Alkali activated earth construction materials

Marsh, Alastair

Award date:
2019

Awarding institution:
University of Bath

Alkali activated earth construction materials

Marsh, Alastair

Award date:
2019

Awarding institution:
University of Bath

Alkali activated earth construction materials

submitted by

Alastair Marsh

for the degree of Doctor of Philosophy

University of Bath

Department of Architecture & Civil Engineering

November 2018

COPYRIGHT

DECLARATION OF AUTHORSHIP

I am the author of this thesis, and the work described therein was carried out by myself personally, with the exception of Chapters 4, 5, 6, 7 and 8 where some of the work was carried out by other researchers. Further details are provided in the declaration of authorship forms which are located prior to each of these chapters.

Acknowledgements

These acknowledgements will be presented in two sections – firstly, academic and scientific support, and secondly, wider social and moral support.

In the first section, my ever-expanding supervisory squad has been a reliable source of guidance and wisdom throughout the PhD journey – Andrew Heath, Mark Evernden, Pete Walker, Pascaline Patureau and Venkat Reddy. With regards to technical and other academic help, I'd like to thank: Philip Fletcher, Diana Lednitzky and Ursula Potter in MAS and Rémi Castaing in CCAF for help with characterisation, as well as Fernando Acosta in Chemical Engineering and Gabriele Kociok-Köhn in Chemistry; David Surgenor and the other 6East technicians for providing assistance and much-needed joviality; Venkat Reddy and Amal Balila for kindly sharing soils and data; Bhavna Sharma for pep talks and reminders of the need to seek gainful employment; Severine Deneulin and Sarah White for early discussions about the role of housing in quality of life and wellbeing; University Library staff for fielding my interminable requests for inter-library loans. I would also like to thank the University of Bath and dCarb CDT for funding, and allowing me the flexibility to pursue my own research proposal. In the same vein, thanks also to Indian Institute of Science, Bangalore and UKIERI for supporting my research placement there. Additional funding thanks to Clay Minerals Group, Applied Mineralogy Group, Armourers and Brasiers', Institute of Materials, Minerals and Mining (IOM3) and the Journal of the European Ceramic Society (JECS) Trust for supporting me to attend conferences once I'd spent all my budget on clays and microscopes.

In the second section, for general social and moral support I'd like to thank: the other doctoral students in Architecture & Civil Engineering, particularly in the "Research Hub" for being part of a fun and surprisingly productive work environment; Claire Hogg and others in the department reception for all manner of things such as finding lost post; Russell Matcham and Mauricia Nambatya from HYT Uganda for inspiring me to enter the field of earth-based construction to begin with; all the communities, in both the city and in the university, to which I have had the privilege to be a part of during my time living in Bath, and finally, to my friends and family, for being understanding and supportive in so many ways.

Abstract

There is a shortage of adequate housing in urban areas of less economically developed countries (LEDCs), which is likely to be exacerbated by high population growth. Conventional walling materials typically used for this application include unstabilised earth, fired brick and concrete block. None of these conventional materials are sufficient to meet the multi-dimensional requirements for sustainable urban growth. There is therefore a demand for new materials that fulfil the criteria of being practical, sustainable and affordable, which is currently unmet. Alkali-activated earth materials are an emerging category of construction materials which could have the potential to fulfil these criteria. In these materials, the clay minerals in soil are transformed into a stabilising phase by the addition of an alkaline activator, in order to give the soil greater strength and durability. These materials have two main potential advantages over conventional walling materials. Firstly, soils are low cost, low environmental impact precursors; secondly, alkali-activated stabilisation has the potential for lower environmental impact than Portland cement stabilisation as it does not require high temperatures or the direct release of CO_2 in the life cycle. Despite these potential advantages, there is a significant knowledge gap around which soils are suitable to use in alkali-activated earth materials. The aims of this thesis are firstly, to establish a fundamental understanding of which soil compositions are suitable for alkali activation, and secondly, to assess the overall viability of alkali-activated earth materials as walling materials suitable for mass housing in this application.

An experimental programme was devised to understand the behaviour of the different components of soil in alkali activation. In this programme, the complexity of the precursors was built up progressively, starting from individual clay minerals commonly found in soils (kaolinite, montmorillonite and illite), followed by mixtures of these clay minerals, natural and synthetic soils, and finishing with soils containing an addition of aggregate. In a simple production process, clay or soil precursors were activated using an aqueous solution of NaOH and then cured at a low temperature of 80°C. Phase formation behaviour was investigated using a range of characterisation techniques. Constraints were specified to make the systems relevant to construction in urban areas of LEDCs. Firstly, an innovative consistency constraint was used, to ensure that the mixes would be appropriate for brickmaking processes. Secondly, the clay and soil precursors were used in their uncalcined form to minimise both the environmental impacts and the technological complexity of the process.

The findings from each experimental stage were used to inform the understanding of the next stage in the series. At the start of the series - the individual clay minerals, the

product phases formed by alkali activation were hydrosodalite for kaolinite, a N-A-S-H or (N,C)-A-S-H geopolymer for montmorillonite, and illite did not form a product phase but underwent alteration. Under the range of conditions used, the clay minerals were never fully consumed. For the mixtures of clay minerals, phase formation behaviour deviated from an ideal rule of mixtures model, which suggested there was a hierarchy of reactivity and influence between the individual clay minerals. For the natural and synthetic soils, it was shown that the clay mineralogy largely determined phase formation behaviour. In contrast, the non-clay components generally had little or no effect on phase formation behaviour, although they did produce a retarding effect on geopolymer formation in one natural soil. In addition, the plasticity of soil was shown to be an important factor in the practical suitability of soils for alkali activation. For the soil mixed with aggregate, it was shown that neither the production of a larger sample, nor the addition of inert aggregate, made any fundamental differences to the alkali activation process.

From this improved technical understanding, it can be stated that using this production process, kaolinitic soils are suitable for alkali activation, whilst montmorillonitic and illitic soils are unsuitable. However, building on this improved fundamental understanding, there is scope for a wider range of soils to be used by tailoring their composition with reactive additives and admixtures. Future research should develop how to tailor soils in this way, and also lower the environmental and financial cost of NaOH-based activators. This research has made an important contribution to the fundamental understanding of how the different components of soil behave in the alkali activation process. Going forward, alkali-activated earth materials have the potential to be part of the solution in providing practical, sustainable and affordable walling materials for housing.

Table of Contents

List of Figures

List of Tables

Chapter 1 - Introduction

The overall research question of this thesis is an investigation into whether alkali-activated earth materials are feasible for construction of housing in urban areas of Less Economically Developed Countries (LEDCs). This chapter introduces the problem area of inadequate housing in urban areas of LEDCs, describes the demand for new materials and the requirements they must meet, and explains why alkali-activated earth materials are a promising candidate for this application.

This thesis is presented in the University of Bath alternative format, in which some chapters are in traditional format and some are in journal article format. For chapters in journal article format, the article is preceded by a linking commentary putting the study in context, and a declaration of authorship explaining the authors' contributions. Some chapters in journal article format include an appendix – the existing numbering system for sections, figures and tables is extended to the appendix in these chapters.

1.1 Problem area: housing in urban areas of LEDCs

Urban areas of LEDCs are some of the most rapidly growing areas in the world. This section will briefly explain the ways in which the insufficient supply of adequate housing in these areas is a problem than needs urgent attention.

By 2050, it is predicted that the world's population will increase by around 2 billion people (UN-DESA, 2015) and there will therefore be a demand for hundreds of millions of new homes over the next three decades. Most of this population growth will be in the continents of Africa and Asia (Figure 1-1). Within these regions, much of this growth will be in LEDCs, which are some of the most rapidly growing countries (UN-DESA, 2015). Within these countries, population growth is tending to be concentrated in urban areas (UN-HABITAT, 2014).

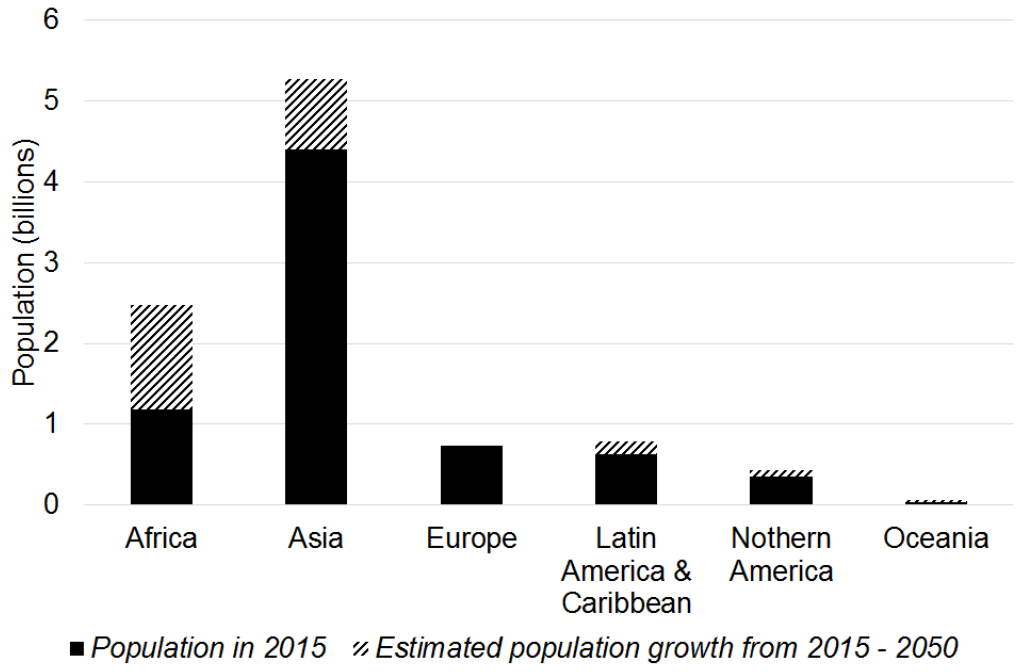

Figure 1-1: Projected global population growth, by region, to 2050. Prepared using data from UNDESA (2015).

In addition to this new demand for housing in these areas, there is simultaneously a need to improve much of the existing housing of inadequate quality. Inadequate housing often makes up large slum areas in cities and is broadly defined by the UN as being deficient in any dimension of habitability, affordability or cultural suitability amongst others (OHCHR and UN-HABITAT, 2014). It is projected that a large proportion of new housing built over the next 30 years in these areas will be of inadequate quality (Figure 1-2) (UN-DESA, 2014, 2015; UN-HABITAT, 2014). Inadequate housing has negative consequences for residents' health, economic

opportunities and resilience (Du Plessis, 2002; Mitchell and Macció, 2018; Wekesa *et al.*, 2011).

The provision of adequate housing is recognised as a priority issue in these regions (Du Plessis, 2005). This is a cross-cutting issue across several of the UN Sustainable Development Goals, including a specific target to "*ensure access for all to adequate, safe and affordable housing and basic services and upgrade slums*" (pg.21, United Nations, 2015). The continued prevalence of inadequate housing is a multi-facetted problem, caused by factors including land ownership, access to finance and planning policy (Du Plessis, 2005; Okpala, 1992; UN-CHS, 1993). However, the lack of adequate construction materials contributes to the problem - and hence the development of new materials has the potential to help alleviate the problem (UN-CHS, 1993).

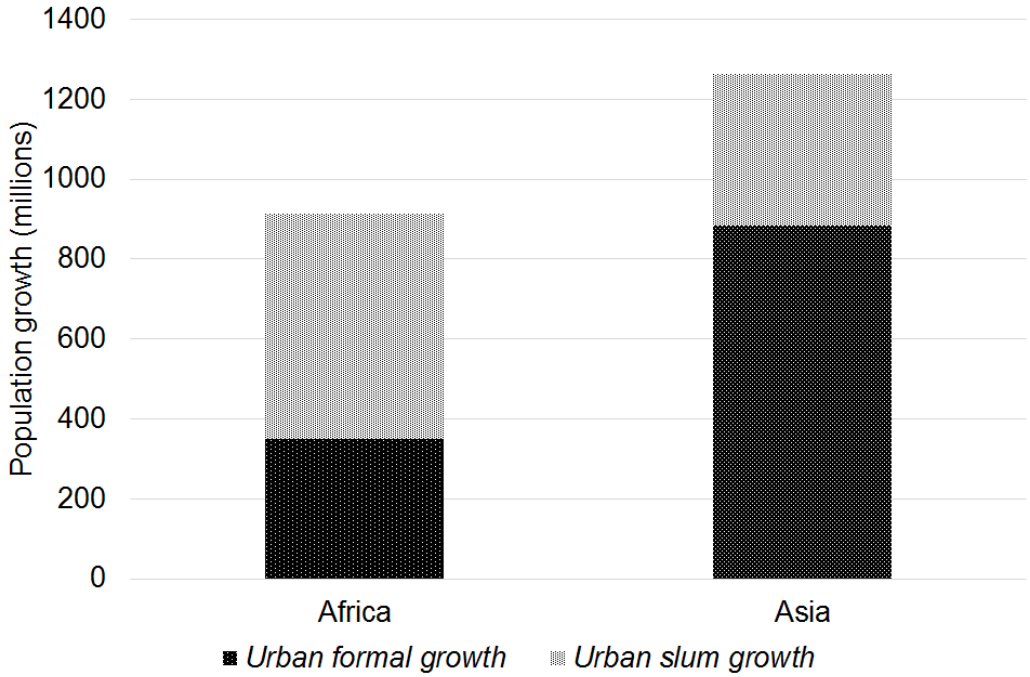

Figure 1-2: Predicted urban population growth in formal and slum areas in Africa and Asia, from 2015 – 2050. Prepared using data from UN-DESA (2014, 2015) and UN-HABITAT (2014).

1.2 Demand for new materials

This section explains the advantages and drawbacks of conventional materials typically used for urban housing in LEDCs, and the requirements of practicality, sustainability and affordability that any new materials must meet.

The scope of this thesis will be limited to walling materials (Figure 1-3), as they typically make up the largest element in one or two storey dwellings, the typologies found in this application (Praseeda *et al.*, 2016). A fairly limited range of conventional materials is typically used for walling in this application: fired brick, concrete blocks and unstabilised earth with natural materials (Okpala, 1992; Wells, 1995). Each has its own advantages and disadvantages.

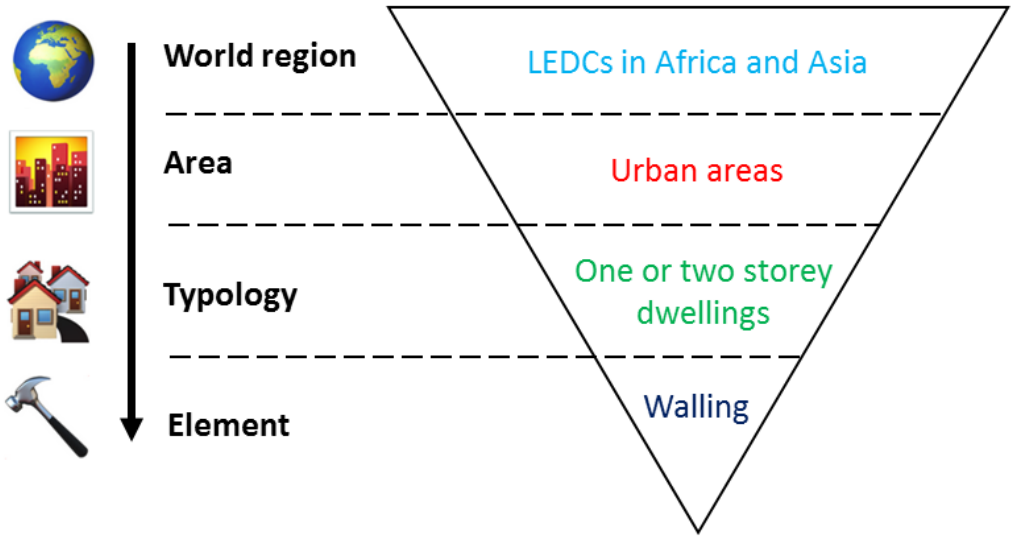

Figure 1-3: A diagram demonstrating how the scope of investigation has been narrowed down. Images generated from iemoji.com.

Fired brick and concrete are socially desirable, generally robust and familiar to build with in LEDCs. However, they often provide poor indoor environmental quality (Sanya, 2012), are relatively expensive and have a high environmental impact through embodied global warming potential (Hashemi *et al.*, 2015). This is a particular concern on a local scale for fired bricks from small manufacturers in many LEDCs, as gathering firewood for brick kilns contributes to deforestation (Hashemi and Cruickshank, 2015).

In contrast, housing built with unstabilised earth materials, using traditional methods such as wattle and daub, can have low environmental impact and provide good indoor environmental quality (Sanya, 2012). However, they can have poor durability (Figure 1-4) (Adegun and Adedeji, 2017), requiring continuing, labour intensive maintenance. They can also be linked to low social status of occupants (Nambatya, 2015; Yeboah, 2005). In addition, some natural resources used in combination with earth, such as

reed poles, have become overexploited in areas of high population growth (Wells *et al.*, 1998). The prevaling trend in recent decades has therefore been to move away from traditional unstabilised earth materials towards fired brick and concrete, when it is affordable to do so (Okpala, 1992; Wells, 1995; Yeboah, 2005).

There have long been calls for new materials in housing (UN-CHS, 1993), as none of the traditional or modern conventional materials meet contemporary needs. New materials must fulfil multidimensional demands in the categories of economic, technical, socio-cultural and environmental sufficiency (Marsh *et al.*, 2016). For the purposes of this thesis, this will be simplified down to three requirements for success: practical, sustainable and affordable.

Figure 1-4: An example of damage sustained by an unstabilised earth building, which can suffer from low durability. Image courtesy of Prof. Pete Walker.

1.2.1 Practical

Construction in urban areas of LEDCs is dominated by the informal sector - this typically involves small scale, unregulated construction, with self-building common (Du Plessis, 2002; Okpala, 1992). Several production practices are typical in the informal sector, such as stockpiling. Because of the lack of formal finance, materials are often bought in an ad hoc manner and stockpiled on site, until there is enough for the construction of the next building element (Aina, 1988; Yeboah, 2005). This means that construction can take months or even years (Awanyo *et al.*, 2014). Unskilled labour is used for most housing construction, with the exception of certain elements such as the

foundation (Aina, 1988). This puts constraints on the complexity of unfamiliar technology that is advisable to be used.

1.2.2 Sustainable

Attention has recently increased on the contribution of the built environment towards global warming through embodied $CO_{2eq.}$ emissions, rather than just through operational emissions (Ibn-Mohammed *et al.*, 2013). In order to keep the global average temperature rise < 1.5°C (relative to pre-industrial levels), it's predicted that global $CO_{2eq.}$ emissions will need to reach net zero by 2050 (IPCC, 2018). Therefore, whilst providing new housing on such a large scale, the embodied $CO_{2eq.}$ emissions should be considerably lower than the conventional materials of fired brick and concrete. However, there are a range of other life cycle impact indicators (Pennington *et al.*, 2004), whose impacts are more relevant on a local level. These can include human toxicity and ecotoxity (Dahmen *et al.*, 2018; Heath *et al.*, 2014), and are especially relevant to informal sector construction, where the regulatory environment and safety practices are generally looser than in more economically developed countries (MEDCs). Social acceptability of housing is another - often neglected - aspect of sustainability. Whilst this is beyond the direct influence of materials researchers, a conscious effort can be made to design materials that appeal to people's aesthetic preferences in a given context. In this case, this would be that the finished form is similar in appearance to conventional construction materials.

1.2.3 Affordable

In informal sector construction, there is typically a lack of access to formal credit, as well as limited financial resources in general (Aina, 1988; Okpala, 1992). Given the prevalence of self-building and low cost of labour in informal construction, the cost of materials typically dominates the overall cost of construction (Baiden *et al.*, 2014; Wells *et al.*, 1998). Therefore, new materials should be more affordable than the conventional modern materials such as fired brick and concrete, which are often unaffordable for many people (Baiden *et al.*, 2014; UN-CHS, 1993).

Based on these three requirements, there are several emerging materials which have the potential to meet this demand. One of these emerging materials is alkali-activated earth materials.

1.3 Alkali-activated earth materials

Alkali-activated earth materials are a hybrid of two categories of materials: earthen materials and alkali-activated materials. This section explains the background of these materials, how they relate to other construction materials, and the potential advantages they have for this application.

Earth construction is an ancient form of construction used for thousands of years and still practiced around the world (Fabbri and Morel, 2016; Houben and Guillaud, 1994). Earth is advantageous in its widespread availability, allowing for use of local resources and reduction of transport costs and impacts (Morel *et al.*, 2001). However, as described in the preceding section, there has been a move away from traditional, unstabilised earthen materials in this application. This is due to their need for labour-intensive repair and maintenance, as well as low social status. Stabilisation of soils to improve their durability and strength has been practised for a long time using natural products (Houben and Guillaud, 1994). Recently, the use of stabilising agents such as cement and lime has been used in a methodical way, to improve the performance of earth (Kinuthia, 2016). Cement-stabilised earth can have a lower environmental impact than concrete blocks and especially fired bricks, whilst still having adequate performance (Figure 1-5) (Dahmen *et al.*, 2018; Reddy and Jagadish, 2003). The use of cement and lime as stabilising agents is undesirable from the point of view of environmental impacts and cost. There is the potential for stabilisation by alkali activation to improve upon the environmental performance and affordability of these materials (Figure 1-6).

Figure 1-5: An example of cement-stabilised soil construction using interlocking stabilised soil blocks (ISSB). Image courtesy of Haileybury Youth Trust.

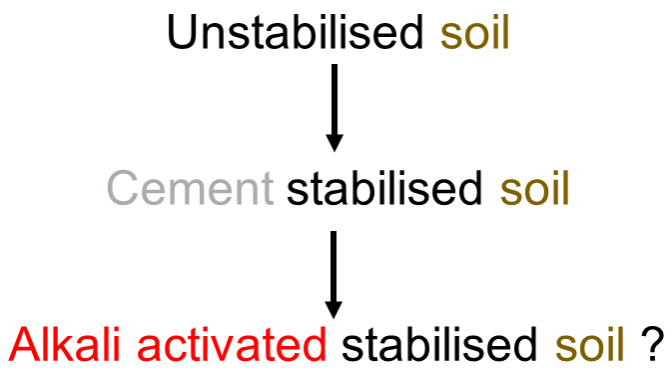

Figure 1-6: Development of soil as a construction material.

Alkali activation is a way of transforming an aluminosilicate precursor into an alkali aluminosilicate phase (Provis, 2014). In the case of soils, this involves transforming the clay minerals into a durable product phase, either a geopolymer or a zeolite, which can perform the function of stabilising the soil (Figure 1-7). This works in a different way to cement stabilisation. Instead of adding in a wholesale new material (such as cement) into the soil as a stabilising phase, alkali activation transforms the clay in soil into a stabilising phase. A technical explanation of this process will be provided in Chapter 2.

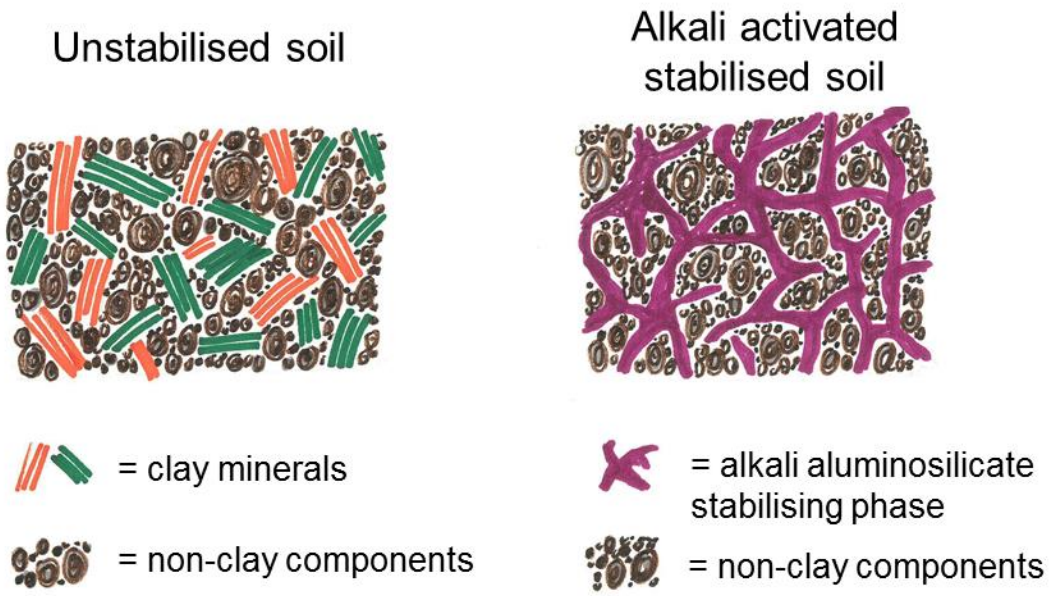

Figure 1-7: Schematic diagrams of unstabilised soil, and soil stabilised by alkali activation.

Alkali-activated materials have been a growing topic of interest given their potential to have lower environmental impact than Portland cement based materials (Habert and Ouellet-Plamondon, 2016). This is primarily due to the fact that there is no requirement for high temperature heating or chemically driven CO_2 release during calcination as in the production of Portland cement or lime. By combining this advantage with the affordability, widespread availability and low environmental impact of soil as a precursor, there is the potential for alkali-activated earth materials to fulfil the requirements of being practical, affordable and sustainable.

The potential of these materials as construction materials has been shown for a small number of prototype systems, and it is a growing research area. However, there is a significant knowledge gap around understanding what range of soil compositions are suitable precursors for alkali activation. This range of suitability will determine whether alkali-activated earth materials could make a major contribution to meeting this material demand across large regions, or be limited to a small portion in certain areas. There is also limited research on linking materials behaviour to suitability in processing and construction. The literature on this subject is reviewed in Chapter 2.

1.4 Overview of thesis

The overall research question of this thesis is: are alkali-activated earth materials feasible for construction of housing in urban areas of LEDCs? This is carried out by pursuing specific technical questions, and then linking these findings back to the broader application, as will be described in Chapter 3. This Introduction chapter has: introduced the problem area of inadequate housing in urban areas of LEDCs; described the demand for new materials and the requirements they must meet, and explained why alkali-activated earth materials are a promising candidate for this application.

The rest of this thesis is organised to answer this research question. A brief summary of each chapter is given below, and schematically summarised in Figure 1-8.

Chapter Two – Clays, soils and alkali activation – a literature review

> A technical description of clay minerals, soils, and the alkali activation process. This identifies the key knowledge gap in the fundamental understanding of soil composition and alkali activation.

Chapter Three – Research approach

> A statement of the technical research questions, and an explanation of the overall methodology used to answer these research questions. This is followed by a description of the choices and assumptions made for mix design, synthesis methods (including how these were made relevant to production processes in LEDCs), characterisation techniques, and the clay and soil precursors.

Chapter Four – Alkali activation of kaolinite

> An investigation of alkali activation of kaolinite, the most common 1:1 clay mineral in soil. A hydrosodalite is formed as the product phase.

Chapter Five – Alkali activation of montmorillonite and illite

> Investigation of alkali activation of montmorillonite and illite, the two most common 2:1 clay minerals in soil. A N-A-S-H or (N,C)-A-S-H geopolymer is formed as the product phase for montmorillonite, and the illite does not form an identified product phase but undergoes alteration.

Chapter Six – Alkali activation of clay mixtures

Investigation of alkali activation of binary and ternary mixtures of kaolinite, montmorillonite and illite. Phase formation is mostly determined by the dominant clay mineral in a mixture, but does not completely follow a simple rule of mixtures model.

Chapter Seven – Alkali activation of natural and synthetic soils

Investigation of the influence of non-clay components in soils, by the alkali activation of natural and synthetic soils. Clay minerals are the primary determinants of phase formation, but non-clay components can have a retarding effect.

Chapter Eight – Alkali activation of soil blocks

Investigation of differences in phase formation behaviour within scaled-up blocks. There are no large phase differences between the centre and edge regions of the block, and addition of aggregate makes no fundamental change to the alkali activation products.

Chapter Nine – Conclusions and future research

The technical research questions are answered, explaining how the systematic investigation of the compositional effects of soil on alkali activation fill the research gap. The overall research question is answered, discussing how the findings of this thesis inform the advantages and disadvantages of alkali-activated earth materials. Priorities for further research include linking phase composition to strength and durability, tailoring the composition and workability of soils and developing lower impact alkaline activators.

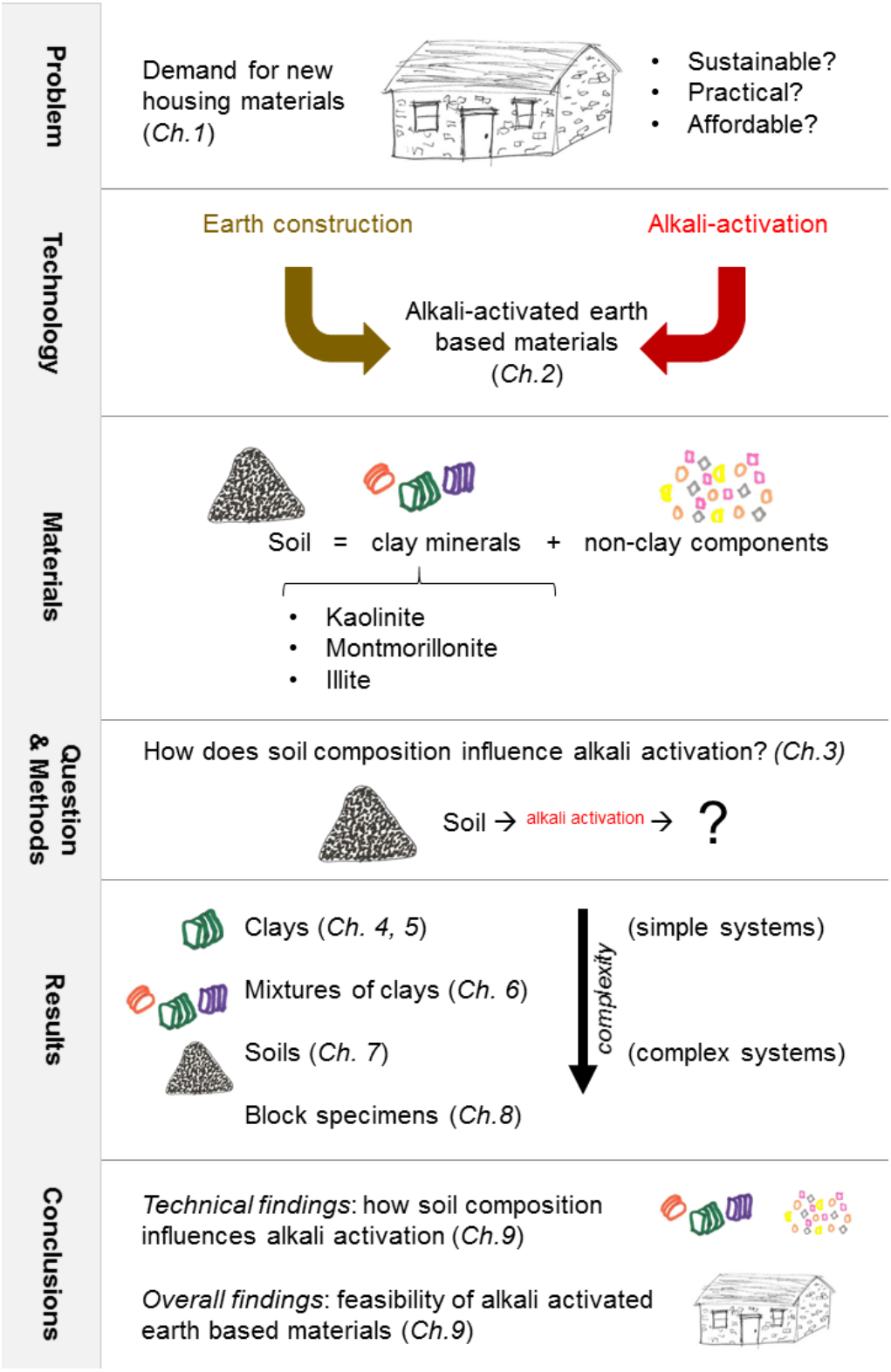

Figure 1-8: Schematic summary of the layout of the thesis.

References

Adegun, O.B. & Adedeji, Y.M.D., 2017. Review of economic and environmental benefits of earthen materials for housing in Africa. *Frontiers of Architectural Research,* 6(4), pp. 519-528.

Aina, T.A., 1988. The construction of housing for the urban poor of Lagos. *Habitat International,* 12(1), pp. 31-48.

Awanyo, L., McCarron, M. & Morgan Attua, E., 2014. Affordable housing options for all in a context of developing capitalism: can housing transformations play a role in the Greater Accra Region, Ghana? *African Geographical Review*, pp. 1-18.

Baiden, B.K., Agyekum, K. & Ofori-Kuragu, J.K., 2014. Perceptions on Barriers to the Use of Burnt Clay Bricks for Housing Construction. *Journal of Construction Engineering,* 2014(502961).

Dahmen, J., Kim, J. & Ouellet-Plamondon, C.M., 2018. Life cycle assessment of emergent masonry blocks. *Journal of Cleaner Production,* 171, pp. 1622-1637.

Du Plessis, C., 2002. *Agenda 21 for Sustainable Construction in Developing Countries.* Pretoria, South Africa: C.B.a.C. Technology.

Du Plessis, C., 2005. Action for sustainability: preparing an African plan for sustainable building and construction. *Building Research & Information,* 33(5), pp. 405-415.

Fabbri, A. & Morel, J.C., 2016. 10 - Earthen materials and constructions. In: K.A. Harries & B. Sharma, eds. *Nonconventional and Vernacular Construction Materials.* Woodhead Publishing, pp. 273-299.

Habert, G. & Ouellet-Plamondon, C., 2016. Recent update on the environmental impact of geopolymers. *RILEM Technical Letters,* 1, pp. 17-23.

Hashemi, A. & Cruickshank, H., 2015. Embodied Energy of Fired Bricks: The Case of Uganda and Tanzania. *14th International Conference on Sustainable Energy Technologies (SET 2015).* Nottingham, UK.

Hashemi, A., Cruickshank, H. & Cheshmehzangi, A., 2015. Environmental Impacts and Embodied Energy of Construction Methods and Materials in Low-Income Tropical Housing. *Sustainability,* 7(6), p. 7866.

Heath, A., Paine, K. & McManus, M., 2014. Minimising the global warming potential of clay based geopolymers. *Journal of Cleaner Production,* 78, pp. 75-83.

Houben, H. & Guillaud, H., 1994. *Earth Construction: A comprehensive guide.* Rugby, U.K.: Practical Action Publishing.

Ibn-Mohammed, T., Greenough, R., Taylor, S., Ozawa-Meida, L. & Acquaye, A., 2013. Operational vs. embodied emissions in buildings—A review of current trends. *Energy and Buildings,* 66, pp. 232-245.

IPCC, 2018. *Chapter 2: Mitigation pathways compatible with 1.5°C in the context of sustainable development.*

Kinuthia, J.M., 2016. 9 - Unfired clay materials and construction. *Nonconventional and Vernacular Construction Materials.* Woodhead Publishing, pp. 251-272.

Marsh, A., Heath, A., Reddy, B.V.V. & Evernden, M., 2016. A Holistic Materials Design Requirements Framework (HoMDReF) For Future Housing Materials. In: S. Emmitt & K. Adeyeye, eds. *ID@50 Integrated Design Conference 2016.* Bath, U.K.

Mitchell, A. & Macció, J., 2018. *Evaluating the Effects of Housing Interventions on Multidimensional Poverty: The Case of TECHO-Argentina.* Oxford, U.K.: Oxford Poverty & Human Development Initiative, (Working Paper No.120).

Morel, J.C., Mesbah, A., Oggero, M. & Walker, P., 2001. Building houses with local materials: means to drastically reduce the environmental impact of construction. *Building and Environment,* 36(10), pp. 1119-1126.

Nambatya, M.M., 2015. *Investigating the rationale for material selection in tropical housing projects in Uganda – a case for Interlocking Stabilised Soil Blocks (ISSB) technology.* MPhil, University of Cambridge.

OHCHR & UN-HABITAT, 2014. *The Right to Adequate Housing.* Geneva, Switzerland: UNHCHR, (Fact Sheet No.21/Rev.1).

Okpala, D.C.I., 1992. Housing production systems and technologies in developing countries: a review of the experiences and possible future trends/prospects. *Habitat International,* 16(3), pp. 9-32.

Pennington, D.W., Potting, J., Finnveden, G., Lindeijer, E., Jolliet, O., Rydberg, T. & Rebitzer, G., 2004. Life cycle assessment Part 2: Current impact assessment practice. *Environment International,* 30(5), pp. 721-739.

Praseeda, K.I., Reddy, B.V.V. & Mani, M., 2016. Embodied and operational energy of urban residential buildings in India. *Energy and Buildings,* 110, pp. 211-219.

Provis, J.L., 2014. Geopolymers and other alkali activated materials: why, how, and what? *Mat. Struct.,* 47(1), pp. 11-25.

Reddy, B.V.V. & Jagadish, K.S., 2003. Embodied energy of common and alternative building materials and technologies. *Energy and Buildings,* 35(2), pp. 129-137.

Sanya, T., 2012. Sustainable architecture evaluation method in an African context: transgressing discipline boundaries with a systems approach. *Sustainability Science,* 7(1), pp. 55-65.

UN-CHS, 1993. Building materials for housing : Report of the executive director, United Nations Commission on Human Settlements. *Habitat International,* 17(2), pp. 1-20.

UN-DESA, 2014. *World Urbanization Prospects: The 2014 Revision, Highlights.* New York, U.S.A., (ST/ESA/SER.A/352).

UN-DESA, 2015. *World Population Prospects: The 2015 Revision, Key Findings and Advance Tables.* New York, U.S.A., (Working Paper No. ESA/P/WP.241.).

UN-HABITAT, 2014. *World Habitat Day: Background Paper.* Nairobi, Kenya: UN-HABITAT.

United Nations, 2015. Transforming our world: The 2030 agenda for sustainable development. *Resolution adopted by the General Assembly.*

Wekesa, B.W., Steyn, G.S. & Otieno, F.A.O., 2011. A review of physical and socio-economic characteristics and intervention approaches of informal settlements. *Habitat International,* 35(2), pp. 238-245.

Wells, J., 1995. Population, settlements and the environment: The provision of organic materials for shelter: A literature review. *Habitat International,* 19(1), pp. 73-90.

Wells, J., Sinda, S.H. & Haddar, F., 1998. Housing and building materials in low-income settlements in Dar es Salaam. *Habitat International,* 22(4), pp. 397-409.

Yeboah, I.E.A., 2005. Housing the urban poor in twenty-first century Sub-Saharan Africa: Policy mismatch and a way forward for Ghana. *GeoJournal,* 62(1-2), pp. 147-161.

Chapter 2 - Alkali activation of clay minerals and soils – a literature review

In this chapter, background descriptions are provided for the structure and properties of clay minerals, soils, as well as the fundamentals of the alkali activation process. This is followed by a literature review of the alkali activation behaviour of individual clay minerals (kaolinite, halloysite, montmorillonite and illite) as well as feedstocks containing clays (common clays and soils).

The scope of the literature review includes some precursors which are not included within the experimental work in this thesis: namely, the clay mineral halloysite, and common clay deposits. Although these are not considered after this chapter, they provide useful context to understanding the alkali activation behaviour of a range of clay minerals and natural feedstocks that contain clay.

Also included in the scope of the literature review are studies which use treatments to increase reactivity, such as thermal activation. There is a dearth of studies on clay minerals and clay-containing feedstocks without any form of treatment. Studies which use reactivity-enhancing treatments have therefore been considered here, because they help provide a more complete picture of the behaviour of clay minerals and natural feedstocks.

From the conclusions from the literature review, two scientific knowledge gaps are presented. The first is around understanding the range of treatment and processing conditions required to form a given product phase. This is highly relevant for the wider development of alkali-activated materials, but for the application of housing in urban areas in LEDCs, constraints on the level of technological complexity preclude the use of the full range of treatments and processing conditions. Therefore, this knowledge gap is not applicable to the research undertaken in this thesis.

The second key knowledge gap is around fundamental understanding of alkali activation for a range of clay-containing feedstocks. This is applicable to soils, and it is this knowledge gap which forms the motivation for the research in this thesis. It is noted that within this review, a key part of the evidence of the behaviour of the untreated individual clay minerals is provided by studies undertaken as part of this thesis.

Declaration of authorship

This declaration concerns the article entitled:									
Alkali activation and geopolymerisation behaviour of clay minerals, common clays and soils: a review									
Publication status (tick one)									
draft manuscript	✓	**Submitted**		**In review**		**Accepted**		**Published**	
Publication details (reference)	Khalifa, A., Marsh, A., Cizer, Ö., Patureau, P., Heath, A. (in preparation). "Alkali activation and geopolymerisation behaviour of clay minerals, common clays and soils: a review"								
Candidate's contribution to the paper (detailed, and also given as a percentage).	The candidate considerably contributed to… Formulation of ideas: Both A.Marsh (50%) and A.Khalifa (50%) independently came up with the idea to write a review on this subject, and decided to co-author together. Design of methodology: Both A.Marsh (50%) and A.Khalifa (50%) decided the aims and scope of the review together. Experimental work: Both A.Marsh and A.Khalifa undertook the reviewing and writing. A.Marsh (55%) focussed on phase formation and the alkali activation process, whilst A.Khalifa (30%) focussed on thermal treatments and clay structures. A.Heath (5%), P.Patureau (5%) and O.Cizer (5%) gave comments and feedback on the manuscript. Presentation of data in journal format: Both A.Marsh (50%) and A.Khalifa (50%) contributed to formatting.								
Statement from Candidate	This paper reports on original research I conducted during the period of my Higher Degree by Research candidature.								
Signed							**Date**	30/10/2018	

Alkali activation and geopolymerisation behaviour of clay minerals, common clays and soils: a review

Abstract

The use of clay minerals as aluminosilicate precursors in alkali-activated materials has grown rapidly, for many potential applications including construction materials. Their abundance in nature makes them an attractive resource. A large number of studies have focused on the alkali activation of calcined kaolinite with a view to forming geopolymers. Recently, other types of clay minerals, common clays and soils have also been used as feedstocks. This paper reviews the factors in mineralogy, treatment and synthesis which influence phase formation in alkali activation of these feedstocks. Studies were grouped into individual clay minerals, and common clays and soils. In the activation of individual clay minerals, it is shown that treatment methods have arguably the largest influence in determining phase formation. Kaolinite, halloysite, montmorillonite and illite can be used to form geopolymers, albeit with different requirements for treatment, activating solution composition and processing conditions. In the activation of common clays and soils, it is shown that overall behaviour is approximately in line with the respective dominant clay minerals. It is promising for the prospects of scaled up production that many deposits of lower conventional quality are in fact better suited for use in alkali activation than those of higher conventional quality. There has been significant progress made in this field, and clay minerals remain a promising feedstock in alkali activation. However, there is still a lack of understanding in how mineralogical factors control material behaviour. It is recommended that further research be directed towards a more complete understanding of the effects of mineralogy and chemical composition in the alkali activation process.

2.1 Introduction

Alkali-activated materials cover a broad range of systems, defined as "*the reaction of a solid aluminosilicate (termed the 'precursor') under alkaline conditions (induced by the 'alkali activator'), to produce a hardened binder which is based on a combination of hydrous alkali-aluminosilicate and/or alkali-alkali earth-aluminosilicate phases*" (pg.2, Provis, 2018a). The alkali activation of clay minerals, common clays and soils lies at the intersection of the fields of clay science and other disciplines including civil engineering, materials science and inorganic chemistry. It is an example of the recent development of collaborations between different subjects for the motivation of sustainability and improved material performance. Recent reviews have been published on related topics including: sustainable brick production (Murmu and Patel, 2018); earth-based construction (Pacheco-Torgal and Jalali, 2012); alkali activation of solely kaolinite and metakaolin (Liew *et al.*, 2016; Provis, 2018b; Rashad, 2013); alkali activation of waste materials (Mehta and Siddique, 2016; Payá *et al.*, 2015; Toniolo and Boccaccini, 2017; Zhang, 2013); geopolymer construction in general (Obonyo *et al.*, 2011); the applications of alkali-activated materials for masonry blocks (Ahmari and Zhang, 2015) and groundworks stabilisation (Sargent, 2015); methods of increasing precursors' reactivity (Tchadjie and Ekolu, 2018); environmental impacts (Habert and Ouellet-Plamondon, 2016); advances in characterisation including measuring durability (Provis *et al.*, 2015), and the fundamental mechanisms of the alkali activation process (Duxson *et al.*, 2007a; Garcia-Lodeiro *et al.*, 2015; Komnitsas and Zaharaki, 2007; Pacheco-Torgal *et al.*, 2008). Alkali-activated materials can be used for a wide range of applications such as functional nanomaterials (MacKenzie, 2015; Medpelli *et al.*, 2014), fire resistance and refractory bricks (Bernal *et al.*, 2014; Kovalchuk and Krienko, 2009), heavy metals immobilization (Lancellotti *et al.*, 2015; Provis, 2009b; Van Jaarsveld *et al.*, 1997) and nuclear waste storage (Shi and Fernández-Jiménez, 2006; Vance and Perera, 2009). Most attention is focussed on construction and building materials, including: cast concrete (Provis *et al.*, 2014a), reinforced concrete (Ding *et al.*, 2016), blocks (Ahmari and Zhang, 2015), thermal insulation (Bernal *et al.*, 2014; Zhang *et al.*, 2014), and repair mortars (Pacheco-Torgal *et al.*, 2012). The potential benefits of alkali-activated materials in construction are well described in the review articles and books cited above – in brief, their main attraction is the potential to have a much lower environmental impact and higher durability than Portland cement based materials (van Deventer *et al.*, 2010).

The most desirable product phase of alkali activation is a geopolymer, due to its strength, stability and durability. Geopolymer is a commonly used term, which falls within the broader domain of alkali activation. Invented by Davidovits (1989), the term

geopolymer generally refers to a system where "*the binding phase comprises an alkali aluminosilicate gel, with aluminium and silicon linked in a three-dimensional tetrahedral gel framework.*" (pg.4, Provis and van Deventer, 2009), and is used mainly to describe low-calcium alkali-activated aluminosilicate binders (Davidovits, 1989; Provis, 2018a). Broadly speaking, any material which has a certain amount of silica and alumina in reactive form – being either sufficiently disordered, or having a structure that is highly soluble in an alkaline media - can be used as a precursor in alkali activation. Among the most popular are: fly ash, ground granulated blast furnace slag (GGBS), building residues and calcined kaolinite (metakaolin). These are important precursors due to their amorphous character and high reactivity. Despite their useful properties, there is a growing move to look beyond these core materials (Scrivener *et al.*, 2016). With regards to fly ash and GGBS, trends in industrial production and geographical location mean they are not guaranteed to be universal mass-scale concrete replacement materials. Utilisation rates of coal combustion products (including fly ash) are already as high as >90% in Europe and Japan, although this is lower in other regions such as Middle East, Africa and Asia <15% (Heidrich *et al.*, 2013). Although construction is still the biggest use, there are numerous other possible applications for fly ash (Blissett and Rowson, 2012; Yao *et al.*, 2015), and emerging uses for GGBS such as carbon sequestration and soil remediation in farmland (Beerling *et al.*, 2018). In addition, questions remain over how to fairly assign their environmental impacts as by-products of industrial processes, rather than waste (Habert *et al.*, 2011). Unlike fly ash and GGBS, metakaolin is an established processed material resource, rather than an industrial side-stream. Due to its purity and consistent composition, metakaolin has been a popular choice for alkali activation, both as a single precursor for geopolymers (Davidovits, 2011; Provis *et al.*, 2009; Rahier *et al.*, 1996) and as a supplementary cementitious material for blended cements (Fernandez Lopez, 2009; Scrivener, 2014; Tironi *et al.*, 2013). However, technical issues of poor workability (Provis, 2009a) and high water demand (Provis *et al.*, 2010) are problematic in alkali activation of pure metakaolin. Methods to address these issues include tailoring the viscosity of the alkaline activating solution (Provis, 2009a) and/or the metakaolin particle morphology from the calcination process (San Nicolas *et al.*, 2013). Beyond technical issues, scale-up is also problematic for metakaolin. The processing costs and lack of abundance of high quality kaolin deposits mean that high purity metakaolin is not sufficient to be the sole precursor for mass-scale cement replacement materials - a wider range of lower purity precursors is needed instead (Gharzouni *et al.*, 2016; McIntosh *et al.*, 2015; Provis, 2018b). In response, increasing attention has been given to using other clay minerals (e.g. 2:1 dioctahedral layer silicates), common clay deposits and soils as precursors. Common clays and soils are both widely available in large quantities.

Global resources for all common industrial clays are extremely large (U.S. Geological Survey, 2018), and it has been estimated that 6 GT/year supply could be available (Scrivener *et al.,* 2016). Soils are abundant in many parts of the world, as shown by their use in construction throughout human history (Houben and Guillaud, 1994). As well as their natural abundance, they are also a waste stream - soils typically make up the single largest component of construction waste (Llatas, 2011).

The alkali activation of clay minerals is a challenging topic, due to the complex nature of clay minerals, and the highly variable influence of formation and weathering conditions on their mineralogy (Meunier, 2005). Several factors control the chemical and physical properties of clays, including: the mineralogy of the layers; exchangeable interlayer cations; the type and quantity of associated minerals; presence of organic matter and soluble salts, and particle size distribution (Brigatti *et al.*, 2013; Murray, 2006). Regarding other feedstocks, “common clays” define a variety of clay-containing deposits, having a wide range of mineralogical compositions (Murray, 2006). Given that soils represent an extensive and widely available source of clay minerals, it is a logical step to consider their behaviour too. Soils have long been stabilised by using alkali additions to change the interlayer cation state and/or flocculation state of the clay minerals (Sargent, 2015), but not by a phase transformation. Alkali-activated soils are an emerging strand for the stabilisation of sub-soils in situ for construction (Sargent, 2015), as well as for the manufacture of construction materials. Although the compositional variability and quality of these feedstocks are much less advantageous than in high-purity metakaolin, they have a far better potential to be scalable (Provis, 2018a). The adoption of lower purity resources is not a trivial step, as both the exact nature of the clay mineral and presence of impurities can both affect phase formation (Autef *et al.*, 2013). Thus, in order to unlock this wider range of resources and use alkali-activated materials as a mass-scale replacement for Portland cement based materials, there is a need to understand the effects of mineralogy and impurities in other clay minerals, common clay deposits and soils.

Given the growing number of alkali activation studies on these feedstocks, now is a timely moment to review: the state of scientific knowledge in this field, the opportunities and potential benefits, the areas in which further research is most needed, and the practical barriers to adoption. The scope of this review considers the alkaline activation of low calcium clay or soil systems, with no additional reactive feedstock such as fly ash, GGBS or other industrial wastes. The purpose of this restriction is to focus on the alkali activation behaviour of the clay minerals themselves. For the purpose of this review, alkali aluminosilicate reaction products are classified as either crystalline zeolitic phases, or amorphous geopolymer phases. Emphasis is given to geopolymer

phases rather than zeolites, as the former is believed to be more beneficial for the applications of construction materials and soil stabilisation. Zeolitic formation is considered only as far as to understand the influences of clay mineralogy and processing conditions on alkali activation behaviour as a whole. Although acid activation has been demonstrated to form geopolymeric products in several systems (Guo *et al.*, 2016; Liu *et al.*, 2012; Wang *et al.*, 2017a), this review is restricted to alkaline activation, as the majority of studies continue to use this method.

Within the phyllosilicate clay minerals, attention has been paid to the three most common clay minerals, especially in soils (Nickovic *et al.*, 2012), namely kaolinite, montmorillonite and illite. Consideration has been extended to the mineralogical groups to which these clay minerals belong: serpentine-kaolin, smectite, and true mica respectively. Given that kaolinite and in particular its calcined version, metakaolin, have been widely studied (Liew *et al.*, 2016; Zhang *et al.*, 2016), kaolinitic systems are considered largely as reference points for systems using other clay minerals.

This article firstly provides a brief overview of clay minerals' structures and fundamental aspects of alkali activation. Secondly, the alkali activation of individual clay minerals – including the use of treatments - is reviewed before going further with the alkali activation of common clays and soils. Finally, the remaining knowledge gaps in this field are identified.

2.2 Structure of clay minerals

Clay minerals are phyllosilicates (layered silicates). Their crystallographic structure consists of regular repetition of tetrahedral and octahedral sheets forming layers. The two-dimensional tetrahedral sheets (Figure 2-1) have the general formula T_2O_5. T is the cation, usually Si^{4+}, Al^{3+}, or Fe^{3+}, with each cation surrounded by four oxygens in a tetrahedral geometry. Each tetrahedron is linked to adjacent tetrahedra by three shared corners (the basal oxygen atoms, O_b) to form a hexagonal mesh pattern. The fourth corners (the tetrahedral apical oxygen atoms, O_a) form octahedra of formula MO_6, which together make two-dimensional octahedral sheets (Figure 2-2). M is either a divalent (Mg^{2+}, Fe^{2+}) or trivalent (Al^{3+}, Fe^{3+}) cation. For a divalent cation, the side-sharing octahedra belong to a trioctahedral sheet, whereas for a trivalent cation, the sheet is called dioctahedral. The positioning of the octahedral anions O_o (most commonly OH^-, but can also be other anions such as F^- or Cl^-) in the octahedra can form either cis- or trans- types of octahedra. These features, and their effect on clay properties, will be described in Section 2.4.2.

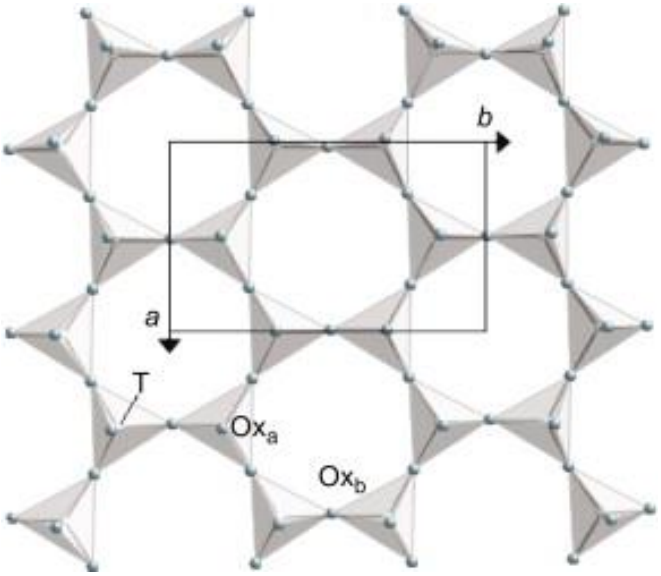

Figure 2-1: Overhead diagram of the tetrahedral sheet. Ox_a = apical oxygen atoms; Ox_b = basal oxygen atoms; T = tetrahedral cations; a and b refer to unit cell parameters (Brigatti et al., 2013).

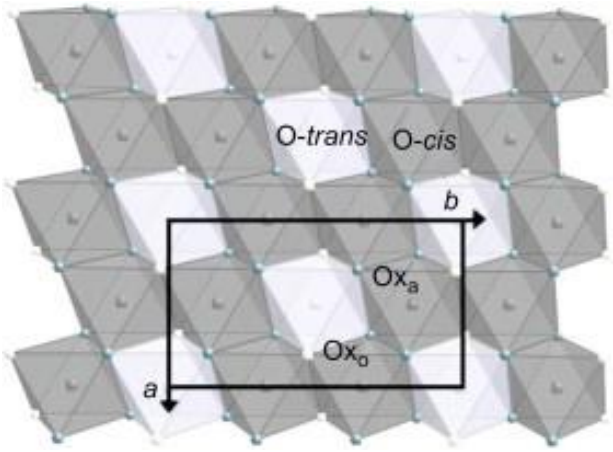

Figure 2-2: Overhead diagram of the octahedral sheet. Ox_a = apical oxygen atoms; Ox_o = octahedral anions (typically OH). O-trans = trans-oriented octahedra; O-cis = cis-oriented octahedra; a and b refer to unit cell parameters (Brigatti et al., 2013).

The stack of layers formed by one tetrahedral sheet and one octahedral sheet defines the 1:1 clay minerals' crystallographic structure (e.g. kaolinite) while in the 2:1 clay minerals, the layer consists of an octahedral sheet sandwiched between two tetrahedral sheets (e.g. smectite). The arrangement and composition of the octahedral and tetrahedral sheets can vary, and this accounts for most of the differences in the physical and chemical properties of the clay minerals (Brigatti *et al.*, 2013; Christidis, 2011; Murray, 2006; Schaetzl and Anderson, 2005).

2.2.1 The 1:1 layer silicates

2.2.1.1 Serpentine-Kaolin group

The 1:1 layer silicates are divided into three subgroups: Trioctahedral 1:1 Minerals (Serpentine sub-group); Dioctahedral 1:1 Minerals (Kaolin sub-group), and a mixed sub-group. Serpentine sub-group minerals have the unit formula of $Mg_6Si_4O_{10}(OH)_8$, in which all the six sites of the octahedral sheet are occupied by Mg^{2+} cations. Kaolin sub-group minerals have the unit formula $Al_4Si_4O_{10}(OH)_8$, in which four sites of the octahedral sheet are occupied by Al^{3+} cations and two are vacant. Kaolinite is the most common member of this subgroup (Figure 2-3). It can be formed by the dissolution of Al and Si by weathering of primary and secondary minerals (Brigatti *et al.*, 2013; Christidis, 2011; Murray, 2006; Schaetzl and Anderson, 2005). Unlike the 2:1 layer silicates, minerals in this group do not tend to have much atomic substitution and do not have a permanent layer charge. This gives them non-swelling behaviour.

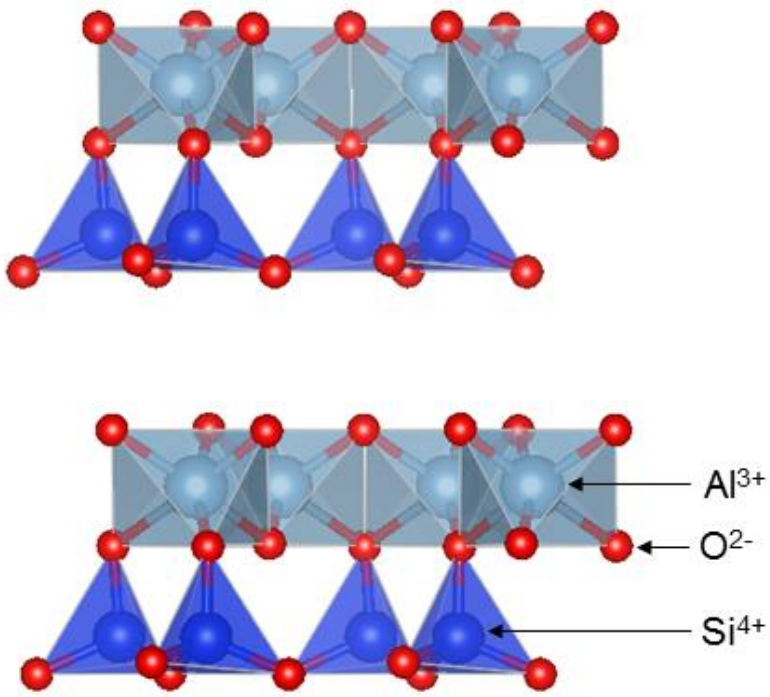

Figure 2-3: Atomic diagram of kaolinite, showing two layers. Image generated in VESTA using structural parameters from Bish (1993).

2.2.1.2 Halloysite - Hydrated Halloysite group

The halloysite minerals can be found in two forms: one hydrated, in which there is a layer of water molecules between the alumino-silicate layers, and one dehydrated. In contrast to the plate-like structure of kaolinite, halloysite has a tubular or spherical structure (Brigatti *et al.*, 2013; Murray, 2006; Schaetzl and Anderson, 2005; Schulze, 2005).

2.2.2 The 2:1 layer silicates

The classifications of 2:1 clay minerals are based on the permanent layer charge, which is caused by cationic substitution in the octahedral or the tetrahedral sheet. In addition to these factors, the 2:1 clay mineral groups are also distinguished by differences in interlayer cations, and their hydration ability (Bergaya and Lagaly, 2013).

2.2.2.1 Smectite group

The smectite group is defined by a layer charge of 0.2-0.6 equivalents per half unit cell, and hydrated exchangeable interlayer cations (Bergaya and Lagaly, 2013). Emmerich et al. (2009) suggested five key features to describe a smectite mineral: (1) identification of the smectite structure, whether it is a dioctahedral or trioctahedral smectite; (2) layer charge; (3) the distribution of the charges in the octahedral and

tetrahedral sheets; (4) the distribution of the cations in the octahedral sheet; and (5) Fe content.

Within the smectite group, the most commonly occurring mineral is montmorillonite (Figure 2-4). It is defined as dioctahedral smectite with little or no tetrahedral charge. Most of the layer charge is generated by the cationic substitution of Mg^{2+} for Al^{3+} in the octahedral sheet.

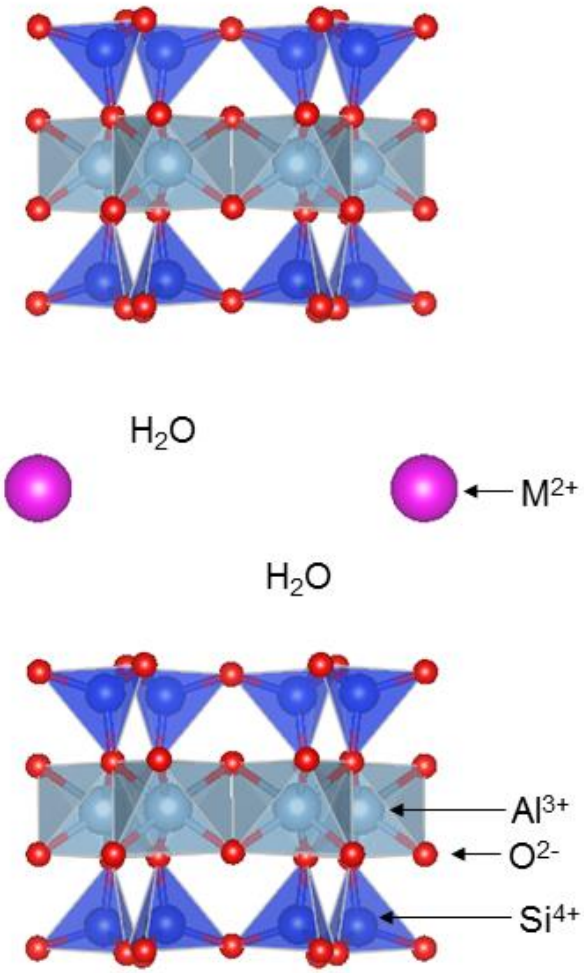

Figure 2-4: Atomic diagram of montmorillonite, showing two layers. M = metallic interlayer cation. Image generated in VESTA using structural parameters from Viani et al. (2002).

2.2.2.2 True mica group

The true mica group is defined by a layer charge of 0.6-1.0 equivalents per half unit cell and non-hydrated monovalent interlayer cations (Bergaya and Lagaly, 2013).

Within this group, the most commonly occurring minerals are illite (Figure 2-5) and muscovite. As a result of the non-hydrated nature of the interlayer cations, these clay minerals are non-swelling, in contrast to the smectite group. The main difference between illite and muscovite is that there is less substitution of Al^{3+} for Si^{4+} in the tetrahedral sheet of muscovite (Murray, 2006).

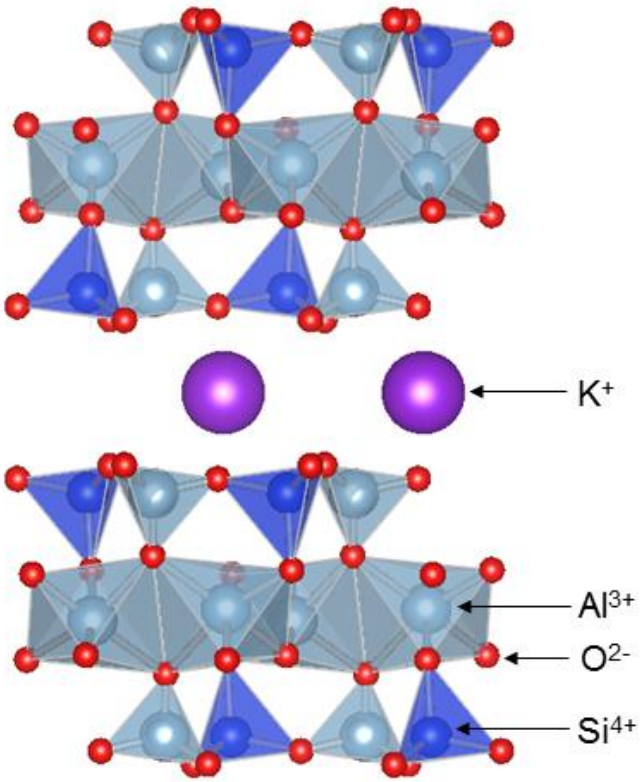

Figure 2-5: Atomic diagram of illite, showing two layers. Image generated in VESTA using structural parameters from Gualtieri (2000).

2.3 Fundamental aspects of alkali activation

The mechanisms of alkali activation are still not fully understood, although in recent decades there have been great advances in understanding complex reaction mechanisms. Fundamentals of alkali activation have been described and discussed in detail elsewhere (Duxson *et al.*, 2007a; Garcia-Lodeiro *et al.*, 2015; Provis, 2014; Provis *et al.*, 2015). Here, a short summary is presented for the alkali activation of clays, together with an overview of possible treatment processes and other factors affecting their activation (Figure 2-6).

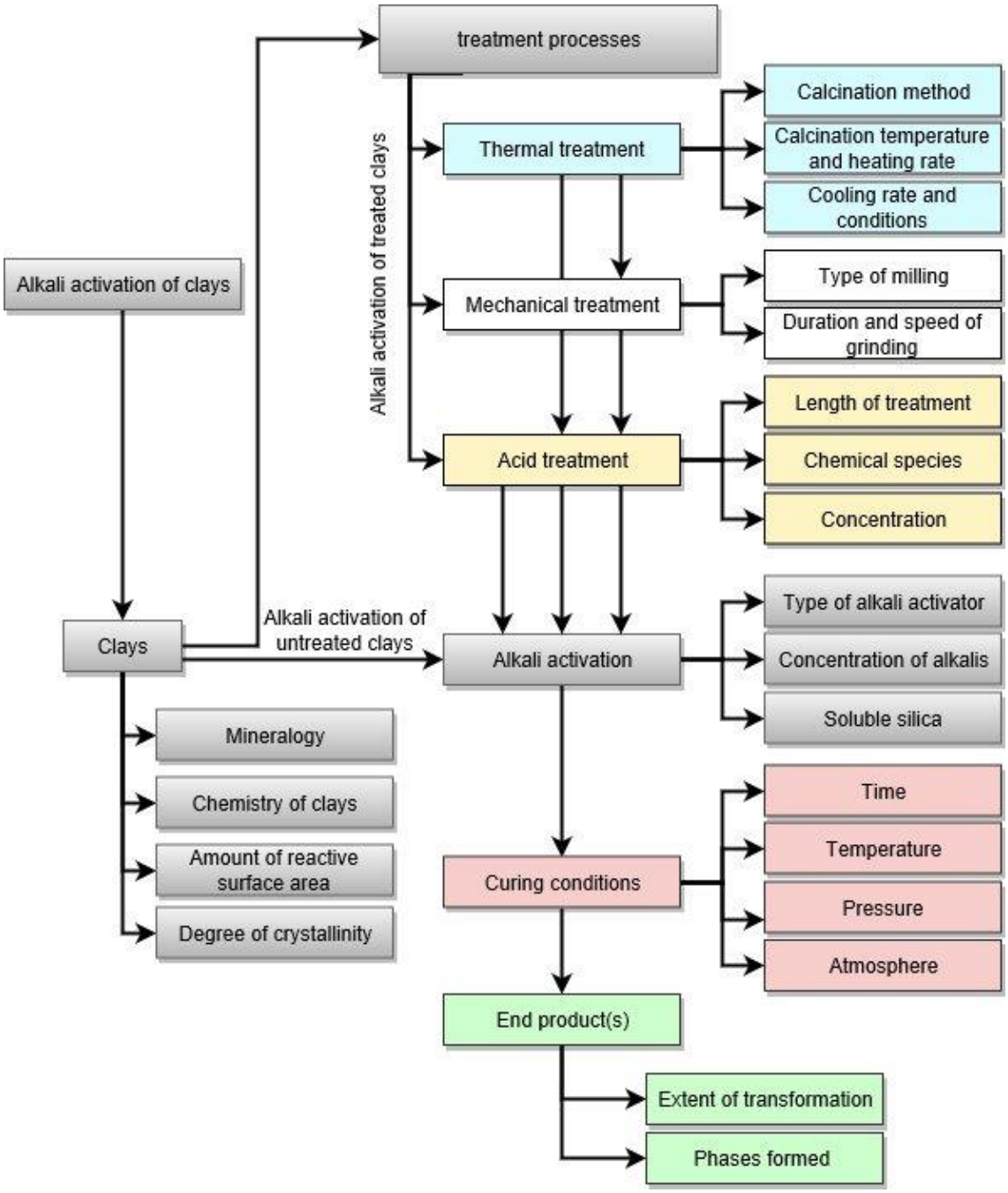

Figure 2-6: A summary of the factors that affect the alkali activation process of clays.

2.3.1 Reaction process

Dissolution of one or more aluminosilicate precursors in a highly concentrated alkaline solution is required to break the precursors down into aluminate and silicate monomers (Weng and Sagoe-Crentsil, 2007). These species then undergo a polycondensation process to form a geopolymer (Duxson *et al.*, 2007a) or a nucleation and growth process to form a crystalline zeolite phase (Cundy and Cox, 2005).

The dissolution behaviour of clay minerals is a well-studied area (Cama and Ganor, 2015). Much of previous research is limited to the range of pH 2-12 as the context is typically either natural rock-forming and pedogenic processes (Golubev *et al.*, 2006) or barrier linings in deep geological storage of radioactive waste (Metz *et al.*, 2005). In contrast, alkali activation typically requires alkaline solutions of [OH] ≥ 5 M at the minimum (Provis *et al.*, 2014b) corresponding to pH ≥ 14. For clays as precursors, an optimal range is 8 – 12 M (Diop and Grutzeck, 2008a; Heah *et al.*, 2013; Hounsi *et al.*, 2014; Lemougna *et al.*, 2014; Xu and Van Deventer, 2000). As a result, although useful insights can be obtained from existing studies, it is still somewhat unknown whether the dissolution mechanisms and behaviour are the same in highly concentrated solutions. The dissolution mechanisms for each clay mineral group are described in Section 2.4. Although there is recently growing attention paid to one-part geopolymers (water added to a dry mixture of aluminosilicate and alkali source) (Luukkonen *et al.*, 2018), the majority of studies reviewed here belong to the two-part process (aqueous activating solution added to a solid aluminosilicate), which is typically used.

2.3.2 Reaction products

Alkali aluminosilicate reaction products are classified as either crystalline zeolitic phases, or amorphous geopolymer phases. The exact nature of the low-Ca amorphous binder phases, known as geopolymers, is still a matter of debate, with previous suggestions made that they are in fact composed of nanocrystalline zeolites (Provis *et al.*, 2005), and others that they are a zeolitic precursor (Fernández-Jiménez *et al.*, 2006). A key difference between zeolites and geopolymers is that the former has fixed stoichiometric compositions (Abdullahi *et al.*, 2017), whereas the latter can have a continuous range of compositions due to the coexistence of a range of $Q_4(mAl)$ tetrahedra in the disordered gel (Duxson *et al.*, 2005b; Provis *et al.*, 2009). For geopolymers, the charge balancing required for the presence of Al atoms in the inorganic polymeric framework requires one alkali metal (M^+) cation for each Al atom (Barbosa *et al.*, 2000; Walkley *et al.*, 2018). Within the broad term of geopolymers, there are distinct phase categories, differing in structure and calcium composition. These are N-A-S-H, C-A-S-H and (N,C)-A-S-H (the following cement chemistry

notation is used to abbreviate chemical formulae: N = Na_2O; C = CaO; A = Al_2O_3; S = SiO_2; H = H_2O) (Garcia-Lodeiro *et al.*, 2015). Given the low calcium content of clays, N-A-S-H or (N,C)-A-S-H typically form, which have only small microstructural differences between them (García-Lodeiro *et al.*, 2010). Therefore, throughout the rest of this article, it is assumed that when the term geopolymer is used, it refers to a N-A-S-H or (N,C)-A-S-H phase.

2.3.3 Compositional variables

The element, quantity and concentration of alkaline metal cation in the activating solution is critical in determining both the type and the amount of product phases formed. Regarding zeolites, the stoichiometry of M, Al and Si depends on the exact species that has been formed. The composition of the aluminosilicate framework is $Al_xSi_{(2-x)}O_4$ (within the range of $0 \leq x \leq 2$), and includes sufficient framework cations M^+ required to balance the anionic charge in the framework arising from the inclusion of aluminium (Newsam, 1986). The metal cations used in the alkaline solution have a crucial effect on the dissolution behaviour and properties of the end material. NaOH and KOH are the compounds most commonly used (Provis, 2009a). Xu and van Deventer (2000) compared NaOH and KOH activators for a range of aluminosilicates. The extent of dissolution was higher in NaOH solutions, but samples activated with KOH solution had higher compressive strength. This was suggested to be due to the larger K^+ ions forming larger silicate oligomers, resulting in more cohesive geopolymeric setting behaviour, although more recently it has been shown that isolating the effects of alkali cation species is not straightforward (Duxson *et al.*, 2007b). There is a general tendency of NaOH to be more conducive to zeolite - rather than geopolymer - formation (Criado *et al.*, 2006), but other factors such as cost and viscosity also influence the choice of compound (Provis, 2009a). When Na_2SiO_3 solution is used, the speciation of the silicate oligomers can influence final properties (Provis, 2009a; Singh *et al.*, 2005), as well as setting time (Arnoult *et al.*, 2018).

The Si:Al molar ratio is also influential in determining the phases formed. This refers to mobile Si and Al ions that are in the solution and free to react. This may differ from the Si:Al ratio of the system as a whole, depending on the dissolution rates and mechanisms of the precursor phases. The implications of this for each clay mineral group are discussed individually in Section 2.4. When processing conditions conducive to geopolymer formation are used, geopolymers are typically formed for systems with Si:Al >1.5 (Duxson *et al.*, 2007b), with zeolite formation tending for systems with Si:Al <1.5. At intermediate ranges of Si:Al = 1-1.5, zeolites and geopolymers can be formed simultaneously (Buchwald *et al.*, 2011; Rahier *et al.*, 1997; Zibouche *et al.*, 2009).

As the silicon proportion of a geopolymer framework increases, the proportion of Al linkages in the chains decreases, which induces strengthening of the network (Fernández-Jiménez *et al.*, 2006). Geopolymers have been formed at Si:Al molar ratios of up to 600, although deformation behaviour was reported to become elastic at Si:Al > 48 (Fletcher *et al.*, 2005). In addition, a system containing too much silica may not fully react, resulting in lower strength beyond an optimal Si:Al ratio (Duxson *et al.*, 2005a). When processing conditions conducive to zeolite formation are used, the zeolite species formed depends on the Si:Al ratio used, with different groups tending to form either side of Si:Al = 5 (Abdullahi *et al.*, 2017; Johnson and Arshad, 2014). Higher Si:Al ratios also result in longer setting times (Silva *et al.*, 2007).

2.3.4 Processing variables

The optimal temperature and time of curing depends on the precursor used, as well as the activation conditions. Highly reactive precursors such as metakaolin can form a geopolymer at room temperature (Rahier *et al.*, 1996; Zhang *et al.*, 2012), but uncalcined kaolin reacts most successfully in the range of 60-100°C (Hounsi *et al.*, 2013). Curing temperature influences the rate of geopolymerisation (Mo *et al.*, 2014), and also affects mechanical properties by influencing pore volume and size distribution (Rovnaník, 2010). For some compositions, extended curing times can result in a secondary transformation from a geopolymer into a zeolite (Duxson *et al.*, 2007b). Pressure plays a role too by altering the solvent's dielectric constant and density, but the effects are specific to each system and also linked to temperature (Byrappa and Adschiri, 2007). Higher pressures can result in formation of finer zeolite particles (Tong *et al.*, 2014).

2.3.5 Thermal treatment to increase reactivity

Thermal treatment is the most common route to increase the reactivity of clay minerals. This involves heating the clay mineral to a specific temperature so that the octahedral layer undergoes dehydroxylation. This then results in a reduction in the bonding coordination number of the Al atoms, making them more reactive (Massiot *et al.*, 1995). The structural transformation upon thermal treatment depends on many factors associated with the treatment, including: heating rate, holding temperature and time, atmosphere (oxidizing or reducing) and cooling rate (Seiffarth *et al.*, 2013; Tchadjie and Ekolu, 2018). The transformation also depends on factors associated with the precursor, including: particle size (Dietel *et al.*, 2017; Heller-Kallai, 2013; Louati *et al.*, 2016), clay mineralogy (Buchwald *et al.*, 2009; Heller-Kallai, 2013; Hollanders *et al.*, 2016), degree of ordering (Hollanders *et al.*, 2016), as well as the amount and type of associated minerals present (Hollanders, 2017). It often seems to be an unstated

assumption in alkali activation studies that once a clay mineral has been dehydroxylated, it stays dehydroxylated. In fact, rehydroxylation is possible under certain conditions. This is discussed in Sections 2.4.1 and 2.4.2 for each clay mineral group.

One of the major effects of calcination is decreased specific surface area with increasing calcination temperature. This is due to the agglomeration of the clay particles at high temperatures, caused by dehydration and then dehydroxylation. For the same reason, the particle size distribution is coarser after calcination (Figure 2-7) (Fernandez *et al.*, 2011; He *et al.*, 1994; Seiffarth *et al.*, 2013).

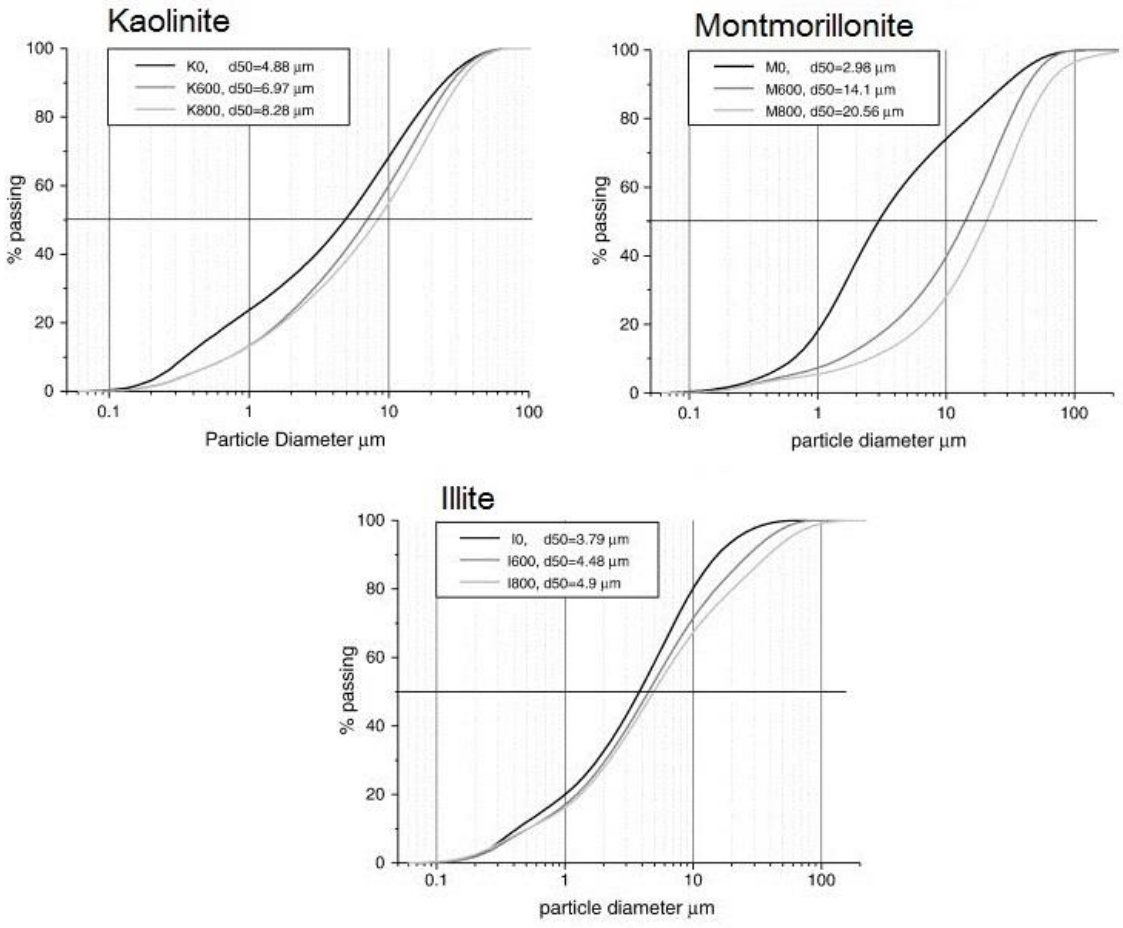

Figure 2-7: Particle size distribution of clay minerals (series 0) and their products calcined at 600°C (series 600) and 800°C (series 800), for a) Kaolinite, b) Montmorillonite, and c) Illite. Adapted from Fernandez et al. (2011).

2.3.6 Other treatments to increase reactivity

There are several other methods to increase the reactivity of aluminosilicates in clay minerals (Tchadjie and Ekolu, 2018). Mechanical treatment aims to have the combined effect of increasing disorder and amorphisation within the clay mineral structures, as well as reducing particle size to increase the specific surface area and therefore the reactivity (Hounsi *et al.*, 2013; MacKenzie *et al.*, 2007). Chemical treatment has also

been used. This includes both acid and alkali fusion treatment (MacKenzie *et al.*, 2007), sometimes used in combination with calcination (Belviso *et al.*, 2017).

2.4 Alkali activation of individual clay minerals

Alkali activation of the most common phyllosilicate clay minerals within the serpentine-kaolin, smectite, and true mica groups are reviewed in this section. Within these groups, the breadth of understanding is not even: some minerals have been the subject of numerous studies, whilst for others, no relevant studies have yet been done. For each clay mineral group, this section has been structured based on dissolution mechanisms, treatments used to increase reactivity, and phase formations.

2.4.1 1:1 clay minerals

2.4.1.1 Dissolution mechanisms

Dissolution behaviour of aluminosilicates can be categorised as either congruent - if the dissolution ratio of Si:Al in the alkaline solution is similar to the Si:Al ratio in the solid raw material, or incongruent - if the dissolution ratio of Si:Al is not similar to the Si:Al ratio of the solid raw material.

Dissolution has been shown to be approximately congruent for a range of aluminosilicate minerals, including phyllosilicates (Xu and Van Deventer, 2000). However, it is also argued that dissolution is congruent for kaolinite, but incongruent for smectite-rich clays (Aldabsheh *et al.*, 2015). There are competing theories to describe the kinetics involved (Cama and Ganor, 2015), but it is widely agreed that the dissolution rate of kaolinite as a whole is controlled by the dissolution of the layer edges (Bauer and Berger, 1998; Huertas *et al.*, 1999; Liew *et al.*, 2016), and it is highly dependent on pH above pH 10 (Huertas *et al.*, 1999).

2.4.1.2 Thermal treatment

Among all the clay minerals, kaolinite is the most used clay mineral for alkali activation. Many studies have tested different calcination temperatures and concluded that the complete dehydroxylation of kaolinite occurs in the temperature range of 650-700°C (Hollanders *et al.*, 2016; Ilić *et al.*, 2010; Tironi *et al.*, 2013). As a result of the dehydroxylation, the coordination of Al atoms in the octahedral sheet is reduced (Massiot *et al.*, 1995), delamination of the layers occurs, and available surface area decreases (He *et al.*, 1994). The dehydroxylated form is known as metakaolin - this is more reactive in geopolymerization than kaolinite as a result of undergoing these changes.

Metakaolin can be partially re-hydroxylated, but this has required conditions of heating at 250°C for 6 days in an excess of water (Rocha and Klinowski, 1991). When the re-hydroxylated metakaolin was then re-de-hydroxylated, the resulting metakaolin was found to be even more disordered than after the first dehydroxylation (Rocha and Klinowski, 1991).

2.4.1.3 Phase formation behaviour

Activation of kaolinite without additional silica tends to form hydrosodalite using hydrothermal synthesis (Barrer *et al.*, 1968; Engelhardt *et al.*, 1992; Heller-Kallai and Lapides, 2007) as well as in lower liquid:solid conditions (Marsh *et al.*, 2018b). Metakaolin, formed by thermal activation of kaolinite, can form zeolitic phases including hydrosodalite, Zeolites A and X (Barrer and Mainwaring, 1972; Heller-Kallai and Lapides, 2007), or a geopolymer phase (Zhang *et al.*, 2012), depending on the processing conditions.

With the addition of soluble silica, both kaolinite (Heah *et al.*, 2012; Hounsi *et al.*, 2013) and metakaolin (Lapides and Heller-Kallai, 2007; Rahier *et al.*, 1996; Zhang *et al.*, 2013) tend towards forming geopolymers. However, if the additional silicate makes the system Si:Al = ~1.5, geopolymers and zeolites can co-form (Rahier *et al.*, 1997).

Although Si:Al molar ratio is important, phase formation does not simply depend on this alone. Curing temperature and duration are highly influential, and these variables cause different behaviours in systems with the same Si:Al molar ratio. In recent reviews of hydrothermal synthesis of zeolites from metakaolin, it is concluded that: for systems with Si:Al ≤ 5, products can be SAPOs, X zeolites, hydrosodalite or other LTA zeolites; for systems with Si:Al ≥ 5, products can be zeolite β, zeolite Y, ZSM-5, ZDM-11 (Abdullahi *et al.*, 2017; Johnson and Arshad, 2014). In several of these systems, the overall Si:Al molar ratio was conducive to geopolymer formation but a range of zeolites were formed instead, due to the curing conditions. The optimum conditions for zeolite synthesis are given as 70-200°C for 16-120 h (Abdullahi *et al.*, 2017; Johnson and Arshad, 2014). These involve higher temperatures and longer periods than those typically used for synthesis of geopolymers. The metastable nature of geopolymers means that they can continue transforming into more stable zeolitic phases when cured at higher temperatures and/or longer periods than their optimal range (Johnson and Arshad, 2014). This was observed for the silica-doped metakaolin systems of Lapides and Heller-Kallai (2007), where further curing at 72 h and beyond transformed the geopolymers into zeolites. This is supported by the findings of Zhang et al. (2012), that crystalline phases form preferentially over geopolymers in systems with higher curing temperatures.

The concentration of the activating solution also has an influence. Johnson and Arshad (2014) and Wang et al. (2017b), recommend an NaOH concentration of <3 M for tailored zeolite synthesis, as higher concentrations decrease the relative crystallinity. This zeolite perspective agrees with studies optimising for the production of geopolymers, as these typically use an NaOH concentration of >5 M (Provis *et al.*, 2014b), with an optimal range for clays of 8 – 12 M (Diop and Grutzeck, 2008a; Heah *et al.*, 2013; Hounsi *et al.*, 2014; Lemougna *et al.*, 2014; Xu and Van Deventer, 2000). In summary, even for relatively simple and well-understood minerals such as kaolinite and metakaolin, there can be a significant variety in product phases formed depending on the variables of additional soluble silica added and curing regime.

Halloysite is much less studied than kaolinite, due to its comparative rarity. Activation of uncalcined halloysite with NaOH solution was shown to result in some structural changes but no product phase (Wang *et al.*, 2013), although this was likely due to the short synthesis time used of 1 h at 50°C. The use of treatments has been more successful - calcination between 550 and 800°C, followed by activation with a combined NaOH and Na_2SiO_3 solution, has succeeded in forming a geopolymer (MacKenzie *et al.*, 2007).

Regarding the synthesis methods used for the 1:1 clay minerals, syntheses optimising for zeolite production mostly use hydrothermal synthesis, which is rarely used in geopolymer syntheses. There are two reasons for this. Firstly, considering reaction conditions, the effects of processing variables in hydrothermal synthesis are still not fully understood and it is not generally considered as an appropriate method for making amorphous phases such as geopolymers. Secondly, considering scalable processing, hydrothermal synthesis is appropriate for high purity reactions in small quantities (Byrappa and Adschiri, 2007), but is less appropriate for the manufacture of construction materials in bulk. This principle also applies to the other clay minerals and clay-containing feedstocks.

2.4.2 2:1 clay minerals

2.4.2.1 Dissolution mechanisms

Similar to the 1:1 clay minerals, dissolution of 2:1 clay minerals as a whole is limited by the dissolution rate of the crystal edges (Bauer and Berger, 1998; Köhler *et al.*, 2003; Yokoyama *et al.*, 2005). For this reason, dissolution rate is dependent on the edge surface area available rather than the total surface area (Yokoyama *et al.*, 2005), in addition to the concentration of the alkali activator(s) (Aldabsheh *et al.*, 2015).

2.4.2.2 Thermal treatment

In contrast to the 1:1 clay minerals described previously, the thermal and chemical stability of 2:1 clay minerals is more variable due to the greater variety in composition and structure. In montmorillonite, thermal and chemical stability is affected by: the distribution of the octahedral cations over cis- and trans- sites; the type of interlayer cations, and the Fe content (Emmerich *et al.*, 1999; Emmerich *et al.*, 2009). However, the principles are the same, in that reactivity is increased by the changes in Al coordination and other structural features that occur during the dehydroxylation process. Here it is useful to emphasise the distinction between dehydroxylation and amorphisation: dehydroxylation is the loss of hydroxyl groups from the octahedral layer, whereas amorphisation is the increase in disorder of the layer structure so it is no longer crystalline. Amorphisation is desirable for increasing precursor reactivity; dehydroxylation can also result in amorphisation in some systems, but this is not a direct correlation between the two.

Cis- and trans- sites describe different types of atomic position in the octahedral sheet (Figure 2-8). In the cis-sites, OH^- groups are located on a shared edge of a triangular face on either the right or left side of the octahedron. In the trans-sites, OH^- groups are located on the top and bottom vertices of the octahedron. In the half-unit cell of a dioctahedral clay mineral, there are two cis-sites and one trans-site, of which only two are occupied. This gives the possibility of different structures depending on which sites are occupied (Figure 2-9). If a sheet is cis-vacant (cv), one trans-site and one cis-site are occupied. If a sheet is trans-vacant (tv), both cis-sites are occupied (Brigatti *et al.*, 2013). These can also be defined by planes of symmetry (Meunier, 2005). Most montmorillonites consist of cv 2:1 layers and most illites consist of tv 2:1 layers, although the reverse can also be true (Drits *et al.*, 1995; Tsipursky and Drits, 1984).

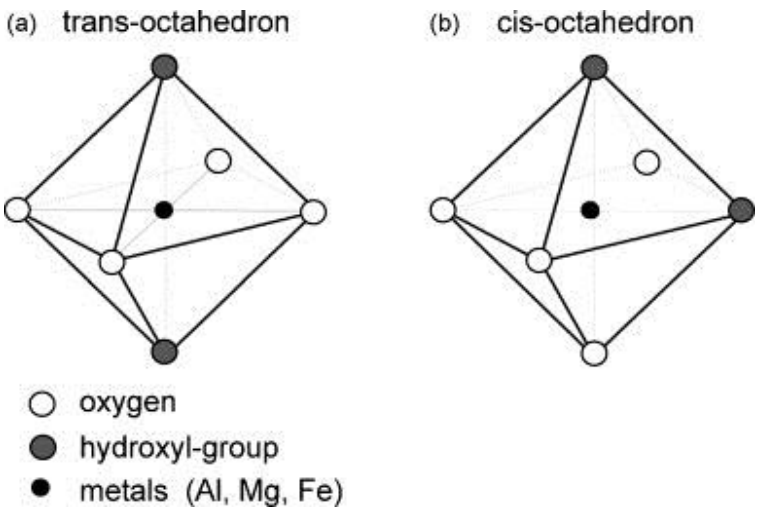

Figure 2-8: Atomic diagrams of a) trans- and b) cis- configurations of octahedral sites, defined by the positions of the octahedral anion - usually a hydroxyl group (Wolters and Emmerich, 2007).

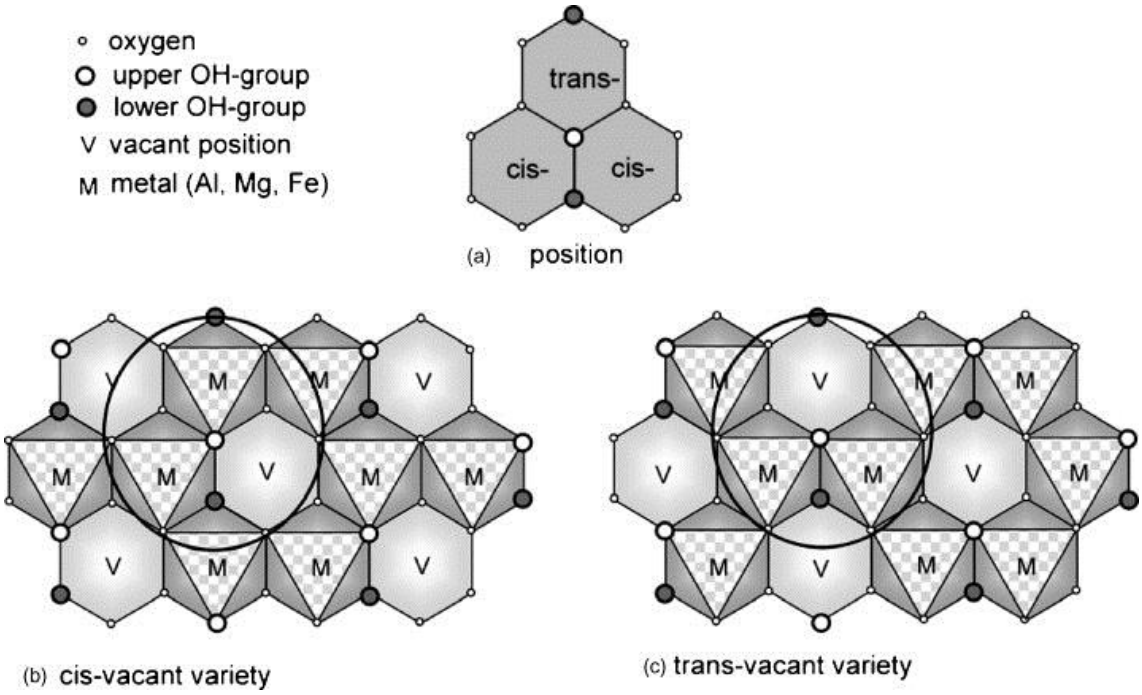

Figure 2-9: Overhead diagrams of a) trans- and cis- configurations of octahedral sites; b) a cis-vacant sheet, in which both trans- sites are occupied; c) a trans-vacant sheet, in which both cis-sites are occupied (Wolters and Emmerich, 2007).

During dehydroxylation, the structural changes are different between the two sheet structures. A common feature is the reaction of two hydroxyl groups to form a water molecule (which evolves) and a residual oxygen, resulting in either a reduction or distortion of octahedral coordination. However, the behaviour of the octahedral cations themselves differs. In a cv smectite, the Al^{3+} ions move from the trans-sites to the cis-sites, which requires additional thermal energy (Heller-Kallai and Rozenson, 1980), and the octahedra transform to a range of coordination states (Muller, 2000). In a tv smectite, no Al^{3+} migration occurs, and octahedra transform to five-coordination (Muller, 2000). The results of these two dehydroxylation pathways is that regardless of

the initial sheet structure, the dehydroxylated structures of dioctahedral 2:1 layer silicates always have tv octahedral sheets (Muller, 2000). This difference in structural change is reflected in dehydroxylation temperature ranges: most cv 2:1 clay minerals dehydroxylate at >600°C, whereas tv clay minerals dehydroxylate at <600°C (Emmerich *et al.*, 2009; Wolters and Emmerich, 2007). This temperature difference is usually large - the dehydroxylation temperature of a clay mineral with a cv sheet structure is typically higher by 150°C to 200°C than the same mineral with a tv sheet structure (Drits *et al.*, 1995). This is due to the shorter bond length of the OH-OH edges in tv sheets compared to cv sheets, since less energy is required for the hydrogen to jump to the closest OH group and form a water molecule (Drits *et al.*, 1995).

As well as the influence of the sheet structures, the dehydroxylation temperature of 2:1 clay minerals is dependent on the valency and ionic radius of the interlayer cations (Derkowski and Kuligiewicz, 2017; Drits *et al.*, 1995; Emmerich *et al.*, 1999; Fernandez *et al.*, 2011; Garg and Skibsted, 2014; He *et al.*, 1994; Hollanders *et al.*, 2016; Tironi *et al.*, 2013). Regarding valency, divalent exchangeable cations (e.g. Ca^{2+}) in clay minerals bind more water, and bind more tightly, to the clay surface than the monovalent exchangeable cations (e.g. Na^{+}) in ambient temperature – therefore, higher dehydroxylation temperatures are needed to remove the additional water for divalent compared to monovalent interlayer cations (He *et al.*, 1994). Regarding ionic radius, dehydroxylation temperature increases for interlayer cations with larger ionic radius. Emmerich et al. (1999) studied the behaviour of homoionic cv montmorillonites and found that the dehydroxylation temperature increased between 625-685°C in the following order: $Li^{+} < Cu^{2+} < Zn^{2+} < Ca^{2+} < Na^{+} < Sr^{2+}$.

Similarly to the dehydroxylation of kaolinite, the dehydroxylation of 2:1 clay minerals can also be seen in powder X-ray diffraction (XRD). He et al. (1994) and Hollanders et al. (2016) claimed that at around 700°C the 001 reflection will be weakened but not fully collapsed due to the non-complete dehydroxylation of the clays. At 800°C and above, the reflection will have fully collapsed and the background of the XRD pattern increased, which indicates complete dehydroxylation (Figure 2-10). Higher temperatures than the optimum calcination temperature causes formation of new phases. In montmorillonite, Garg and Skibsted (2014) showed that above 1000°C, the SiO_4 tetrahedra across the collapsed interlayer space in the dehydroxylated structure recrystallize and form cristobalite, cordierite and anorthite. In a pure smectite clay, at 900°C, magnesium aluminium silicate ($MgAl_2Si_4O_{12}$) was formed (Figure 2-10) (Hollanders *et al.*, 2016). The side-effect of new phase formation is a decrease in the amount of reactive material in the clay, as shown by decreasing background intensity in an XRD pattern.

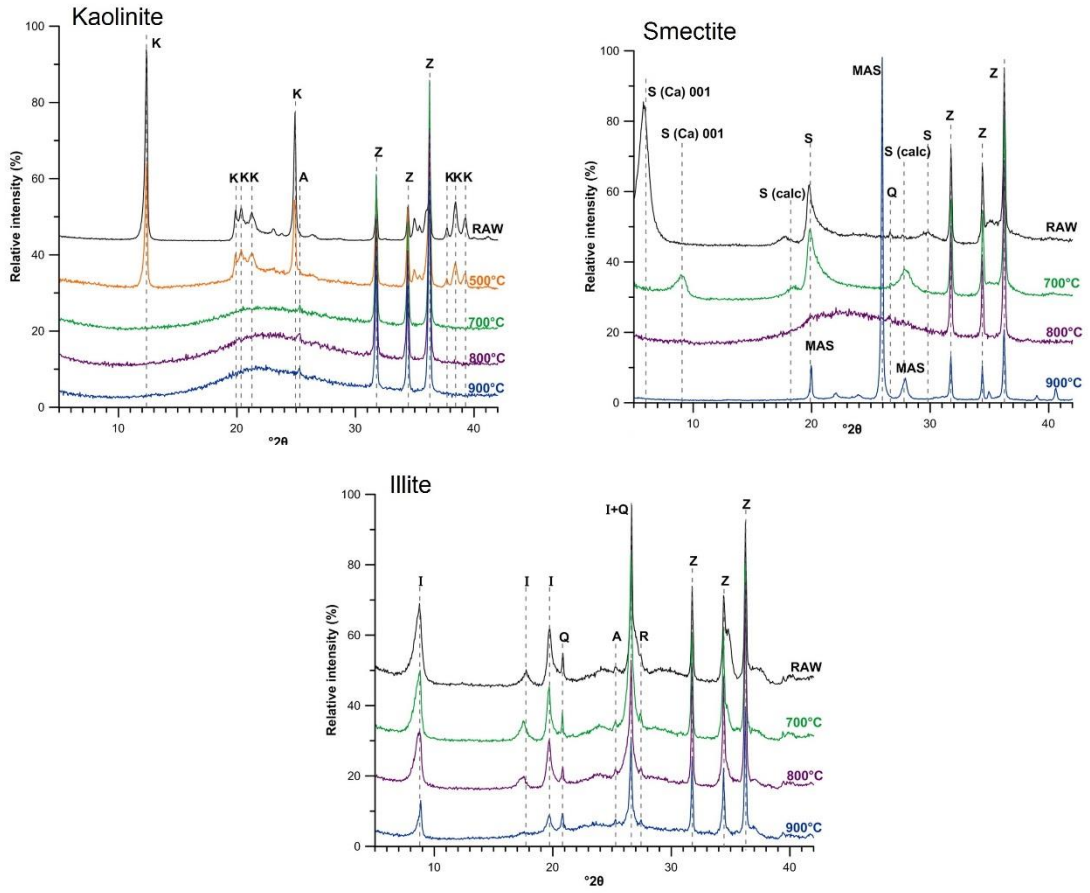

Figure 2-10: XRD patterns of untreated clays (RAW) and after calcination at various temperatures, for a) Kaolinite, b) Smectite, and c) Illite. The identified minerals are: K: kaolinite, H: halloysite, S: smectite (with Ca or Na), He: hectorite, Q: quartz, A: anatase R: rutile and Z: zincite (internal standard), MAS: magnesium aluminum silicate. Adapted from Hollanders et al. (2016).

Unlike kaolinite, dioctahedral 2:1 clays retain their layer structure after dehydroxylation (Heller-Kallai, 2013). The Al coordination changes are reversible as they can undergo varying degrees of rehydroxylation, including under ambient conditions. Rehydroxylation can happen because the clay structure is under stress by lattice distortions and by the cations in the hexagonal holes (Emmerich, 2000; Muller, 2000). Other studies showed that dehydroxylated montmorillonite regains many of the hydroxyl groups by treatment under steam between 200-300°C. The rehydroxylation of the 2:1 clay minerals affects the reactivity of these clays under chemical activation. More details on the structural transformation of 2:1 dioctahedral layer silicates during dehydroxylation-rehydroxylation reactions can be found in Muller et al. (2000).

2.4.2.3 Chemical treatment

Acid treatment can also be used to increase reactivity. This process has been investigated more extensively for smectites, which causes dehydroxylation and dissolution of the octahedral sheet, and turns the tetrahedral sheet into a "*three-dimensional framework of protonated amorphous silica*" (pg.129, Komadel, 2003). This

can eventually transform the smectite into a "*hydrous amorphous silica phase*" (pg.1405, Madejová *et al.*, 1998). The extent of this process depends on: the composition of the octahedral sheet; the strength of the acid treatment, and the length of time. This increases reactivity by increasing the surface area, making the structure more disordered, and also increases the clay's Si:Al ratio by dissolution of octahedral Al (Komadel and Madejová, 2013).

The extent of this process depends on the treatment conditions used and the composition of the clay mineral. Montmorillonite can be almost fully amorphised given a treatment of sufficient concentration and time (Figure 2-11) (Steudel *et al.*, 2009b). Belviso et al. (2017) found that a 5 M HCl treatment resulted in a greater extent of amorphisation for Ca- than Na-montmorillonite. The authors attributed this to a higher dissolution rate of the Ca-montmorillonite, due to a higher proportion of Mg and/or Fe substitutions in the octahedral layer (Madejová *et al.*, 1998). Behaviour is similar for illite, with degree of amorphisation dependent on concentration and length of treatment, and near complete amorphisation achievable (Figure 2-11) (Steudel *et al.*, 2009a).

Acid treatment behaviour has different mechanisms in smectite and mica group clay minerals. Attack of the octahedral sheet occurs via layer edges for both groups, whereas in swelling clays attack can occur via the interlayer faces too (Steudel *et al.*, 2009a, b). Since interlayer faces are accessible to protons in swelling layers, this increases the rate of dissolution (Komadel *et al.*, 1996). As a result, acid dissolution is slower for the mica group (Steudel *et al.*, 2009a).

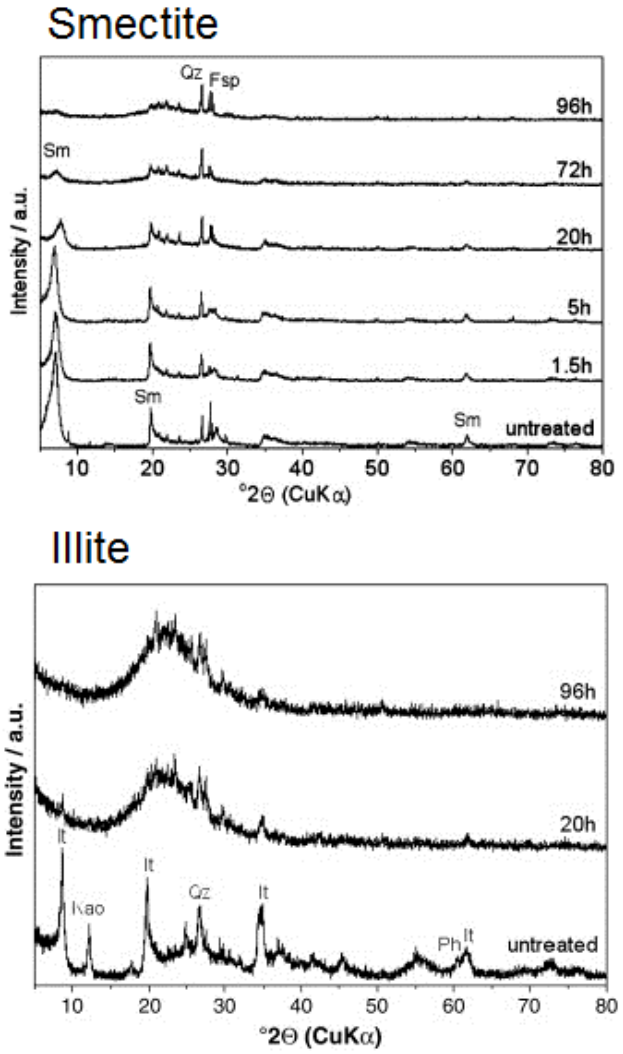

Figure 2-11 XRD patterns showing amorphisation of a) smectite, and b) illite after acid-washing in 5 M H_2SO_4 at 80°C for up to 96 h. Adapted from Steudel et al. (2009a, b).

2.4.2.4 Phase formation behaviour in smectite group

There are few studies on the alkali activation of montmorillonite. This preference may partly be due to the known difficulties of using montmorillonite-based materials for construction, given its expansive behaviour. It also has a more variable composition compared to kaolinite, particularly with regard to octahedral and interlayer cation substitutions, as described in Section 2.2.2.

Early studies investigated uncalcined montmorillonite, but not with the intention of geopolymer formation as more recent studies have. Ingles et al. (1970) activated an uncalcined montmorillonite without additional silica using a range of activators. Using NaOH and KOH, no aluminosilicate product phase was formed, and much of the activator was not consumed, possibly due to the low curing temperature of 25°C. Richardson et al. (1986) activated a similar system, but using higher temperature curing. For oven curing, this resulted in a decrease in montmorillonite XRD reflection

intensity, and for microwave curing, partial dehydration of the montmorillonite. No product phases were reported from XRD characterisation, but geopolymer formation cannot be excluded as no consideration of the formation of amorphous phases was made. Belviso et al. (2017) activated a calcined montmorillonite which did not undergo a phase transformation. Marsh et al. (2018a) activated both an acid-washed K10 Montmorillonite and an untreated Bentonite with NaOH solution, forming a geopolymer when the system molar ratio of Na:Al ≥ 1.

When thermal treatment is used, phase formation behaviour is more dependent on the relative amounts of Al and Si present in the system that are soluble under the given activation conditions. Belviso et al. (2017), reported probable geopolymer formation by 1 M NaOH hydrothermal alkali activation of Na- and Ca-montmorillonites which were acid washed (80°C for 48 h in 5 M HCl) and then calcined at 700°C. However, when samples were calcined without a preceding acid treatment, no changes were reported. This difference is likely due to the partial amorphisation and dissolution of the octahedral sheet observed from the acid treatment, and the relatively low NaOH concentration used in synthesis.

When additional soluble silica is added, a geopolymer is formed. Prud'homme et al. (2011) activated an uncalcined montmorillonite with KOH and K-silicate solution, and the later addition of silica fume as a foaming agent. Characterisation results and visible strengthening suggested that the montmorillonite contributed to the formation of a geopolymer, as the montmorillonite's structure was destroyed during activation. Seiffarth et al. (2013) reported a geopolymer was formed from a silica-doped smectite clay calcined at various temperatures from 550–950°C. In this study, explicit evidence for geopolymer formation from phase characterisation was not given, but rather inferred from increased strength of the alkali-activated samples. When Belviso et al. (2017) used an additional NaOH fusion step at 700°C, zeolites were much more readily formed.

No studies were found on the alkali activation of other members of the smectite group. In summary, montmorillonite can be used to form a geopolymer in its uncalcined form, if the activating solution and curing conditions are sufficient. The same is also true for its calcined form, although zeolites can also be formed, depending on the activating solution and processing conditions.

2.4.2.5 Phase formation behaviour in true mica group

As for montmorillonite, few studies have been performed on the alkali activation of illite, and most of these have used thermal treatment.

For un-calcined illites, reaction products are not generally formed, but there are exceptions. Richardson et al. (1986) activated an uncalcined illite with NaOH solution. No reaction products were formed for oven heating, but nepheline was formed when microwave heating was used. Sedmale et al. (2013) mixed illite-rich clay with KOH solution, which underwent only small changes in strength. It is likely that no geopolymer was formed, and this could have partly been due to the very short curing time used. Marsh et al. (2018a) activated an illite with NaOH without treatment. No product phase was formed, but the illite underwent a kind of structural breakdown. In contrast, Prud'homme et al. (2011) activated an uncalcined illite with KOH and K-silicate solution, and the addition of silica fume as a foaming agent. After a full set of characterizations, they concluded that the illite partially dissolved and contributed to the formation of a geopolymer.

When calcination is used, the results are not always in agreement. Belviso et al. (2017) showed that an illite calcined at 700°C underwent no obvious changes by 1 M NaOH hydrothermal alkali activation, with the addition of a preceding acid treatment making no difference. In contrast, Sperberga et al. (2011) mixed a calcined (700–900°C) illite with KOH solution, and a geopolymer was believed to be formed.

When additional soluble silica is added in addition to a thermal treatment, a geopolymer is possibly formed. Seiffarth et al. (2013) thermally treated illite clay between 550–950°C, and activated it with additional silica. Geopolymerisation was inferred from increased strength, but without proof provided by phase characterisation. When Belviso et al. (2017) used an additional NaOH fusion step, a sodalite was formed, and a variety of other sodalites were formed using various combinations of treatment processes.

The inference of a geopolymer phase through increased strength after activation is simple but has drawbacks, as will be discussed in Section 2.5.5. However, in the case of illite as the dominant clay phase, no formation of zeolitic phases has been reported for the conditions typically used for geopolymer synthesis, so could be a reasonable assumption in this instance.

In summary, the alkali activation behaviour of illite does not seem to be consistent between studies. In its uncalcined form, geopolymers have been formed under some

conditions but not others. If illite is calcined, geopolymer formation is also possible, but from the evaluation of these studies, it does not seem to be a reliable reaction.

2.4.3 Comparison of individual clay studies

In terms of having the potential to form a geopolymer, the evidence suggests that any of the clay minerals considered here can be transformed into a geopolymer. Comparing clay minerals and the different treatments used (Table 2-1), the different clay minerals require different extents of treatments to become reactive enough, and to get a suitable Si:Al molar ratio, to make this happen.

The most obvious comparison is the difference between the 1:1 and 2:1 clay minerals. One expects different phase formation behaviour between them, due to a large difference in Si:Al molar ratio. It seems that it is more reliable to form a geopolymer from kaolinite, but only given the use of additional soluble silicate. In contrast, it is possible to form a geopolymer from the 2:1 clay minerals without additional soluble silicate, but the reaction is less reliable. Within 1:1 clay minerals, despite the dearth of studies on halloysite, it is tentatively suggested that halloysite is less prone to form a geopolymer than kaolinite. Within 2:1 clay minerals, geopolymers are formed more readily from montmorillonite than illite. Given their similarity in layer chemistry, this could be partly attributed to smectites' swelling behaviour giving a higher specific surface area for reaction in a wet mix, as has been shown for acidic dissolution (Komadel *et al.*, 1996).

The majority of studies use calcined clays in alkali activation. It is likely that calcined clays will be more highly used than uncalcined clays in future products due to their amorphous structure and high reactivity towards alkali activation. However, it is still necessary to study the alkali activation of uncalcined clays. Firstly, from a perspective of understanding the fundamentals of their behaviour, and secondly, for investigating the feasibility of uncalcined clay products for applications where comparable performance to Portland cement based materials is less critical.

From the comparison of studies by clay mineral and treatments used (Table 2-1), the most reliable route to forming a geopolymer for all of the clay minerals considered is calcination followed by activation with additional soluble silica. Whilst acid washing and NaOH fusion do seem to increase reactivity, they do not necessarily make it more likely to form a geopolymer rather than a zeolite. This conclusion supports previous recommendations for alkali-activated materials in general, that lower impact routes of soluble silicate production is a research priority (Provis, 2018a, 2018b; Scrivener *et al.*, 2016). Other potentially energy-saving measures such as flash-calcination (Salvador, 1995) should also be investigated further.

Table 2-1: Summary of reaction products for alkali activation of individual clays in the studies reviewed, showing effects of different treatments and system additions. The default activation process in this context is with NaOH only.

		1:1 clay minerals		2:1 clay minerals	
Treatment	**System additions**	**Kaolinite**	**Halloysite**	**Montmorillonite**	**Illite**
None	None	Hydrosodalite (Barrer *et al.*, 1968; Engelhardt *et al.*, 1992; Heller-Kallai and Lapides, 2007; Marsh *et al.*, 2018b)	None (Wang *et al.*, 2013)	None (Ingles, 1970; Richardson *et al.*, 1986) Geopolymer (Marsh *et al.*, 2018a)	None (Marsh *et al.*, 2018a; Richardson *et al.*, 1986; Sedmale *et al.*, 2013)
None	Soluble silicate	Geopolymer (Heah *et al.*, 2012, 2013; Hounsi *et al.*, 2014; Hounsi *et al.*, 2013; Prud'homme *et al.*, 2011)	---	Geopolymer (Prud'homme et al., 2011)	Geopolymer (Prud'homme et al., 2011)
Acid wash	None	---	---	None (Belviso *et al.*, 2017) Geopolymer (Marsh *et al.*, 2018a)	---
Calcination	None	Hydrosodalite (Barrer and Mainwaring, 1972) Various zeolites (Barrer and Mainwaring, 1972; Heller-Kallai and Lapides, 2007; Zhang *et al.*, 2012) Geopolymer + hydrosodalite (Zhang *et al.*, 2012)	---	None (Belviso *et al.*, 2017)	None (Belviso *et al.*, 2017) Possible geopolymer (Sperberga *et al.*, 2011)
Acid wash + calcination	None	---	---	Geopolymer (Belviso *et al.*, 2017)	None (Belviso *et al.*, 2017)
Calcination + NaOH fusion	None	---	---	Various zeolites (Belviso *et al.*, 2017)	Sodalite (Belviso *et al.*, 2017)
Calcination	Soluble silicate	Geopolymer (Lapides and Heller-Kallai, 2007; Rahier *et al.*, 1996; Zhang *et al.*, 2013) Geopolymer + hydrosodalite (Rahier *et al.*, 1997)	Geopolymer (MacKenzie *et al.*, 2007)	Possible geopolymer (Seiffarth *et al.*, 2013)	Possible geopolymer (Seiffarth *et al.*, 2013)

2.5 Alkali activation of common clays and soils

2.5.1 Nature and composition of common clays and soils

In line with the purpose of this review, the focus of this section will be on the alkaline activation behaviour of the clay minerals within common clays and soils. As previously stated, common clay deposits and soils are an abundant source of clay minerals. These are more scalable compared to the high purity deposits and refined products currently used - but also more complex and variable. Using kaolinite for example, primary residual deposits are the most common type, but are generally small and contain limited quantities of reserves (Murray and Keller, 1993). Thus, there is a need for research on a wider range of deposits than the small number of large deposits currently exploited in other industries. This argument extends to the other clay minerals as well as soils.

Understanding the influence of mineralogical aspects is key to unlocking their potential as scalable precursors. Given the scope of this review, the majority of attention is paid to clay mineral factors with only brief consideration given to the role of associated minerals and organic content.

Very small amounts of certain clay minerals may exert a large influence on the physical properties of a common clay or soil. The degree of crystallinity is important for some industrial applications, especially paper coatings (Murray and Lyons, 1956). Crystallinity is of particular importance here, since, as discussed in Section 2.3, clay minerals with poorer crystallinity are generally thought to be more reactive.

The clay minerals and other components can vary greatly within common clays and soils in different locations. Soils around the world contain clay minerals in different amounts (Abe *et al.*, 2006; Nickovic *et al.*, 2012), depending on climate, lithology and weathering history (Christidis, 2011). In addition, the distribution of clay minerals in soil in a single location can vary with depth (Claret *et al.*, 2002; Dixon and Weed, 1989), due to varying extents of weathering (Meunier, 2005). Further information on pedogenic processes, the occurrence of clay minerals in soils and their mineralogical and physical properties are given elsewhere (Huang *et al.*, 2011; Meunier, 2005).

In addition to differences in the amounts present, there can be large differences in the nature of the clay minerals in different locations, including substitutions and crystallinity (Meunier, 2005). For example, the kaolinite from a mixed hydrothermal and residual kaolin deposit in Cornwall, U.K. is well crystallised, whereas kaolinite from a sedimentary deposit in Georgia, U.S.A. varies between extremely well crystallised and

poorly crystallised (Murray and Keller, 1993; Murray and Lyons, 1956). Other clay minerals can also vary in crystallinity depending on their formation and weathering history - for example, smectite in vertisol soils from undergoing wetting-drying cycles (Meunier, 2005). Decreased stacking order and degree of crystallinity could contribute to the reactivity of clays, even without explicit treatment to increase disorder. This is relevant to the different formation routes of clays, suggesting that some deposits may require less treatment, as their geological history has made them more reactive (Prud'homme *et al.*, 2011).

2.5.2 Overview of types of systems

Because common clays and soils frequently contain more than one clay mineral, this section also reviews studies on synthetic mixtures of the individual clays. This is helpful to understand the interactions between different clay minerals in more complex systems such as soils. Many studies have mixed an additional reactive aluminosilicate (e.g. fly ash, refined metakaolin) with a soil before activation. Although potentially beneficial in terms of properties achieved, these systems are not as useful for understanding the behaviour of clay minerals and associated minerals in common clays and soils. In these systems, it is often unclear whether the soil is simply acting as an aggregate, or whether its components are actively contributing to the alkali activation process and phase formation. For this reason, these systems have not been reviewed here, and so only a small number of studies in this field meet the scope of this review. In the following sections, studies are grouped by the dominant clay in each soil.

2.5.3 Common clays and soils containing a single dominant clay mineral

Kaolinite-dominant soils are the most studied ones, for the same reason described for individual clays. In an early study, Boutterin and Davidovits (1988) activated a kaolinitic soil with NaOH, giving increased compressive strength. The authors attributed this to a zeolitic product, but no characterisation was given. Lateritic soils containing kaolinite as the sole clay mineral are a popular feedstock. Lemougna et al. (2014) and Diop and Grutzeck (2008a) activated uncalcined kaolinitic lateritic soils with NaOH, forming a hydrosodalite as the product phase. Lemougna et al. (2014) suggested a geopolymer phase may also have formed, but the characterisation evidence presented was not conclusive. In a very similar study, Yousef et al. (2012) identified the reaction product to be plagioclase feldspar and a geopolymer, but given the system, it is thought far more likely to be a hydrosodalite too. Lassinantti Gualtieri et al. (2015) also studied a kaolinitic lateritic soil. Activation with NaOH and Na_2SiO_3 apparently had no effect on

the uncalcined soil, but a geopolymer formed as the main reaction product for the calcined soil. Muñoz et al. (2015) studied a synthetic montmorillonite-dominated soil, using clay and mining waste. Activation of the uncalcined soil with NaOH and Na-silicate seemed to form a geopolymer, although the relatively modest gains in strength suggest that much of the montmorillonite remained undissolved, albeit exfoliated. Notably, the use of mineral additives seemed to encourage geopolymerisation.

In summary, in feedstocks containing a single dominant clay mineral, phase formation behaviour is generally in line with that expected from alkali activation of individual clay minerals. However, the majority of studies are on kaolinitic feedstocks.

2.5.4 Common clays and soils containing multiple clay minerals

For studies on feedstocks containing multiple clay minerals, those containing two clay minerals will be reviewed first, followed by those containing three.

Amongst feedstocks containing two clay minerals, kaolinite-illite is the most common clay combination. El Hafid and Hajjaji (2015) calcined an illite-kaolinite clay sample at 700°C and mixed it with NaOH solutions, producing the zeolites chabazite and natrolite. It was unclear what exact roles the kaolinite and the illite played in the development of these product phases. However, the formation of zeolites in this study is most likely due to the metakaolin supplying enough Al to solution, to give a lower Si:Al solution ratio that was more conducive to zeolite formation. On another kaolinite-illite soil, Zibouche et al. (2009) found that activation of the calcined soil with NaOH solution formed zeolites, geopolymers or both, depending on the amount of soluble silica used in the activating solution. The illite did not fully react in the process. Essaidi et al. (2014) studied two kaolinite-illite clays, one of which had a lower kaolinite and higher illite content than the other. The soils were activated in the uncalcined and calcined states with KOH and K-silicate, forming geopolymers for all systems. Among the activated samples, the more illite-rich soil was the stronger of the two when calcined but weaker when uncalcined. However, the authors suggested this might be partly attributable to the surface defects in the kaolinite in the illite-rich soil, leading to more amorphous content after calcination. Xu and van Deventer (2000) used a synthetic mixture of illite and kaolinite, activated in its uncalcined state using NaOH and Na_2SiO_3. No chemical characterisation of the activated sample was given, but it did result in mechanical strength gain. Richardson et al. (1986) activated binary mixtures of kaolinite, montmorillonite and illite clays with aqueous NaOH solution, producing zeolites and/or nepheline. None of the phases formed had not been formed during activation of the individual clays. However, no mention of geopolymers or amorphous

phases was made, and the activated systems were not fully characterised. The use of microwave curing and very short curing times (less than 30 minutes) means there is limited comparability with other systems.

There are fewer studies on feedstocks containing three clay minerals. Richardson et al. (1986) extended the previous study to a ternary mixture, which produced zeolites and nepheline. Diop and Grutzeck (2008b) activated a raw clay containing kaolinite, montmorillonite and illite, although the relative quantities were not given. Activation of the uncalcined clay with NaOH formed a hydrosodalite. Dietel et al. (2017) studied a different clay containing all three minerals, using thermal treatment and activation with KOH. A geopolymer was formed.

In summary, in common clays or soils containing multiple clay minerals, phase formation behaviour and clay mineral consumption is generally less easily determined that in those with a single dominant clay mineral. However, no studies have observed radically different behaviour between multiple and single clay mineral feedstocks.

2.5.5 Comparison of common clays and soil studies

Compared with individual clays, there is greater complexity but also greater potential with using common clays and soils as feedstocks. Key challenges are to understand the effect of this complexity on phase formation behaviour and other material properties.

As previously described, there can be great variation in clay mineralogy - including crystallinity - in common clays and soils, depending on pedogenic conditions. Since poorer crystallinity is generally thought to make for a more reactive clay mineral in alkali activation, several treatment methods (Sections 2.3.5 and 2.3.6) have been used to artificially improve reactivity. The purposeful use of clay minerals with naturally occurring low crystallinity, such as by Essaidi et al. (2014) is an under-investigated aspect in this field so far. It is promising that clay minerals from low crystallinity deposits could be better suited for alkali activation, thereby avoiding competition with other industries for high crystallinity deposits.

A general trend throughout this field is the proliferation of different units used to describe a system’s composition – this makes meaningful comparisons between systems more difficult. The most useful units are deemed to be: oxide/elemental molar ratios (i.e. Si:Al, M:Al, M:Si) - for system composition of Al, Si and metal cation M; molarity - for alkali activating solution, and liquid:solid mass ratio - for describing the wet mix used.

In testing of mechanical properties, dry strength is usually tested rather than wet strength. Although reported dry strength values are often impressive, this is not necessarily the most important measurement for the commercial development of alkali-activated materials as replacements for fired clay bricks and Portland cement based materials. If increased dry strength is not also accompanied with increased wet strength and durability, then use will be limited. In addition, when Na_2SiO_3 is used, it is rarely mentioned that this is an adhesive used to strengthen other materials, most commonly cardboard (Fawer *et al.*, 1999). The development of appropriate testing methods for alkali-activated construction materials is being progressed by RILEM Technical Commitee 224-AAM amongst others (Abora *et al.*, 2014). There is now a voluntary standard for alkali-activated cementitious materials in the British Standards, PAS 8820:2016 (BSI, 2016).

Studies on soils are usually carried out with the purpose of demonstrating a particular common clay deposit or soil is suitable for use as an alkali-activated material. For this reason, there is usually an emphasis on optimising the processing variables to get the best mechanical properties. In general, the depth of microstructural characterisation is less than for studies on individual clay minerals. This is understandable as they are more complex systems, but at the same time is less useful for developing a fundamental understanding of common clays' and soils' behaviour. Calcination is generally used less often for common clays and soils than in studies of individual clay minerals.

For common clays and soils that contain a single clay mineral plus associated minerals, phase formation behaviour is in line with that expected from the alkali activation of individual clay minerals. This suggests that associated minerals do not play a large role in determining alkali activation behaviour. However, this cannot yet be taken as universally applicable, as only a very limited compositional range of clay-containing feedstocks has been studied so far. A summary of basic details, including clay composition, of all the reviewed alkali activation studies is given in Table 2-2. As described above, studies on single clay feedstocks are dominated by kaolinite, and multiple clay feedstocks are dominated by kaolinite-illite. In order to improve the fundamental understanding of these systems, a broader range of compositions should be studied. Lastly, there is still limited understanding on the strengthening mechanisms between geopolymers and aggregates (Dietel *et al.*, 2017; Lee and van Deventer, 2004; Pacheco-Torgal *et al.*, 2007). This may be a key difference between 'pure' individual clays and common clays or soils with a high content of unreactive particles.

Table 2-2: A summary of basic details of the alkali activation studies reviewed (Kaol = kaolinite, Mt = montmorillonite, I = illite)

Study	Feedstock category	Clay mineral(s)	Treatments used	Alkali solution compound(s)	Phases formed
Barrer et al. (1968)	Individual clay	Kaol	None	NaOH	Hydrosodalite
Engelhardt et al. (1992)	Individual clay	Kaol	None	NaOH	Hydrosodalite
Heller-Keller and Lapides (2007)	Individual clay	Kaol	None	NaOH	Hydrosodalite
Marsh et al. (2018b)	Individual clay	Kaol	None	NaOH	Hydrosodalite
Barrer and Mainwaring (1972)	Individual clay	Kaol	Thermal	NaOH	Hydrosodalite; various zeolites
Heller-Keller and Lapides (2007)	Individual clay	Kaol	Thermal	NaOH	Hydrosodalite; Zeolite A; Zeolite X
Zhang et al. (2012)	Individual clay	Kaol	Thermal	NaOH	Geopolymer + hydrosodalite
Heah et al. (2012)	Individual clay	Kaol	None	NaOH + Na_2SiO_3	Geopolymer
Heah et al. (2013)	Individual clay	Kaol	None	NaOH + Na_2SiO_3	Geopolymer
Rahier et al. (1996)	Individual clay	Kaol	Thermal	NaOH + Na_2SiO_3	Geopolymer
Lapides and Heller-Kallai (2007)	Individual clay	Kaol	Thermal	NaOH + Na_2SiO_3	Geopolymer
Zhang et al. (2013)	Individual clay	Kaol	Thermal	NaOH + Na_2SiO_3	Geopolymer
Rahier et al. (1997)	Individual clay	Kaol	Thermal	NaOH + Na_2SiO_3	Geopolymer + hydrosodalite
Wang et al. (2013)	Individual clay	Halloysite	None	NaOH	None
MacKenzie et al. (2007)	Individual clay	Halloysite	Thermal	NaOH + Na_2SiO_3	Geopolymer
Ingles et al. (1970)	Individual clay	Mt	None	NaOH	None
Richardson et al. (1986)	Individual clay	Mt	None	NaOH	None
Marsh et al. (2018a)	Individual clay	Mt	None	NaOH	Geopolymer
Marsh et al. (2018a)	Individual clay	Mt	Acid	NaOH	Geopolymer
Belviso et al. (2017)	Individual clay	Mt	Acid	NaOH	Geopolymer
Belviso et al. (2017)	Individual clay	Mt	Acid + thermal	NaOH	Geopolymer
Prud'homme et al. (2011)	Individual clay	Mt	None	KOH + K_2SiO_3	Geopolymer
Seiffarth et al. (2013)	Individual clay	Mt	Thermal	NaOH + Na_2SiO_3	Possible geopolymer
Belviso et al. (2017)	Individual clay	Mt	Thermal + NaOH fusion	NaOH	Sodalite + zeolite + faujasite
Richardson et al. (1986)	Individual clay	I	None	NaOH	None
Sedmale et al. (2013)	Individual clay	I	None	KOH	None

Marsh et al. (2018b)	Individual clay	I	None	NaOH	None
Prud'homme et al. (2011)	Individual clay	I	None	KOH + K_2SiO_3	Geopolymer
Belviso et al. (2017)	Individual clay	I	Thermal	NaOH	None
Sperberga et al. (2011)	Individual clay	I	Thermal	KOH	Possible geopolymer
Seiffarth et al. (2013)	Individual clay	I	Thermal	NaOH + Na_2SiO_3	Possible geopolymer
Belviso et al. (2017)	Individual clay	I	Thermal + NaOH fusion	NaOH	Sodalite
Boutterin and Davidovits (1988)	Single clay soil	Kaol	None	NaOH + KOH	Zeolite
Lemougna et al. (2014)	Single clay soil	Kaol	None	NaOH	Hydrosodalite
Lassinanti Gualtieri et al. (2015)	Single clay soil	Kaol	Thermal	NaOH + Na_2SiO_3	Geopolymer
Diop and Grutzeck (2008a)	Single clay soil	Kaol	None	NaOH	Hydrosodalite
Yousef et al. (2012)	Single clay soil	Kaol	None	NaOH	Hydrosodalite
Munoz et al. (2015)	Single clay soil	Mt	None	NaOH + Na_2SiO_3	Geopolymer
El Hafid and Hajjaji (2015)	Multiple clay deposit	Kaol + I	Thermal	NaOH	Chabazite + natrolite
Zibouche et al. (2009)	Multiple clay soil	Kaol + I	Thermal	NaOH + Na_2SiO_3	Geopolymer + faujasite
Essaidi et al. (2014)	Multiple clay deposit	Kaol + I	None	KOH + K_2SiO_3	Geopolymer
Essaidi et al. (2014)	Multiple clay deposit	Kaol + I	Thermal	KOH + K_2SiO_3	Geopolymer
Xu and Van Deventer (2000)	Multiple clay mixture	Kaol + I	None	NaOH + Na_2SiO_3	Possible geopolymer
Richardson et al. (1986)	Multiple clay mixture	Kaol + I	None	NaOH	Zeolites + Nepheline
Richardson et al. (1986)	Multiple clay mixture	Kaol + Mt	None	NaOH	Zeolites
Richardson et al. (1986)	Multiple clay mixture	Mt + I	None	NaOH	Nepheline
Richardson et al. (1986)	Multiple clay mixture	Kaol + Mt + I	None	NaOH	Zeolites + Nepheline
Diop and Grutzeck (2008b)	Multiple clay deposit	Kaol + Mt + I	None	NaOH	Hydrosodalite
Dietel et al. (2017)	Multiple clay deposit	Mt + I + Kaol	Thermal	KOH	Geopolymer

2.6 Conclusions

Clay-containing feedstocks have high potential as scalable precursors in alkali-activated materials, which can help achieve sustainable development in the construction industry. To meet this potential, it is necessary to utilise both non-kaolinitic clay minerals, as well as clay-containing feedstocks of variable composition and lower purity than those typically used, such as common clays and soils. Attention has been concentrated on production of geopolymer phases through alkali activation, as these are the most desirable phases for use as construction materials.

Kaolinite is the most reliable clay mineral precursor to produce a geopolymer, but only given the use of additional soluble silicate. Montmorillonite and illite (both 2:1 clay minerals) have the potential to form geopolymers without the addition of soluble silicate. Montmorillonite is less reliable for geopolymer formation compared to kaolinite, and is more dependent on treatment and processing parameters. Illite can form a geopolymer, but there is less agreement between studies on what optimal conditions are. Whilst it is the available Si:Al molar ratio that determines the potential phases that a system may form, it is a combination of treatment and processing conditions that determines what phase, if at all, is actually formed. For all the clay minerals, the most effective route for geopolymer production in general is a combination of calcination treatment and additional of soluble silicate.

With regard to common clay deposits and soils, phase formation behaviour is controlled by the dominant clay mineral in the composition. Clay mineral crystallinity varies depending on geological and diagenetic conditions. A lower degree of crystallinity gives higher reactivity in alkali activation. Given that several industrial applications for clays prefer high crystallinity, further exploitation of clay deposits for alkali activation precursors would not directly compete with existing industries.

The potential for the exploitation of common clays and soils as precursors for scalable alkali-activated materials is bright, as it is possible to form geopolymer phases from individual clay minerals, and from low-purity common clays and soils. There are two chief scientific barriers to further development and commercial production. Firstly, understanding of how restrictive the range of processing conditions is to achieving desired phase formation. Secondly, improving our fundamental understanding of these systems by investigating a broader compositional range of feedstocks. Engineering barriers include whether materials can have the strength and durability to displace Portland cement based materials. Further questions remain about the cost-effectiveness, environmental impact and scalability of different treatment methods.

Acknowledgements

A. Marsh was supported by the EPSRC Centre for Decarbonisation of the Built Environment (dCarb) [grant number EP/L016869/1] and a University of Bath Research Scholarship. A. Khalifa is supported by the FWO research project (grant number G0C2615N)

Figures 2-1 and 2-2 reprinted from Developments in Clay Science. Ed. F. Bergaya, 5, Brigatti, M.F., Galan, E., Theng, B.K.G., Chapter 2 - Structure and Mineralogy of Clay Minerals, pg.22, Copyright (2013), with permission from Elsevier.

Figure 2-7 adapted from Cement and Concrete Research, 41, Fernandez, R., Martirena, F., Scrivener, K.L., The origin of the pozzolanic activity of calcined clay minerals: A comparison between kaolinite, illite and montmorillonite, pg.117, Copyright (2011), with permission from Elsevier.

Figures 2-8 and 2-9 reprinted from Thermochimica Acta, 462, Wolters, F. and Emmerich, K., Thermal reactions of smectites - relation of dehydroxylation temperature to octahedral structure, pg.81-82, Copyright (2007), with permission from Elsevier.

Figure 2-10 adapted from Applied Clay Science, 132-133, Hollanders, S., Adriaens, R., Skibsted, J., Cizer, Ö.,Elsen, J., Pozzolanic reactivity of pure calcined clays, pg.554, Copyright (2016), with permission from Elsevier.

Figure 2-11 adapted from Applied Clay Science, 44, Steudel, A., Batenburg, L.F., Fischer, H.R., Weidler, P.G. and Emmerich, K., Alteration of non-swelling clay minerals and magadiite by acid activation, pg.98, Copyright (2009), and from Applied Clay Science, 44, Steudel, A., Batenburg, L.F., Fischer, H.R., Weidler, P.G. and Emmerich, K., Alteration of non-swelling clay minerals and magadiite by acid activation, pg.110, Copyright (2009), with permission from Elsevier.

References

Abdullahi, T., Harun, Z. & Othman, M.H.D., 2017. A review on sustainable synthesis of zeolite from kaolinite resources via hydrothermal process. *Advanced Powder Technology,* 28(8), pp. 1827-1840.

Abe, S.S., Masunaga, T., Yamamoto, S., Honna, T. & Wakatsuki, T., 2006. Comprehensive assessment of the clay mineralogical composition of lowland soils in West Africa. *Soil Science & Plant Nutrition,* 52(4), pp. 479-488.

Abora, K., Beleña, I., Bernal, S.A., Dunster, A., Nixon, P.A., Provis, J.L., Tagnit-Hamou, A. & Winnefeld, F., 2014. Durability and Testing – Chemical Matrix Degradation Processes. In: J.L. Provis & J.S.J. van Deventer, eds. *Alkali Activated Materials: State-of-the-Art Report, RILEM TC 224-AAM.* Dordrecht: Springer Netherlands, pp. 177-221.

Ahmari, S. & Zhang, L., 2015. 24 - The properties and durability of alkali-activated masonry units. *Handbook of Alkali-Activated Cements, Mortars and Concretes.* Oxford: Woodhead Publishing, pp. 643-660.

Aldabsheh, I., Khoury, H., Wastiels, J. & Rahier, H., 2015. Dissolution behavior of Jordanian clay-rich materials in alkaline solutions for alkali activation purpose. Part I. *Applied Clay Science,* 115, pp. 238-247.

Arnoult, M., Perronnet, M., Autef, A. & Rossignol, S., 2018. How to control the geopolymer setting time with the alkaline silicate solution. *Journal of Non-Crystalline Solids,* 495, pp. 59-66.

Autef, A., Joussein, E., Poulesquen, A., Gasgnier, G., Pronier, S., Sobrados, I., Sanz, J. & Rossignol, S., 2013. Influence of metakaolin purities on potassium geopolymer formulation: The existence of several networks. *Journal of Colloid and Interface Science,* 408, pp. 43-53.

Barbosa, V.F.F., MacKenzie, K.J.D. & Thaumaturgo, C., 2000. Synthesis and characterisation of materials based on inorganic polymers of alumina and silica: sodium polysialate polymers. *International Journal of Inorganic Materials,* 2(4), pp. 309-317.

Barrer, R., Cole, J. & Sticher, H., 1968. Chemistry of soil minerals. Part V. Low temperature hydrothermal transformations of kaolinite. *Journal of the Chemical Society A: Inorganic, Physical, Theoretical*, pp. 2475-2485.

Barrer, R.M. & Mainwaring, D.E., 1972. Chemistry of soil minerals. Part XIII. Reactions of metakaolinite with single and mixed bases. *Journal of the Chemical Society, Dalton Transactions,* (22), pp. 2534-2546.

Bauer, A. & Berger, G., 1998. Kaolinite and smectite dissolution rate in high molar KOH solutions at 35° and 80°C. *Applied Geochemistry,* 13(7), pp. 905-916.

Beerling, D.J., Leake, J.R., Long, S.P., Scholes, J.D., Ton, J., Nelson, P.N., Bird, M., Kantzas, E., Taylor, L.L., Sarkar, B., Kelland, M., DeLucia, E., Kantola, I., Müller, C., Rau, G. & Hansen, J., 2018. Farming with crops and rocks to address global climate, food and soil security. *Nature Plants,* 4(3), pp. 138-147.

Belviso, C., Cavalcante, F., Niceforo, G. & Lettino, A., 2017. Sodalite, faujasite and A-type zeolite from 2:1 dioctahedral and 2:1:1 trioctahedral clay minerals. A singular

review of synthesis methods through laboratory trials at a low incubation temperature. *Powder Technology,* 320, pp. 483-497.

Bergaya, F. & Lagaly, G., 2013. Chapter 1 - General Introduction: Clays, Clay Minerals, and Clay Science. In: F. Bergaya & G. Lagaly, eds. *Developments in Clay Science.* Elsevier, pp. 1-19.

Bernal, S.A., Krivenko, P.V., Provis, J.L., Puertas, F., Rickard, W.D.A., Shi, C. & van Riessen, A., 2014. Other Potential Applications for Alkali-Activated Materials. In: J.L. Provis & J.S.J. van Deventer, eds. *Alkali Activated Materials: State-of-the-Art Report, RILEM TC 224-AAM.* Dordrecht: Springer Netherlands, pp. 339-379.

Bish, D.L., 1993. Rietveld refinement of the kaolinite structure at 1.5 K. *Clays and Clay Minerals,* 41(6), pp. 738-744.

Blissett, R.S. & Rowson, N.A., 2012. A review of the multi-component utilisation of coal fly ash. *Fuel,* 97, pp. 1-23.

Boutterin, C. & Davidovits, J., 1988. Geopolymeric Cross-Linking (LTGS) and Building materials. In: Geopolymer ' 88, 1988.

Brigatti, M.F., Galán, E. & Theng, B.K.G., 2013. Chapter 2 - Structure and Mineralogy of Clay Minerals. In: F. Bergaya & G. Lagaly, eds. *Handbook of Clay Science.* 2nd ed. Amsterdam: Elsevier, pp. 21-81.

BSI, 2016. PAS 8820:2016. Construction materials. Alkali-activated cementitious material and concrete. Specification BSI.

Buchwald, A., Hohmann, M., Posern, K. & Brendler, E., 2009. The suitability of thermally activated illite/smectite clay as raw material for geopolymer binders. *Applied Clay Science,* 46(3), pp. 300-304.

Buchwald, A., Zellmann, H.D. & Kaps, C., 2011. Condensation of aluminosilicate gels—model system for geopolymer binders. *Journal of Non-Crystalline Solids,* 357(5), pp. 1376-1382.

Byrappa, K. & Adschiri, T., 2007. Hydrothermal technology for nanotechnology. *Progress in Crystal Growth and Characterization of Materials,* 53(2), pp. 117-166.

Cama, J. & Ganor, J., 2015. Chapter 4 - Dissolution Kinetics of Clay Minerals. In: C. Tournassat, C.I. Steefel, I.C. Bourg & F. Bergaya, eds. *Developments in Clay Science.* Elsevier, pp. 101-153.

Christidis, G.E., 2011. *Advances in the characterization of industrial minerals.* London: The Mineralogical Society of Great Britain and Ireland.

Claret, F., Bauer, A., Schäfer, T., Griffault, L. & Lanson, B., 2002. Experimental investigation of the interaction of clays with high-pH solutions: A case study from the Callovo-Oxfordian formation, Meuse-Haute Marne underground laboratory (France). *Clays and Clay Minerals,* 50(5), pp. 633-646.

Criado, M., Palomo, A. & Fernández-Jiménez, A., 2006. Alkali activated fly ash binders. A comparative study between sodium and potassium activators. *Materiales de Construccion,* 56(281), pp. 51-65.

Cundy, C.S. & Cox, P.A., 2005. The hydrothermal synthesis of zeolites: Precursors, intermediates and reaction mechanism. *Microporous and Mesoporous Materials,* 82(1), pp. 1-78.

Davidovits, J., 1989. Geopolymers and geopolymeric materials. *Journal of Thermal Analysis and Calorimetry,* 35(2), pp. 429-441.

Davidovits, J., 2011. *Geopolymer chemistry and applications.* 3rd ed. Saint-Quentin: Institut Geopolymere.

Derkowski, A. & Kuligiewicz, A., 2017. Rehydroxylation in smectites and other clay minerals observed in-situ with a modified thermogravimetric system. *Applied Clay Science,* 136, pp. 219-229.

Dietel, J., Warr, L.N., Bertmer, M., Steudel, A., Grathoff, G.H. & Emmerich, K., 2017. The importance of specific surface area in the geopolymerization of heated illitic clay. *Applied Clay Science,* 139, pp. 99-107.

Ding, Y., Dai, J.-G. & Shi, C.-J., 2016. Mechanical properties of alkali-activated concrete: A state-of-the-art review. *Construction and Building Materials,* 127, pp. 68-79.

Diop, M.B. & Grutzeck, M.W., 2008a. Low temperature process to create brick. *Construction and Building Materials,* 22(6), pp. 1114-1121.

Diop, M.B. & Grutzeck, M.W., 2008b. Sodium silicate activated clay brick. *B Eng Geol Environ,* 67(4), pp. 499-505.

Dixon, J.B. & Weed, S.B., 1989. *Minerals in Soil Environments.* 2nd ed. Madison, WI: Soil Science Society of America.

Drits, V., Besson, G. & Muller, F., 1995. An improved model for structural transformation of heat-treated aluminous dioctahedral 2: 1 layer silicates. *Clays and Clay Minerals,* 43(6), pp. 718-731.

Duxson, P., Fernández-Jiménez, A., Provis, J.L., Lukey, G.C., Palomo, A. & van Deventer, J.S.J., 2007a. Geopolymer technology: the current state of the art. *J Mater Sci,* 42(9), pp. 2917-2933.

Duxson, P., Mallicoat, S.W., Lukey, G.C., Kriven, W.M. & van Deventer, J.S.J., 2007b. The effect of alkali and Si/Al ratio on the development of mechanical properties of metakaolin-based geopolymers. *Colloids and Surfaces A: Physicochemical and Engineering Aspects,* 292(1), pp. 8-20.

Duxson, P., Provis, J.L., Lukey, G.C., Mallicoat, S.W., Kriven, W.M. & van Deventer, J.S.J., 2005a. Understanding the relationship between geopolymer composition, microstructure and mechanical properties. *Colloids and Surfaces A: Physicochemical and Engineering Aspects,* 269(1), pp. 47-58.

Duxson, P., Provis, J.L., Lukey, G.C., Separovic, F. & van Deventer, J.S.J., 2005b. 29Si NMR Study of Structural Ordering in Aluminosilicate Geopolymer Gels. *Langmuir,* 21(7), pp. 3028-3036.

El Hafid, K. & Hajjaji, M., 2015. Effects of the experimental factors on the microstructure and the properties of cured alkali-activated heated clay. *Applied Clay Science,* 116–117, pp. 202-210.

Emmerich, K., 2000. Spontaneous rehydroxylation of a dehydroxylated cis-vacant montmorillonite. *Clays and Clay Minerals,* 48(3), pp. 405-408.

Emmerich, K., Madsen, F.T. & Kahr, G., 1999. Dehydroxylation behavior of heat-treated and stream-treated homoionic Cis-vacant montmorillonites. *Clays and Clay Minerals,* 47(5), pp. 591-604.

Emmerich, K., Wolters, F., Kahr, G. & Lagaly, G., 2009. Clay Profiling: The Classification of Montmorillonites. *Clays and Clay Minerals,* 57(1), pp. 104-114.

Engelhardt, G., Felsche, J. & Sieger, P., 1992. The hydrosodalite system Na6+ x [SiAlO4] 6 (OH) x. cntdot. nH2O: formation, phase composition, and de-and rehydration studied by 1H, 23Na, and 29Si MAS-NMR spectroscopy in tandem with thermal analysis, x-ray diffraction, and IR spectroscopy. *Journal of the American Chemical Society,* 114(4), pp. 1173-1182.

Essaidi, N., Samet, B., Baklouti, S. & Rossignol, S., 2014. Feasibility of producing geopolymers from two different Tunisian clays before and after calcination at various temperatures. *Applied Clay Science,* 88-89, pp. 221-227.

Fawer, M., Concannon, M. & Rieber, W., 1999. Life cycle inventories for the production of sodium silicates. *The International Journal of Life Cycle Assessment,* 4(4), p. 207.

Fernández-Jiménez, A., Palomo, A., Sobrados, I. & Sanz, J., 2006. The role played by the reactive alumina content in the alkaline activation of fly ashes. *Microporous and Mesoporous Materials,* 91(1), pp. 111-119.

Fernandez Lopez, R., 2009. *Calcined clayey soils as a potential replacement for cement in developing countries.* PhD, École Polytechnique Fédérale de Lausanne.

Fernandez, R., Martirena, F. & Scrivener, K.L., 2011. The origin of the pozzolanic activity of calcined clay minerals: A comparison between kaolinite, illite and montmorillonite. *Cement and Concrete Research,* 41(1), pp. 113-122.

Fletcher, R.A., MacKenzie, K.J.D., Nicholson, C.L. & Shimada, S., 2005. The composition range of aluminosilicate geopolymers. *Journal of the European Ceramic Society,* 25(9), pp. 1471-1477.

García-Lodeiro, I., Fernández-Jiménez, A., Palomo, A. & Macphee, D.E., 2010. Effect of Calcium Additions on N–A–S–H Cementitious Gels. *Journal of the American Ceramic Society,* 93(7), pp. 1934-1940.

Garcia-Lodeiro, I., Palomo, A. & Fernández-Jiménez, A., 2015. 2 - An overview of the chemistry of alkali-activated cement-based binders. *Handbook of Alkali-Activated Cements, Mortars and Concretes.* Oxford: Woodhead Publishing, pp. 19-47.

Garg, N. & Skibsted, J., 2014. Thermal Activation of a Pure Montmorillonite Clay and Its Reactivity in Cementitious Systems. *The Journal of Physical Chemistry C,* 118(21), pp. 11464-11477.

Gharzouni, A., Samet, B., Baklouti, S., Joussein, E. & Rossignol, S., 2016. Addition of low reactive clay into metakaolin-based geopolymer formulation: Synthesis, existence domains and properties. *Powder Technology,* 288, pp. 212-220.

Golubev, S.V., Bauer, A. & Pokrovsky, O.S., 2006. Effect of pH and organic ligands on the kinetics of smectite dissolution at 25°C. *Geochimica et Cosmochimica Acta,* 70(17), pp. 4436-4451.

Gualtieri, A.F., 2000. Accuracy of XRPD QPA using the combined Rietveld-RIR method. *Journal of Applied Crystallography,* 33(2), pp. 267-278.

Guo, C.-m., Wang, K.-t., Liu, M.-y., Li, X.-h. & Cui, X.-m., 2016. Preparation and characterization of acid-based geopolymer using metakaolin and disused polishing liquid. *Ceramics International,* 42(7), pp. 9287-9291.

Habert, G., d'Espinose de Lacaillerie, J.B. & Roussel, N., 2011. An environmental evaluation of geopolymer based concrete production: reviewing current research trends. *Journal of Cleaner Production,* 19(11), pp. 1229-1238.

Habert, G. & Ouellet-Plamondon, C., 2016. Recent update on the environmental impact of geopolymers. *RILEM Technical Letters,* 1, pp. 17-23.

He, C., Makovicky, E. & Osbæck, B., 1994. Thermal stability and pozzolanic activity of calcined kaolin. *Applied Clay Science,* 9(3), pp. 165-187.

Heah, C.Y., Kamarudin, H., Mustafa Al Bakri, A.M., Bnhussain, M., Luqman, M., Khairul Nizar, I., Ruzaidi, C.M. & Liew, Y.M., 2012. Study on solids-to-liquid and alkaline activator ratios on kaolin-based geopolymers. *Construction and Building Materials,* 35, pp. 912-922.

Heah, C.Y., Kamarudin, H., Mustafa Al Bakri, A.M., Bnhussain, M., Luqman, M., Khairul Nizar, I., Ruzaidi, C.M. & Liew, Y.M., 2013. Kaolin-based geopolymers with various NaOH concentrations. *Int J Miner Metall Mater,* 20(3), pp. 313-322.

Heidrich, C., Feuerborn, H.-J. & Weir, A., 2013. Coal combustion products: a global perspective. In: World of Coal Ash Conference, April 22-25 2013 Lexington, Kentucky.

Heller-Kallai, L., 2013. Chapter 10.2 - Thermally Modified Clay Minerals. In: F. Bergaya & G. Lagaly, eds. *Handbook of Clay Science.* 2nd ed.: Elsevier, pp. 411-433.

Heller-Kallai, L. & Lapides, I., 2007. Reactions of kaolinites and metakaolinites with NaOH—comparison of different samples (Part 1). *Applied Clay Science,* 35(1–2), pp. 99-107.

Heller-Kallai, L. & Rozenson, I., 1980. Dehydroxylation of dioctahedral phyllosilicates. *Clays and Clay Minerals,* 28(5), pp. 355-368.

Hollanders, S., 2017. *Mineralogical study of the pozzolanic properties of calcined clays.* DSc, KU Leuven.

Hollanders, S., Adriaens, R., Skibsted, J., Cizer, Ö. & Elsen, J., 2016. Pozzolanic reactivity of pure calcined clays. *Applied Clay Science,* 132-133, pp. 552-560.

Houben, H. & Guillaud, H., 1994. *Earth Construction: A comprehensive guide.* Rugby, U.K.: Practical Action Publishing.

Hounsi, A.D., Lecomte-Nana, G., Djétéli, G., Blanchart, P., Alowanou, D., Kpelou, P., Napo, K., Tchangbédji, G. & Praisler, M., 2014. How does Na, K alkali metal concentration change the early age structural characteristic of kaolin-based geopolymers. *Ceramics International,* 40(7, Part A), pp. 8953-8962.

Hounsi, A.D., Lecomte-Nana, G.L., Djétéli, G. & Blanchart, P., 2013. Kaolin-based geopolymers: Effect of mechanical activation and curing process. *Construction and Building Materials,* 42, pp. 105-113.

Huang, P.M., Li, Y. & Sumner, M.E., 2011. *Handbook of Soil Sciences.* Boca Raton: CRC Press

Huertas, F.J., Chou, L. & Wollast, R., 1999. Mechanism of kaolinite dissolution at room temperature and pressure Part II: kinetic study. *Geochimica et Cosmochimica Acta,* 63(19–20), pp. 3261-3275.

Ilić, B.R., Mitrović, A.A. & Miličić, L.R., 2010. Thermal treatment of kaolin clay to obtain metakaolin. *Hemijska industrija,* 64(4), pp. 351-356.

Ingles, O., 1970. Mechanisms of clay stabilization with inorganic acids and alkalis. *Soil Research,* 8(1), pp. 81-85.

Johnson, E.B.G. & Arshad, S.E., 2014. Hydrothermally synthesized zeolites based on kaolinite: A review. *Applied Clay Science,* 97-98, pp. 215-221.

Köhler, S.J., Dufaud, F. & Oelkers, E.H., 2003. An experimental study of illite dissolution kinetics as a function of ph from 1.4 to 12.4 and temperature from 5 to 50°C. *Geochimica et Cosmochimica Acta,* 67(19), pp. 3583-3594.

Komadel, P., 2003. Chemically modified smectites. *Clay Miner,* 38(1), pp. 127-138.

Komadel, P., Bujdák, J., Madejová, J., Šucha, V. & Elsass, F., 1996. Effect of Non-Swelling Layers on the Dissolution of Reduced-Charge Montmorillonite in Hydrochloric Acid. *Clay Miner.* p. 333.

Komadel, P. & Madejová, J., 2013. Chapter 10.1 - Acid Activation of Clay Minerals. In: F. Bergaya & G. Lagaly, eds. *Handbook of Clay Science.* 2nd ed.: Elsevier, pp. 385-409.

Komnitsas, K. & Zaharaki, D., 2007. Geopolymerisation: A review and prospects for the minerals industry. *Minerals Engineering,* 20(14), pp. 1261-1277.

Kovalchuk, G. & Krienko, P.V., 2009. 12 - Producing fire- and heat-resistant geopolymers. In: J.L. Provis & J.S.J. van Deventer, eds. *Geopolymers.* Woodhead Publishing, pp. 227-266.

Lancellotti, I., Barbieri, L. & Leonelli, C., 2015. 20 - Use of alkali-activated concrete binders for toxic waste immobilization. In: F. Pacheco-Torgal, J.A. Labrincha, C. Leonelli, A. Palomo & P. Chindaprasirt, eds. *Handbook of Alkali-Activated Cements, Mortars and Concretes.* Oxford: Woodhead Publishing, pp. 539-554.

Lapides, I. & Heller-Kallai, L., 2007. Reactions of metakaolinite with NaOH and colloidal silica — Comparison of different samples (part 2). *Applied Clay Science,* 35(1–2), pp. 94-98.

Lassinantti Gualtieri, M., Romagnoli, M., Pollastri, S. & Gualtieri, A.F., 2015. Inorganic polymers from laterite using activation with phosphoric acid and alkaline sodium silicate solution: Mechanical and microstructural properties. *Cement and Concrete Research,* 67, pp. 259-270.

Lee, W.K.W. & van Deventer, J.S.J., 2004. The interface between natural siliceous aggregates and geopolymers. *Cement and Concrete Research,* 34(2), pp. 195-206.

Lemougna, P.N., Madi, A.B., Kamseu, E., Melo, U.C., Delplancke, M.P. & Rahier, H., 2014. Influence of the processing temperature on the compressive strength of Na

activated lateritic soil for building applications. *Construction and Building Materials,* 65, pp. 60-66.

Liew, Y.M., Heah, C.Y., Mohd Mustafa, A.B. & Kamarudin, H., 2016. Structure and properties of clay-based geopolymer cements: A review. *Progress in Materials Science,* 83, pp. 595-629.

Liu, L.-P., Cui, X.-M., He, Y., Liu, S.-D. & Gong, S.-Y., 2012. The phase evolution of phosphoric acid-based geopolymers at elevated temperatures. *Materials Letters,* 66(1), pp. 10-12.

Llatas, C., 2011. A model for quantifying construction waste in projects according to the European waste list. *Waste Management,* 31(6), pp. 1261-1276.

Louati, S., Baklouti, S. & Samet, B., 2016. Acid based geopolymerization kinetics: Effect of clay particle size. *Applied Clay Science,* 132-133, pp. 571-578.

Luukkonen, T., Abdollahnejad, Z., Yliniemi, J., Kinnunen, P. & Illikainen, M., 2018. One-part alkali-activated materials: A review. *Cement and Concrete Research,* 103, pp. 21-34.

MacKenzie, K.J.D., 2015. 28 - Innovative applications of inorganic polymers (geopolymers). In: F. Pacheco-Torgal, J.A. Labrincha, C. Leonelli, A. Palomo & P. Chindaprasirt, eds. *Handbook of Alkali-Activated Cements, Mortars and Concretes.* Oxford: Woodhead Publishing, pp. 777-805.

MacKenzie, K.J.D., Brew, D.R.M., Fletcher, R.A. & Vagana, R., 2007. Formation of aluminosilicate geopolymers from 1:1 layer-lattice minerals pre-treated by various methods: a comparative study. *J Mater Sci,* 42(12), pp. 4667-4674.

Madejová, J., Bujdák, J., Janek, M. & Komadel, P., 1998. Comparative FT-IR study of structural modifications during acid treatment of dioctahedral smectites and hectorite. *Spectrochimica Acta Part A: Molecular and Biomolecular Spectroscopy,* 54(10), pp. 1397-1406.

Marsh, A., Heath, A., Patureau, P., Evernden, M. & Walker, P., 2018a. Alkali activation behaviour of un-calcined montmorillonite and illite clay minerals. *Applied Clay Science,* 166, pp. 250-261.

Marsh, A., Heath, A., Patureau, P., Evernden, M. & Walker, P., 2018b. A mild conditions synthesis route to produce hydrosodalite from kaolinite, compatible with extrusion processing. *Microporous and Mesoporous Materials,* 264, pp. 125-132.

Massiot, D., Dion, P., Alcover, J.F. & Bergaya, F., 1995. 27Al and 29Si MAS NMR Study of Kaolinite Thermal Decomposition by Controlled Rate Thermal Analysis. *Journal of the American Ceramic Society,* 78(11), pp. 2940-2944.

McIntosh, A., Lawther, S.E.M., Kwasny, J., Soutsos, M.N., Cleland, D. & Nanukuttan, S., 2015. Selection and characterisation of geological materials for use as geopolymer precursors. *Advances in Applied Ceramics,* 114(7), pp. 378-385.

Medpelli, D., Seo, J.M. & Seo, D.K., 2014. Geopolymer with Hierarchically Meso-/Macroporous Structures from Reactive Emulsion Templating. *Journal of the American Ceramic Society,* 97(1), pp. 70-73.

Mehta, A. & Siddique, R., 2016. An overview of geopolymers derived from industrial by-products. *Construction and Building Materials,* 127, pp. 183-198.

Metz, V., Amram, K. & Ganor, J., 2005. Stoichiometry of smectite dissolution reaction. *Geochimica et Cosmochimica Acta,* 69(7), pp. 1755-1772.

Meunier, A., 2005. *Clays.* Berlin: Springer-Verlag Berlin Heidelberg.

Mo, B.-H., Zhu, H., Cui, X.-M., He, Y. & Gong, S.-Y., 2014. Effect of curing temperature on geopolymerization of metakaolin-based geopolymers. *Applied Clay Science,* 99, pp. 144-148.

Muller, F.D., V.; Plançon, A.; Robert, J.-L., 2000. Structural transformation of 2:1 dioctahedral layer silicates during dehydroxylation-rehydroxylation reactions. *Clays and Clay Minerals,* 48(5), pp. 572-585.

Muñoz, J.F., Easton, T. & Dahmen, J., 2015. Using alkali-activated natural aluminosilicate minerals to produce compressed masonry construction materials. *Construction and Building Materials,* 95, pp. 86-95.

Murmu, A.L. & Patel, A., 2018. Towards sustainable bricks production: An overview. *Construction and Building Materials,* 165, pp. 112-125.

Murray, H.H., 2006. Chapter 2 Structure and Composition of the Clay Minerals and their Physical and Chemical Properties. In: H.H. Murray, ed. *Applied Clay Mineralogy: Occurrences, Processing and Application of Kaolins, Bentonites, Palygorskite-Sepiolite, and Common Clays.* Elsevier, pp. 7-31.

Murray, H.H. & Keller, W.D., 1993. Kaolins, Kaolins and Kaolins. In: H.H. Murray, W.M. Bundy & C.C. Harvey, eds. *Kaolin Genesis and Utilization.* Clay Minerals Society.

Murray, H.H. & Lyons, S.C., 1956. Correlation of Paper-Coating Quality with Degree of Crystal Perfection of Kaolinite. In: A. Swineford, ed. Fourth National Conference On Clays and Clay Minerals, 1956 Pennsylvania, USA. National Academy of Sciences - National Research Council, pp. 31-40.

Newsam, J.M., 1986. The Zeolite Cage Structure. *Science,* 231(4742), pp. 1093-1099.

Nickovic, S., Vukovic, A., Vujadinovic, M., Djurdjevic, V. & Pejanovic, G., 2012. High-resolution mineralogical database of dust-productive soils for atmospheric dust modeling. *Atmospheric Chemistry and Physics,* 12(2), pp. 845-855.

Obonyo, E., Kamseu, E., Melo, U. & Leonelli, C., 2011. Advancing the Use of Secondary Inputs in Geopolymer Binders for Sustainable Cementitious Composites: A Review. *Sustainability,* 3(2), pp. 410-423.

Pacheco-Torgal, F., Abdollahnejad, Z., Miraldo, S., Baklouti, S. & Ding, Y., 2012. An overview on the potential of geopolymers for concrete infrastructure rehabilitation. *Construction and Building Materials,* 36, pp. 1053-1058.

Pacheco-Torgal, F., Castro-Gomes, J. & Jalali, S., 2007. Investigations about the effect of aggregates on strength and microstructure of geopolymeric mine waste mud binders. *Cement and Concrete Research,* 37(6), pp. 933-941.

Pacheco-Torgal, F., Castro-Gomes, J. & Jalali, S., 2008. Alkali-activated binders: A review. *Construction and Building Materials,* 22(7), pp. 1305-1314.

Pacheco-Torgal, F. & Jalali, S., 2012. Earth construction: Lessons from the past for future eco-efficient construction. *Construction and Building Materials,* 29, pp. 512-519.

Payá, J., Monzó, J., Borrachero, M.V. & Tashima, M.M., 2015. 18 - Reuse of aluminosilicate industrial waste materials in the production of alkali-activated concrete binders. In: F. Pacheco-Torgal, J.A. Labrincha, C. Leonelli, A. Palomo & P. Chindaprasirt, eds. *Handbook of Alkali-Activated Cements, Mortars and Concretes.* Oxford: Woodhead Publishing, pp. 487-518.

Provis, J.L., 2009a. 4 - Activating solution chemistry for geopolymers. In: J.L. Provis & J.S.J. van Deventer, eds. *Geopolymers - Structure, Processing, Properties and Industrial Applications.* Woodhead Publishing, pp. 50-71.

Provis, J.L., 2009b. 19 - Immobilisation of toxic wastes in geopolymers. In: J.L. Provis & J.S.J. van Deventer, eds. *Geopolymers.* Woodhead Publishing, pp. 421-440.

Provis, J.L., 2014. Geopolymers and other alkali activated materials: why, how, and what? *Mat. Struct.,* 47(1), pp. 11-25.

Provis, J.L., 2018a. Alkali-activated materials. *Cement and Concrete Research,* 114, pp. 40-48.

Provis, J.L., 2018b. Alkali-Activation of Calcined Clays – Past, Present and Future. In: F. Martirena, A. Favier & K. Scrivener, eds. Calcined Clays for Sustainable Concrete, 2018 Dordrecht. Springer Netherlands, pp. 372-376.

Provis, J.L., Brice, D.G., Buchwald, A., Duxson, P., Kavalerova, E., Krivenko, P.V., Shi, C., van Deventer, J.S.J. & Wiercx, J.A.L.M., 2014a. Demonstration Projects and Applications in Building and Civil Infrastructure. In: J.L. Provis & J.S.J. van Deventer, eds. *Alkali Activated Materials: State-of-the-Art Report, RILEM TC 224-AAM.* Dordrecht: Springer Netherlands, pp. 309-338.

Provis, J.L., Duxson, P., Kavalerova, E., Krivenko, P.V., Pan, Z., Puertas, F. & van Deventer, J.S.J., 2014b. Historical Aspects and Overview. In: J.L. Provis & J.S.J. van Deventer, eds. *Alkali Activated Materials: State-of-the-Art Report, RILEM TC 224-AAM.* Dordrecht: Springer Netherlands, pp. 11-57.

Provis, J.L., Duxson, P. & van Deventer, J.S.J., 2010. The role of particle technology in developing sustainable construction materials. *Advanced Powder Technology,* 21(1), pp. 2-7.

Provis, J.L., Lukey, G.C. & van Deventer, J.S., 2005. Do geopolymers actually contain nanocrystalline zeolites? A reexamination of existing results. *Chemistry of Materials,* 17(12), pp. 3075-3085.

Provis, J.L., Palomo, A. & Shi, C., 2015. Advances in understanding alkali-activated materials. *Cement and Concrete Research,* 78, pp. 110-125.

Provis, J.L. & van Deventer, J.S.J., 2009. 1.1 History of Geopolymer Technology. In: J.L. Provis & J.S.J. van Deventer, eds. *Geopolymers - Structure, Processing, Properties and Industrial Applications.* Woodhead Publishing.

Provis, J.L., Yong, S.L. & Duxson, P., 2009. 5 - Nanostructure/microstructure of metakaolin geopolymers. In: J.L. Provis & J.S.J. van Deventer, eds. *Geopolymers - Structure, Processing, Properties and Industrial Applications.* Woodhead Publishing, pp. 72-88.

Prud'homme, E., Michaud, P., Joussein, E., Peyratout, C., Smith, A. & Rossignol, S., 2011. In situ inorganic foams prepared from various clays at low temperature. *Applied Clay Science,* 51(1), pp. 15-22.

Rahier, H., Simons, W., Van Mele, B. & Biesemans, M., 1997. Low-temperature synthesized aluminosilicate glasses: Part III Influence of the composition of the silicate solution on production, structure and properties. *J Mater Sci,* 32(9), pp. 2237-2247.

Rahier, H., Van Mele, B., Biesemans, M., Wastiels, J. & Wu, X., 1996. Low-temperature synthesized aluminosilicate glasses. Part I Low-temperature reaction stoichiometry and structure of a model compound. *J Mater Sci,* 31(1), pp. 71-79.

Rashad, A.M., 2013. Alkali-activated metakaolin: A short guide for civil Engineer – An overview. *Construction and Building Materials,* 41, pp. 751-765.

Richardson, C.K., Markuszewski, R., Durham, K.S. & Bluhm, D.D., 1986. Effect of Caustic and Microwave Treatment on Clay Minerals Associated with Coal. *Mineral Matter and Ash in Coal.* American Chemical Society, pp. 513-523.

Rocha, J. & Klinowski, J., 1991. The rehydration of metakaolinite to kaolinite. *Journal of the Chemical Society, Chemical Communications,* (8), pp. 582-584.

Rovnaník, P., 2010. Effect of curing temperature on the development of hard structure of metakaolin-based geopolymer. *Construction and Building Materials,* 24(7), pp. 1176-1183.

Salvador, S., 1995. Pozzolanic properties of flash-calcined kaolinite: A comparative study with soak-calcined products. *Cement and Concrete Research,* 25(1), pp. 102-112.

San Nicolas, R., Cyr, M. & Escadeillas, G., 2013. Characteristics and applications of flash metakaolins. *Applied Clay Science,* 83-84, pp. 253-262.

Sargent, P., 2015. 21 - The development of alkali-activated mixtures for soil stabilisation. *Handbook of Alkali-Activated Cements, Mortars and Concretes.* Oxford: Woodhead Publishing, pp. 555-604.

Schaetzl, R. & Anderson, S., 2005. *Soils: Genesis and Geomorphology.* 1st ed. New York: Cambridge University Press.

Schulze, D.G., 2005. Clay Minerals. In: D. Hillel, ed. *Encyclopedia of Soils in the Environment.* Oxford: Elsevier, pp. 246-254.

Scrivener, K.L., 2014. Options for the future of cement. *Indian Concrete Journal,* 88(7), pp. 11-21.

Scrivener, K.L., John, V.M. & Gartner, E.M., 2016. *Eco-efficient cements: potential, economically viable solutions for a low-CO2, cement-based materials industry.* UNEP.

Sedmale, G., Korovkins, A., Seglins, V. & Lindina, L., 2013. Application of chemical trated illite clay for development of ceramics products. In: G.A. László, ed. *Iop Conf Ser-Mat Sci.* Miskolc-Lillafüred, Hungary: IOP Publishing, p. 012056.

Seiffarth, T., Hohmann, M., Posern, K. & Kaps, C., 2013. Effect of thermal pre-treatment conditions of common clays on the performance of clay-based geopolymeric binders. *Applied Clay Science,* 73, pp. 35-41.

Shi, C. & Fernández-Jiménez, A., 2006. Stabilization/solidification of hazardous and radioactive wastes with alkali-activated cements. *Journal of Hazardous Materials,* 137(3), pp. 1656-1663.

Silva, P.D., Sagoe-Crenstil, K. & Sirivivatnanon, V., 2007. Kinetics of geopolymerization: Role of Al2O3 and SiO2. *Cement and Concrete Research,* 37(4), pp. 512-518.

Singh, P.S., Trigg, M., Burgar, I. & Bastow, T., 2005. Geopolymer formation processes at room temperature studied by 29Si and 27Al MAS-NMR. *Materials Science and Engineering: A,* 396(1), pp. 392-402.

Sperberga, I., Sedmale, G., Stinkulis, G., Zeila, K. & Ulme, D., 2011. Comparative study of illite clay and illite-based geopolymer products. In: K. Niihara, T. Ohji & Y. Sakka, eds. *3rd International Congress on Ceramics (ICC3).* Osaka, Japan: IOP Publishing, p. 222027.

Steudel, A., Batenburg, L.F., Fischer, H.R., Weidler, P.G. & Emmerich, K., 2009a. Alteration of non-swelling clay minerals and magadiite by acid activation. *Applied Clay Science,* 44(1), pp. 95-104.

Steudel, A., Batenburg, L.F., Fischer, H.R., Weidler, P.G. & Emmerich, K., 2009b. Alteration of swelling clay minerals by acid activation. *Applied Clay Science,* 44(1), pp. 105-115.

Tchadjie, L.N. & Ekolu, S.O., 2018. Enhancing the reactivity of aluminosilicate materials toward geopolymer synthesis. *J Mater Sci,* 53(7), pp. 4709-4733.

Tironi, A., Trezza, M.A., Scian, A.N. & Irassar, E.F., 2013. Assessment of pozzolanic activity of different calcined clays. *Cement and Concrete Composites,* 37, pp. 319-327.

Tong, F., Ji, W., Li, M., Zeng, C. & Zhang, L., 2014. Investigation of the crystallization of zeolite A from hydrogels aged under high pressure. *CrystEngComm,* 16(36), pp. 8563-8569.

Toniolo, N. & Boccaccini, A.R., 2017. Fly ash-based geopolymers containing added silicate waste. A review. *Ceramics International,* 43(17), pp. 14545-14551.

Tsipursky, S.I. & Drits, V., 1984. The distribution of octahedral cations in the 2: 1 layers of dioctahedral smectites studied by oblique-texture electron diffraction. *Clay Miner,* 19(2), pp. 177-193.

U.S. Geological Survey, 2018. *Mineral commodity summaries 2018.* U.S. Geological Survey.

van Deventer, J.S.J., Provis, J.L., Duxson, P. & Brice, D.G., 2010. Chemical Research and Climate Change as Drivers in the Commercial Adoption of Alkali Activated Materials. *Waste and Biomass Valorization,* 1(1), pp. 145-155.

Van Jaarsveld, J.G.S., Van Deventer, J.S.J. & Lorenzen, L., 1997. The potential use of geopolymeric materials to immobilise toxic metals: Part I. Theory and applications. *Minerals Engineering,* 10(7), pp. 659-669.

Vance, E.R. & Perera, D.S., 2009. 18 - Geopolymers for nuclear waste immobilisation. In: J.L. Provis & J.S.J. van Deventer, eds. *Geopolymers.* Woodhead Publishing, pp. 401-420.

Viani, A., Gualtieri Alessandro, F. & Artioli, G., 2002. The nature of disorder in montmorillonite by simulation of X-ray powder patterns. *Am Mineral.* pp. 966-975.

Walkley, B., Rees, G.J., San Nicolas, R., van Deventer, J.S.J., Hanna, J.V. & Provis, J.L., 2018. New Structural Model of Hydrous Sodium Aluminosilicate Gels and the Role of Charge-Balancing Extra-Framework Al. *The Journal of Physical Chemistry C,* 122(10), pp. 5673-5685.

Wang, Q., Zhang, J. & Wang, A., 2013. Alkali activation of halloysite for adsorption and release of ofloxacin. *Applied Surface Science,* 287, pp. 54-61.

Wang, Y.-S., Dai, J.-G., Ding, Z. & Xu, W.-T., 2017a. Phosphate-based geopolymer: Formation mechanism and thermal stability. *Materials Letters,* 190, pp. 209-212.

Wang, Y., Chen, J., Wu, H. & Lei, X., 2017b. Controllable preparation of zeolite P1 from metakaolin-based geopolymers via a hydrothermal method. *Clays and Clay Minerals,* 65(1), pp. 42-51.

Weng, L. & Sagoe-Crentsil, K., 2007. Dissolution processes, hydrolysis and condensation reactions during geopolymer synthesis: Part I—Low Si/Al ratio systems. *J Mater Sci,* 42(9), pp. 2997-3006.

Wolters, F. & Emmerich, K., 2007. Thermal reactions of smectites—Relation of dehydroxylation temperature to octahedral structure. *Thermochimica Acta,* 462(1), pp. 80-88.

Xu, H. & Van Deventer, J.S.J., 2000. The geopolymerisation of alumino-silicate minerals. *International Journal of Mineral Processing,* 59(3), pp. 247-266.

Yao, Z.T., Ji, X.S., Sarker, P.K., Tang, J.H., Ge, L.Q., Xia, M.S. & Xi, Y.Q., 2015. A comprehensive review on the applications of coal fly ash. *Earth-Science Reviews,* 141, pp. 105-121.

Yokoyama, S., Kuroda, M. & Sato, T., 2005. Atomic force microscopy study of montmorillonite dissolution under highly alkaline conditions. *Clays and Clay Minerals,* 53(2), pp. 147-154.

Yousef, R.I., El-Eswed, B., Alshaaer, M., Khalili, F. & Rahier, H., 2012. Degree of reactivity of two kaolinitic minerals in alkali solution using zeolitic tuff or silica sand filler. *Ceramics International,* 38(6), pp. 5061-5067.

Zhang, L., 2013. Production of bricks from waste materials – A review. *Construction and Building Materials,* 47, pp. 643-655.

Zhang, Z., Provis, J.L., Reid, A. & Wang, H., 2014. Geopolymer foam concrete: An emerging material for sustainable construction. *Construction and Building Materials,* 56, pp. 113-127.

Zhang, Z., Provis, J.L., Wang, H., Bullen, F. & Reid, A., 2013. Quantitative kinetic and structural analysis of geopolymers. Part 2. Thermodynamics of sodium silicate activation of metakaolin. *Thermochimica Acta,* 565, pp. 163-171.

Zhang, Z., Wang, H., Provis, J.L., Bullen, F., Reid, A. & Zhu, Y., 2012. Quantitative kinetic and structural analysis of geopolymers. Part 1. The activation of metakaolin with sodium hydroxide. *Thermochimica Acta,* 539(Supplement C), pp. 23-33.

Zhang, Z.H., Zhu, H.J., Zhou, C.H. & Wang, H., 2016. Geopolymer from kaolin in China: An overview. *Applied Clay Science,* 119, Part 1, pp. 31-41.

Zibouche, F., Kerdjoudj, H., de Lacaillerie, J.-B.d.E. & Van Damme, H., 2009. Geopolymers from Algerian metakaolin. Influence of secondary minerals. *Applied Clay Science,* 43(3), pp. 453-458.

Chapter 3 - Research approach

This chapter: defines the scope of investigation and the research questions; explains the overall methodology used; justifies the specific methods and materials used, and describes how the following results chapters link to each other.

3.1 Scope of investigation and research questions

In Chapter 1, it was shown that there is an unmet demand for sustainable, practical and affordable construction materials to provide adequate housing in urban areas of LEDCs. Alkali-activated earth materials are an emerging construction material that may have the potential to fulfil the requirements. From this context, the overall research question is presented:

- Are alkali-activated earth materials viable walling materials for sustainable, practical and affordable mass housing in LEDCs?

In Chapter 2, a review of the literature review showed there is a knowledge gap around the influence of soil compositions on the alkali activation process. Therefore, in order to answer the overall research question, the following technical research questions needed to be answered:

- What are the alkali activation potentials of kaolinite, montmorillonite and illite as individual clay minerals?
- What contribution do the non-clay minerals in soil make to alkali activation?
- Which soil compositions are most suited to stabilisation by alkali activation?

These questions defined the scope of the investigation. The varied and controlled parameters are listed in Table 3-1, and these were assessed through considering the products formed. This excluded other variables from the scope of investigation, including: processing conditions, treatments (such as calcination), and the use of reactive additives (such as fly ash).

The aim of this investigation was not product design – it was not intended to make a construction product from one specific soil. Rather, the aim was to improve the fundamental understanding of this materials family, and its potential to solve a civil engineering problem. As shown in Chapter 2, it is common for studies in this field to perform detailed testing on mechanical properties, but the most pressing knowledge gap in this field is around the effect of soil composition on phase formation. Accordingly, the focus of this investigation was the characterisation of precursors and product phases, rather than detailed measurements of mechanical properties such as strength and durability.

Table 3-1: A list of the parameters that are varied and controlled in the investigations in this thesis.

Varied parameters	**Controlled parameters**
Precursor composition Na:Al molar ratio	Alkaline solution compound Mix consistency Curing temperature Curing time Ageing time

3.2 Methodology

The experimentation for this thesis was designed to understand the behaviour of complex natural materials by isolating their components. As described in Chapter 2, soils have highly variable compositions, simplified as consisting of clay minerals and non-clay components. In addition to this natural complexity, from the precedent of cement-stabilised soil blocks, aggregate would be added to an alkali-activated soil mix.

To break down this multi-component complexity into bitesize parts, a sequence of experiments was designed to build up from simple (individual clay minerals) to complex precursors (an alkali-activated soil and aggregate mix), as shown in Figure 3-1. Firstly, the alkali activation behaviour of kaolinite (Chapter 4), montmorillonite and illite (Chapter 5) in clay minerals in isolation were investigated. As described in Chapter 2, clay minerals are understood to be the largest reactive component of soils in alkali activation, and these three clay minerals are the most common in soils. Secondly, mixtures of clays in different proportions were used as precursors, to understand if their behaviour in a mixture deviated from their behaviour as individuals (Chapter 6). Thirdly, synthetic soils were manufactured, based on the composition of three natural soils, in order to isolate the influence of non-clay components (Chapter 7). Lastly, aggregate was added to one of the natural soils (Chapter 8) and used to produce large scale block specimens, as used in real wall construction. Each experiment built on the results of the previous experiments, to refine understanding of how the different components of soil influence alkali activation behaviour.

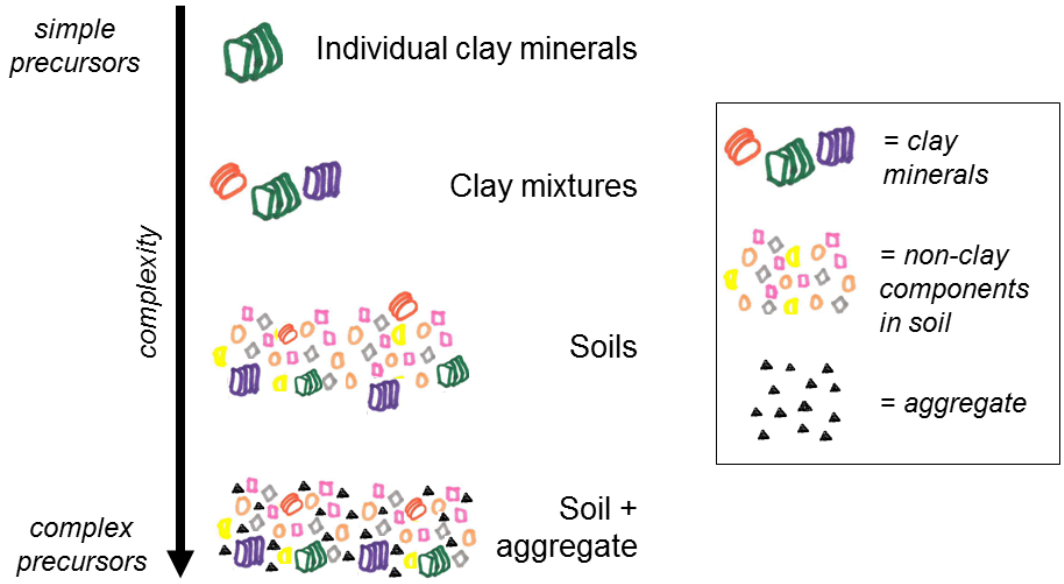

Figure 3-1: Schematic diagram showing the development of precursor complexity throughout the thesis investigation.

The typical methodology used in this research area is to use a single soil precursor, and vary the parameters regarding the activating solution and curing conditions. As described in Chapter 2, this has given a detailed level of knowledge for optimising these processing conditions, but only for a single soil composition in each research project. In contrast, the overall methodology of this thesis and the constituent studies was to vary soil composition factors in a systematic way, as shown visually in Figure 3-2. Complexity was built with each following study to include mixtures of minerals, real soils and larger scale blocks with aggregates. Through this innovative approach, it was intended to determine in a systematic way which soil compositions are most promising for alkali activation, rather than just optimising the activation of a single soil.

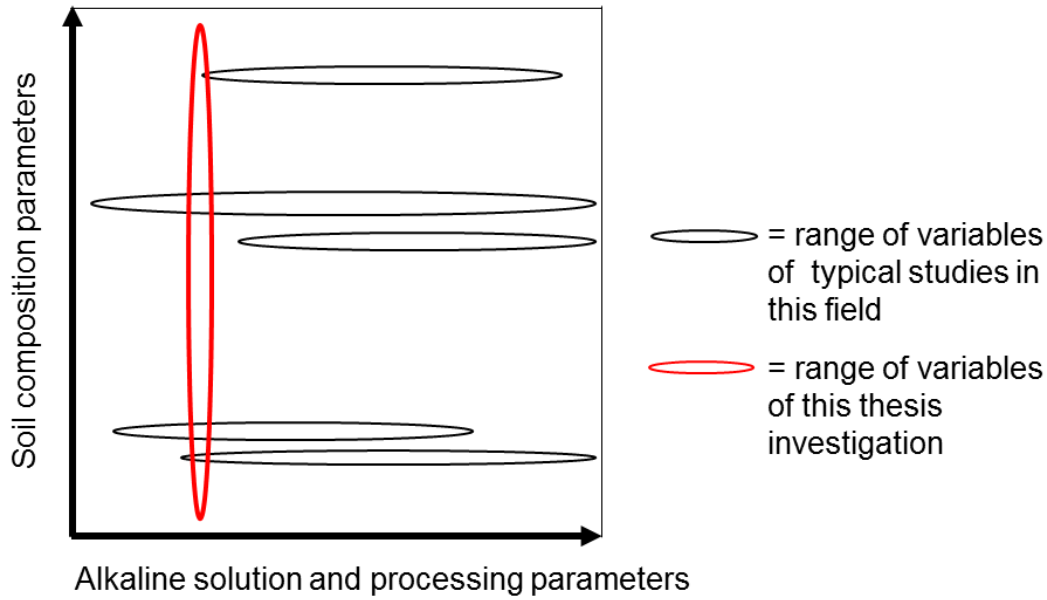

Figure 3-2: Schematic diagram comparing the range of variables investigated in this thesis and in typical studies in this field.

3.3 Materials

3.3.1 Clays and soils

Regarding the clays used, a balance was sought between what is representative of clays in soils, purity and previous characterisation in other studies (Table 3-2). As a result, purified clays were sourced for kaolinite (Imerys Speswhite Kaolin) and montmorillonite (Sigma-Aldrich K10 Montmorillonite #69866, and Honeywell Fluka Bentonite #285234). Illite in isolation has no commercial purpose, so a purified form could not be sourced. An unpurified but well-characterised illite was used instead (Clay Minerals Society Illite IMt-2 Silver Hill, Montana). The cost of the montmorillonite and illite clays was much more expensive than the kaolinite, which limited some experiments.

Table 3-2: Summary of clays used

Clay used	**Clay mineral**	**Treatment**
Imerys Speswhite Kaolin	Kaolinite	Purified
Sigma-Aldrich K10 Montmorillonite #69866.	Montmorillonite	Purified and acid-washed
Honeywell Fluka Bentonite #285234.	Montmorillonite	Purified
Clay Minerals Society Illite IMt-2 Silver Hill, Montana	Illite	none

Regarding the soils used, a balance was sought between having a spread of geographical locations near to urban areas, a variety of mineralogical compositions, and previous characterisation in other studies (Table 3-3).

Table 3-3: Summary of soils used

Soil used	**Clay minerals** (in descending order of wt.%)
Bristol	Kaolinite, illite, montmorillonite
Bengaluru	Kaolinite
Khartoum	Montmorillonite, kaolinite, illite

Regarding treatments, none were used. Amongst the different treatments, it is well-established that thermal activation in particular increases the reactivity of clay minerals in alkali activation (as explained in Chapter 2). However, this additional process would not be feasible for this construction context, as it requires tightly controlled temperatures tailored to the clay mineralogy (Hollanders *et al.*, 2016). It would also

increase the embodied impacts of the material considerably (Habert and Ouellet-Plamondon, 2016).

3.3.2 Alkaline activators

Regarding activating solution composition, although it is well-established that additional soluble silicates - such as solutions from $Na_2O{\cdot}nSiO_3$ (with a typical range of n = 1.55 – 3.97) (Lagaly *et al.*, 2000) - are conducive to geopolymer formation (as explained in Chapter 2), these were not used. Firstly, this would have added another variable into the experimental design, giving an unfeasible number of systems. Secondly, it would have obstructed the aim of understanding the fundamental behaviour of the clay minerals themselves. Therefore, NaOH was chosen as the sole activating solution compound. It is the most commonly used compound in previous studies (as described in Chapter 2), and is cheaper and more widely available than KOH or other alkali metal hydroxides.

3.4 Synthesis methods

A simple synthesis process was used to make small cylinder samples. This was designed to mimic production processes appropriate to LEDCs as far as possible in a laboratory setting. This process was kept as consistent as possible between the different studies. In each study, a control sample was also made, using water, rather than an activating solution.

The stages in synthesis were (also shown visually in Figure 3-3):

1. Preparing the activating solution
2. Preparing the dry clay/soil (includes mixing clay/soil components in Chapters 6, 7 and 8)
3. Mixing the dry clay/soil with the activating solution
4. Tamping the wet mixture into the mould
5. Curing in an oven
6. Demoulding

A variation on this process was used for the synthesis of scaled-up blocks – this is described in Chapter 8.

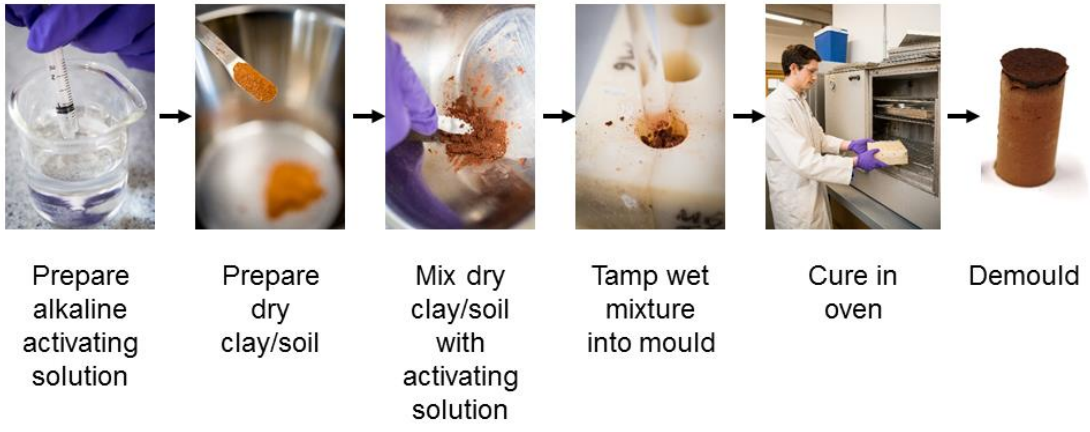

Figure 3-3: Visual summary of the stages in the synthesis process

The activating solution composition was determined from the desired Na:Al molar ratio, and the plasticity properties of a given clay or soil. Because the behaviour of the individual clays had not previously been systematically investigated using comparable conditions, an Na:Al range from 0.25 - 1.5 was used in Chapters 4 and 5. Once it was established that Na:Al = 1 was sufficient to cause the majority of the clay precursor to react without using a theoretical excess of Na, this was used as the fixed Na:Al value in Chapters 6 and 7.

To calculate the quantities of dry NaOH and water required to meet a specified Na:Al value whilst maintaining plastic limit consistency, an iterative solving function was used. This was required given the interdependence of the system parameters, as shown schematically in Figure 3-4. The change in the precursors' plastic limit with NaOH concentration was measured experimentally, and by fitting a best fit line to those data, the plastic limit of each precursor could be predicted for a given NaOH concentration. By using the equation for the best fit line, amounts of water and NaOH were iteratively generated to achieve a system where the conditions of desired Na:Al ratio and plastic limit consistency were both met. Further details are provided in the Methods and Materials sections of Chapters 4, 5, 6 and 7.

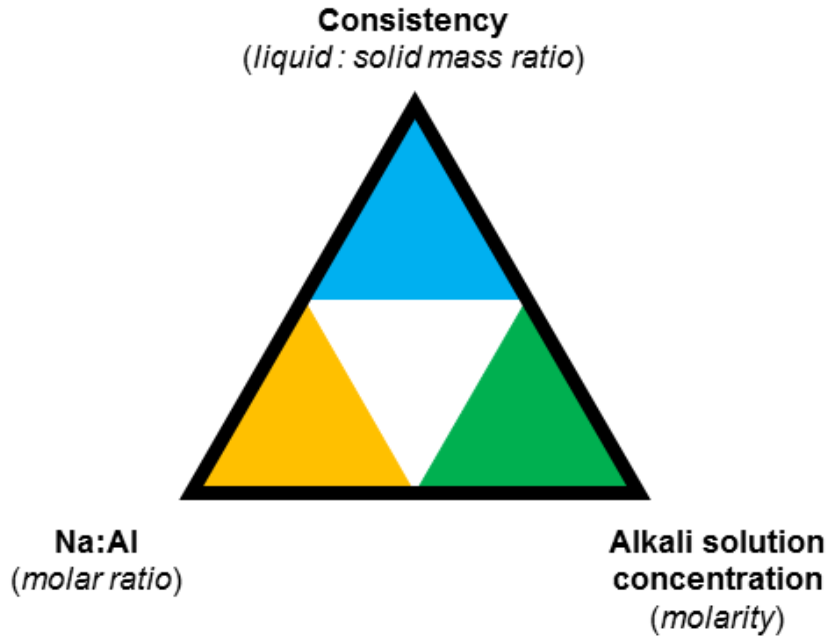

Figure 3-4: Schematic diagram showing the interdependence of consistency, Na:Al and alkali solution concentration, with their respective units.

The curing conditions of 80°C for 24 h were chosen based on optimal values identified by previous studies investigating curing conditions for uncalcined clays and soils (Chapter 2).

3.5 Characterisation techniques

Characterisation techniques were chosen based on established methods for clay minerals (Christidis, 2011), soils (Ulery and Drees, 2008) and alkali activated materials (Duxson et al., 2007; Provis et al., 2015). Techniques were used to characterise the precursors as well as identify phase transformations and microstructural changes in the alkali-activated samples. Determining the phase assemblages in each system was not possible with a single technique. It was therefore crucial to use a range of techniques, as each technique gave complementary information to the others. However, due to the constraints of cost, availability and time, the full range of techniques were not used in all studies. Characterisations of the alkali-activated materials were done at 28 days ageing time. This time was a compromise between a sufficiently long time for the reaction to occur, and a practical length for testing. This is also an ageing time commonly used in the testing of cementitious materials. Testing conditions used for each technique varied between the constituent studies, so full details are specific to each chapter and are provided there. A brief description of why each technique was used is given here:

Powder X-ray diffraction (PXRD) was used to identify crystalline phases, as well as to determine whether a large quantity of an amorphous phase was present. In all cases, oriented powder samples were used, prepared using a glass slide to press down the powder onto another glass slide. This preparation was chosen in order to achieve preferential orientation of the plate-like clay minerals along their basal plane, and thus make them easier to identify when present in small quantities (Brindley and Brown, 1980).

Scanning electron microscopy (SEM) was used to examine systems' microstructure. Fracture surfaces of samples were used, to examine the morphology of phases more clearly. Polished cross-sections were not used due to the friability of many of the samples. Secondary electrons were used for the image signal, to give a clearer image of the topography.

Thermal gravimetric analysis (TGA) with mass spectrometry (MS) of the evolved gases was primarily used to determine the amount of H_2O and OH groups present in different phases. C and CO_2 were also monitored to assist in identifying the presence of phases containing carbon.

^{27}Al and ^{29}Si magic angle spinning (MAS) nuclear magnetic resonance (NMR) spectrometry were used to measure the distribution of bonding environments for Al and Si atoms in the samples. The observed coordination changes were used to describe the effects of alkali activation.

Fourier Transform Infrared (FTIR) spectroscopy was used to give supplementary information about the bonding environments of atoms, particularly the Si-O-T bonding environment. The Si-O-T bands gave information about bonding in the precursor clay minerals as well as the zeolite and geopolymer reaction products.

Unconfined compressive strength (UCS) testing was used in Chapter 8 to measure the load-bearing capacity of cured blocks. As previously described, structural characterisation was not the primary aim of this thesis, so these were treated as indicative measurements to supplement the chemical and microstructural characterisation.

Photos of the cured samples were taken to show the macroscopic changes that happened during curing, such as shrinkage, expansion and colour changes. Where possible, these changes were then related to the phase and microstructural analysis.

In addition to these, some techniques were used for the precursors only:

Brunauer-Emmett-Teller (BET) nitrogen porosimetry was used to measure the specific surface area of the precursors, to indicate how much surface area was available for the alkali activation reaction.

Energy Dispersive X-ray (EDX) spectroscopy was used to measure chemical oxide composition of the precursors, and in particular to assess the presence of minor elements.

Plastic limits of precursors were measured using the Atterberg test (BSI, 1990) to determine the amount of water required to attain the plastic state. When in the plastic state, a plastic material – such as a clay or soil - can be moulded without breaking, and hold its shape (Reeves *et al.,* 2006). This concept is mostly used in soil mechanics but also has industrial relevance to construction materials, as a soil in its plastic state can be extruded to form a block (Maskell *et al.,* 2013). Depending on the blockmaking process used (e.g. block press) and exact conditions used, the optimal amount of water required to form a block will differ from the plastic limit. However, given the plastic limit is an easily measured property that is comparable across clays and soils, this was used to determine the amount of water or NaOH solution to add to the precursor. When determining the amount of NaOH solution required for a precursor to achieve the plastic state, the Atterberg test was adapted to exclude the mass of NaOH from being considered with the mass of clay in the dried sample (Bain, 1971).

For the natural soils, particle size distribution was measured using a combination of wet-sieving, to measure particle grading from 2 mm – 63 μm, and hydrometer testing, to measure particle grading < 63 μm by using the principle of Stokes' Law to measure

particle size by the time taken for particles to fall out of suspension in water (BSI, 1990).

3.6 Outline of results chapters

The following five chapters each describe and interpret the results of an individual study (Table 3-4). These build up in precursor complexity, from individual clays (Chapters 4 and 5) to mixtures of clays (Chapter 6), natural and synthetic soils (Chapter 7) and finally to natural soils mixed with aggregates (Chapter 8).

Table 3-4: An outline of the systems studied in Chapters 4-8.

Chapter#	**Material system**	**Aspect of soils tested**	**Characterisation**
4	Clay	Behaviour of 1:1 clay (kaolinite)	PXRD, SEM, TGA, FTIR, ^{27}Al and ^{29}Si MAS-NMR, FTIR, photos
5	Clay	Behaviour of 2:1 clays (montmorillonite and illite)	PXRD, SEM, TGA, FTIR, ^{27}Al and ^{29}Si MAS-NMR, FTIR, photos
6	Mixtures of clays	Differences in behaviour of clays when present in mixtures	PXRD, SEM, FTIR, photos
7	Natural and synthetic soils	Influence of non-clay components	PXRD, SEM, TGA, FTIR, photos
8	Natural soil mixed with aggregate	Influence of addition of aggregate and scaling up	PXRD, SEM, photos, UCS, drying.

References

Bain, J., 1971. A plasticity chart as an aid to the identification and assessment of industrial clays. *Clay Miner,* 9(1), pp. 1-17.

Brindley, G.W. & Brown, G., 1980. *Crystal structures of clay minerals and their X-ray identification.* London: Mineralogical Society.

BSI, 1990. BS 1377-2:1990 Methods of test for soils for civil engineering purposes. Classification tests

Christidis, G.E., 2011. *Advances in the characterization of industrial minerals.* London: The Mineralogical Society of Great Britain and Ireland.

Duxson, P., Fernández-Jiménez, A., Provis, J.L., Lukey, G.C., Palomo, A. & van Deventer, J.S.J., 2007. Geopolymer technology: the current state of the art. *J Mater Sci,* 42(9), pp. 2917-2933.

Habert, G. & Ouellet-Plamondon, C., 2016. Recent update on the environmental impact of geopolymers. *RILEM Technical Letters,* 1, pp. 17-23.

Hollanders, S., Adriaens, R., Skibsted, J., Cizer, Ö. & Elsen, J., 2016. Pozzolanic reactivity of pure calcined clays. *Applied Clay Science,* 132-133, pp. 552-560.

Lagaly, G., Tufar, W., Minihan, A. & Lovell, A., 2000. Silicates. In: B. Elvers, ed. *Ullmann's Encyclopedia of Industrial Chemistry.* Hoboken, USA: Wiley-VCH.

Maskell, D., Heath, A. & Walker, P., 2013. Laboratory scale testing of extruded earth masonry units. *Materials & Design,* 45, pp. 359-364.

Provis, J.L., Palomo, A. & Shi, C., 2015. Advances in understanding alkali-activated materials. *Cement and Concrete Research,* 78, pp. 110-125.

Reeves, G.M., Sims, I. & Cripps, J.C., 2006. *Clay materials used in construction.* London: Geological Society.

Ulery, A.L. & Drees, L.R., 2008. *Methods of Soil Analysis Part 5—Mineralogical Methods.* Madison, WI: Soil Science Society of America.

Chapter 4 - Alkali activation of kaolinite

In this chapter, the alkali activation behaviour of kaolinite, the most common 1:1 clay mineral in soils, is investigated. This is presented as a separate chapter to montmorillonite and illite (Chapter 5) - these are 2:1 clays and are therefore better suited to comparisons between each other.

This chapter has been revised following suggestions from the examiners, so the article presented here has minor differences compared to the published article.

Declaration of authorship

This declaration concerns the article entitled:									
A mild conditions synthesis route to produce hydrosodalite from kaolinite, compatible with extrusion processing									
Publication status (tick one)									
draft manuscript		**Submitted**		**In review**		**Accepted**		**Published**	✓
Publication details (reference)	Marsh, A., Heath, A., Patureau, P., Evernden, M., Walker, P. (2018). "A mild conditions synthesis route to produce hydrosodalite from kaolinite, compatible with extrusion processing." Microporous and Mesoporous Materials 264: 125-132.								
Candidate's contribution to the paper (detailed, and also given as a percentage).	The candidate predominantly executed the… Formulation of ideas: A.Marsh (80%) developed the idea for this study, with suggestions and guidance given by the co-authors (20%) (i.e. supervisors). Design of methodology: A.Marsh (80%) developed the methodology for this study, with suggestions and guidance given by the co-authors (20%) (i.e. supervisors). Experimental work: A.Marsh undertook the majority of experimental work and analysis (80%). P.Patureau undertook the Le Bail and Rietveld refinements of the powder XRD data (20%). ^{27}Al and ^{29}Si MAS-NMR measurements were undertaken by the EPSRC Solid-State NMR Service, and analysed by A.Marsh. Presentation of data in journal format: A.Marsh (90%) undertook all formatting except for Figures 4-4 and 4-5, by P.Patureau (10%).								
Statement from Candidate	This paper reports on original research I conducted during the period of my Higher Degree by Research candidature.								
Signed						**Date**	30/10/2018		

Published as Marsh, A, Heath, A, Patureau, P, Evernden, M & Walker, P 2018, 'A mild conditions synthesis route to produce hydrosodalite from kaolinite, compatible with extrusion processing', Microporous and Mesoporous Materials, vol. 264, pp. 125-132 and available online via: https://doi.org/10.1016/j.micromeso.2018.01.014

A mild conditions synthesis route to produce hydrosodalite from kaolinite, compatible with extrusion processing

Abstract

Hydrosodalites are a family of zeolitic materials which have a diverse range of possible applications such as water desalination. Typical synthesis methods are relatively complex, using hydrothermal production and pre-processing and it is desirable to use lower energy and more cost-effective processing routes. For the first time, a low temperature, non-hydrothermal synthesis procedure for hydrosodalites, compatible with extrusion processing, is demonstrated. Kaolinite precursor, without calcination, was activated with a sodium hydroxide solution and formed at a workability consistent with extrusion. The cured samples were characterised using a range of advanced analytical techniques including PXRD, SEM, TGA, ^{27}Al and ^{29}Si-MAS-NMR, and FTIR to confirm and quantify conversion of the precursor to product phases. The synthesis consistently formed a 8:2:2 basic hydroxysodalite phase and the reaction was shown to follow a largely linear relationship with Na:Al until full conversion to the hydrosodalite phase was approached. The hydrosodalite became more ordered for Na:Al ≥ 1. There is good agreement between quantitative measurements made using PXRD, TGA and ^{29}Si-MAS-NMR methods, providing confidence in the results. It has been shown that it is possible to synthesise hydrosodalite materials in a consistent and predictable manner, using non-hydrothermal methods, at the viscosity used for extrusion processing. This novel processing route could reduce production costs, production impacts and open up new applications for this important family of materials.

4.1 Introduction

Hydrosodalites are a member of the zeolite family. Their defining features are their aluminosilicate framework of cubic symmetry (S.G. *P*-43*n*) (Wiebcke *et al.*, 1992), formed by alternating SiO_4 and AlO_4 tetrahedras shown in Figure 4-1 (Pauling, 1930). These sodalite cages (β-cages) can contain a wide range of guest species (Engelhardt *et al.*, 1992; Newsam, 1986). The sub-family of hydrosodalites itself contains two separate groups within the general chemical formula $Na_{6+x}(Al_6Si_6O_{24})(OH)_x \cdot nH_2O$. These are: basic hydrosodalite (or hydroxysodalite hydrate) for x = 2, n= 8, with a chemical formula of $Na_8(Al_6Si_6O_{24})(OH)_2 \cdot 2H_2O$ (abbreviated as 8:2:2), and non-basic hydrosodalite for x = 0, n =2, with a chemical formula $Na_6(Al_6Si_6O_{24}) \cdot 8H_2O$ (abbreviated as 6:0:8) (Felsche and Luger, 1987; Wiebcke *et al.*, 1992). The cage structure of sodalites gives them desirable properties including selective adsorption (Newsam, 1986), fluorescence (Kirk, 1955) and thermal stability. Previous research has considered applications as diverse as wastewater treatment (Johnson and Worrall, 2007), water desalination (Khajavi *et al.*, 2010; Wang *et al.*, 2016), admixtures in cement mortars (Sasnauskas and Palubinskaite, 2005), and use in optics and computation (Stucky and James, 1990).

It is well established that kaolinite can be reacted with sodium hydroxide solutions to form hydrosodalite under hydrothermal conditions (Barrer *et al.*, 1968). Kaolinite is a phyllosilicate mineral, with an ideal chemical formula $Al_2(Si_2O_5)(OH)_4$. Each layer is formed of a gibbsite and silica sheet, with the unit cell having the *C*1 space group (Bish, 1993), as shown in Figure 4-1. Hydrogen bonding between layers forms large stacks, giving little opportunity for interlayer cation adsorption (Bergaya *et al.*, 2013). Kaolinite is a common clay mineral found in soils and deposits, and is an inexpensive feedstock if not highly purified. Purified kaolinite is readily available and is used in ceramics, paper production, medicines and numerous other applications.

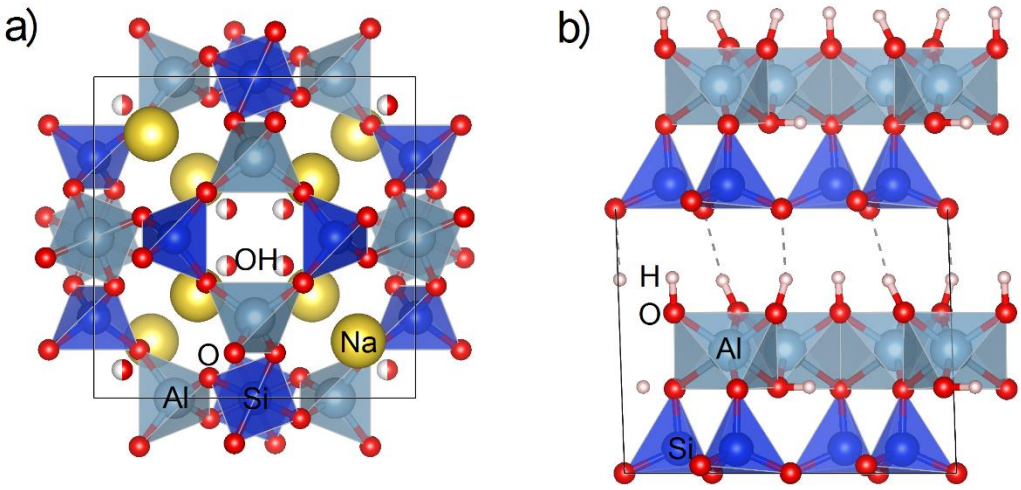

Figure 4-1: The structures of a) sodalite (8:2:2 hydroxysodalite), using structural parameters by Kendrick and Dann (2004), and b) kaolinite, using structural parameters by Bish (1993). Both structures are viewed along the a axis with coordination polyhedra shown for Al and Si. Images were generated in VESTA.

The synthesis of zeolitic products is generally by alkali activation of an aluminosilicate and the product phase is strongly determined by the processing conditions used. Hydrosodalite has been shown to be favoured over formation of other zeolitic phases by the following processing conditions: synthesis time between 24 and 72 hours (Temuujin *et al.*, 2002); solid:liquid ratios of > 5 (Alkan *et al.*, 2005); NaOH solution concentrations of > 3 M, and synthesis temperatures of 150-200 °C (Querol *et al.*, 2002). Hydrothermal synthesis is by far the most commonly used method (Querol *et al.*, 2002), whilst more complex two-step synthesis methods have also been used involving alkali pre-fusion at elevated temperatures (Belviso *et al.*, 2017). It is also common to calcine kaolinite by heating above 700 °C to form metakaolin, in order to increase reactivity before synthesis (Passos *et al.*, 2017).

Even for hydrosodalite which prefers low solid:liquid ratios (Alkan *et al.*, 2005), synthesis routes typically use an excess quantity of NaOH solution, which makes them incompatible for processing involving extrusion, a technique which is frequently used for production of ceramics. Extrusion is an adaptable, continuous processing technique, which requires that a clay-based feedstock is a wetted mixture in its plastic state (Maskell *et al.*, 2013). In the plastic state, a clay-based material is able to be moulded without cracking and has the ability to hold its new shape without support (Barnes, 2000). This is typically done at a moisture content between the plastic limit and liquid limit (Wagner, 2013), which is the moisture content range over which the clay

can be moulded but will not flow as a liquid. Extrusion processing could increase the types of products and applications where hydrosodalites could be used.

Given that calcination and mid-temperature synthesis both involve an additional heating step, a synthesis route at low temperature involving no thermal pre-treatment could be desirable for reducing energy and for practicality. The proportions of phases formed by the reaction of kaolinite with sodium hydroxide have previously been investigated in relation to the nature of kaolinite used (Heller-Kallai and Lapides, 2007), or addition of different volumes of an activating solution at given pH (Sruthi and Reddy P, 2017), rather than the Na:Al molar ratio for a mixture of constant workability. Whilst Heller-Kallai and Lapides demonstrated proof of concept for non-hydrothermal synthesis (Heller-Kallai and Lapides, 2007), a systematic understanding of the reaction for these conditions has not previously been developed. A synthesis route using lower temperature and atmospheric conditions would make production cheaper and less energy-intensive.

In this study, hydrosodalite-kaolinite samples were made with a range of Na:Al ratios from 0.25-1.5. They were characterised to determine the amounts of hydrosodalite formed and unreacted kaolinite for each Na:Al ratio, comparing measurements made using PXRD, ^{29}Si MAS-NMR and TGA.

4.2 Experimental

4.2.1 Materials

Imerys Speswhite (mined from Cornwall, U.K.) kaolinite was used as the aluminosilicate precursor. The chemical composition was determined by energy dispersive X-rays (JEOL SEM6480LV with Oxford INCA X-Act SDD X-ray detector), at an accelerating voltage of 20 kV, a chamber pressure of between 10 – 30 Pa, a Si wafer as a standard, and measuring 4 scan areas. The precursor powder was mounted on a sticky carbon tab on top of an aluminium stub, and was not coated. Standard errors in composition were calculated from the variation in values between the different area scans. This showed minor amounts of iron, potassium and magnesium were present (Table 4-1), believed to be unreactive in the present conditions. Specific surface area was determined using the BET method (Brunauer *et al.*, 1938), using a Micromeritics 3Flex. 1 g of precursor powder was degassed under vacuum conditions at 150°C for 14 h, before testing. The measured specific surface area was 11.9 m^2g^{-1}. It was activated using sodium hydroxide pellets of >98% purity (Sigma-Aldrich, product no. 06203).

Table 4-1: Chemical composition of kaolinite precursor in oxide wt%.

Oxide	**Al_2O_3**	**Fe_2O_3**	**K_2O**	**MgO**	**SiO_2**	**Total**
wt % (std error)	40.11 (0.15)	0.95 (0.06)	2.06 (0.09)	0.04 (0.04)	56.83 (0.15)	100

4.2.2 Synthesis procedure

The compositions in Table 4-2 were determined to provide samples of pre-determined Na:Al ratio, whilst maintaining the wet mix workability at the plastic limit. This was done by initially undertaking Atterberg plastic limit measurements (Wagner, 2013) for kaolinite over a range of sodium hydroxide solution concentrations (BSI, 1990). From these data a best fit line was plotted to extrapolate the volume of solution required to reach plastic limit consistency for a given concentration (Figure 4-2). A correction was made to exclude the mass of the sodium hydroxide from the solids mass in the plastic limit calculations (Bain, 1971). Only small changes in plastic limit were observed, as expected due to kaolinite's low cation exchange capacity (Bergaya *et al.*, 2013).

Table 4-2: Composition of hydrosodalite samples for chemical characterisation.

Name	0.25-Na:Al	0.5-Na:Al	0.75-Na:Al	1-Na:Al	1.25-Na:Al	1.5-Na:Al
Na:Al molar ratio	0.25	0.5	0.75	1	1.25	1.5
Concentration of activating solution (molarity)	5.2	9.5	13.2	16.2	18.3	19.7

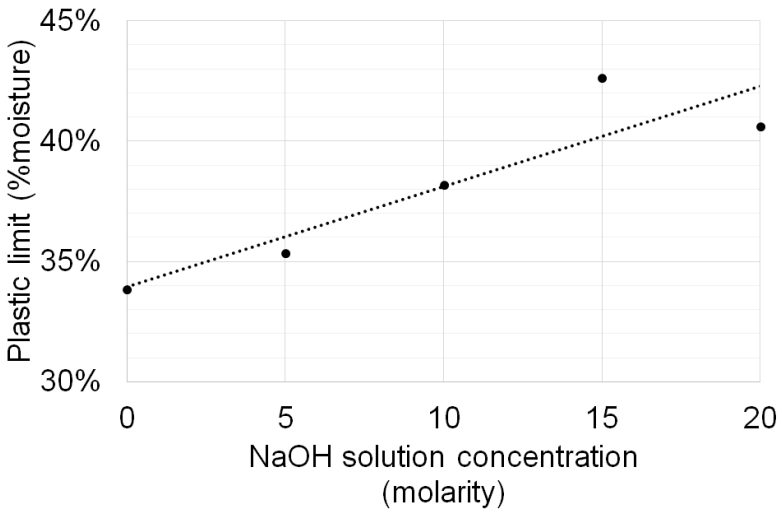

Figure 4-2: The change in kaolinite's plastic limit with sodium hydroxide solution concentration.

The kaolinite was activated by adding a sodium hydroxide solution. Solutions of different concentrations were prepared by adding sodium hydroxide pellets to distilled water, mixed with a magnetic stirrer (Stuart UC152 heat-stir) for a minimum of 2 hours until fully dissolved and then allowed to cool. Kaolinite was pre-dried in a 105 °C oven, and left to cool. Varying quantities of activating solutions were added to 25 g of kaolinite, as given in Table 4-2. The mixture of activating solution and kaolinite was mixed by hand for 3 minutes, providing a consistent and well-distributed mixture. The high viscosity of the samples allowed them to be compacted by hand into 18mm x 36mm cylindrical Teflon moulds by tamping with a glass rod in three layers for each sample, using 25 blows for each layer. Samples were cured in an air atmosphere in a 80°C oven for 24 hours in their moulds, and after demoulding stored in a controlled environmental room at 20 ± 0.5°C and 50 ± 2.5 % relative humidity.

4.2.3 Characterisation methods

The set of characterisations was performed at 28 ± 2 days ageing time, and (with the exception of SEM imaging) was done using powders prepared from the cured samples. These were ground by hand, having been wetted with isopropanol to avoid damaging the kaolinite's crystal structure (Moore and Reynolds, 1997). Powders were ground

until there was no further discernible reduction in particle size, and so were comparable between samples. Any variation in particle size of the ground powders was not expected to have any noticeable effect on characterisation results. The intention of the testing was to attempt to quantify kaolinite to hydrosodalite conversion, and develop a fundamental understanding of the mechanisms and products formed.

Powder X-ray diffraction (PXRD) analysis was undertaken to identify phases with a Bruker D8 Advance instrument using monochromatic CuKα1 L3 (λ = 1.540598 Å) X-radiation and a Vantec superspeed detector. A step size of $0.016^0(2\theta)$ and step duration of 0.3 seconds were used. Phase identification was performed using Bruker EVA software, using reference patterns from the Joint Committee on Powder Diffraction Standards (JCPDS) database. Le Bail extractions and Rietveld refinements of the structure were performed using JANA 2006 (Petříček *et al.*, 2014) and the Cheary Coelho fundamental approach for XRD profile parameters (Cheary and Coelho, 1992). Quartz was used as an internal standard. The refined patterns were plotted in arbitrary units, without normalisation. For determining relative differences of a given pattern to a well-defined pattern (the original precursor material) prepared in the same manner, the limitations of hand grinding and Rietveld refinement for semi-quantitative XRD analysis were deemed acceptable (Kahle *et al.*, 2002).

Thermogravimetric analysis (TGA) was undertaken using a Setaram Setsys Evolution TGA over a range of 30 to 1000 °C at a heating rate of 10 °C/minute. An air atmosphere was used, with a flow rate of 20 ml/minute. A connected mass spectrometer was used (Pfeiffer Omni) to identify whether evolved gas species contained OH, H_2O, C or CO_2.

Fourier Transform Infrared Spectroscopy (FTIR) was used to characterise molecular bonding, using a Perkin-Elmer Frontier with a diamond Attenuated Total Reflectance (ATR) head. Spectra were collected over a range of 4000-600 cm^{-1} using a resolution of 4cm^{-1} and 5 scans per spectrum. Corrections were made for ATR and background using Perkin-Elmer Spectrum software.

Magic angle spinning (MAS) nuclear magnetic resonance (NMR) spectra were measured for ^{27}Al and ^{29}Si to characterise coordination states, using a Varian VNMRS (9.4 T) in direct excitation. The ^{27}Al spectra were obtained with a 104.199 MHz field, using a sample spinning frequency of 14 kHz in a 4 mm rotor, a pulse duration of 1 µs, an acquisition time of 10 ms, a recycle time of 0.2 s, line broadening of 0.005 s, and between 6000 - 7000 scans were used for each spectrum. The ^{29}Si spectra were obtained with a 79.438 MHz field (79.435 MHz for Kao), using a sample spinning frequency of 6.08 kHz (6 kHz for Kao) in a 6 mm rotor, a pulse duration of 4 µs, an acquisition time of 20 ms, a recycle time of 2 s, line broadening of 0.02 s, and between

1360 - 3000 scans were used for each spectrum. Proton decoupling was used at 61.0 kHz for Kao, and at 62.5 kHz for Kao-0.25Na:Al, Kao-0.5Na:Al and Kao-0.75Na:Al. The other spectra were recorded without decoupling, which appeared to make very little difference to the appearance of the spectra. Chemical shifts were referenced to 1 M aq. $Al(NO_3)_3$ for ^{27}Al and tetramethylsilane for ^{29}Si. Spectra have been normalised to the height of the most intense line in the spectrum.

The proportion of kaolinite consumed was estimated by integrating the peaks corresponding to kaolinite and hydrosodalite in the ^{29}Si MAS-NMR spectra (deconvoluted as required when overlapping) (Kinsey *et al.,* 1985). The area fraction of the kaolinite peak from the total peak area in a given sample's spectrum was assumed as equivalent to phase proportion, since ^{29}Si is a spin-half nucleus and does not suffer quadrupolar effects (Apperley *et al.,* 2012). A Lorentzian profile was used for deconvolution as it gave a better fit to the measured curves than a Gaussian profile. These results are presented collectively alongside the values from the other techniques in Section 4.4.2. A detailed description of the deconvolution process is given in the Appendix.

Scanning electron microscope (SEM) imaging was used to characterise phase size and morphology, using a JEOL SEM6480LV in secondary electron mode with an accelerating voltage (AV) of 10kV. Bulk specimens were sputter coated with gold for 3 minutes. Because the SEM used a tungsten filament, an AV of 10 kV was selected as an optimal balance between the tendencies towards a noisy image at lower AV, and lower resolution at higher AV. Unpolished samples were used to enable easier distinction of particle morphology in the microstructures, and also because of the friability of some of the samples.

4.3 Results

4.3.1 PXRD phase analysis

The PXRD pattern of the precursor clay gave kaolinite clay mineral (Powder Diffraction File (PDF)# 01-079-1570) as the major phase, with muscovite (PDF# 01-084-1304) and quartz (PDF# 00-046-1045) present as minor phases (Figure 4-3), as expected from a Cornish residual deposit (Thurlow, 2005). X-Ray diffraction patterns were also recorded for each cured sample and compared with the kaolinite precursor (Figure 4-4). New peaks in the cured samples were assigned to hydrosodalite (PDF# 00-042-0215), with a basic hydroxysodalite 8:2:2 structure. The patterns presented in Figure 4-4 shows that the intensity of the kaolinite peaks decreases while the intensity of the hydrosodalite peaks increases with increasing Na:Al ratio, indicating kaolinite was consumed during the production of hydrosodalite, as expected. As no evidence was found of the formation of a disordered phase, it was assumed that all the phases present in the samples are either hydrosodalite or the crystalline structures in the kaolinite precursor.

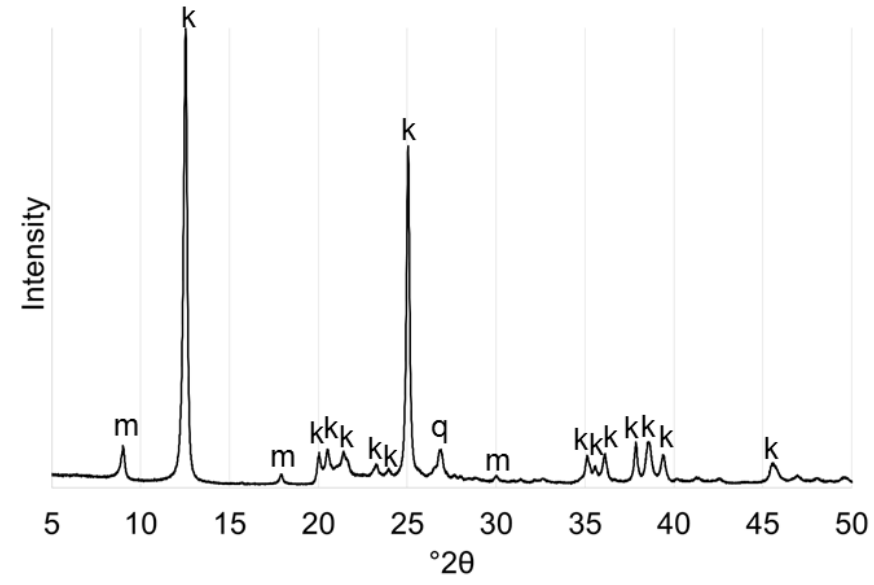

Figure 4-3: PXRD pattern of kaolinite precursor, indexed as: k = kaolinite; m = muscovite; q = quartz.

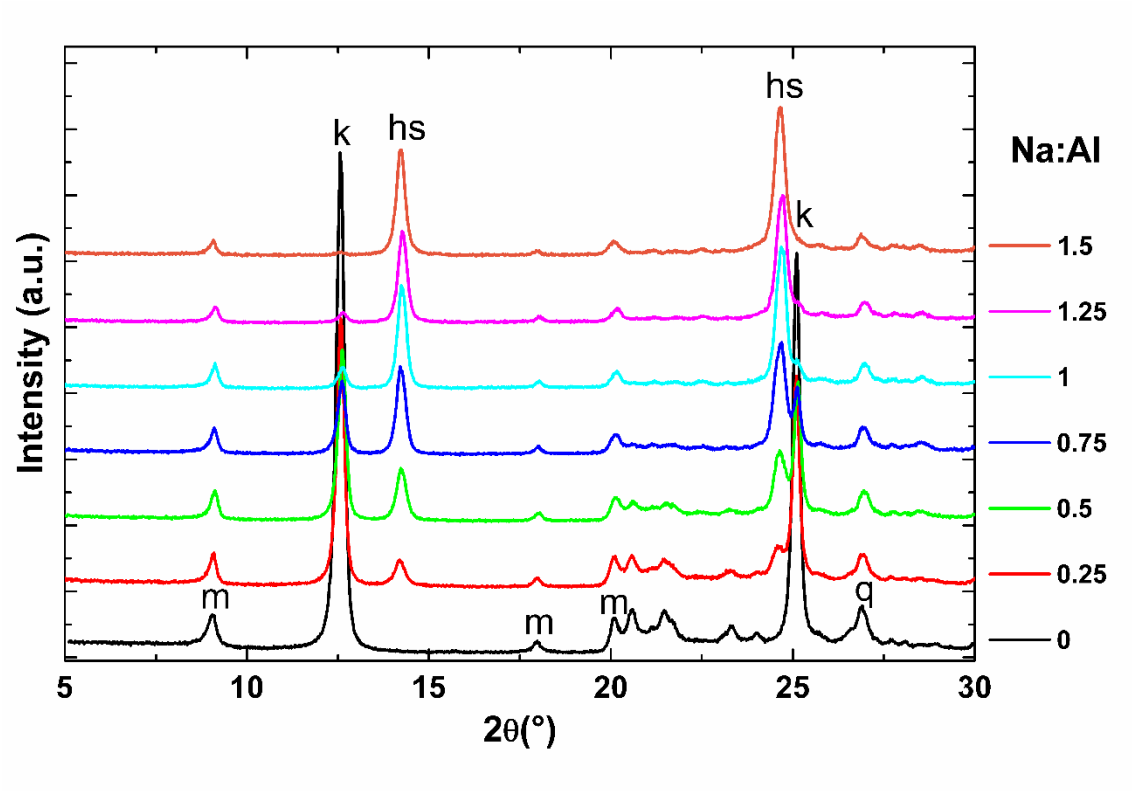

Figure 4-4: PXRD patterns of the initial kaolinite clay and the cured samples. Peaks which do not change are labelled on the Na:Al = 0 pattern, as m = muscovite, q = quartz. Peaks which do change are labelled on the Na:Al = 1.5 pattern, as k = kaolinite, hs = hydrosodalite.

LeBail structure extractions were performed for the clay and each cured sample using structural models for kaolinite (Bish, 1993), quartz (Dusek *et al.*, 2001), muscovite (Guggenheim *et al.*, 1987) and hydroxysodalite (Kendrick and Dann, 2004) from the literature. The only observable change in the kaolinite phase's lattice parameters with the increase of Na:Al ratio was the monotone increase of the α-angle from 91.6° to 92.5°. Although the magnitude of this increase is significant, this distortion is rather small considering the triclinic lattice of kaolinite, and neither does it affect the structure of the aluminosilicate layers or the distance between them. On the other hand, the sodalite cubic lattice shrinks from Na:Al = 0.25 - 1, then stabilizes for Na:Al> 1. This difference of 0.03 Å is probably due to slight disorder in the lowest Na:Al ratio samples.

The good agreement achieved between the models cited above and the experimental data allowed Rietveld refinements to be undertaken for each pattern in order to estimate the proportion of kaolinite consumed in function of the Na:Al molar ratio, and an example is shown in Figure 4-5. Rietveld refinement of kaolinite PXRD pattern at room temperature has been shown to be difficult (Bish, 1993) and this study is not intended to improve knowledge of the kaolinite structure. Instead Rietveld refinements were used as a comparison tool to study the formation of hydrosodalite under the synthesis conditions used.

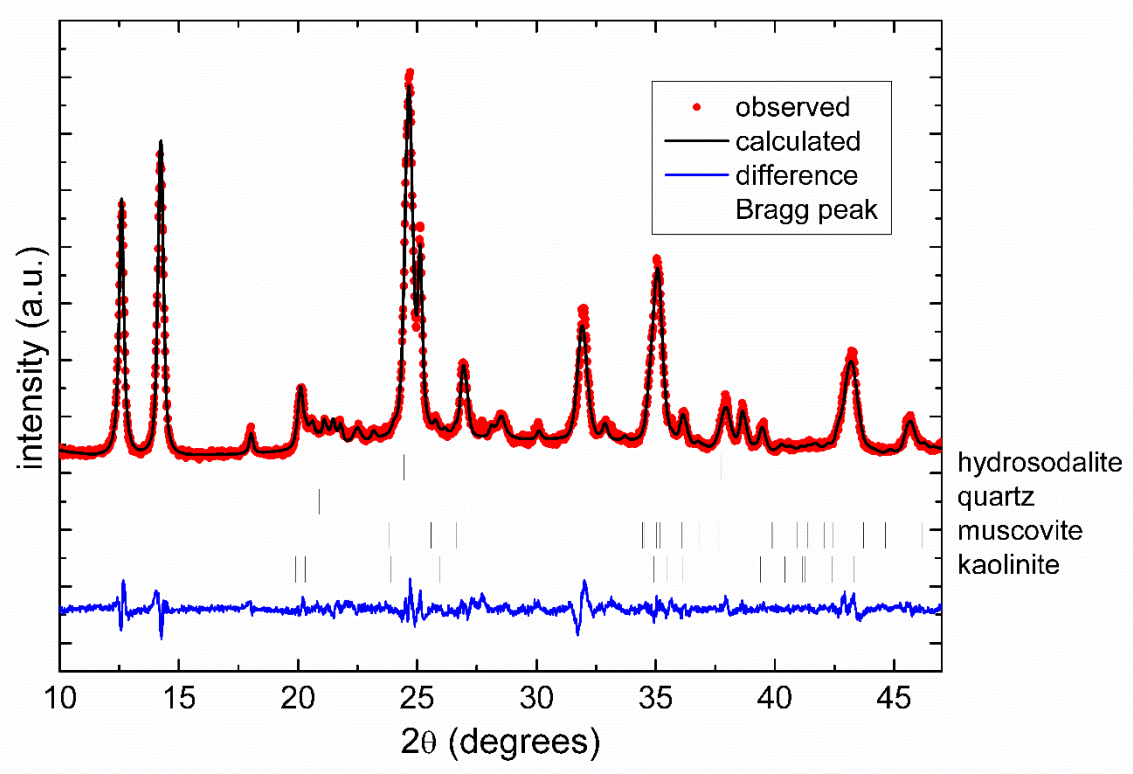

Figure 4-5: Refined XRD patterns of the 0.75 Na:Al sample with the structural models for kaolinite (ICSD #80082), quartz (ICSD #93093), muscovite (ICSD #202262) and 8:2:2 hydroxysodalite (ICSD# 413496).

Owing to the higher symmetry and ordering of the phases present in the kaolinite precursor, these refinements permitted the percentage of each phase in the cured samples to be estimated. The percentages of muscovite and quartz phases remained consistent in all the samples. These species are considered unaffected by the synthesis process, in agreement with previous studies on muscovite (Zografou, 2015) and quartz (Autef *et al.*, 2012).

As expected, the quantity of hydrosodalite in the samples increased in a linear trend with the increase of Na:Al ratio, confirming expectations for this system (Heller-Kallai and Lapides, 2007; Sruthi and Reddy P, 2017). A chart summarizing these results is provided in Section 4.4.2.

4.3.2 SEM phase size and morphology

SEM images were taken to investigate the microstructure of the cured samples, in particular the size, morphology and distribution of hydrosodalite crystallites. As shown in Figure 4-6, two dominant particle types were present in the cured samples: plate-like particles typically between 0.5 – 5 μm, spheroidal crystallites typically ≤1 μm. The plate-like particles were attributed to kaolinite, as these were the only particle type observed in the precursor, and it was known from the PXRD results that kaolinite was the dominant phase in the precursor. The spheroidal particles were attributed to

hydrosodalite. It was known from the PXRD results that the amount of hydrosodalite in the cured samples increased with increasing Na:Al molar ratio – this matched the observations of increasing amounts of the spheroidal particles in the SEM images. The difference between kaolinite's 2D morphology and hydrosodalite's 3D morphology was expected given the nature of their crystallographic cells as shown in Figure 4-1, and was consistent with the known morphology of hydrosodalite (Moloy *et al.,* 2016). The small size and irregular shape for the hydrosodalite were as expected for short curing time non-hydrothermal conditions (Engelhardt *et al.*, 1992). As Na:Al increased, the average size of hydrosodalite crystallites increased from around 0.5 to 1μm. The observed phase proportions of hydrosodalite and kaolinite respectively increased and decreased in the cured samples as Na:Al increased. Knowing that these observations are only qualitative, the changes in microstructure showed by SEM imaging still broadly agreed with the results of the PXRD refinement.

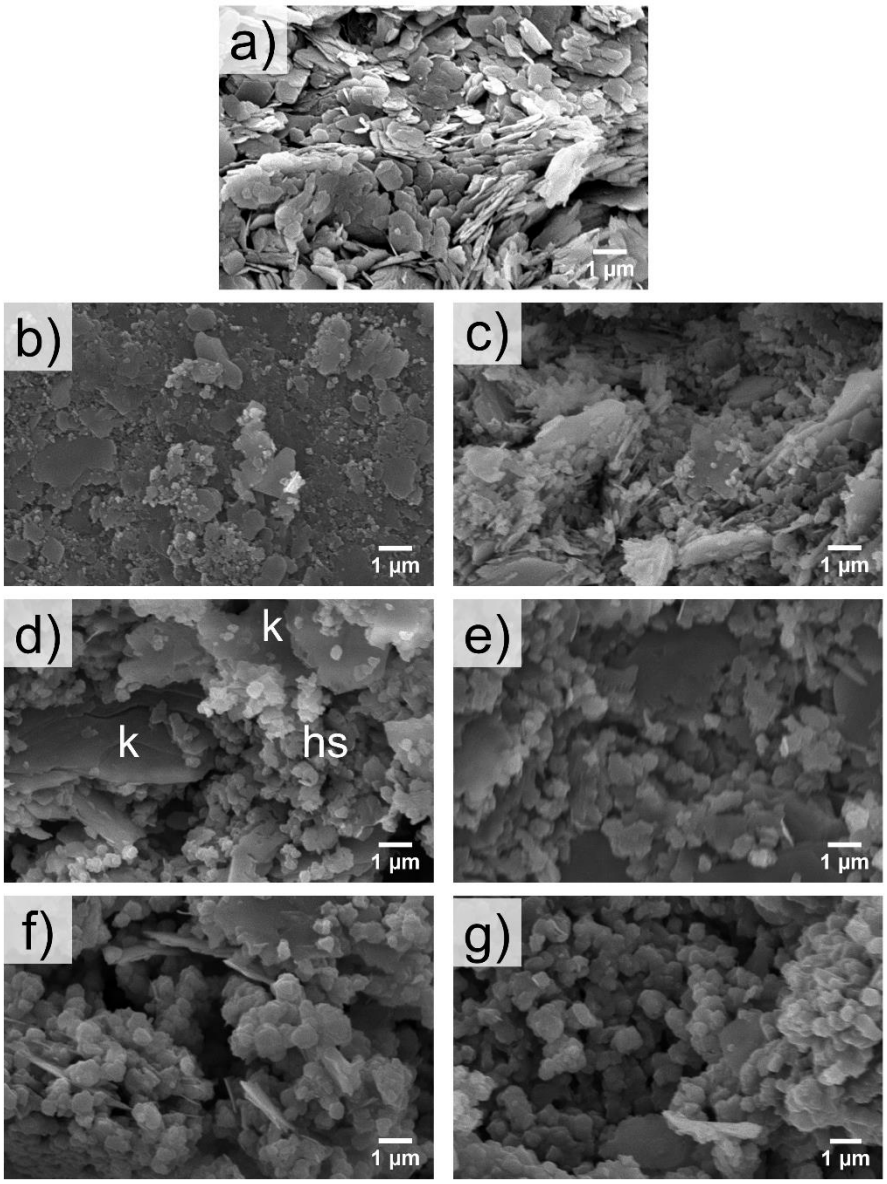

Figure 4-6: SEM images of the kaolinite precursor a), and cured samples with the following Na:Al values: b) 0.25, c) 0.5, d) 0.75, e) 1, f) 1.25, g) 1.5. Annotations in d) give examples of kaolinite (k) and hydrosodalite (hs) phases.

4.3.3 TGA thermal behaviour

Thermal behaviour was investigated to give more detailed information about the possible composition of the hydrosodalite phase, as well as thermal stability and quantity of kaolinite present. The proportion of kaolinite consumed was estimated by integrating the peak attributed to the dehydroxylation of kaolinite in the dTG spectrum (plotted in %mass loss / minute to normalise between samples). This peak area was then expressed as an area fraction of the equivalent peak in the dTG spectrum for the starting kaolinite precursor. The area fraction was then assumed as equivalent to proportion of kaolinite remaining in the sample. These results are presented collectively alongside the values from the other techniques in Section 4.4.2. The accompanying mass spectrometry data is presented in the Appendix.

Overall mass loss decreased slightly as Na:Al increased, with the exception of 1.5-Na:Al (Figure 4-7), indicating that the hydrosodalite phase had a slightly lower overall content of evolvable H_2O and/or OH groups than the kaolinite precursor. The changes in the profile of the TG curve were clarified by taking the derivative (dTG) (Figure 4-7). In the dTG curve of the kaolinite precursor, the peak at 500°C was attributed to dehydroxylation of kaolinite's octahedral sheet, and the broad peak from 50 to 100°C to surface adsorbed moisture (Földvári, 1991). The dehydroxylation peak decreased in intensity as Na:Al increased, which indicated an increased consumption of kaolinite in confirmation of XRD and SEM observations. The dTG curves of the cured samples all had two or three new peaks between 80 and 230°C, attributed to the H_2O molecules in the β-cage of the hydrosodalite (Engelhardt *et al.*, 1992).The dTG curves of 1.25-Na:Al and 1.5-Na:Al had an additional peak at 740°C, possibly indicating a carbonated hydrosodalite (Buhl, 1993) which could have occurred from interaction with atmospheric carbon dioxide during the curing phase. The reasons why this is more likely at higher Na:Al ratios is discussed later.

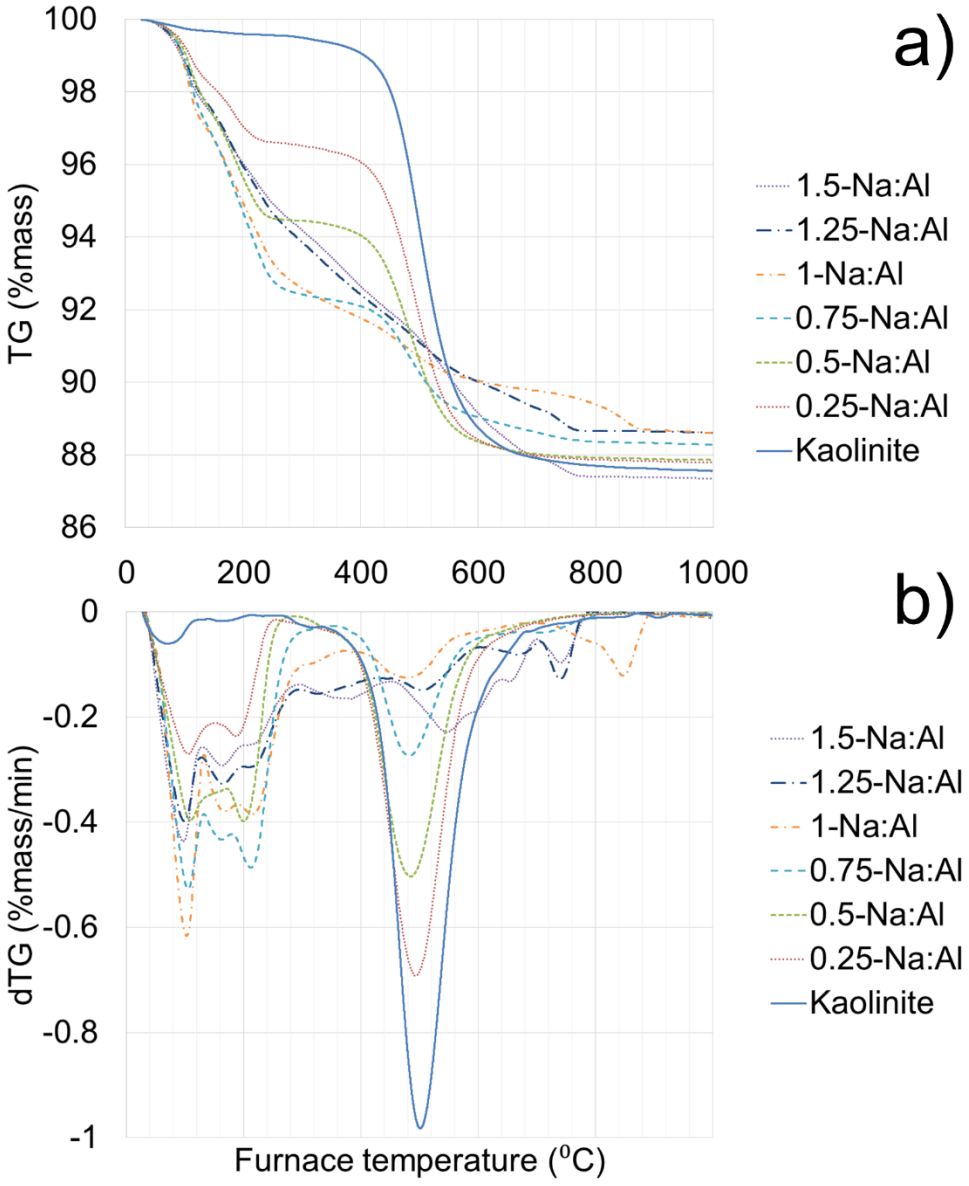

Figure 4-7: TGA (a) and dTG (b) spectra for kaolinite and cured samples

4.3.4 ^{27}Al and ^{29}Si MAS-NMR bonding coordination

MAS-NMR spectra were measured to determine whether the curing process had transformed aluminium and silicon bonding from 3-fold sheet coordination in kaolinite into 4-fold network coordination in hydrosodalite.

For kaolinite, the ^{27}Al spectrum (Figure 4-8) had a single peak at 1.5 ppm, attributed to Al in the octahedral sheet (Fitzgerald *et al.*, 1989), and the ^{29}Si spectrum (Figure 4-9) had a single peak at -91 ppm, attributed to Si in the tetrahedral sheet in Q^3 coordination (Fitzgerald *et al.*, 1989). In the ^{27}Al spectra of the cured samples (Figure 4-8), the kaolinite peak at 1.5 ppm decreased as Na:Al increased, as expected from increased consumption of the kaolinite. New peaks emerged in the range of 60 to 63 ppm which are indicative of Al(4Si) coordination (Sturm *et al.*, 2015), and was attributed to hydrosodalite as this was known to be the product phase from PXRD. Within this range there are two peaks, at 60 and 63 ppm, which overlap in the spectra of samples in the range Na:Al = 0.75 – 1.25. The small difference in chemical shift between the two peaks, despite them both having Al(4Si) coordination, is likely due to differences in other structural parameters such as the next-nearest neighbour environment and β-cage contents (Kirkpatrick *et al.*, 1985).

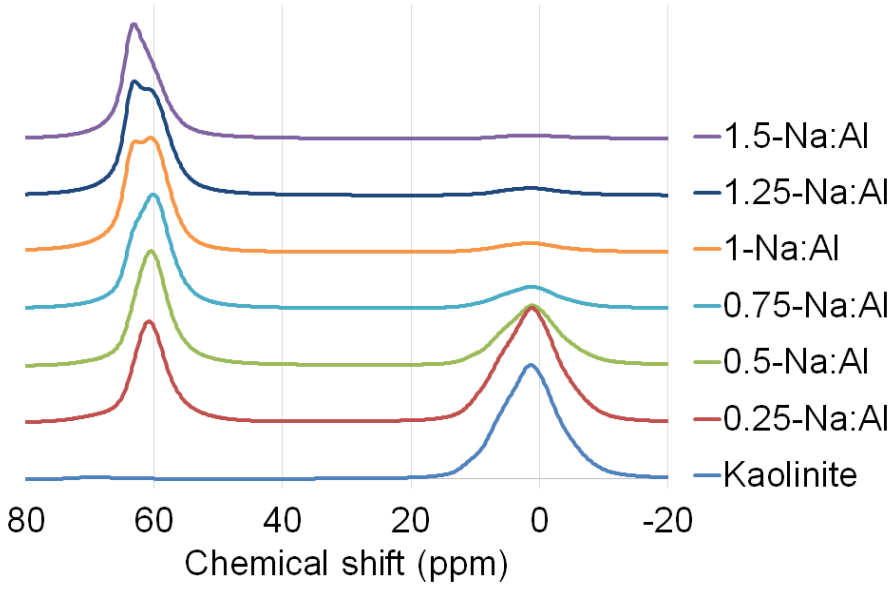

Figure 4-8: ^{27}Al MAS-NMR spectra of kaolinite precursor and cured samples

In the ^{29}Si spectra of the cured samples (Figure 4-9), the kaolinite peak at -91ppm decreased as Na:Al increased, also as expected from increased consumption of the kaolinite. New peaks emerged in the range of -83.5 to -86.5 ppm which are indicative of Q^4(4Al) bonding in a zeolitic framework (Klinowski, 1988), and were therefore attributed to hydrosodalite (Engelhardt *et al.*, 1992). In a similar manner to the ^{27}Al spectra, the location and intensity of peaks within this region changed with Na:Al molar ratio. For both ^{27}Al and ^{29}Si spectra, the recession and emergence of distinct peaks suggest that the system is disordered, with different local environments within the hydrosodalite (Kirkpatrick *et al.*, 1985).

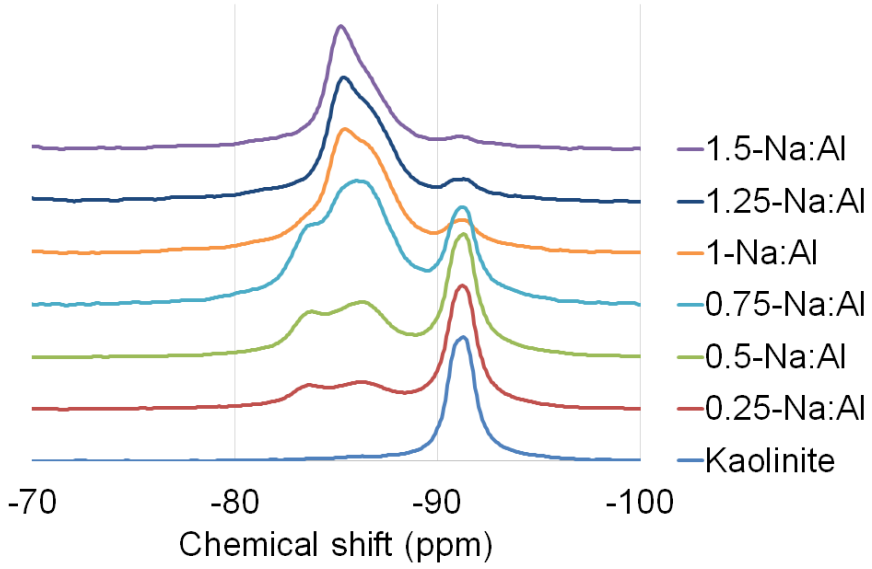

Figure 4-9: ^{29}Si MAS-NMR spectra of kaolinite precursor and cured samples.

4.3.5 FTIR molecular bonding

FTIR spectra were collected to determine the changes in molecular bonding, in particular for aluminium and silicon. The range of 1800 – 600 cm^{-1} is shown (Figure 4-10) along with the indexed peaks (Table 4-3) as the most intense aluminosilicate bands occur in this range. As Na:Al increased, the kaolinite bands progressively decreased in intensity to become only shoulders at most in the1.5-Na:Al spectrum, whereas the hydrosodalite bands emerged from 0.25-Na:Al to become dominant in 1.5-Na:Al. The two carbonate bands are only detectable for Na:Al = 1.25 to 1.5. These spectra confirm the progressive consumption of kaolinite to form hydrosodalite as Na:Al increased. The presence of carbonate bands in spectra with higher Na:Al indicated either the presence of sodium carbonate (Barbosa *et al.*, 2000) or a carbonate-enclathrated variety of hydrosodalite (Buhl, 1993).

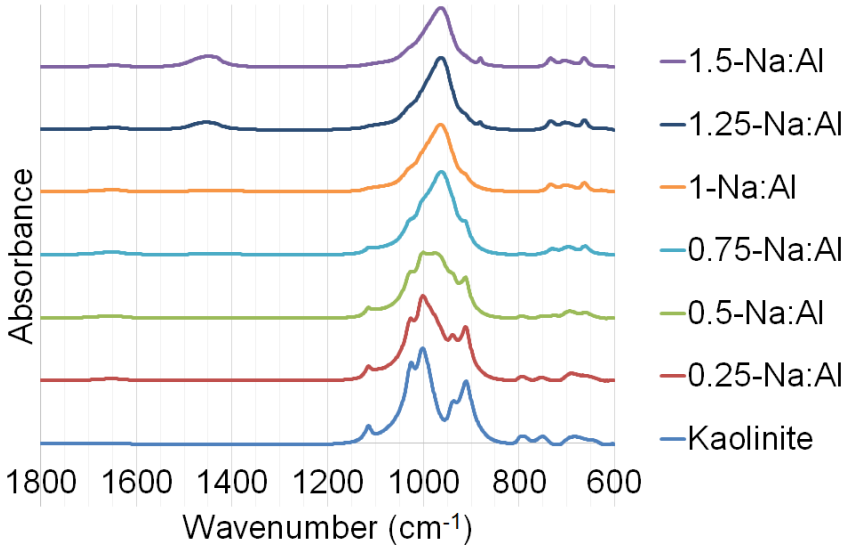

Figure 4-10: FTIR spectra of kaolinite precursor and activated samples

Table 4-3: Indexed absorption bands in FTIR spectra. Wavenumbers given are from kaolinite precursor spectrum for kaolinite phase bands, and from 1.5-Na:Al spectrum for hydrosodalite phase bands. ⊥ = stretching vibration, ∥ = bending vibration.

Band	Wavenumber (cm^{-1})	Intensity	Phase	Reference
Si-O	683.5	vw	Kaolinite	(Madejova and Komadel, 2001)
Si-O	750.8	vw	Kaolinite	(Madejova and Komadel, 2001)
Si-O	788.5	vw	Kaolinite	(Van der Marel and Beutelspacher, 1976)
Si-O (⊥)	1114.6	w	Kaolinite	(Van der Marel and Beutelspacher, 1976)
Al—O-H (∥)	911.0	s	Kaolinite	(Russell and Fraser, 1994)
Al—O-H (∥)	936.3	s/sh	Kaolinite	(Russell and Fraser, 1994)
Si-O-Si (⊥)	1025.5	vs	Kaolinite	(Madejova and Komadel, 2001)
Si-O-Si (⊥)	1114.6	w	Kaolinite	(Van der Marel and Beutelspacher, 1976)
Si-O-T (⊥,symmetric)	663.4	w	Hydrosodalite	(Henderson and Taylor, 1977; Mikuła *et al.*, 2015)
Si-O-T (⊥,symmetric)	706.1	w	Hydrosodalite	(Henderson and Taylor, 1977; Mikuła *et al.*, 2015)
Si-O-T (∥,asymmetric)	734.0	w	Hydrosodalite	(Henderson and Taylor, 1977; Mikuła *et al.*, 2015)
Si-O-T (∥,asymmetric)	963.2	vs	Hydrosodalite	(Henderson and Taylor, 1977; Mikuła *et al.*, 2015)
O-H (∥)	1644.6	vw	Hydrosodalite	(Engelhardt *et al.*, 1992; Farmer, 1974)
C-O	881.1	w	Hydrosodalite	(Barbosa *et al.*, 2000; Buhl, 1993)
C-O	1452.2	w	Hydrosodalite	(Barbosa *et al.*, 2000; Buhl, 1993)

4.4 Discussion

4.4.1 Nature of the hydrosodalite product phase

XRD patterns showed that the product phase was a hydrosodalite. The lattice parameters of the hydrosodalite, obtained through Le Bail refinement, did not change significantly over the Na:Al range tested. Given that an increase in hydration ratio would increase the lattice parameter, it can be deduced that the same hydrosodalite phase is formed for each composition. Other characterisation results were analysed in an attempt to identify the exact phase present. Given the processing conditions of 80°C in an atmosphere of air with no applied pressure, the candidate hydrosodalite phases are limited to 8:2:2, 6:0:8 (Engelhardt *et al.*, 1992) and carbon-enclathrated 8:1:3 (Buhl, 1993). The TG and dTG curves agreed broadly with XRD and SEM results, but showed evidence of possible changes in the hydrosodalite β-cage contents at different Na:Al values, confirming some of the SEM observations. The peaks in the dTG curves (Figure 4-7) between 80 and 230°C seemingly question the possibility of 8:2:2, as its characteristic dTG peak is much higher at around 600°C (Engelhardt *et al.*, 1992).The presence of the 6:0:8 phase would be surprising, as 8:2:2 is known to be the primary phase formed in this reaction, which only transforms to 6:0:8 phase upon washing with water (Engelhardt *et al.*, 1992).

The presence of multiple peaks attributed to hydrosodalite in the ^{29}Si MAS-NMR spectrum (Figure 4-9) indicates different local environments, and hence a degree of disorder in the hydrosodalite (Kirkpatrick *et al.*, 1985). The number of different peaks and overall spread was greatest for Na:Al ≤ 0.75, reducing progressively for Na:Al ≥ 1.This trend is corroborated by the observed stabilisation of hydrosodalite lattice parameters for Na:Al > 1, as described in section 4.3.1. An in-depth study of local environments is beyond the scope of this article, but this trend clearly indicates that the hydrosodalite becomes more ordered at higher Na:Al values.

Carbonates are key to determining if another product phase was present, or whether they were also part of a hydrosodalite. Sodium carbonate would be expected to form in the higher Na:Al samples, given that not all Na was consumed in the reaction (see Section 4.4.3) leaving some Na in solution, and that the curing process involved heating in an atmosphere of air containing carbon dioxide. dTG peaks strongly associated with release of CO_2 were present at 840°C for 1-Na:Al and at 740°C for 1.25-Na:Al and 1.5-Na:Al (Figure 4-7). The mass loss at 740°C in 1.25-Na:Al and 1.5-Na:Al could have been from a carbon-enclathrated sodalite, which has previously been shown to lose mass between 693-750 °C (Buhl, 1993). The mass loss at 840°C in 1-Na:Al is possibly from sodium carbonate, as this does not lose mass until above 800°C

(Newkirk and Aliferis, 1958). Carbonate bands emerged in the FTIR spectra for Na:Al≥1.25, but these are not enough to distinguish whether the carbonates are part of a hydrosodalite phase or a separate carbonate salt, possibly sodium carbonate from the reaction of any excess sodium hydroxide with atmospheric carbon dioxide.

Whilst there is not total agreement between the different characterisation methods, given the synthesis conditions used, the product phases are most likely to be dominated by a 8:2:2 basic hydroxysodalite, which becomes more ordered with higher Na:Al. There is evidence of minor carbonate products, particularly at the higher Na:Al ratios.

4.4.2 Measurements of kaolinite consumption with Na:Al molar ratio

The consumption of kaolinite in each sample was compared for measurements made by methods in PXRD, TGA and ^{29}Si-MAS-NMR (Figure 4-11). Each data point corresponds to a single sample, rather than an average taken from several samples. For this reason, error bars have not been plotted. Caution should be taken in considering the precision of individual data points, and so discussion is about the overall trends rather than specific values. The R^2 value of the linear best fit line taken over all the data points from the different techniques (plotted in Figure 4-11) is 0.816. The R^2 values of the linear best fit lines for the data points for each individual technique (not plotted in Figure 4-11 for clarity) are 0.946 for Rietveld XRD, 0.987 for TGA and 0.967 for ^{29}Si MAS NMR.

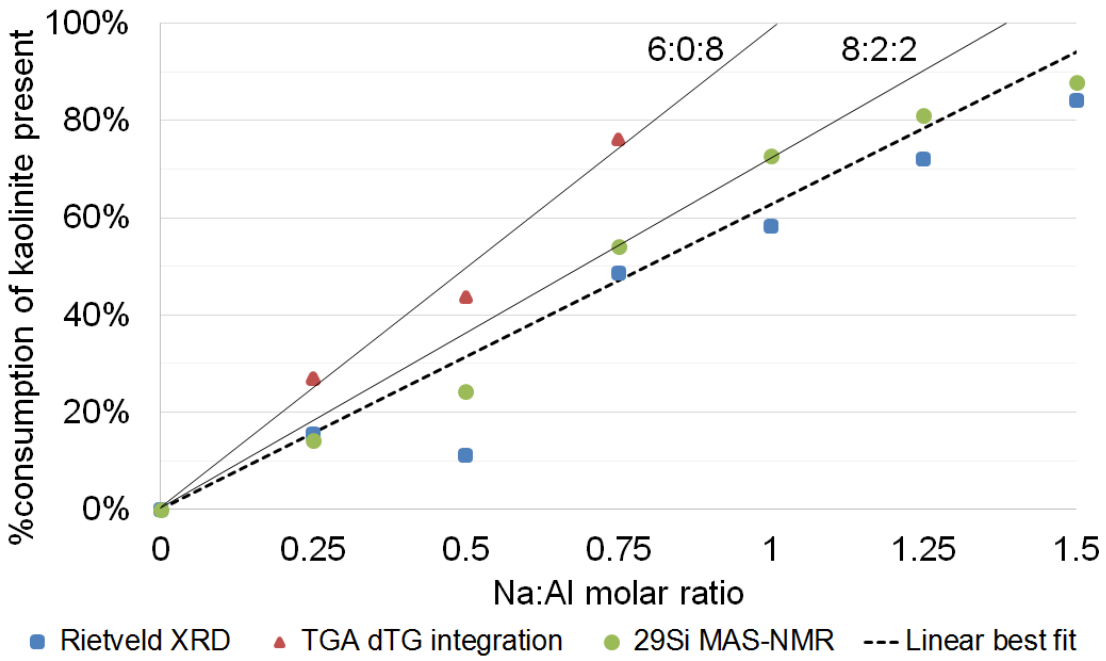

Figure 4-11: Consumption of kaolinite for different Na:Al values, estimated from Rietveld XRD, TGA and ^{29}Si MAS-NMR techniques. The dotted line is the linear best fit. The two solid lines represent the lines expected for ideal formation of 6:0:8 and 8:2:2.

Only values up to Na:Al = 0.75 are plotted for TGA, as after this point in the series the baseline of the dTG curve was too noisy. Evaluation using FTIR was also attempted, by comparing the intensity of the Al—O-H stretching vibration at ~3690cm^{-1} between the activated samples and the starting kaolinite (Russell and Fraser, 1994). However, given these spectra were taken using ATR rather than KBr pellet technique, this method was discounted as too unreliable and imprecise (Farmer, 1974).

There is good agreement between the remaining different techniques, with each showing an approximately linear trend between consumption of kaolinite and Na:Al. There is some variability in outcomes, particularly for PXRD at 0.5-Na:Al and TGA at 0.75-Na:Al, but some discrepancy is expected with experimental data with automatic data processing. The method for ^{29}Si MAS-NMR is straightforward, but relies on having a simple spectrum in which the peaks do not overlap too much. Likewise, the accuracy of the TGA method depends on having a consistent baseline and well-spaced dTG peaks. The different techniques give good agreement for measurement of phase consumption, but as described in Section 4.4.1, each still provides distinct, complementary phase information.

4.4.3 Nature of the reaction

Under the conditions used, the reaction of kaolinite produced hydrosodalite as the only major phase. Whilst the TGA and FTIR analysis suggests there could be formation of minor quantities of carbonate salts at Na:Al≥ 1.25, the majority of Na was consumed in the production of hydrosodalite. In addition to the advantages of low temperature and simple conditions, this indicates this could also be a clean process.

The Na:Al ratio expected to result in transformation of all the kaolinite in the precursor depends on the type of hydrosodalite formed. Each sodalite framework of $(AlSiO_4)_6$ requires either 6 or 8 Na atoms (as shown in the unit cell in Figure 4-1) depending on whether a 6:0:8, 8:2:2 or 8:1:3 phase is formed. These correspond to ideal Na:Al molar ratios of 1 and 1.33 respectively. Given that at an experimental Na:Al ratio of 1.5 there was approximately 10% unreacted kaolinite, the reaction under these conditions did not reach equilibrium and can be assumed was limited by kinetics.

A linear line provides a good fit ($R^2 = 0.82$) to the values of kaolinite consumption taken from the different methods (Figure 4-11). The deviation of the 0.5-Na:Al point is explained by lower values given by all of the methods, and in particular the lower XRD value, whilst that of 0.75-Na:Al is skewed by the TGA result, as affected by baseline selection as mentioned above. For Na:Al ≥ 1.25, there is some evidence of a plateau beginning. This cannot be attributed to the dissolution process, as the surface area:mass ratio of kaolinite has been shown to remain constant throughout (Bauer and Berger, 1998), with the faster dissolution of particularly fine particles only making a small contribution to the overall process (Huertas *et al.*, 1999). A plateau indicates increased unreacted sodium, which correlates with the potential for increased carbonates identified in the FTIR spectra at Na:Al > 1.25.

Extending the linear best fit line predicts that the reaction would reach completion at a Na:Al molar ratio of 1.6. In practice, the reaction is unlikely to go to completion, as the alkalinity of the remaining solution decreases as more kaolinite is dissolved. The predicted Na:Al ratio to completion of 1.6 would present difficulties for this process, as the number of moles of Na required in solution would then exceed the saturation limit of a sodium hydroxide solution at room temperature (Budtova and Navard, 2016). If the questionable TGA data at 0.75-Na:Al is ignored, the average would be closer to 50% kaolin consumption which would place it below the theoretical maximum for an 8:2:2 hydrosodalite, indicating this form of hydrosodalite is not excluded by the data.

4.5 Conclusions

A novel synthesis method has been shown to produce hydrosodalite from kaolinite by activation with sodium hydroxide solution with no prior activation of the precursor and no hydrothermal conditions required. A rational study of the effect of the alkaline concentration has been performed and gave consistent and repeatable results across different analytical techniques. This demonstrates the possibility of easy, cheap and efficient production of semi-condensed aluminosilicates. The numerous applications of the latter as well as the extrusion compatibility of this process also increases its potential for larger scale production.

Acknowledgements

This study was supported by the EPSRC Centre for Decarbonisation of the Built Environment (dCarb) [grant number EP/L016869/1]; a University of Bath Research Scholarship; the Clay Minerals Group of the Mineralogical Society of Great Britain and Ireland, and the Armourers & Brasiers Gauntlet Trust. Solid-state NMR spectra were obtained at the EPSRC UK National Solid-state NMR Service at Durham. Thanks are given to Dr Asel Sartbaeva, University of Bath, and Dr Tony Fraser, James Hutton Institute, for helpful discussions about MAS-NMR and FTIR respectively. All data created during this research are openly available from the University of Bath data archive at https://doi.org/10.15125/BATH-00436.

References

Alkan, M., Hopa, Ç., Yilmaz, Z. & Güler, H., 2005. The effect of alkali concentration and solid/liquid ratio on the hydrothermal synthesis of zeolite NaA from natural kaolinite. *Microporous and Mesoporous Materials,* 86(1), pp. 176-184.

Apperley, D.C., Harris, R.K. & Hodgkinson, P., 2012. *Solid-State NMR: Basic Principles and Practice.* New York: Momentum Press.

Autef, A., Joussein, E., Gasgnier, G. & Rossignol, S., 2012. Parameters That Influence Silica Dissolution in Alkaline Media. *Developments in Strategic Materials and Computational Design III.* John Wiley & Sons, Inc., pp. 13-24.

Bain, J., 1971. A plasticity chart as an aid to the identification and assessment of industrial clays. *Clay Miner,* 9(1), pp. 1-17.

Barbosa, V.F.F., MacKenzie, K.J.D. & Thaumaturgo, C., 2000. Synthesis and characterisation of materials based on inorganic polymers of alumina and silica: sodium polysialate polymers. *International Journal of Inorganic Materials,* 2(4), pp. 309-317.

Barnes, G.E., 2000. *Soil mechanics : principles and practice.* 2nd ed. Basingstoke: Macmillan.

Barrer, R., Cole, J. & Sticher, H., 1968. Chemistry of soil minerals. Part V. Low temperature hydrothermal transformations of kaolinite. *Journal of the Chemical Society A: Inorganic, Physical, Theoretical*, pp. 2475-2485.

Bauer, A. & Berger, G., 1998. Kaolinite and smectite dissolution rate in high molar KOH solutions at 35° and 80°C. *Applied Geochemistry,* 13(7), pp. 905-916.

Belviso, C., Cavalcante, F., Niceforo, G. & Lettino, A., 2017. Sodalite, faujasite and A-type zeolite from 2:1 dioctahedral and 2:1:1 trioctahedral clay minerals. A singular review of synthesis methods through laboratory trials at a low incubation temperature. *Powder Technology,* 320, pp. 483-497.

Bergaya, F., Lagaly, G. & Vayer, M., 2013. Chapter 2.11 – Cation and Anion Exchange. In: F. Bergaya & G. Lagaly, eds. *Developments in Clay Science.* Elsevier, pp. 333-359.

Bish, D.L., 1993. Rietveld refinement of the kaolinite structure at 1.5 K. *Clays and Clay Minerals,* 41(6), pp. 738-744.

Brunauer, S., Emmett, P.H. & Teller, E., 1938. Adsorption of gases in multimolecular layers. *Journal of the American chemical society,* 60(2), pp. 309-319.

BSI, 1990. BS 1377-2:1990 Methods of test for soils for civil engineering purposes. Classification tests

Budtova, T. & Navard, P., 2016. Cellulose in NaOH–water based solvents: a review. *Cellulose,* 23(1), pp. 5-55.

Buhl, J.C., 1993. The properties of salt-filled sodalites. *Thermochimica Acta,* 219, pp. 205-214.

Cheary, R.W. & Coelho, A., 1992. A fundamental parameters approach to X-ray line-profile fitting. *Journal of Applied Crystallography,* 25(2), pp. 109-121.

Dusek, M., Petricek, V., Wunschel, M., Dinnebier, R.E. & van Smaalen, S., 2001. Refinement of modulated structures against X-ray powder diffraction data with JANA2000. *Journal of Applied Crystallography,* 34(3), pp. 398-404.

Engelhardt, G., Felsche, J. & Sieger, P., 1992. The hydrosodalite system Na6+ x [SiAlO4] 6 (OH) x. cntdot. nH2O: formation, phase composition, and de-and rehydration studied by 1H, 23Na, and 29Si MAS-NMR spectroscopy in tandem with thermal analysis, x-ray diffraction, and IR spectroscopy. *Journal of the American Chemical Society,* 114(4), pp. 1173-1182.

Farmer, V.C., 1974. *Infrared spectra of minerals.* London: Mineralogical society.

Felsche, J. & Luger, S., 1987. Phases and thermal decomposition characteristics of hydro-sodalites Na6+x,[AlSiO4]6,(OH)x·nH2O. *Thermochimica Acta,* 118, pp. 35-55.

Fitzgerald, J.J., Hamza, A.I., Bronnimann, C.E. & Dec, S.F., 1989. Solid-state 27Al and 29Si NMR studies of the reactivity of the aluminum-containing clay mineral kaolinite. *Solid State Ionics,* 32, pp. 378-388.

Földvári, M., 1991. Measurement of different water species in minerals by means of thermal derivatography. In: W. Smykatz-Kloss & S.S.J. Warne, eds. *Thermal Analysis in the Geosciences.* Berlin, Heidelberg: Springer Berlin Heidelberg, pp. 84-100.

Guggenheim, S., Chang, Y. & van Groos, A., 1987. Muscovite dehydroxylation: High-temperature studies. *Am Mineral,* 72.

Heller-Kallai, L. & Lapides, I., 2007. Reactions of kaolinites and metakaolinites with NaOH—comparison of different samples (Part 1). *Applied Clay Science,* 35(1–2), pp. 99-107.

Henderson, C. & Taylor, D., 1977. Infrared spectra of anhydrous members of the sodalite family. *Spectrochimica Acta Part A: Molecular Spectroscopy,* 33(3-4), pp. 283-290.

Huertas, F.J., Chou, L. & Wollast, R., 1999. Mechanism of kaolinite dissolution at room temperature and pressure Part II: kinetic study. *Geochimica et Cosmochimica Acta,* 63(19–20), pp. 3261-3275.

Johnson, C.D. & Worrall, F., 2007. Novel granular materials with microcrystalline active surfaces—Waste water treatment applications of zeolite/vermiculite composites. *Water Research,* 41(10), pp. 2229-2235.

Kahle, M., Kleber, M. & Jahn, R., 2002. Review of XRD-based quantitative analyses of clay minerals in soils: the suitability of mineral intensity factors. *Geoderma,* 109(3), pp. 191-205.

Kendrick, E. & Dann, S., 2004. Synthesis, properties and structure of ion exchanged hydrosodalite. *Journal of Solid State Chemistry,* 177(4–5), pp. 1513-1519.

Khajavi, S., Jansen, J.C. & Kapteijn, F., 2010. Production of ultra pure water by desalination of seawater using a hydroxy sodalite membrane. *Journal of Membrane Science,* 356(1), pp. 52-57.

Kinsey, R.A., Kirkpatrick, R.J., Hower, J., Smith, K.A. & Oldfield, E., 1985. High resolution aluminum-27 and silicon-29 nuclear magnetic resonance spectroscopic study of layer silicates, including clay minerals. *Am Mineral,* 70(5-6), pp. 537-548.

Kirk, R.J., 1955. The Luminescence and Ternebrescence of Natural and Synthetic Sodalite. *Am Mineral,* 40, pp. 22-31.

Kirkpatrick, R.J., Smith, K.A., Schramm, S., Turner, G. & Yang, W.-H., 1985. Solid-state nuclear magnetic resonance spectroscopy of minerals. *Annual Review of Earth and Planetary Sciences,* 13(1), pp. 29-47.

Klinowski, J., 1988. Recent advances in solid-state NMR of zeolites. *Annual Review of Materials Science,* 18(1), pp. 189-218.

Madejova, J. & Komadel, P., 2001. Baseline studies of the clay minerals society source clays: infrared methods. *Clays and Clay Minerals,* 49(5), pp. 410-432.

Maskell, D., Heath, A. & Walker, P., 2013. Laboratory scale testing of extruded earth masonry units. *Materials & Design,* 45, pp. 359-364.

Mikuła, A., Król, M. & Koleżyński, A., 2015. The influence of the long-range order on the vibrational spectra of structures based on sodalite cage. *Spectrochimica Acta Part A: Molecular and Biomolecular Spectroscopy,* 144, pp. 273-280.

Moloy, E.C., Liu, Q. & Navrotsky, A., 2006. Formation and hydration enthalpies of the hydrosodalite family of materials. *Microporous and Mesoporous Materials,* 88(1), pp. 283-292.

Moore, D.M. & Reynolds, R.C., 1997. *X-ray diffraction and the identification and analysis of clay minerals.* 2nd ed. Oxford: Oxford University Press.

Newkirk, A. & Aliferis, I., 1958. Drying and decomposition of sodium carbonate. *Analytical Chemistry,* 30(5), pp. 982-984.

Newsam, J.M., 1986. The Zeolite Cage Structure. *Science,* 231(4742), pp. 1093-1099.

Passos, F.A.C.M., Castro, D.C., Ferreira, K.K., Simões, K.M.A., Bertolino, L.C., Barbato, C.N., Garrido, F.M.S., Felix, A.A.S. & Silva, F.A.N.G., 2017. Synthesis and Characterization of Sodalite and Cancrinite from Kaolin. In: S. Ikhmayies, B. Li, J.S. Carpenter, J. Li, J.-Y. Hwang, S.N. Monteiro, D. Firrao, M. Zhang, Z. Peng, J.P. Escobedo-Diaz, C. Bai, Y.E. Kalay, R. Goswami & J. Kim, eds. *Characterization of Minerals, Metals, and Materials 2017.* Cham: Springer International Publishing, pp. 279-288.

Pauling, L., 1930. XXII. The Structure of Sodalite and Helvite. *Zeitschrift für Kristallographie – Crystalline Materials,* 74(1-6), pp. 213-225.

Petříček, V., Dušek, M. & Palatinus, L., 2014. Crystallographic Computing System JANA2006: General features. *Zeitschrift für Kristallographie – Crystalline Materials,* 229(5), pp. 345-352.

Querol, X., Moreno, N., Umaña, J.C., Alastuey, A., Hernández, E., López-Soler, A. & Plana, F., 2002. Synthesis of zeolites from coal fly ash: an overview. *International Journal of Coal Geology,* 50(1), pp. 413-423.

Russell, J.D. & Fraser, A.R., 1994. Infrared methods. In: M.J. Wilson, ed. *Clay Mineralogy: Spectroscopic and Chemical Determinative Methods.* Dordrecht: Springer Netherlands, pp. 11-67.

Sasnauskas, V. & Palubinskaite, D., 2005. The synthesis of hydrosodalite and its use in mortar technology. *Materials Science-Poland,* 23(3), p. 793.

Sruthi, P.L. & Reddy P, H.P., 2017. Characterization of kaolinitic clays subjected to alkali contamination. *Applied Clay Science,* 146, pp. 535-547.

Stucky, G.D. & James, E.M.D., 1990. Quantum Confinement and Host/Guest Chemistry: Probing a New Dimension. *Science,* 247(4943), pp. 669-678.

Sturm, P., Greiser, S., Gluth, G.J.G., Jäger, C. & Brouwers, H.J.H., 2015. Degree of reaction and phase content of silica-based one-part geopolymers investigated using chemical and NMR spectroscopic methods. *J Mater Sci,* 50(20), pp. 6768-6778.

Temuujin, J., Okada, K. & MacKenzie, K.J.D., 2002. Zeolite formation by hydrothermal treatment of waste solution from selectively leached kaolinite. *Materials Letters,* 52(1), pp. 91-95.

Thurlow, C., 2005. *China Clay from Cornwall & Devon: An Illustrated Account of the Modern China Clay Industry.* 4th ed.: Cornish Hillside Publications.

Van der Marel, H.W. & Beutelspacher, H., 1976. *Atlas of infrared spectroscopy of clay minerals and their admixtures.* Amsterdam; New York: Elsevier Scientific Publishing Company.

Wagner, J.F., 2013. Chapter 9 – Mechanical Properties of Clays and Clay Minerals. In: F. Bergaya & G. Lagaly, eds. *Handbook of Clay Science.* 2nd ed. Amsterdam: Elsevier, pp. 347-381.

Wang, Q., Li, N., Bolto, B., Hoang, M. & Xie, Z., 2016. Desalination by pervaporation: A review. *Desalination,* 387(Supplement C), pp. 46-60.

Wiebcke, M., Engelhardt, G., Felsche, J., Kempa, P.B., Sieger, P., Schefer, J. & Fischer, P., 1992. Orientational disorder of the hydrogen dihydroxide anion,(O2H3-) in sodium hydroxosodalite dihydrate (Na8 [Al6Si6O24](OH)2.2H2O): single-crystal x-ray and powder neutron diffraction and MAS NMR and FT IR spectroscopy. *The Journal of Physical Chemistry,* 96(1), pp. 392-397.

Zografou, A., 2015. *The use of china clay waste as a construction material using alkali-activated cement technology.* PhD, University of Bath.

Appendix

Additional details are given here regarding three aspects of the main article: firstly, the mass spectrometry data accompanying the thermogravimetric results; secondly, an explanation of the deconvolution procedure used for analysis of the ^{29}Si MAS-NMR spectra, and lastly, the water and hydroxyl bands of the FTIR spectra.

4.6 Mass spectrometry data

The mass spectrometry (MS) data that was collected alongside the thermogravimetric (TG) data is presented here (Figure 4-12).

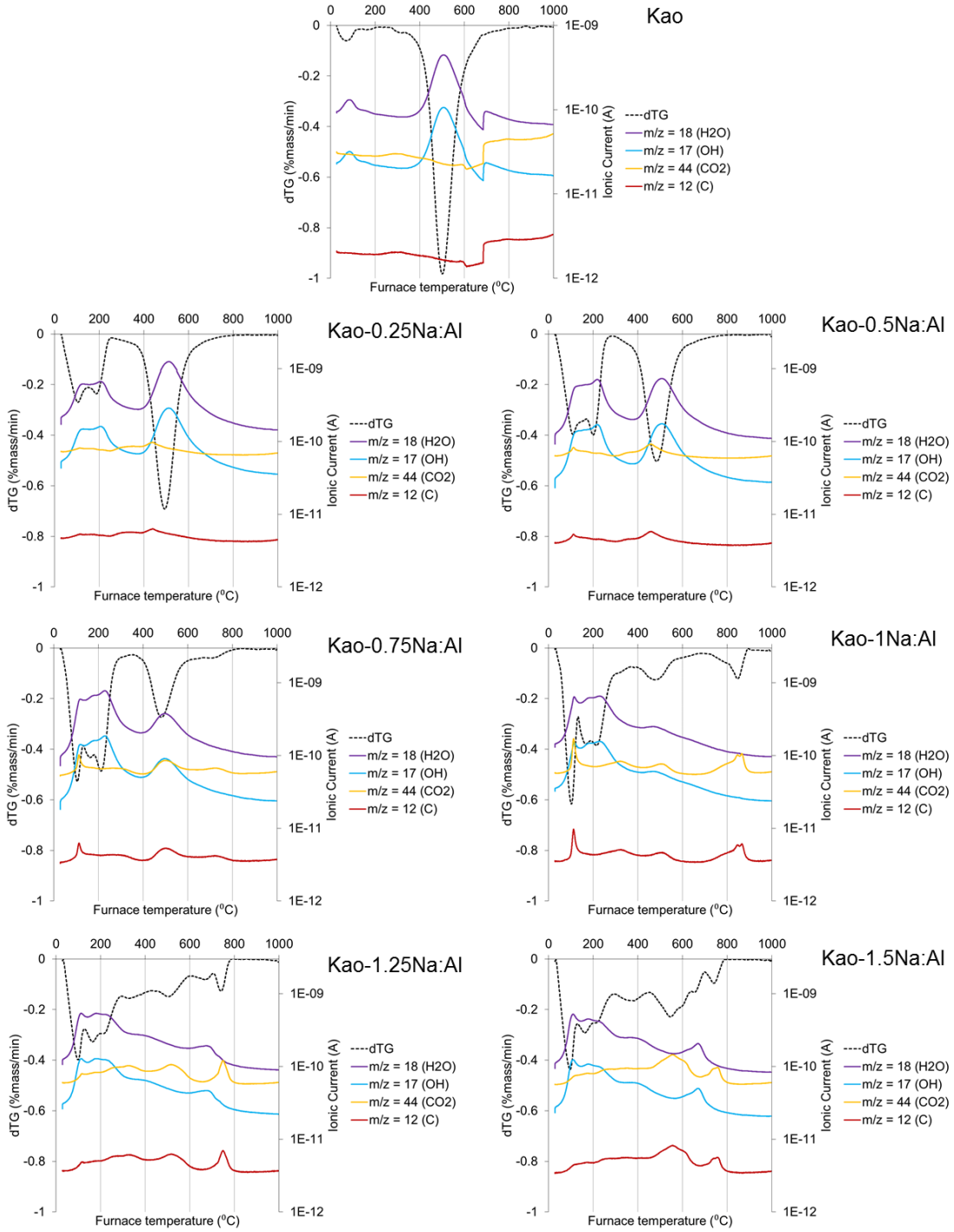

Figure 4-12: MS and dTG data for Kao and activated Kao samples.

4.7 ^{29}Si MAS-NMR deconvolution procedure

The process used for the deconvolution and analysis of the ^{29}Si MAS-NMR spectra will be explained in detail here. Firstly, a flat-line baseline correction was made on the spectra so that there were no negative values. Deconvolution of the spectra was carried out using OriginPro software and fitted to Lorentzian peak profiles, as this gave a better fit to the measured peaks than Gaussian profiles. Peak centre values for the fitted curves were not pre-determined and were allowed to vary.

A total of five different peaks were fitted over the range of samples analysed. For simplicity, it was assumed that all Si in a Q^3 environment was present in kaolinite, and all Si in a Q^4 environment was present in hydrosodalite. It was beyond the necessary scope of this study to identify the exact bonding environment of each of the four fitted Q^4 peaks (labelled a – d). It is acknowledged that this approach did not consider the contributions of Q^3 Si in muscovite or Q^4 Si in quartz – however, it is known from the PXRD analysis that both of these are only present as minor impurity phases in the precursor. Therefore this assumption is not expected to make a significant difference to the values. It was also assumed the dissolution of Al and Si from the kaolinite was congruent, and the possible contribution of Al and Si from muscovite was not considered to be significant. For each spectrum, the cumulative fitted curve was deemed to be an acceptable match for the measured spectrum. An example is given in Figure 4-13 below.

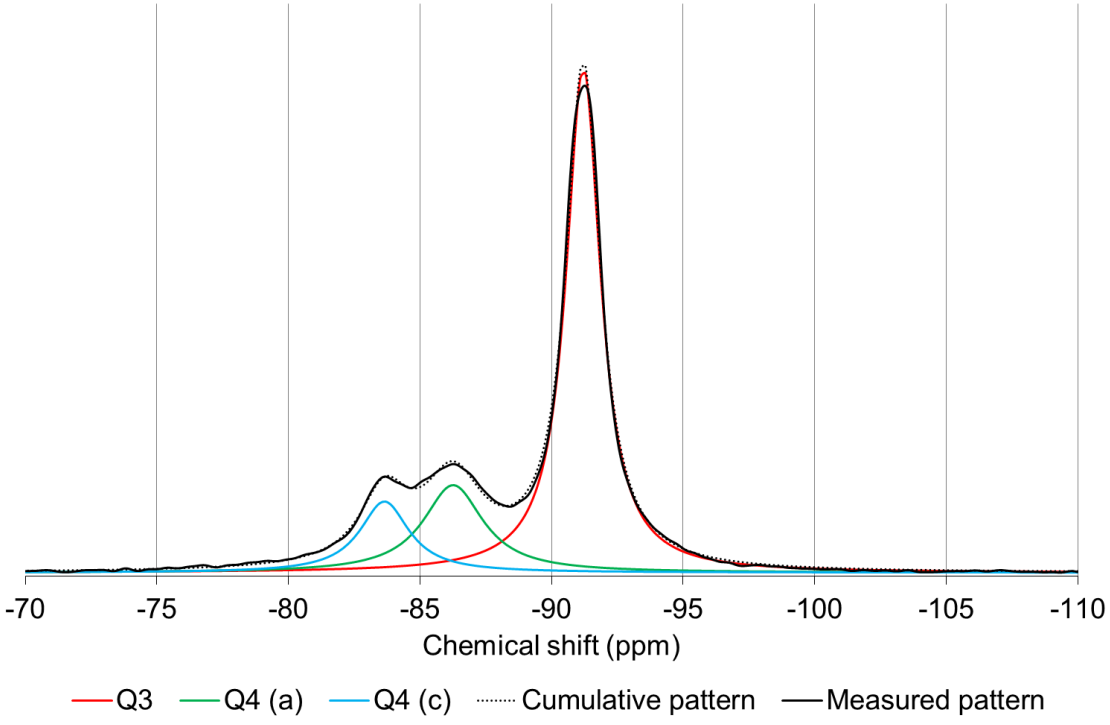

Figure 4-13: Peak deconvolution of the 29Si MAS-NMR spectra, demonstrated for Kao-0.25Na:Al.

The area under each of the fitted curves was integrated, and then expressed as a % of the total integrated area. These values are given in Table 4-4 below.

Table 4-4: Estimates for the proportion of different Si environments found in each sample.

	Si environments (average peak centre given in ppm)				
	Q^3	Q^4 (a)	Q^4 (b)	Q^4 (c)	Q^4 (d)
	-91.3 ppm	-86.5 ppm	-85.3 ppm	-83.6 ppm	-80.4 ppm
Kao	100%	0%	0%	0%	0%
Kao-0.25Na:Al	67%	20%	0%	13%	0%
Kao-0.5Na:Al	51%	17%	16%	16%	0%
Kao-0.75Na:Al	22%	66%	0%	12%	0%
Kao-1Na:Al	11%	44%	36%	9%	0%
Kao-1.25Na:Al	7%	46%	40%	0%	7%
Kao-1.5Na:Al	4%	46%	44%	0%	6%

The % values from the different Q^4 curves were summed to give the estimated signal contribution from hydrosodalite, and hence the proportion of Si atoms. The % values for Q^3 were used to get the equivalent proportion for kaolinite. These values were then factored by the relative number of Si atoms in one mole of the respective phases (2 moles of Si per mole of kaolinite, 6 moles of Si per mole of hydrosodalite). This then gave the estimated proportions of each phase. The results for each sample are given in Table 4-5 below.

Table 4-5: Estimates for the phase distribution of each sample in terms of proportion of Si atoms, and phase composition.

	% of Si atoms		% molar proportion	
	Kaolinite	Hydrosodalite	Kaolinite	Hydrosodalite
Kao	100%	0%	100%	0%
Kao-0.25Na:Al	67%	33%	86%	14%
Kao-0.5Na:Al	51%	49%	76%	24%
Kao-0.75Na:Al	22%	78%	46%	54%
Kao-1Na:Al	11%	89%	27%	73%
Kao-1.25Na:Al	7%	93%	19%	81%
Kao-1.5Na:Al	4%	96%	12%	88%

4.8 Hydroxyl and water bands in FTIR spectra

Due to the difference in absorbance of bands in different regions of the spectra, only the range of 600 – 1800 cm^{-1} was presented in the main article. The Si-O-Al bands in that range are the most useful for phase identification, but the water and hydroxyl bands in the range of 3000 – 4000 cm^{-1} can also provide information (Figure 4-14).

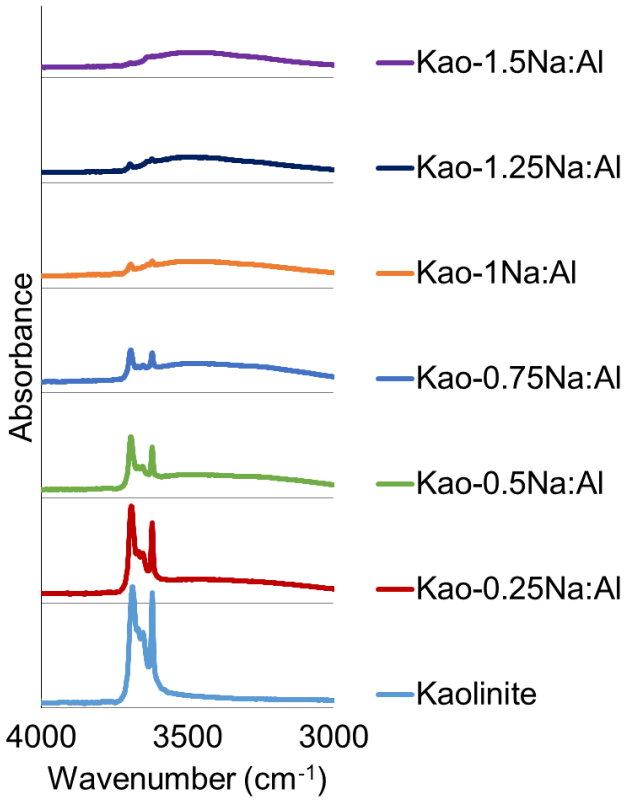

Figure 4-14: FTIR spectra of kaolinite precursor and activated samples in the 3000 – 4000 cm^{-1} range.

The bands at 3687, 3669, 365 and 3620 cm^{-1} are OH stretching bands, which are characteristic of kaolinite (Russell and Fraser, 1994). As the Na:Al molar ratio increased, the intensity of these bands decreased but never fully disappeared. This is in agreement with analysis in the main article on the phase composition of these samples. As the kaolinite OH bands receded, they were replaced with a broad band in the range of 3200 – 3700 cm^{-1}. This was attributed to OH groups in water-water hydrogen bonds (Farmer, 1974). This trend corresponds with the TGA observations of increasing amounts of zeolitic water with increasing Na:Al molar ratio. It would therefore be expected that this emerging band is attributable to OH and/or water groups in the β-cage of the hydrosodalite (Engelhardt *et al.*, 1992).

Chapter 5 - Alkali activation of montmorillonite and illite

In this chapter, the alkali activation behaviour of montmorillonite and illite, the most common 2:1 clay minerals in soils, is investigated. This is presented as a separate chapter to kaolinite, as montmorillonite and illite are both 2:1 clays and are therefore better suited to comparisons between each other.

The additional experimentation on interlayer cation exchange presented in the Appendix was undertaken on the recommendation of the journal reviewers. Whilst not of direct applicability to the motivations of this research, it helps to provide a more thorough understanding of the phenomena observed in the alkali activation of montmorillonite.

This chapter has been revised following suggestions from the examiners, so the article presented here has minor differences compared to the published article.

Declaration of authorship

This declaration concerns the article entitled:									
Alkali activation behaviour of un-calcined montmorillonite and illite clay minerals									
Publication status (tick one)									
draft manuscript		**Submitted**		**In review**		**Accepted**		**Published**	✓
Publication details (reference)	Marsh, A., Heath, A., Patureau, P., Evernden, M., Walker, P. (2018). "Alkali activation behaviour of un-calcined montmorillonite and illite clay minerals." Applied Clay Science 166: 250-261.								
Candidate's contribution to the paper (detailed, and also given as a percentage).	The candidate predominantly executed the… Formulation of ideas: A.Marsh (80%) developed the idea for this study, with suggestions and guidance given by the co-authors (20%) (i.e. supervisors). Design of methodology: A.Marsh (70%) developed the methodology for this study, with suggestions and guidance given by the co-authors (30%) (i.e. supervisors). Experimental work: A.Marsh undertook the majority of experimental work and analysis (80%). P.Patureau (20%) undertook the Le Bail refinements of the powder XRD data and assisted with the interlayer cation exchange experiments. ^{27}Al and ^{29}Si MAS-NMR measurements were undertaken by the EPSRC Solid-State NMR Service, and analysed by A.Marsh. Presentation of data in journal format: A.Marsh (100%) undertook all formatting.								
Statement from Candidate	This paper reports on original research I conducted during the period of my Higher Degree by Research candidature.								
Signed							**Date**	30/10/2018	

Published as Marsh, A, Heath, A, Patureau, P, Evernden, M & Walker, P 2018, 'Alkali activation behaviour of un-calcined montmorillonite and illite clay minerals', Applied Clay Science, vol. 166, pp. 250-261 and available online via: https://doi.org/10.1016/j.clay.2018.09.011

Alkali activation behaviour of un-calcined montmorillonite and illite clay minerals

Abstract

Using alkali activation, un-calcined soils have potential as precursors for low carbon, low cost, geopolymer-stabilised construction materials. This technology has been recently promoted as a lower impact alternative to cement stabilisation for walling materials in construction around the world. There is a lack of fundamental understanding around the alkali activation of un-calcined montmorillonite and illite, which, along with kaolinite, are clay minerals commonly found in soils. Kaolinite, as a 1:1 clay mineral, has been shown to form crystalline hydrosodalite when alkali-activated, but 2:1 montmorillonite and illite could form stronger geopolymer structures due to the higher Si:Al ratio in the precursor mineral. The lack of understanding of the underlying mechanisms at work with 2:1 clay minerals is a barrier to knowing how viable un-calcined geopolymer stabilised soil materials are for the range of soil types found in nature. In this study, montmorillonite and illite precursors were activated with a range of sodium hydroxide concentrations, compacted, and then cured at 80°C for 24 hours. The cured samples were characterised using a variety of advanced analytical techniques, including powder XRD, SEM, TGA, ^{27}Al and ^{29}Si-MAS-NMR, and FTIR. For the first time it was confirmed that alkali activation of uncalcined montmorillonite forms a N-A-S-H or (N,C)-A-S-H geopolymer as the major product phase, which increases in quantity with increasing Na:Al molar ratio of the system. Although it has a similar Si:Al ratio, alkali activation of illite seems to result in structural alteration and increased porosity for Na:Al ≥ 0.5. The behaviour of these individual clay minerals suggests that the alkali activation of un-calcined 2:1 clay minerals is complex. Although alkali activation of montmorillonite can form a geopolymer, alkali activation of soils containing illite may lead to poor quality materials. This research has shown that the focus of future development work should be around montmorillonite-based clays.

5.1 Introduction

Alkali activation of aluminosilicates for construction materials has been the focus of extensive research in recent years, due to the potential of lower energy and carbon costs compared to conventional materials such as Portland cement based concrete (Provis, 2014). Alongside industrial by-products such as fly ash (Fernández-Jiménez *et al.*, 2006; van Jaarsveld *et al.*, 2002) and rice husk ash (Zhang, 2013), alkali activation of clays and soils has been investigated, due to their abundance and low cost (Diop and Grutzeck, 2008; MacKenzie, 2009). Clays can be used not only as supplementary cementitious materials (Fernandez *et al.*, 2011; Garg and Skibsted, 2014; Hollanders *et al.*, 2016; Tironi *et al.*, 2013), but also as primary aluminosilicate precursors in alkali activation. While a few studies have been done on montmorillonitic and illitic soils, studies of clay minerals in isolation have been dominated by kaolinite and metakaolin (Liew *et al.*, 2016). At the same time, a wide range of soils found around the world contain montmorillonite and/or illite (Nickovic *et al.*, 2012). An improved fundamental understanding of the alkali activation behaviour of these two clay minerals in isolation is required. This is in order to develop a better understanding of how mixed mineral soils will behave, and therefore which soils might be suitable or unsuitable for alkali activation.

In the specific application being considered, the goal of alkali activation is to convert clay minerals into strong, durable and water resistant product phases which will allow the manufacture of concrete block replacements, or similar products. A sufficiently reactive aluminosilicate system with a Si:Al molar ratio of 1.5 – 2.5 is expected to form a geopolymer in the presence of a sufficiently concentrated alkaline activating solution (Duxson *et al.*, 2007b). The amount of geopolymer phase formed depends on both the extent of dissolution of the aluminosilicate precursor (i.e. the clay mineral) in the alkaline activating solution (Duxson *et al.*, 2007a), as well as the total amount of metal cation in the system, as required for charge balancing (Barbosa *et al.*, 2000).

Both, montmorillonite and illite are dioctahedral 2:1 clay minerals having layers consisting of one octahedral sheet between two tetrahedral sheets. Montmorillonite is a member of the smectite family; illite, the mica family (Brindley and Brown, 1980). For their crystal structure, montmorillonite has a triclinic lattice, with a P space group (Gualtieri *et al.*, 2001; Viani *et al.*, 2002) while illite has a monoclinic lattice, with a C2/c or C2/m space group for the 1M and 2M1 polytypes respectively (Gualtieri, 2000; Gualtieri *et al.*, 2008). In chemical composition, both minerals have formula ranges rather than fixed stoichiometry, due to substitutions. For montmorillonite, there is substitution of Mg^{2+} for Al^{3+} in the octahedral sheet; for illite there is Al^{3+} substitution for

Si^{4+} in the tetrahedral sheet, and possible Mg^{2+} or Fe^{2+} substitution for Al^{3+} in the octahedral sheet (Brigatti *et al.*, 2013; Brindley and Brown, 1980).

To balance the negative layer charges resulting from these substitutions, both minerals have interlayer cations. Montmorillonite can host a range of different interlayer cations including Ca^{2+}, Na^{+}, Mg^{2+}, K^{+} and Sr^{2+}, whereas illite has only K^{+}. Illite has a much lower cation exchange capacity than montmorillonite (Kahr and Madsen, 1995). This is due to its small interlayer space and the 'fixed' nature of the small potassium ions in the ditrigonal cavities on the surfaces of the tetrahedral sheet (Bergaya *et al.*, 2013; Verburg and Baveye, 1994). The hydration of the interlayer cations and subsequent osmotic behaviour of their diffuse double layers in montmorillonites results in swelling behaviour, whereas the positioning of the K^{+} interlayer cations in illite results in non-swelling behaviour (Van Olphen, 1963).

For application as masonry blocks, alkali-activated soil materials must be able to be manufactured at block scale and placed in a wall at which point dimensional stability is required. Given their swelling behaviour, montmorillonitic soils have usually been avoided in earth construction, even when using chemical stabilisation such as cement or lime (Jagadish, 2007). It remains to be seen whether alkali activation can be used to transform the montmorillonite into a strong and durable stabilising phase, which ensures that any unreacted clay fraction is constrained in its ability to have a detrimental effect on overall properties. The viability of an alkali-activated soil material, especially if containing a swelling clay such as a montmorillonite, therefore depends not only on the ability to form a geopolymer phase, but also how much geopolymer phase is formed and how that geopolymer phase interacts with any unreacted minerals. To be compatible with extrusion processing, an established process used in brickmaking, the consistency of the wet mix needs to be approximately at the plastic limit (Maskell *et al.*, 2013). Practical constraints such as these are not often considered in studies on alkali-activated materials, but are vital to the feasibility of any new material.

In previous studies in this field, a popular processing technique is to heat a clay (or soil containing clay minerals) above its dehydroxylation temperature in order to increase its reactivity (Liew *et al.*, 2016; Tchadjie and Ekolu, 2018). Unlike the dehydroxylation of kaolinite, dioctahedral 2:1 clays retain their layer structure (Heller-Kallai, 2013) but still undergo a reduction in Al coordination in the octahedral layer (Heller-Kallai, 2013; Muller, 2000). However, these coordination changes are reversible as dehydroxylated 2:1 clays can undergo varying degrees of rehydroxylation, even under ambient conditions (Emmerich, 2000; Muller, 2000). Given that the dehydroxylation temperatures for montmorillonite and illite are in the ranges of 620 – 780°C and 520 –

650°C respectively (Földvári, 1991), there is a significant energy investment required for this. Since the main driver for alkali activated materials is a lower energy footprint (MacKenzie, 2009), it is desirable to know under which conditions these two clay minerals might be sufficiently reactive in their uncalcined state.

The behaviour of montmorillonite in alkali solutions is the subject of ongoing research for the application of barrier materials for radioactive waste storage (Dohrmann *et al.*, 2013; Fernández *et al.*, 2014; Nakayama *et al.*, 2004). For example, the transformation of montmorillonite to illite in the presence of K-rich groundwater is of concern, as this leads to loss of swelling capacity (Kaufhold and Dohrmann, 2010; Lee *et al.*, 2010). The transferability of such knowledge is limited for the present application for several reasons: alkaline concentrations are lower ([OH] < 1 M); timescales are longer; liquid:solid ratios are much higher, and alkali solutions used are often complex mixtures of metal hydroxides designed to mimic the composition of Portland cement pore fluids. In contrast, there are few previous studies on alkali activation of montmorillonite for the intentional production of alkali aluminosilicate phases. In early studies, Willoughby et al. (1968) and Ingles (1970) activated uncalcined montmorillonite with a range of alkali hydroxides, showing a loss of strength when sodium hydroxide was used with room temperature curing. Belviso et al. (2017) showed that a 700°C calcined Ca-montmorillonite precursor formed a geopolymer by hydrothermal alkali activation, but formed zeolites when an additional NaOH pre-fusion step was used. Seiffarth et al. (2013) thermally pre-treated a smectite clay sample (550 – 950°C), and mixed it with a sodium silicate solution. Geopolymerisation was inferred from the increased strength of the alkali activated samples, but detailed phase characterisation was not performed. The causal link between geopolymerisation and higher strength is not straightforward since sodium silicate itself is an adhesive, used to strengthen materials such as cardboard (Fawer *et al.*, 1999).

More studies have been done on illite alkali activation, but most of them have focussed on calcined precursors. Seiffarth et al. (2013) thermally pre-treated illite clay between 550 – 950°C, and mixed it with a sodium silicate solution. Again, geopolymerisation was inferred from increased strength, but without detailed phase characterisation. El Hafid and Hajjaji (2015) calcined an illite-kaolinite clay sample at 700°C and mixed it with NaOH solutions, producing the zeolites chabazite and natrolite. It was unclear what role the kaolinite and the illite played in the development of these product phases. Sperberga et al. (2011) mixed a calcined (700 – 900°C) illite deposit with KOH solution, Sedmale et al. (2013) mixed the same illite deposit with KOH solution, but without calcination. In both cases, although improved compressive strength was noted, proof of geopolymer phase production was not definitive. In contrast to their results for

montmorillonite, Belviso et al. (2017) showed that a calcined illite precursor underwent no obvious changes by hydrothermal alkali activation, but did form zeolites when an additional NaOH pre-fusion step was used.

Although the existing range of studies provides some insight, there is still a knowledge gap in the direct comparison of the alkali activation of non-calcined montmorillonite and illite. A recurring obstacle to developing a fuller fundamental understanding of precursor influence on alkali activation behaviour is that given the numbers of variables involved, comparison between studies is difficult. In order to develop a fundamental understanding of the processes at work, this study is a systematic investigation and comparison of the alkali activation behaviour of un-calcined montmorillonite and illite. The aim is to understand phase formation behaviour, in order to determine which conditions might be suitable for producing stabilised soil materials.

5.2 Experimental

5.2.1 Materials

K10 montmorillonite (Sigma-Aldrich, product no. 69866-1KG) and Clay Minerals Society Imt-2 (Silver Hill) illite were used as the aluminosilicate precursors. Chemical compositions were determined by energy dispersive X-rays (EDX) in a scanning electron microscope (JEOL SEM6480LV with Oxford INCA X-Act SDD X-ray detector) at an accelerating voltage of 20 kV, a chamber pressure of between 10 – 30 Pa, a Si wafer as a standard, and measuring 4 scan areas per sample. The precursor powders were mounted on a sticky carbon tab on top of an aluminium stub, and were not coated. Standard errors in composition were calculated from the variation in values between the different area scans for each sample. Specific surface area was determined using the BET method in a Micromeritics 3Flex instrument. The precursor powders (0.2 g of K10 Montmorillonite, and 1 g of Illite) were degassed under vacuum conditions at 150°C for 14 h, before testing.

For the K10 montmorillonite, chemical composition suggested that the dominant clay mineral was a Ca-montmorillonite due to presence of Ca, with a low amount of iron and minor amounts of potassium, magnesium, sodium, sulphur and titanium also present (Table 5-1). The sulphur was likely to be due to either a remnant of the acid treatment, or a trace accessory mineral. BET specific surface area was 265.8 m^2g^{-1}. K10 montmorillonite is produced by acid treatment of naturally occurring Ca-montmorillonite, in which the Ca^{2+} interlayer cations are partially replaced by protons (Varadwaj *et al.*, 2013), and the octahedral sheet cations (mostly Al^{3+}, with some Mg^{2+} substitution) are partially replaced by more divalent cations (Monteiro *et al.*, 2014). This process typically results in a modified clay with increased surface area, micro-porosity and surface acidity (Komadel and Madejová, 2013). This was a proprietary process carried out by the manufacturer, so no details could be obtained. The pre-treatment was not expected to significantly affect the product phases formed in this particular application, and having a consistent and well characterised material was considered more important than having an untreated raw material in developing a fundamental understanding of the mechanisms.

Table 5-1: Chemical composition of K10 montmorillonite and illite used, in oxide %wt.

Oxide	Al_2O_3	CaO	Fe_2O_3	K_2O	MgO	Na_2O	SiO_2	SO_3	TiO_2	Total
K10 Montmorillonite %wt (std error)	13.53 (0.66)	0.47 (0.14)	4.53 (1.05)	1.56 (0.22)	1.67 (0.11)	0.03 (0.03)	77.60 (2.12)	0.12 (0.07)	0.49 (0.02)	100
Illite %wt (std error)	20.80 (0.34)	0.00	8.32 (0.38)	8.67 (0.18)	2.28 (0.06)	0.00	59.14 (0.26)	0.00	0.78 (0.06)	100

For the illite, chemical composition showed minor amounts of iron, potassium, magnesium and titanium present (Table 5-1). BET specific surface area was 19.5 m^2g^{-1}. Unlike for the montmorillonite, there were no easily accessible purified forms of illite available.

The precursors were activated using sodium hydroxide pellets of >98% purity (Sigma-Aldrich, product no. 06203).

5.2.2 Synthesis procedure

As previously described (Marsh *et al.*, 2018), the compositions in Table 5-2 were determined to provide samples of pre-determined Na:Al ratio, whilst maintaining the wet mix workability at the plastic limit. Molar quantities of Al were calculated from generic structural formulae of the clay minerals. Although there were minor impurities in both the precursors, the Na:Al ratios were valid for the purpose of relative comparisons – any small error was consistent within the series of systems for each precursor. Atterberg plastic limit measurements (Wagner, 2013) were taken for montmorillonite and illite over a range of sodium hydroxide solutions (BSI, 1990). From these data a best fit line was plotted to extrapolate the volume of solution required to reach plastic limit consistency for a given concentration (Figure 5-1). A correction was made to exclude the mass of the sodium hydroxide from the solids mass in the plastic limit calculations (Bain, 1971). Montmorillonite demonstrated a significant decrease in plastic limit with increasing NaOH, likely due to partial dissolution. Only small changes were observed for illite. The illite samples were limited to Na:Al of 0.75 as it was not practically possible to produce samples with a higher value while keeping the plasticity constraint.

Table 5-2: Composition of samples in the activated montmorillonite and illite series, each for 25 g of dry precursor.

Name	**Mont-0.25 Na:Al**	**Mont-0.5 Na:Al**	**Mont-0.75 Na:Al**	**Mont-1 Na:Al**	**Mont-1.25 Na:Al**	**Mont-1.5 Na:Al**	**ILL-0.25 Na:Al**	**ILL-0.5 Na:Al**	**ILL-0.75 Na:Al**
Na:Al molar ratio	0.25	0.5	0.75	1	1.25	1.5	0.25	0.5	0.75
Concentration of activating solution (molarity)	1.1	2.5	4.1	6.4	14.0	18.8	8.3	15.3	19.7
Water mass (g)	22.5	20.5	18.2	15.3	8.2	6.5	4.8	4.8	4.8

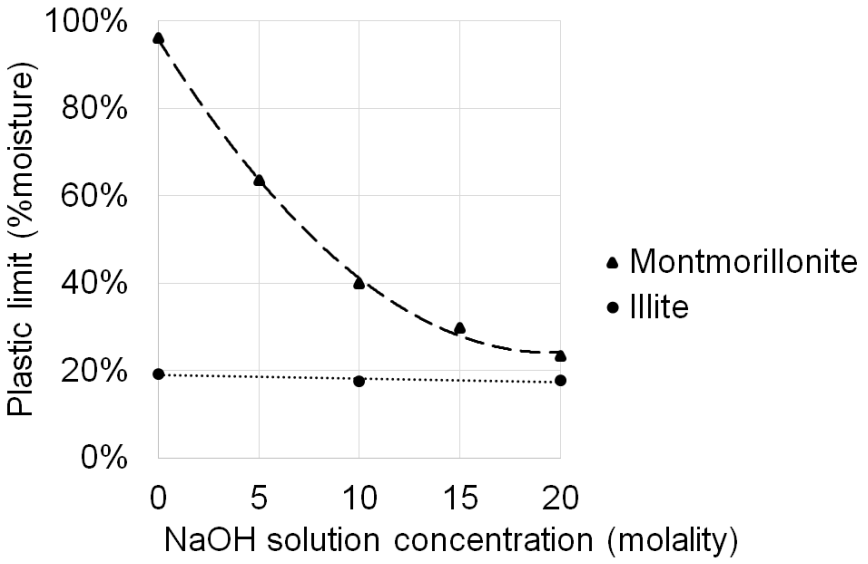

Figure 5-1: The change in plastic limit of montmorillonite and illite precursors with sodium hydroxide solution concentration.

The montmorillonite and illite were activated by adding a sodium hydroxide solution. Solutions of different concentrations were prepared by adding sodium hydroxide pellets to distilled water, mixed with a magnetic stirrer (Stuart UC152 heat-stir) for a minimum of 2 hours until fully dissolved and then allowed to cool. The clays were pre-dried in a 105°C oven, and left to cool. Varying quantities of activating solutions were added to 25 g of each clay, as given in Table 5-2. Each mixture of activating solution and clay was mixed by hand for 3 minutes, providing a consistent and well-distributed mixture. The high viscosity of the samples allowed them to be compacted by hand into 18 mm x 36 mm cylindrical Teflon moulds by tamping with a glass rod in three layers for each sample, using 25 blows for each layer. Samples were cured in an air atmosphere in a 80°C oven for 24 hours in their moulds. After curing, the activated illite samples were not fully dried so required further drying by 72 hours in a vacuum desiccator. After demoulding, samples were aged for 28 days in a controlled environment of 20 ± 0.5°C and 50 ± 2.5% relative humidity. An air atmosphere was intentionally used for both curing and ageing, to provide conditions representative of industrial brickmaking processes. This gave an indication of carbonation behaviour for these clay minerals after alkali activation, a subject of interest as efflorescence is a known problem in alkali-activated materials (Allahverdi *et al.*, 2015), as well as an approximate indication of how much Na was left unused in the activation process itself.

5.2.3 Characterisation methods

The set of characterisations were done at 28 ± 2 days ageing time, and (with the exception of SEM imaging) were done using powders prepared from the cured samples. These were ground by hand, having been wetted with isopropanol to avoid damaging the clay minerals' crystal structures (Moore and Reynolds, 1997). Powders were ground until there was no further discernible reduction in particle size, and so were comparable between samples. Any variation in particle size of the ground powders was not expected to have any noticeable effect on characterisation results. For XRD, TGA and FTIR, all characterisation was carried out on powder samples stored for at least 48 hours at 50% relative humidity, to allow for equal hydration states.

Powder X-ray diffraction (XRD) analysis was done to identify phases with a Bruker D8 Advance instrument using monochromatic CuKα1 L3 (λ = 1.540598 Å) X-radiation and a Vantec superspeed detector. A step size of 0.016 °(2θ) and step duration of 0.3 seconds were used. Phase identification was done using Bruker EVA software, using reference patterns from the Joint Committee on Powder Diffraction Standards (JCPDS) database. Patterns were corrected for sample height shift by calibrating to the most intense quartz reflection (101) at 26.6 °(2θ). The backgrounds have been defined thanks to Le Bail extractions of the XRD patterns using JANA 2006 (Petříček *et al.*, 2014).

SEM imaging was used to characterise phase size and morphology, using a JEOL SEM6480LV in secondary electron mode with an accelerating voltage (AV) of 10kV. Bulk specimens were sputter coated with gold for 3 minutes. Because the SEM used a tungsten filament, an AV of 10 kV was selected as an optimal balance between the tendencies towards a noisy image at lower AV, and lower resolution at higher AV. Unpolished samples were used to enable easier distinction of particle morphology in the microstructures, and also because of the friability of some of the samples.

Thermogravimetric analysis (TGA) was done to characterise thermal behaviour, using a Setaram Setsys Evolution TGA over a range of 30 to 1000°C at a heating rate of 10°C/minute. An air atmosphere was used, with a flow rate of 20 ml/minute. A connected mass spectrometer was used (Pfeiffer Omni) to identify whether evolved gas species contained OH, H_2O, C or CO_2.

Solid state magic angle spinning (MAS) nuclear magnetic resonance (NMR) spectra were measured for ^{27}Al and ^{29}Si to characterise coordination states, using a Varian VNMRS (9.4 T) in direct excitation. The ^{27}Al spectra were obtained with a 104.198 MHz field (104.199 MHz for Mont and ILL), using a sample spinning frequency of 14 kHz in a 4 mm rotor, a pulse duration of 1 µs, an acquisition time of 10 ms (9.8 ms for activated

Mont samples), a recycle time of 0.2 s, line broadening of 0.005 s, and between 3000 – 7000 scans were used for each spectrum. The ^{29}Si spectra were obtained with a 79.435 MHz field (79.438 MHz for activated ILL samples), using a sample spinning frequency of 6 kHz in a 6 mm rotor, a pulse duration of 4 μs, an acquisition time of 20 ms (15 ms for activated ILL samples), a recycle time of 2 s, line broadening of 0.01 s (0.05 s for ILL and activated ILL samples), and between 1220 – 4000 scans were used for each spectrum. Proton decoupling was used at 61.0 kHz for Mont and ILL, at 41.7 kHz for Mont-Na:Al = 0.25 – 1 and ILL-Na:Al = 0.25 – 0.75. The samples Mont-Na:Al = 1.25 – 1.5 were recorded without decoupling, which appeared to make very little difference to the appearance of the spectra. Chemical shifts were referenced to 1 M aq. $Al(NO_3)_3$ for ^{27}Al and tetramethylsilane for ^{29}Si. Spectra have been normalised to the height of the most intense line in the spectrum.

Fourier Transform Infrared Spectroscopy (FTIR) was done to characterise molecular bonding, using a Perkin-Elmer Frontier with a diamond Attenuated Total Reflectance (ATR) head. Spectra were collected over a range of 4000 – 600 cm^{-1} using a resolution of 4 cm^{-1} and 5 scans per spectrum. Corrections were made for ATR and background using Perkin-Elmer Spectrum software.

5.3 Results

5.3.1 XRD phase analysis

The XRD pattern of the plain (control) montmorillonite precursor showed it contained montmorillonite clay mineral (Powder Diffraction File (PDF)# 00-013-0135), muscovite (PDF# 01-084-1304), quartz (PDF# 00-046-1045) and minor amounts of microcline (PDF# 00-019-0932) and kaolinite (PDF# 01-079-1570) (Figure 5-2). The weak intensity and broad peak profile of the montmorillonite 001 reflection is likely a result of internal disorder, and does not necessarily indicate the phase proportion. The basal spacing calculated from the Le Bail refinement is 14.4 Å, which is in the possible range for smectites. Given the oxide composition, this suggests it is either a Ca-, Mg- or mixed Ca-Mg-montmorillonite (Ferrage *et al.*, 2005).

The XRD pattern of the illite showed it contained illite clay mineral (PDF# 00-026-0911) as the major phase, with quartz, microcline and kaolinite present as minor phases (Gailhanou *et al.*, 2007) (Figure 5-2). Previous studies on this source clay identified it to be composed of >90% illite (Gailhanou *et al.*, 2007), and the illite clay mineral to be mostly of the 1M/1Md polytype (Haines and van der Pluijm, 2008).

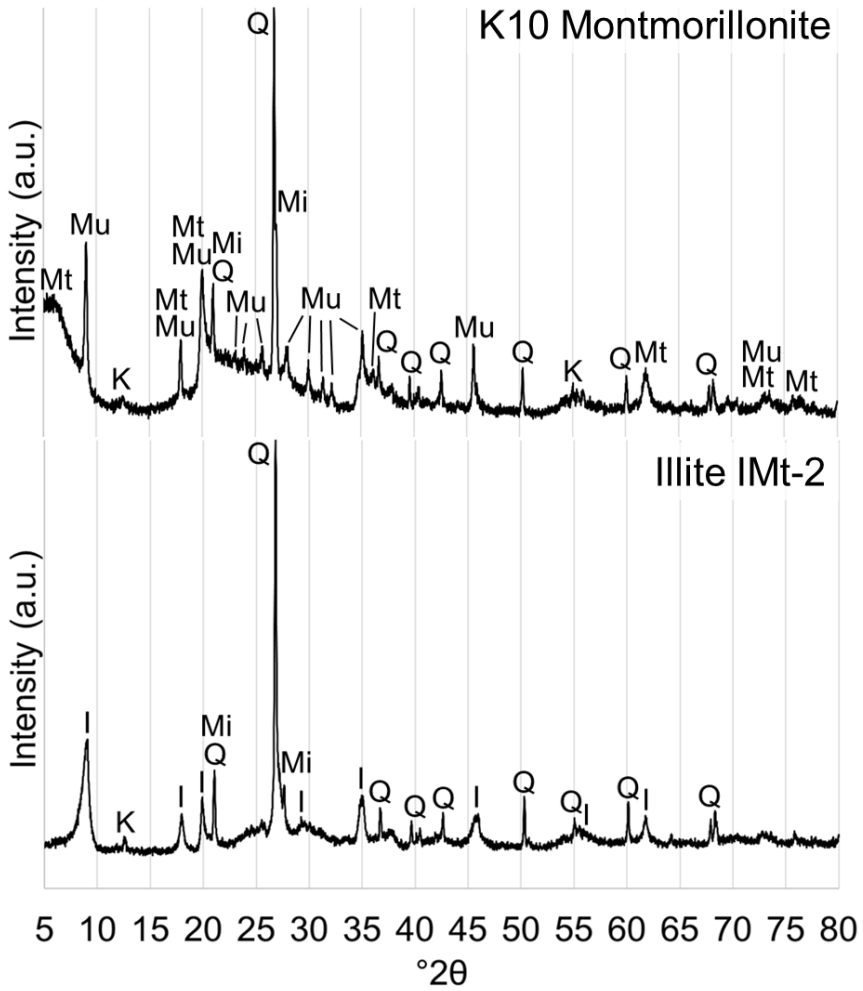

K = kaolinite; I = illite; Mi = microcline; Mu = muscovite; Mt = montmorillonite; Q = quartz.

Figure 5-2: X-Ray powder diffraction patterns of K10 montmorillonite and Illite Imt-2 precursors.

In the activated montmorillonite series, a change in the background profile was observed with increasing Na:Al (Figure 5-3), more clearly visible in the background patterns, extracted from the measured patterns using Le Bail refinement. The 17 – 22 °(2θ) (5.2 – 4.0 Å) hump in the precursor's pattern receded, and a broad hump emerged in the 22 – 35 °(2θ) (4.0 – 2.6 Å) region as Na:Al increased. This emergent hump was attributed to an amorphous geopolymer phase as described by Duxson *et al.* (2007a). No significant new crystalline reflections were observed. Seeming increases in the intensity of the montmorillonite/muscovite reflection at 17.8 °(2θ) (5.0 Å) between patterns were believed to arise from a combination of pattern effects, rather than changes in phase quantity. Firstly, the decrease in intensity of the neighbouring montmorillonite/muscovite reflection at 19.8 °(2θ) (4.5 Å) made the 17.8 °(2θ) (5.0 Å) reflection look more intense in comparison. Secondly, the described background changes affected the intensity of the quartz reflection at 26.6 °(2θ), which each pattern was normalised to. The 001 reflection shifted for all activated samples, corresponding

to a shift in d-value from 14.4 Å for the precursor clay to 11.6 Å. As shown by further experimentation reported in the Appendix, the synthesis conditions used for alkaline activation were not conducive to cation exchange of Na^+ in solution for the initial Ca^{2+} and/or Mg^{2+} in the interlayer sites. There was no significant shift in 2θ position of the muscovite 001 reflection in the activated samples, indicating there was no significant interlayer cation exchange of Na^+ for K^+. This is expected, given that Na^+ has a lower affinity for muscovite than K^+ (Osman *et al.*, 1999), and little exchange happens except on exposed surfaces (Gaines Jr, 1957).

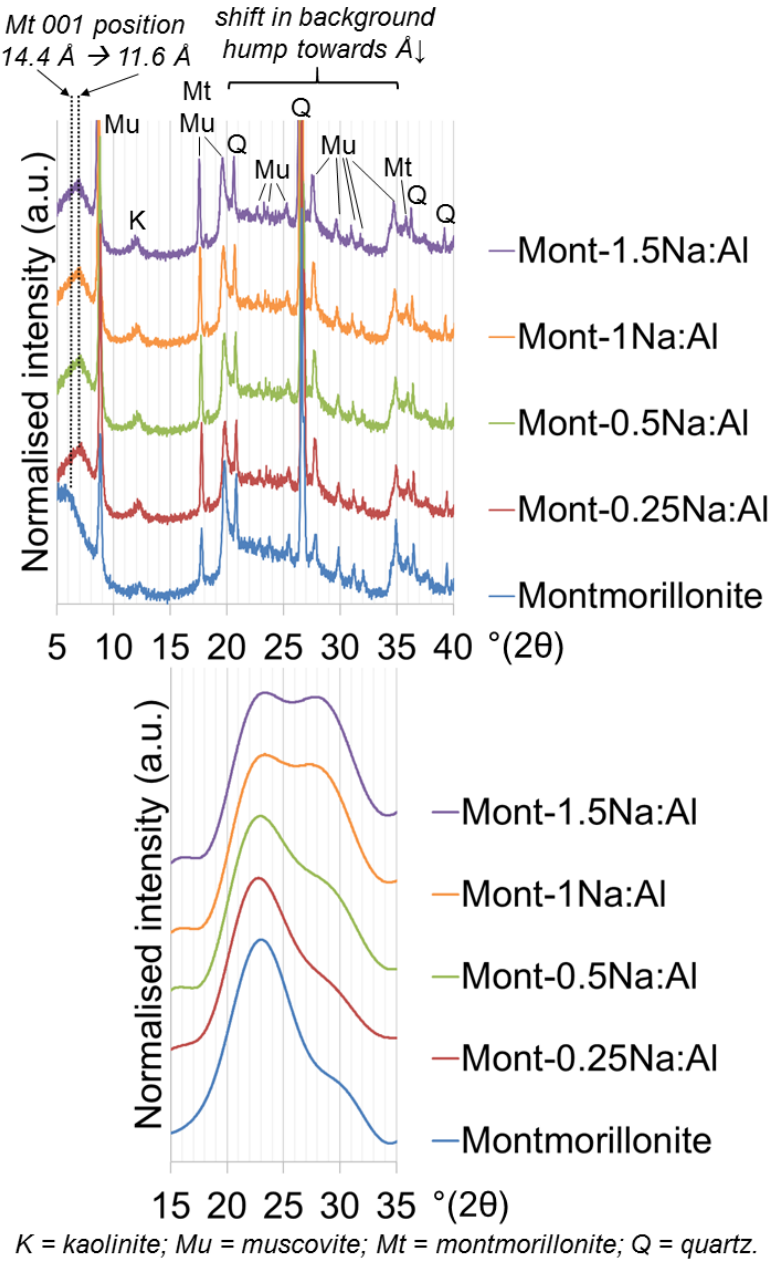

Figure 5-3: X-Ray powder diffraction patterns of the montmorillonite precursor and the cured samples. The lower set of patterns show the changes in extracted background in the 15-35 °2θ range.

In the activated illite series, several new crystalline reflections emerged (Figure 5-4). A small amount of hydrosodalite (PDF# 00-041-0009) was formed as Na:Al increased. This occurred in parallel with the consumption of the minor amount of kaolinite – estimated by Gailhanou *et al.* (2007) to make up <1% of the precursor – as would be expected for this type of synthesis (Marsh *et al.*, 2018). Reflections of natrite (Na_2CO_3) (PDF# 00-037-0451) and thermonatrite ($Na_2CO_3 \cdot H_2O$) (PDF# 00-008-0448) emerged as Na:Al increased, associated with efflorescence arising from an excess of Na in an alkali-activated system (Škvára *et al.*, 2012; Zhang *et al.*, 2014). Unlike the activated montmorillonite series, there were no significant changes in the patterns' backgrounds, or illite lattice parameters.

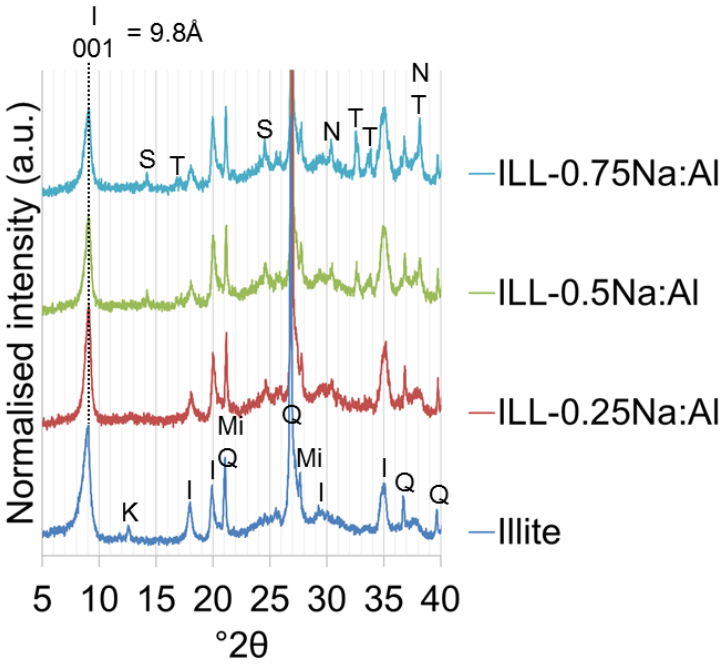

I = illite; K = kaolinite; Mi = microcline; N = natrite; Q = quartz; S = hydrosodalite; T = thermonatrite.

Figure 5-4: X-Ray powder diffraction patterns of the illite precursor and the cured samples.

5.3.2 SEM phase size and morphology

For the montmorillonite series (Figure 5-5), the microstructure changed with increasing Na:Al ratio. For low Na:Al ratios, this was irregularly shaped particles, with rough, flaky edges, typically ≤0.5 μm. As Na:Al increased, these particles formed a continuous phase rather than distinct individual particles.

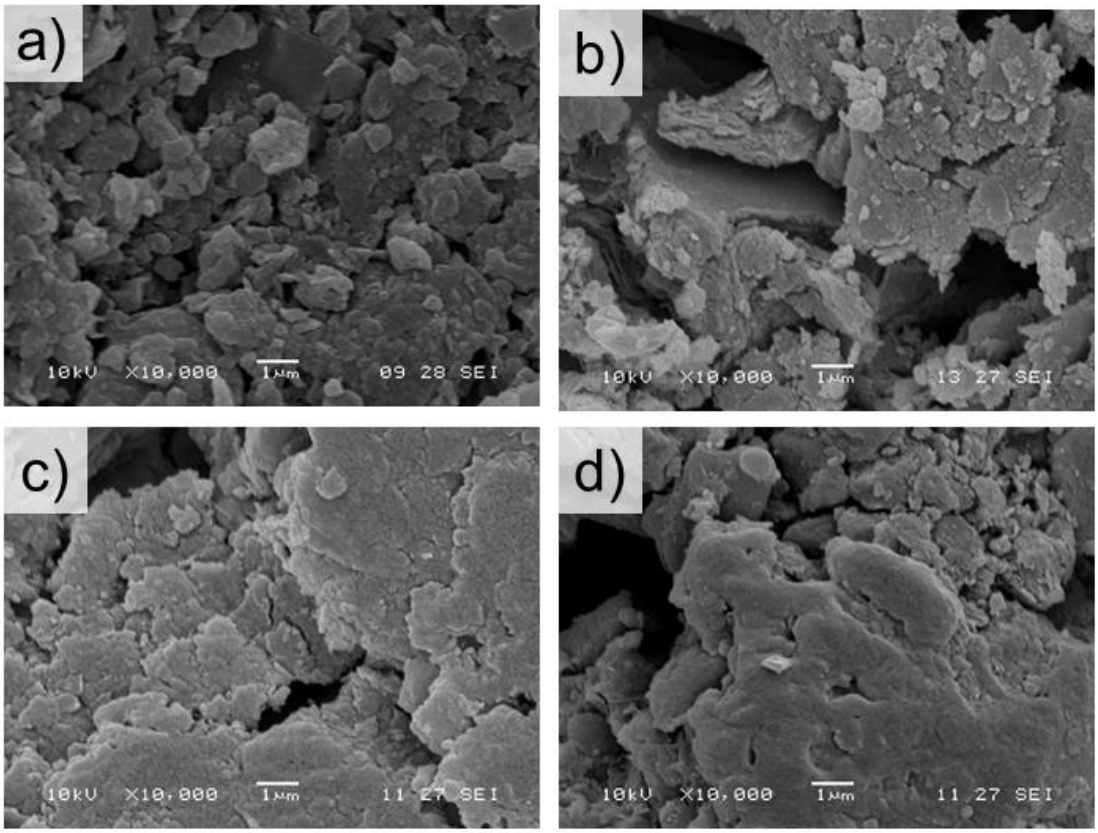

Figure 5-5: SEM images of the montmorillonite precursor a), and cured samples with the following Na:Al values: b) 0.5, c) 1, d) 1.5.

For the illite series (Figure 5-6), there were no significant differences in microstructure between the precursor and Na:Al = 0.25 – 0.5, however there were continuous changes, including the arrangement of particles. For Na:Al = 0.75, the particles had an elongated morphology. Possible explanations for this are explored in Section 5.4.4.

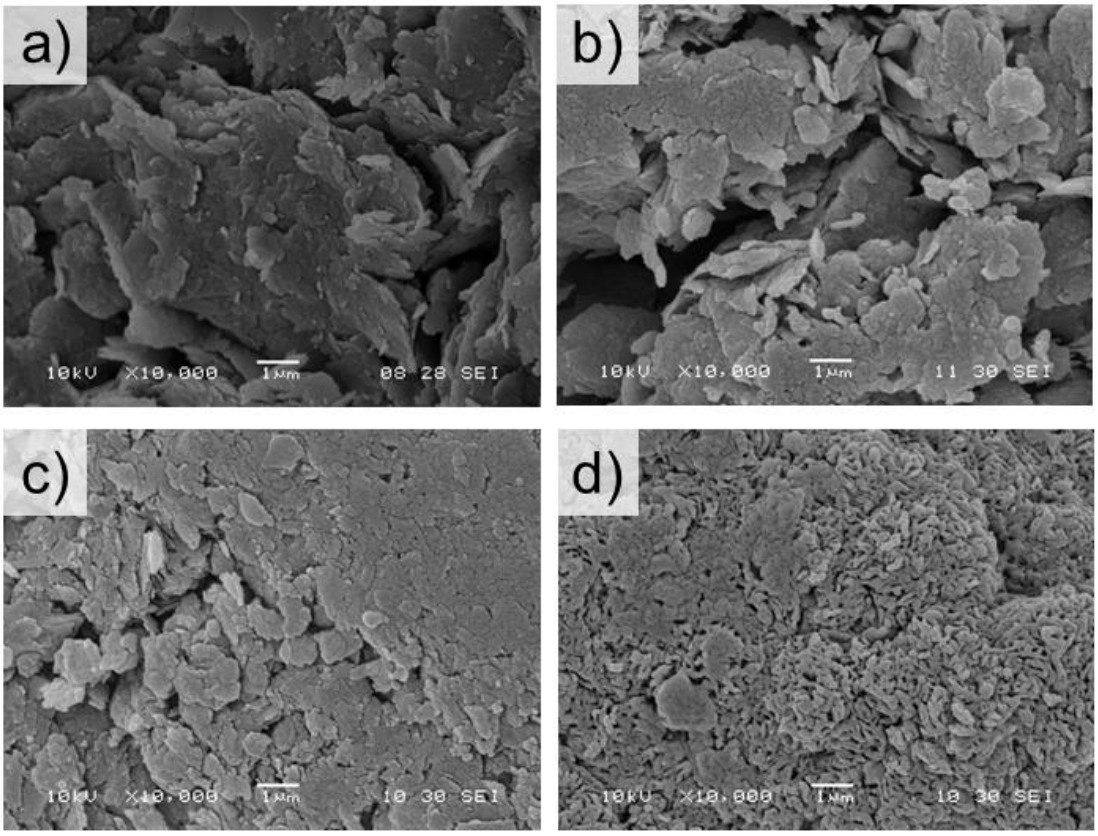

Figure 5-6: SEM images of the illite precursor a), and cured samples with the following Na:Al values: b) 0.25, c) 0.5, d) 0.75.

5.3.3 TGA thermal behaviour

The mass loss events at 30 – 200°C (dTG peak at 86°C) and 200 – 750°C (peak at 564°C) in the montmorillonite precursor (Figure 5-7) were attributed to the loss of surface adsorbed water and the dehydroxylation of the montmorillonite phase respectively (Földvári, 1991). Given that muscovite undergoes dehydroxylation at 780 – 950°C, the absence of a major dTG peak in this region indicates that muscovite is only present as a minor phase. The mass loss in the region of 200 – 1000°C is 4.5%. This is close to the range of theoretical dehydroxylation mass loss for montmorillonites of 4.7 – 4.9wt% (Christidis, 2011). Given that the only notable impurities from the XRD were muscovite and quartz, this indicates that montmorillonite is the majority phase in the precursor. MS data for all spectra is presented in the Appendix.

Overall mass loss increased with Na:Al over the range of Na:Al tested, from ~9.5% to 13%. The constant magnitude of the dTG peak at ~100°C over the Na:Al range was attributed to a simultaneous decrease in surface water desorption from montmorillonite, and increase in surface water desorption from the geopolymer product. This was inferred from a previous observation that metakaolin geopolymers have a water desorption peak at ~100°C (Bernal *et al.*, 2011). A plateau of increasing intensity formed in the dTG spectrum in the range 120 – 380°C. This signal was also attributed to the geopolymer phase, since it resembles a disordered form of zeolitic water desorption peaks in this temperature range (Alshaaer *et al.*, 2016). A distinct single peak has previously been observed at 270°C for simple geopolymer systems, albeit for longer curing times (Walkley *et al.*, 2016), whilst more complex clay-based systems have formed plateaus in that region (Alshaaer, 2013; Alshaaer *et al.*, 2016; Hounsi *et al.*, 2013). In addition, the XRD and SEM results show that a geopolymer is the only product phase present which could contribute to such a significant mass loss signal. Two peaks in the dTG spectra at ~470°C emerged only for Na:Al = 0.75 – 1, strongly associated with CO_2 evolution. These were not attributed to the geopolymer phase as no thermal loss events have been found above 350°C in simple geopolymer systems (Walkley *et al.*, 2016).

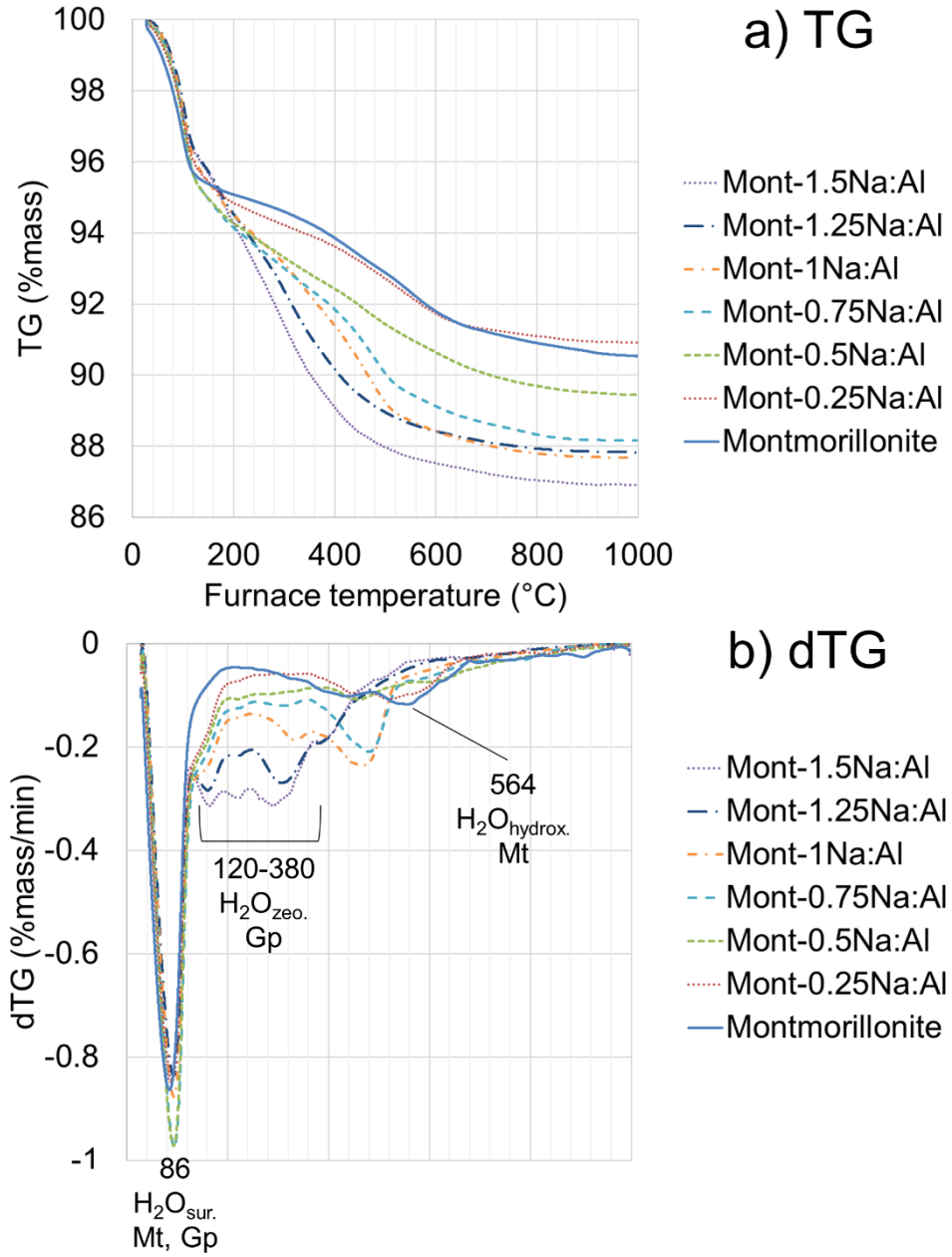

$H_2O_{sur.}$ = surface-adsorbed water; $H_2O_{zeo.}$ = zeolitic water; $H_2O_{hydrox.}$ = dehydroxylation
Mt = montmorillonite; Gp = geopolymer

Figure 5-7: a) TG spectra and b) dTG spectra, for montmorillonite precursor and cured samples.

The mass loss events at 30 – 115°C (dTG peak at 88°C) and 340 – 680°C (dTG peak at 545°C) in the illite precursor (Figure 5-8) were attributed to the loss of surface adsorbed water and the dehydroxylation of illite respectively (Földvári, 1991; Murad and Wagner, 1996).

There was an increase in overall mass loss as Na:Al increased, from 5% in the illite precursor to 14% in ILL-0.75Na:Al. This increase was distributed over thermal loss events in both the 30 – 115°C and 450 – 600°C ranges, which were both associated with evolution of H_2O and CO_2. The significant increase in intensity of the dTG peak at ~90°C with increasing Na:Al suggested that there is a significant increase in surface-adsorbed water, and hence surface area. The significant single dTG peak at 540°C in the activated illite samples was not attributed to a geopolymer, since the dTG signal range for a geopolymer was shown in the activated montmorillonite system to be a broad plateau within the 100 – 400°C range (Figure 5-7). The colour change to a red hue upon heating to 1000°C indicated that hematite had formed once the illite structure broke down completely releasing Fe^{2+} after 900°C (Murad and Wagner, 1996).

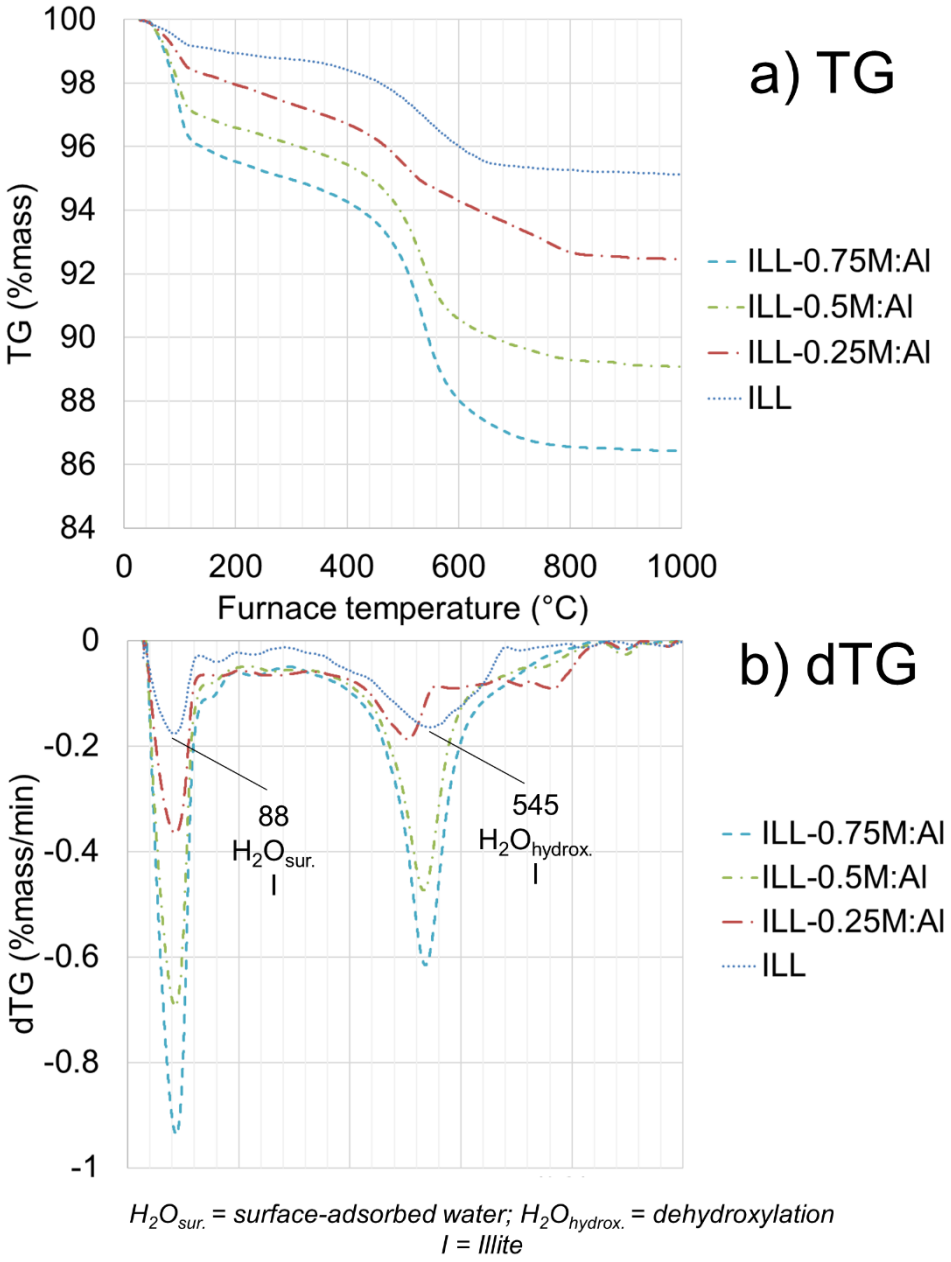

Figure 5-8: a) TG spectra and b) dTG spectra, for illite precursor and cured samples.

5.3.4 ^{27}Al and ^{29}Si MAS-NMR bonding coordination

In the montmorillonite precursor, the ^{27}Al spectrum had peaks at 70, 56 and 4 ppm (Figure 5-9a). The peaks at 70 and 4 ppm were attributed to AlO_4 and AlO_6 coordination respectively ((Engelhardt and Michel, 1987) cited in (Cativiela *et al.*, 1993)). The small amount of AlO_4 coordination was attributed to Al^{3+} substitution for Si^{4+} in the tetrahedral sheet of montmorillonite. These montmorillonite peaks may have overlapped with muscovite, whose peaks would be expected at 4 and 72 ppm (Kinsey *et al.*, 1985). The ^{29}Si spectrum had peaks at -93, -101 and -111 ppm (Figure 5-9b). The peaks at -93 and -101 ppm were both attributed to Si in Q_3(>1Al) coordination in the tetrahedral sheet of the montmorillonite (Cativiela *et al.*, 1993; Magi *et al.*, 1984), since decreased shielding from Al^{3+} substitutions moves Q_4(1Al) peaks to less negative chemical shifts (Kirkpatrick *et al.*, 1985). The peak at -111 ppm was attributed to tetrahedral sheet Si that had transformed from sheet (Q_3) to framework (Q_4) coordination as a result of the acid-washing process (Breen *et al.*, 1995). Another possible contribution is from a siliceous impurity (Magi *et al.*, 1984).

In the activated montmorillonite samples' ^{27}Al spectra, a peak emerged at 56 ppm, corresponding to tetrahedral Al coordination and attributed to a N-A-S-H geopolymer phase (Duxson *et al.*, 2005a; Singh *et al.*, 2005), with the other peaks remaining unchanged (Figure 5-9a). In the ^{29}Si spectra, a broad peak emerged in the -80 to -95 ppm range, corresponding to a range of Si coordination states in terms of non-bridging oxygens (NBOs) and Al next nearest neighbours (NNNs), and attributed to N-A-S-H geopolymer formation (Figure 5-9b) (Duxson *et al.*, 2005c; Fernández-Jiménez *et al.*, 2006). As Na:Al increased, this peak progressively shifted towards less negative chemical shifts, which is associated with a higher proportion of Al in the framework (Lee and Stebbins, 1999). This suggested there was initial preferential dissolution of silica from the clay at low Na:Al values, but becoming less Si-rich at higher Na:Al values. The ^{29}Si spectra had more changes than the ^{27}Al spectra in the activated montmorillonite samples. Despite this inconsistency, the overall evidence showed the formation of a geopolymer phase, in agreement with previous XRD and SEM results.

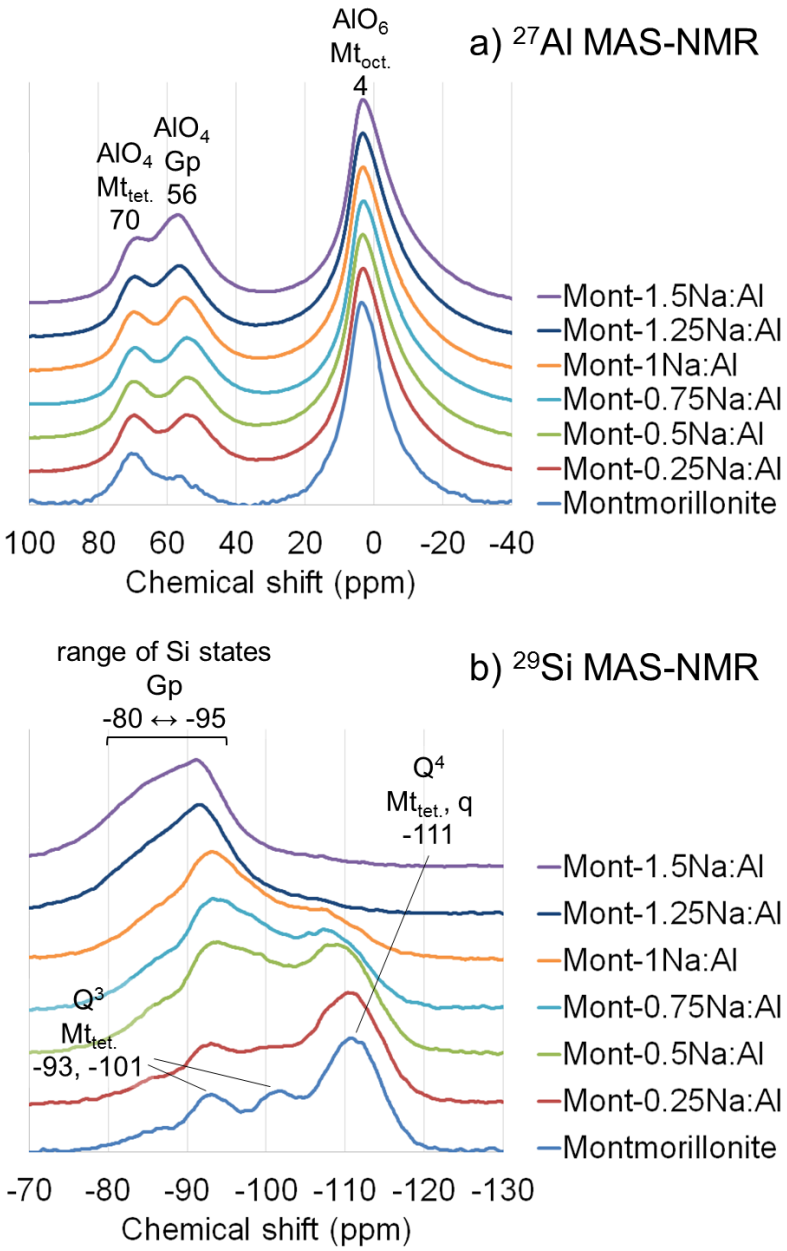

$Mt_{oct.}$ = octahedral sheet of montmorillonite;
$Mt_{tet.}$ = tetrahedral sheet of montmorillonite;
Gp = geopolymer; q = quartz / siliceous impurity

Figure 5-9: a) ^{27}Al MAS-NMR and b) ^{29}Si MAS-NMR spectra of montmorillonite precursor and cured samples.

In the ^{27}Al spectrum of the illite precursor (Figure 5-10a), the largest peak at 2 ppm was attributed to AlO_6 coordination in the octahedral sheet, and a small peak at 66 ppm to AlO_4 coordination of Al^{3+} substitutions in the tetrahedral sheet of illite (Kinsey *et al.*, 1985). In the ^{29}Si spectrum (Figure 5-10b), the largest peak at -90 ppm is attributed to Si in Q_3 coordination in the tetrahedral sheet of illite (Kinsey *et al.*, 1985). The breadth of this peak was caused by paramagnetism of iron atoms (Kirkpatrick *et al.*, 1985). The smaller ^{29}Si peak at -108 ppm was attributed to a quartz impurity (Thompson, 1984).

In the activated illite samples, the AlO_6 (2 ppm) and AlO_4 (66 ppm) illite peaks decreased with increasing Na:Al, indicating increased dissolution of the illite (Figure 5-10a). A peak emerged at 59 ppm, attributed to AlO_4 coordination given its location. Since this is the same coordination as the AlO_4 peak in the illite precursor but at a less positive chemical shift, the emergent peak represented an AlO_4 coordination state with a greater number of Al NNNs (Kirkpatrick *et al.*, 1985). The narrower profile of the emergent peak suggested it was a more ordered bonding environment (Kirkpatrick *et al.*, 1985). This was hence attributed to a hydrosodalite phase, which was known to have formed in small amounts from the XRD, and the peak matched well with sodalite produced in the same synthesis conditions using a kaolinite precursor (Marsh *et al.*, 2018). Unlike the activated montmorillonite samples' spectra, the ^{29}Si spectra changed little with increasing Na:Al (Figure 5-10b). There was some evidence of a peak emerging at -88 ppm, in agreement with observations of hydrosodalite formation under the same synthesis conditions (Marsh *et al.*, 2018), possibly accompanied by a decrease in intensity on the negative side of the tetrahedral peak. The indication of a small amount of hydrosodalite formation agreed with the XRD results, but without an obvious explanation for the microstructural changes observed in SEM images.

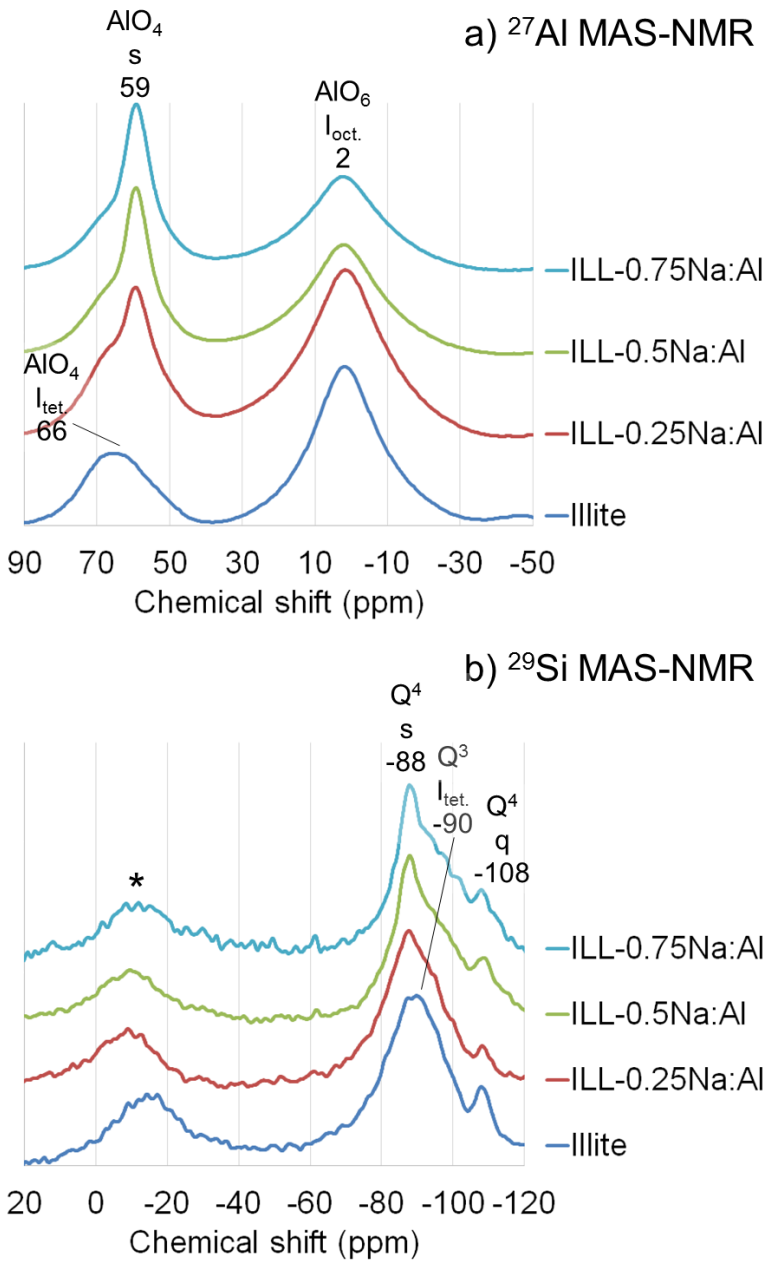

$I_{oct.}$ = octahedral sheet of illite;
$I_{tet.}$ = tetrahedral sheet of illite;
*q = quartz; s = sodalite; * = spinning side-band*

Figure 5-10: a) ^{27}Al MAS-NMR and b) ^{29}Si MAS-NMR spectra of illite precursor and cured samples.

5.3.5 FTIR molecular bonding

In the montmorillonite precursor, the FTIR spectrum (Figure 5-11a) was dominated by a Si-O-Si stretching band at 1031 cm^{-1}, with various shoulders (Van der Marel and Beutelspacher, 1976). Tables of band attributions are provided in the Appendix (Table 5-7). In the activated samples' spectra (Figure 5-11a), the montmorillonite Si-O-Si stretching band decreased as Na:Al increased, but was still present as a shoulder. The emergence of a new, broad band at ~1000 cm^{-1} was attributed to the asymmetric Si-O-T stretching modes of a geopolymer (Lee and van Deventer, 2003; Rees *et al.*, 2007). The lower wavenumber is indicative of a greater proportion of Si-O-Al bonds in the alkali aluminosilicate product phase relative to the precursor (Fernández-Jiménez and Palomo, 2005). As Na:Al increased, the peak position of the Si-O-T band progressively shifted to lower wavenumbers. This phenomenon was previously observed for fly ash (Hajimohammadi *et al.*, 2011), and here was likewise attributed to a decrease in the Si:Al ratio with increasing Na:Al. This interpretation agreed with the changes observed in the ^{29}Si-MAS-NMR spectra (Figure 5-9b). The decrease in wavenumber of the Si-O-T band's peak was the greatest between the precursor and Na:Al = 0.25, followed by (previously described) progressive decreases of smaller magnitude with increasing Na:Al. Given the XRD results showed that a consistent modification of montmorillonite occurred for all Na:Al values, it could be that this phenomenon also made some contribution to the observed band shift between the precursor and Na:Al = 0.25. The breadth of the bands made it difficult to say to what extent the spectral changes could be attributed to montmorillonite modification, and which to montmorillonite consumption and geopolymer formation. In the lower wavenumber range, the Si-O stretching band in the montmorillonite was partly replaced by a broad Si-O band which emerged at 779 cm^{-1} in the activated samples, attributed to a geopolymer (Barbosa *et al.*, 2000). CO_3^{2-} bands at 1441 and 880 cm^{-1} emerged for Na:Al ≥ 0.5 (Barbosa *et al.*, 2000). These corroborated the presence of carbonates, as suggested by the peaks attributed to CO_2 evolution in the dTG spectra (Figure 5-7b).

In the illite precursor, the FTIR spectrum was dominated by a Si-O-Al band at 987 cm^{-1} (Figure 5-11b). Tables of band attributions are provided in the Appendix (Table 5-8). In the activated samples' spectra the dominant band was broader, less intense and at a higher wavenumber (999 cm^{-1}) than the Si-O-Al band in the illite precursor (Figure 5-11b). Given their close proximity in wavenumber, it was unclear whether the dominant band in the activated samples was due to formation of an alkali aluminosilicate product phase, or from modification of the illite. Given that the XRD patterns of the activated patterns did not show a significant geopolymer hump or crystalline alkali aluminosilicate reflections, and retained a significant illite reflection, the

latter explanation was preferred. Similar to the activated montmorillonite samples' spectra, CO_3^{2-} bands at 1436 and 880 cm^{-1} emerged in all activated samples (Barbosa *et al.*, 2000). These corroborated the presence of carbonates, as shown in the XRD patterns (Figure 5-4) and the peaks attributed to CO_2 loss in the dTG spectra (Figure 5-7b). Although carbonate bands have been shown to be an associated product of geopolymer formation from the atmospheric carbonation of unconsumed NaOH in the system (Barbosa *et al.*, 2000), the evidence from the activated illite samples' spectra agreed with the preceding sections' conclusions that no significant amount of alkali aluminosilicate product phase was formed.

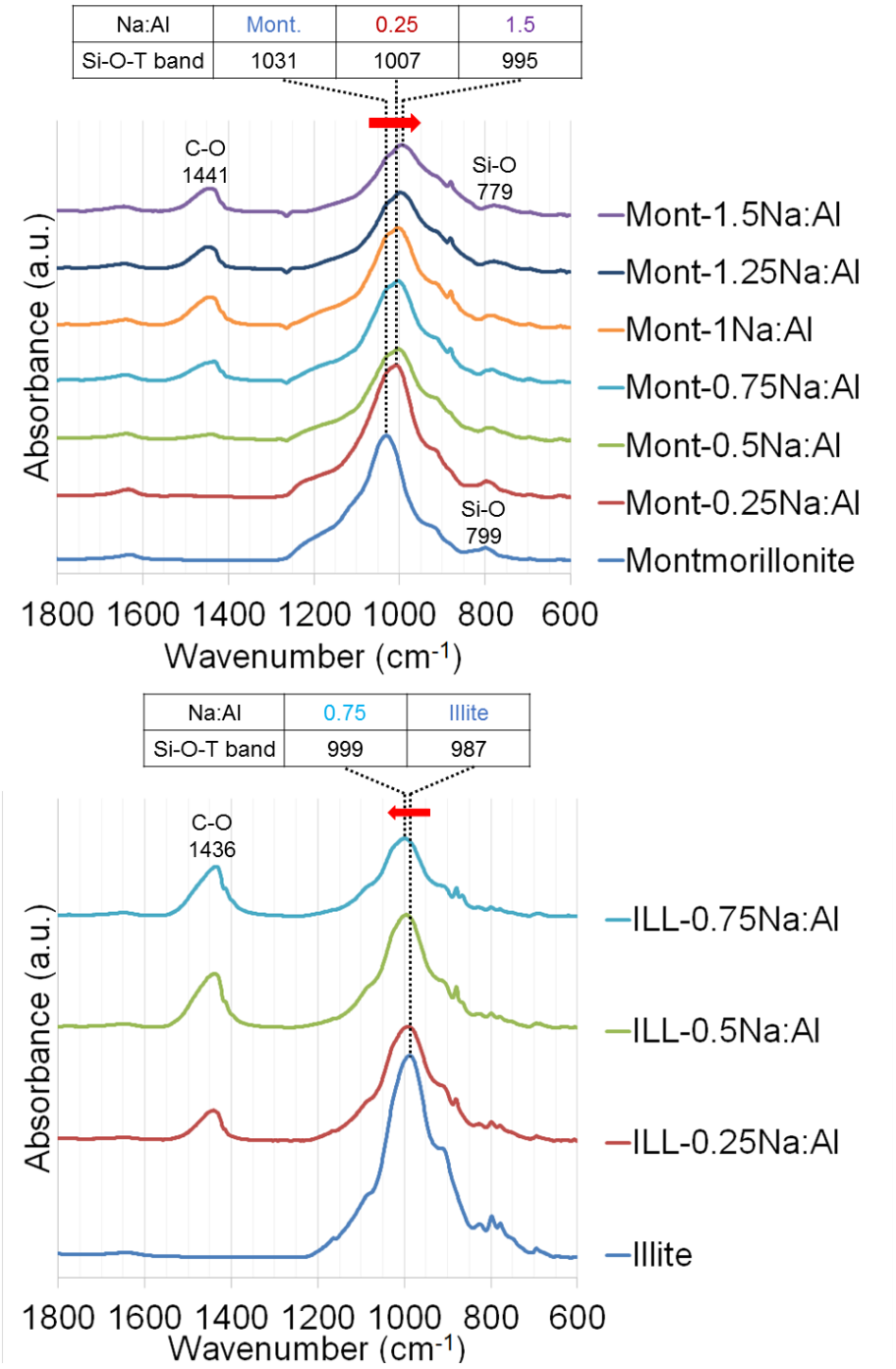

Figure 5-11: FTIR spectra of a) montmorillonite and b) illite precursors and activated samples.

5.3.6 Macroscopic behaviour

Photos taken after demoulding showed differences in curing behaviour between samples (Figure 5-12). In the activated montmorillonite series, samples in the Na:Al = 0.75 – 1 range exhibited angled shrinkage cracks and were noticeably darker in complexion than the others in the series. In the activated illite series, there was a significant trend in expansion as Na:Al increased. ILL-0.75Na:Al expanded beyond the top of the mould by >5 mm, ILL-0.5Na:Al expanded by ≤1 mm, and ≤2 mm shrinkage was observed for ILL-0.25Na:Al.

Figure 5-12: Photos of the cured samples of a) montmorillonite series and b) illite series. Samples were cured in 18 mm diameter, 36 mm height cylindrical moulds.

5.4 Discussion

Having characterised the product phases formed, it is necessary to understand how the differences in the clay minerals resulted in these different behaviours, and the effect of Na:Al molar ratio on the nature and quantity of product phase formed. Given the intended application of construction materials, it is also desirable to understand the relationships between micro- and macro-structures.

5.4.1 Transformations of the precursor clay minerals

Both systems require a qualitative approach to phase analysis as they are incompatible with quantitative methods (Marsh *et al.*, 2018), due to the overlap of signals from the precursor and product phases. In addition, the amorphous nature of geopolymer phases makes quantifying them, particularly using XRD, difficult.

In the montmorillonite series, a geopolymer phase was clearly formed when Na:Al ≥ 1. The activation behaviour was found to be similar to that of an untreated Bentonite (see Appendix for further experimentation). For the spectral measurements, especially dTG (Figure 5-7b) and ^{29}Si-MAS-NMR (Figure 5-9b), there was a progressive emergence of the characteristic signals as Na:Al increased. As for the exact nature of the geopolymer phase formed, it seems likely to have been either N-A-S-H or (N,C)-A-S-H. The latter is a N-A-S-H gel with partial substitution of Ca for Na (Garcia-Lodeiro *et al.*, 2015). The precursor contained a minor amount of calcium (0.5wt% CaO) (Table 5-1). The measured d-value of the montmorillonite suggested that some of this calcium was present as interlayer cations, and hence had potential to be a mobile species that could have been involved in the activation process. The formation of a C-A-S-H phase in large quantities was unlikely, as the amount of calcium in the system was insufficient for this. The $CaO:SiO_2:Al_2O_3$ normalised ratio of the precursor was 0.5% : 84.7% : 14.8%. This is much less than the minimum CaO content of 35% for a C-A-S-H phase, but well within the range for (N,C)-A-S-H (Garcia-Lodeiro *et al.*, 2011).

It has been shown that N-A-S-H and C-A-S-H phases can form together in an activating solution of < 7.5 M (Yip *et al.*, 2005). It is therefore feasible that for samples with Na:Al ≤ 1 (i.e. those with [NaOH] < 7.5 M), a trace amount of C-A-S-H formed in addition to a majority of N-A-S-H. However, this is very difficult to verify, due to the combined effect of the much smaller amount of total product phase formed and the similarity of their respective signals for several of the characterisation methods used. For the samples with Na:Al ≥ 1.25 (i.e. [NaOH] > 7.5 M), a single (N,C)-A-S-H phase is the most likely product. Given that there are no considerable differences in microstructure between (N,C)-A-S-H and pure N-A-S-H (García-Lodeiro *et al.*, 2010), this subtle phase difference is unlikely to be deleterious in a structural application.

In the illite series, there were clearly significant physical changes in both macrostructure (Figure 5-12) and microstructure (Figure 5-6). However, there was little chemical evidence to show transformation of the illite into a product phase for any of the samples in the series, only a small amount of hydrosodalite formed from the kaolinite impurity as well as sodium carbonates. It is therefore concluded that the alkali activation of illite resulted in some kind of structural breakdown. This process could be the alkaline analogy of either: acid activation, in which a three-dimensional, cross-linked structure of amorphous, porous silica is formed (Komadel, 1999; Komadel and Madejová, 2013); or, thermal dehydroxylation, which in kaolinite Al coordination is reduced from 6 to 5 and 4 (Heller-Kallai, 2013; Massiot *et al.*, 1995). This interpretation would be consistent with some of the observed changes: SEM images (Figure 5-6) and the adsorbed water peak in the dTG spectrum (Figure 5-8) indicated a significant increase in porosity.

It is clear from Table 5-3 that the systems in both series changed upon activation. However, the nature of a geopolymer phase, with its amorphous atomic structure, variable composition and variable microstructure, means that it is difficult to conclusively prove that a geopolymer phase has formed using a single characterisation technique. Using a range of advanced corroboratory techniques, the evidence in this study points towards geopolymer formation in the montmorillonite series, and structural alteration of illite with increasing Na:Al ratio.

Table 5-3: A summary of the strength of evidence for the formation of a geopolymer phase for montmorillonite and illite systems.

Characterisation method	Montmorillonite series	Illite series
XRD	Indicative	Undetectable
SEM	Indicative	Undetectable
TGA	Indicative	Undetectable
^{27}Al-MAS-NMR	Indicative	Undetectable
^{29}Si-MAS-NMR	quantitative	Undetectable
FTIR	Indicative	Undetectable

5.4.2 Differences between clay minerals in interlayer cation and dissolution behaviour

Clays in highly alkaline solutions can undergo interlayer cation exchange and/or dissolution. To develop a fuller understanding of differences in behaviour between the two clays, both phenomena will be considered.

With regard to interlayer cation exchange, the mechanism for the decrease in d-value of the montmorillonite during activation is not clear. The synthesis conditions used, particularly the low liquid:solid ratio, mean that it is unlikely that Na^+ exchange took

place to a large extent in the montmorillonite. It is also unlikely that exchange of other cations is responsible for the decrease in d-value. Elucidation of the exact mechanism of this phenomenon is beyond the scope of this study, further results and discussion are included in the Appendix.

With regard to the differing extents of reaction between the two precursors, it could be that the greater total effective surface area of montmorillonite helped to enable much greater dissolution than in the illite. As mentioned earlier, the acid wash pre-treatment could also have increased the surface area for the montmorillonite. Changes in the extent of dissolution through increased surface area alone are unlikely to explain the differences between the product phases. However, the substitution of Al for divalent cations during this process will have altered the Si:Al molar ratio of the clay mineral from its starting state. The extent of this Al removal depends on the acid strength and duration of the pre-treatment process (Komadel and Madejová, 2013).

In contrast to cation exchange, alkaline dissolution – especially at pH > 13 – is generally less well understood. Although a comparison of the precursors' dissolution behaviour is beyond the scope of this study, it needs brief consideration given its influence as the first reaction step in the geopolymerisation process (Duxson *et al.*, 2007a; Weng and Sagoe-Crentsil, 2007). Previous studies on the dissolution of montmorillonite (Bauer and Berger, 1998) and illite (Xu and Van Deventer, 2000) cannot be directly applied to interpret the reactions in this system because no studies have yet made a direct comparison of these two minerals under the same conditions, and in particular the low water contents used in this study. In addition, the solutions used here (pH 14 – 15) are significantly stronger than those typically used in dissolution studies (pH 11 – 13) (Köhler *et al.*, 2003). Although a direct comparative study has not been done, Köhler *et al.*, (2003) noted that alkaline dissolution rates are similar for many clay and micaceous minerals. From a mechanistic perspective of alkaline dissolution, muscovite and montmorillonite dissolve almost solely at particle edges, with negligible dissolution on the basal planes (Kuwahara, 2008; Yokoyama *et al.*, 2005). As described in section 5.3.1, there were significant differences in consumption of the montmorillonite, illite and muscovite phases in these systems, and also compared to the kaolinite phase in the analogous kaolinitic system (Marsh *et al.*, 2018). This could be primarily due to the larger quantities of clay phases in the precursors, compared to muscovite. It seems likely that the difference between the extents of dissolution is also partly attributable to differences in total edge surface area (ESA) of each mineral in the system.

5.4.3 Influence of Na:Al ratio

Na:Al ratio is the primary user-controlled variable in alkali activated soil systems, so it is important to understand its effects on the nature and quantity of products or transformed phases.

A geopolymer N-A-S-H or (N,C)-A-S-H phase was formed for samples in the activated montmorillonite series for Na:Al ≥ 1.25, and likely at lower values too. Whilst the nature of a geopolymer phase does not lend itself to quantitative phase analysis, there is qualitative evidence to suggest that the amount of geopolymer phase formed increased progressively with Na:Al. This molar ratio also seems to influence the nature, as well as quantity of the geopolymer phase formed. The observed decrease in the Si:Al ratio of the geopolymer phase, as described in Sections 5.3.4 and 5.3.5, is inferred to be caused by a decrease in the Si:Al ratio of the pore solution (Buchwald *et al.*, 2011). Although the Si:Al ratio of the geopolymer product is altered from the precursor, the total mix Si:Al ratio remains unchanged – the change in the geopolymer product phase is a function of the different dissolution rate for the Al and Si. The initial preference of silica dissolution is attributed to the increased porosity and disorder in the tetrahedral silica sheet (Komadel, 2003; Shinoda, 1995), which is expected to increase dissolution rate. This would likely have increased the supply of Si from the basal planes, which is negligible for ordered sheet silicates (Kuwahara, 2008). Whilst it is a subtle change in this instance, the ability of the Na:Al ratio to change the Si:Al molar ratio of the geopolymer formed is of fundamental interest due to the influence of Si:Al on the mechanical properties of geopolymers (Duxson *et al.*, 2005b).

For the illite series, increase in the Na:Al molar ratio possibly resulted in progressive decreases in the illite clay mineral signal intensity in the ^{29}Si MAS-NMR spectra (Figure 5-10b), and to a lesser extent in the XRD pattern (Figure 5-4). This suggests that more illite was altered as Na:Al increased. The most dramatic progressive change was in macroscopic behaviour, with increasing degrees of expansion during curing as Na:Al increased (Figure 5-12). Shrinkage was observed at Na:Al = 0.25, some expansion for Na:Al = 0.5, and extreme expansion for Na:Al = 0.75. This suggests that the nature of the alteration was more extreme at higher Na:Al values, in addition to simply more of the illite being altered. Unlike in the montmorillonite series, where increase in Na:Al increased the amount of geopolymer phase formed, in the illite the increase in Na:Al changed both the nature of the transformation product as well as possibly the amount of illite being transformed.

5.4.4 Linking macrostructural and microstructural changes

Given the performance of construction materials depends on both micro- and macro-structural performance and properties, it is important to determine any links between the two as observed in the SEM and photo images.

Two montmorillonite samples Mont-0.75Na:Al and Mont-1Na:Al underwent angled shrinkage cracking during curing (Figure 5-12). Apart from Na:Al molar ratio, there were no compositional differences between these samples and the rest of the series, and the phenomenon was shown to be repeatable. The only remaining explanation is that during the curing process, the NaOH concentration in the pore fluid induced a flocculation effect amongst the unreacted montmorillonite particles, resulting in localised face-face alignment and hence shrinkage cracks around the outside of the sample.

The ILL-0.75Na:Al sample expanded during the curing process, resulting in both macroscopic voids (Figure 5-12) and an altered microstructure (Figure 5-6) in the cured sample. One possible explanation is that a gas-generating reaction took place during curing. The oxidation of fine silica during alkali activation has been shown to produce a hydrogen gas, but the porosity generated by this mechanism is coarser than that observed here (Prud'homme *et al.*, 2010). Trace iron oxide phases could play a role, which are likely present from both the EDX results and the colour change after heating to 1000°C discussed in Section 5.3.3. Another explanation is that the illite underwent an alkali-induced structural breakdown, as already described in Section 5.4.1.

5.5 Conclusions

Montmorillonite and illite are both dioctahedral 2:1 clay minerals, but their alkali activation behaviour is very different. With the precursors and synthesis conditions used in this study, montmorillonite formed a N-A-S-H or (N,C)-A-S-H geopolymer as the major product phase, which increased in quantity but decreased in Si:Al ratio with increasing Na:Al molar ratio of the system. Illite increased in porosity upon alkali activation with Na:Al ≥ 0.5, but without forming a new product phase from the activation of the illite clay mineral itself. Both series displayed deleterious macroscopic changes, including both shrinkage and expansion, which cannot be entirely explained through the observed microstructural phenomena.

The prospect of making geopolymer-stabilised soil materials without calcination has both energy and processing benefits. However, even using a range of characterisation techniques it is extremely difficult to quantify the extent of phase transformations in these more complex aluminosilicate systems. Within the Na:Al ranges compatible with extrusion processing, the activation behaviour of uncalcined illite suggests illite-rich soils are not suitable for earth block construction, whereas montmorillonite-rich soils may be more promising. It remains to be seen whether using higher Si content or calcining the clays can produce a sufficient quantity of geopolymer to use for low impact earth masonry materials.

Acknowledgements

This study was supported by the EPSRC Centre for Decarbonisation of the Built Environment (dCarb) [grant number EP/L016869/1]; a University of Bath Research Scholarship; the Clay Minerals Group of the Mineralogical Society of Great Britain and Ireland, and the Armourers & Brasiers Gauntlet Trust. Solid-state NMR spectra were obtained at the EPSRC UK National Solid-state NMR Service at Durham. Thanks are given to the associate editor and four anonymous reviewers for their helpful comments and suggestions.

All data created during this research are openly available from the University of Bath data archive at https://doi.org/10.15125/BATH-00549.

References

Allahverdi, A., Najafi Kani, E., Hossain, K.M.A. & Lachemi, M., 2015. 17 – Methods to control efflorescence in alkali-activated cement-based materials. *Handbook of Alkali-Activated Cements, Mortars and Concretes.* Oxford: Woodhead Publishing, pp. 463-483.

Alshaaer, M., 2013. Two-phase geopolymerization of kaolinite-based geopolymers. *Applied Clay Science,* 86, pp. 162-168.

Alshaaer, M., El-Eswed, B., Yousef, R.I., Khalili, F. & Rahier, H., 2016. Development of functional geopolymers for water purification, and construction purposes. *Journal of Saudi Chemical Society,* 20, Supplement 1, pp. S85-S92.

Bain, J., 1971. A plasticity chart as an aid to the identification and assessment of industrial clays. *Clay Miner,* 9(1), pp. 1-17.

Barbosa, V.F.F., MacKenzie, K.J.D. & Thaumaturgo, C., 2000. Synthesis and characterisation of materials based on inorganic polymers of alumina and silica: sodium polysialate polymers. *International Journal of Inorganic Materials,* 2(4), pp. 309-317.

Bauer, A. & Berger, G., 1998. Kaolinite and smectite dissolution rate in high molar KOH solutions at 35° and 80°C. *Applied Geochemistry,* 13(7), pp. 905-916.

Belviso, C., Cavalcante, F., Niceforo, G. & Lettino, A., 2017. Sodalite, faujasite and A-type zeolite from 2:1 dioctahedral and 2:1:1 trioctahedral clay minerals. A singular review of synthesis methods through laboratory trials at a low incubation temperature. *Powder Technology,* 320, pp. 483-497.

Bergaya, F., Lagaly, G. & Vayer, M., 2013. Chapter 2.11 – Cation and Anion Exchange. In: F. Bergaya & G. Lagaly, eds. *Developments in Clay Science.* Elsevier, pp. 333-359.

Bernal, S.A., Rodríguez, E.D., Mejía de Gutiérrez, R., Gordillo, M. & Provis, J.L., 2011. Mechanical and thermal characterisation of geopolymers based on silicate-activated metakaolin/slag blends. *J Mater Sci,* 46(16), p. 5477.

Breen, C., Madejová, J. & Komadel, P., 1995. Correlation of catalytic activity with infra-red, 29Si MAS NMR and acidity data for HCl-treated fine fractions of montmorillonites. *Applied Clay Science,* 10(3), pp. 219-230.

Brigatti, M.F., Galán, E. & Theng, B.K.G., 2013. Chapter 2 – Structure and Mineralogy of Clay Minerals. In: F. Bergaya & G. Lagaly, eds. *Handbook of Clay Science.* 2nd ed. Amsterdam: Elsevier, pp. 21-81.

Brindley, G.W. & Brown, G., 1980. *Crystal structures of clay minerals and their X-ray identification.* London: Mineralogical Society.

BSI, 1990. BS 1377-2:1990 Methods of test for soils for civil engineering purposes. Classification tests

Buchwald, A., Zellmann, H.D. & Kaps, C., 2011. Condensation of aluminosilicate gels—model system for geopolymer binders. *Journal of Non-Crystalline Solids,* 357(5), pp. 1376-1382.

Cativiela, C., Figueras, F., Fraile, J.M., Garcia, J.I., Mayoral, J.A., de Me´norval, L.C. & Pires, E., 1993. Comparison of the catalytic properties of protonic zeolites and exchanged clays for Diels-Alder synthesis. *Applied Catalysis A: General,* 101(2), pp. 253-267.

Diop, M.B. & Grutzeck, M.W., 2008. Low temperature process to create brick. *Construction and Building Materials,* 22(6), pp. 1114-1121.

Dohrmann, R., Kaufhold, S. & Lundqvist, B., 2013. Chapter 5.4 – The Role of Clays for Safe Storage of Nuclear Waste. In: F. Bergaya & G. Lagaly, eds. *Developments in Clay Science.* Elsevier, pp. 677-710.

Duxson, P., Fernández-Jiménez, A., Provis, J.L., Lukey, G.C., Palomo, A. & van Deventer, J.S.J., 2007a. Geopolymer technology: the current state of the art. *J Mater Sci,* 42(9), pp. 2917-2933.

Duxson, P., Lukey, G.C., Separovic, F. & van Deventer, J.S.J., 2005a. Effect of Alkali Cations on Aluminum Incorporation in Geopolymeric Gels. *Industrial & Engineering Chemistry Research,* 44(4), pp. 832-839.

Duxson, P., Mallicoat, S.W., Lukey, G.C., Kriven, W.M. & van Deventer, J.S.J., 2007b. The effect of alkali and Si/Al ratio on the development of mechanical properties of metakaolin-based geopolymers. *Colloids and Surfaces A: Physicochemical and Engineering Aspects,* 292(1), pp. 8-20.

Duxson, P., Provis, J.L., Lukey, G.C., Mallicoat, S.W., Kriven, W.M. & van Deventer, J.S.J., 2005b. Understanding the relationship between geopolymer composition, microstructure and mechanical properties. *Colloids and Surfaces A: Physicochemical and Engineering Aspects,* 269(1), pp. 47-58.

Duxson, P., Provis, J.L., Lukey, G.C., Separovic, F. & van Deventer, J.S.J., 2005c. 29Si NMR Study of Structural Ordering in Aluminosilicate Geopolymer Gels. *Langmuir,* 21(7), pp. 3028-3036.

El Hafid, K. & Hajjaji, M., 2015. Effects of the experimental factors on the microstructure and the properties of cured alkali-activated heated clay. *Applied Clay Science,* 116–117, pp. 202-210.

Emmerich, K., 2000. Spontaneous rehydroxylation of a dehydroxylated cis-vacant montmorillonite. *Clays and Clay Minerals,* 48(3), pp. 405-408.

Engelhardt, G. & Michel, D., 1987. *High-resolution solid-state NMR of silicates and zeolites.* New York, NY: John Wiley and Sons.

Fawer, M., Concannon, M. & Rieber, W., 1999. Life cycle inventories for the production of sodium silicates. *The International Journal of Life Cycle Assessment,* 4(4), p. 207.

Fernández-Jiménez, A., de la Torre, A.G., Palomo, A., López-Olmo, G., Alonso, M.M. & Aranda, M.A.G., 2006. Quantitative determination of phases in the alkaline activation of fly ash. Part II: Degree of reaction. *Fuel,* 85(14–15), pp. 1960-1969.

Fernández-Jiménez, A. & Palomo, A., 2005. Mid-infrared spectroscopic studies of alkali-activated fly ash structure. *Microporous and Mesoporous Materials,* 86(1), pp. 207-214.

Fernandez, R., Martirena, F. & Scrivener, K.L., 2011. The origin of the pozzolanic activity of calcined clay minerals: A comparison between kaolinite, illite and montmorillonite. *Cement and Concrete Research,* 41(1), pp. 113-122.

Fernández, R., Ruiz, A.I. & Cuevas, J., 2014. The role of smectite composition on the hyperalkaline alteration of bentonite. *Applied Clay Science,* 95, pp. 83-94.

Ferrage, E., Lanson, B., Sakharov, B.A. & Drits, V.A., 2005. Investigation of smectite hydration properties by modeling experimental X-ray diffraction patterns: Part I. Montmorillonite hydration properties. *Am Mineral,* 90(8-9), pp. 1358-1374.

Földvári, M., 1991. Measurement of different water species in minerals by means of thermal derivatography. In: W. Smykatz-Kloss & S.S.J. Warne, eds. *Thermal Analysis in the Geosciences.* Berlin, Heidelberg: Springer Berlin Heidelberg, pp. 84-100.

Gailhanou, H., van Miltenburg, J.C., Rogez, J., Olives, J., Amouric, M., Gaucher, E.C. & Blanc, P., 2007. Thermodynamic properties of anhydrous smectite MX-80, illite Imt-2 and mixed-layer illite–smectite ISCz-1 as determined by calorimetric methods. Part I: Heat capacities, heat contents and entropies. *Geochimica et Cosmochimica Acta,* 71(22), pp. 5463-5473.

Gaines Jr, G.L., 1957. The ion-exchange properties of muscovite mica. *The Journal of Physical Chemistry,* 61(10), pp. 1408-1413.

García-Lodeiro, I., Fernández-Jiménez, A., Palomo, A. & Macphee, D.E., 2010. Effect of Calcium Additions on N–A–S–H Cementitious Gels. *Journal of the American Ceramic Society,* 93(7), pp. 1934-1940.

Garcia-Lodeiro, I., Palomo, A. & Fernández-Jiménez, A., 2015. 2 – An overview of the chemistry of alkali-activated cement-based binders. *Handbook of Alkali-Activated Cements, Mortars and Concretes.* Oxford: Woodhead Publishing, pp. 19-47.

Garcia-Lodeiro, I., Palomo, A., Fernández-Jiménez, A. & Macphee, D.E., 2011. Compatibility studies between N-A-S-H and C-A-S-H gels. Study in the ternary diagram Na2O–CaO–Al2O3–SiO2–H2O. *Cement and Concrete Research,* 41(9), pp. 923-931.

Garg, N. & Skibsted, J., 2014. Thermal Activation of a Pure Montmorillonite Clay and Its Reactivity in Cementitious Systems. *The Journal of Physical Chemistry C,* 118(21), pp. 11464-11477.

Gualtieri, A., Viani, A., Banchio, G. & Artioli, G., 2001. Quantitative phase analysis of natural raw materials containing montmorillonite. In: R. Delhez & E.J. Mittemeijer, eds. *European Powder Diffraction EPDIC 7*. Barcelona, Spain: Trans Tech Publ, pp. 702-709.
Gualtieri, A.F., 2000. Accuracy of XRPD QPA using the combined Rietveld-RIR method. *Journal of Applied Crystallography,* 33(2), pp. 267-278.

Gualtieri, A.F., Ferrari, S., Leoni, M., Grathoff, G., Hugo, R., Shatnawi, M., Paglia, G. & Billinge, S., 2008. Structural characterization of the clay mineral illite-1M. *Journal of Applied Crystallography,* 41(2), pp. 402-415.

Haines, S.H. & van der Pluijm, B.A., 2008. Clay quantification and Ar–Ar dating of synthetic and natural gouge: Application to the Miocene Sierra Mazatán detachment fault, Sonora, Mexico. *Journal of Structural Geology,* 30(4), pp. 525-538.

Hajimohammadi, A., Provis, J.L. & van Deventer, J.S.J., 2011. The effect of silica availability on the mechanism of geopolymerisation. *Cement and Concrete Research,* 41(3), pp. 210-216.

Heller-Kallai, L., 2013. Chapter 10.2 – Thermally Modified Clay Minerals. In: F. Bergaya & G. Lagaly, eds. *Handbook of Clay Science.* 2nd ed.: Elsevier, pp. 411-433.

Hollanders, S., Adriaens, R., Skibsted, J., Cizer, Ö. & Elsen, J., 2016. Pozzolanic reactivity of pure calcined clays. *Applied Clay Science,* 132-133, pp. 552-560.

Hounsi, A.D., Lecomte-Nana, G.L., Djétéli, G. & Blanchart, P., 2013. Kaolin-based geopolymers: Effect of mechanical activation and curing process. *Construction and Building Materials,* 42, pp. 105-113.

Ingles, O., 1970. Mechanisms of clay stabilization with inorganic acids and alkalis. *Soil Research,* 8(1), pp. 81-85.

Jagadish, K., 2007. *Building with Stabilized Mud.* New Delhi: I.K. International Publishing House Pvt. Ltd.

Kahr, G. & Madsen, F.T., 1995. Determination of the cation exchange capacity and the surface area of bentonite, illite and kaolinite by methylene blue adsorption. *Applied Clay Science,* 9(5), pp. 327-336.

Kaufhold, S. & Dohrmann, R., 2010. Stability of bentonites in salt solutions: II. Potassium chloride solution — Initial step of illitization? *Applied Clay Science,* 49(3), pp. 98-107.

Kinsey, R.A., Kirkpatrick, R.J., Hower, J., Smith, K.A. & Oldfield, E., 1985. High resolution aluminum-27 and silicon-29 nuclear magnetic resonance spectroscopic study of layer silicates, including clay minerals. *Am Mineral,* 70(5-6), pp. 537-548.

Kirkpatrick, R.J., Smith, K.A., Schramm, S., Turner, G. & Yang, W.-H., 1985. Solid-state nuclear magnetic resonance spectroscopy of minerals. *Annual Review of Earth and Planetary Sciences,* 13(1), pp. 29-47.

Köhler, S.J., Dufaud, F. & Oelkers, E.H., 2003. An experimental study of illite dissolution kinetics as a function of ph from 1.4 to 12.4 and temperature from 5 to 50°C. *Geochimica et Cosmochimica Acta,* 67(19), pp. 3583-3594.

Komadel, P., 1999. Structure and Chemical Characteristics of Modified Clays. In: P. Misaelides, F. Macášek, T.J. Pinnavaia & C. Colella, eds. *Natural Microporous Materials in Environmental Technology.* Dordrecht: Springer Netherlands, pp. 3-18.

Komadel, P., 2003. Chemically modified smectites. *Clay Miner,* 38(1), pp. 127-138.

Komadel, P. & Madejová, J., 2013. Chapter 10.1 – Acid Activation of Clay Minerals. In: F. Bergaya & G. Lagaly, eds. *Handbook of Clay Science.* 2nd ed.: Elsevier, pp. 385-409.

Kuwahara, Y., 2008. In situ observations of muscovite dissolution under alkaline conditions at 25–50 °C by AFM with an air/fluid heater system. *Am Mineral,* 93(7), p. 1028.

Lee, J.O., Kang, I.M. & Cho, W.J., 2010. Smectite alteration and its influence on the barrier properties of smectite clay for a repository. *Applied Clay Science,* 47(1), pp. 99-104.

Lee, S.K. & Stebbins, J.F., 1999. The degree of aluminum avoidance in aluminosilicate glasses. *Am Mineral*, 84(5-6), pp. 937-945.

Lee, W.K.W. & van Deventer, J.S.J., 2003. Use of Infrared Spectroscopy to Study Geopolymerization of Heterogeneous Amorphous Aluminosilicates. *Langmuir,* 19(21), pp. 8726-8734.

Liew, Y.M., Heah, C.Y., Mohd Mustafa, A.B. & Kamarudin, H., 2016. Structure and properties of clay-based geopolymer cements: A review. *Progress in Materials Science,* 83, pp. 595-629.

MacKenzie, K.J.D., 2009. Utilisation of non-thermally activated clays in the production of geopolymers. In: J.L. Provis & J.S.J. Van Deventer, eds. *Geopolymers: Structure, Processing, Properties and Industrial Applications.* Pp. 296-316.

Magi, M., Lippmaa, E., Samoson, A., Engelhardt, G. & Grimmer, A.R., 1984. Solid-state high-resolution silicon-29 chemical shifts in silicates. *The Journal of Physical Chemistry,* 88(8), pp. 1518-1522.

Marsh, A., Heath, A., Patureau, P., Evernden, M. & Walker, P., 2018. A mild conditions synthesis route to produce hydrosodalite from kaolinite, compatible with extrusion processing. *Microporous and Mesoporous Materials,* 264, pp. 125-132.

Maskell, D., Heath, A. & Walker, P., 2013. Laboratory scale testing of extruded earth masonry units. *Materials & Design,* 45, pp. 359-364.

Massiot, D., Dion, P., Alcover, J.F. & Bergaya, F., 1995. 27Al and 29Si MAS NMR Study of Kaolinite Thermal Decomposition by Controlled Rate Thermal Analysis. *Journal of the American Ceramic Society,* 78(11), pp. 2940-2944.

Monteiro, A., Jarrais, B., Rocha, I.M., Pereira, C., Pereira, M.F.R. & Freire, C., 2014. Efficient immobilization of montmorillonite onto cotton textiles through their functionalization with organosilanes. *Applied Clay Science,* 101, pp. 304-314.

Moore, D.M. & Reynolds, R.C., 1997. *X-ray diffraction and the identification and analysis of clay minerals.* 2nd ed. Oxford: Oxford University Press.

Muller, F.D., V.; Plançon, A.; Robert, J.-L., 2000. Structural transformation of 2:1 dioctahedral layer silicates during dehydroxylation-rehydroxylation reactions. *Clays and Clay Minerals,* 48(5), pp. 572-585.

Murad, E. & Wagner, U., 1996. The thermal behaviour of an Fe-rich illite. *Clay Miner,* 31(1), pp. 45-52.

Nakayama, S., Sakamoto, Y., Yamaguchi, T., Akai, M., Tanaka, T., Sato, T. & Iida, Y., 2004. Dissolution of montmorillonite in compacted bentonite by highly alkaline aqueous solutions and diffusivity of hydroxide ions. *Applied Clay Science,* 27(1), pp. 53-65.

Nickovic, S., Vukovic, A., Vujadinovic, M., Djurdjevic, V. & Pejanovic, G., 2012. High-resolution mineralogical database of dust-productive soils for atmospheric dust modeling. *Atmospheric Chemistry and Physics,* 12(2), pp. 845-855.

Osman, M.A., Moor, C., Caseri, W.R. & Suter, U.W., 1999. Alkali Metals Ion Exchange on Muscovite Mica. *Journal of Colloid and Interface Science,* 209(1), pp. 232-239.

Petříček, V., Dušek, M. & Palatinus, L., 2014. Crystallographic Computing System JANA2006: General features. *Zeitschrift für Kristallographie – Crystalline Materials,* 229(5), pp. 345-352.

Provis, J.L., 2014. Geopolymers and other alkali activated materials: why, how, and what? *Mat. Struct.,* 47(1), pp. 11-25.

Prud'homme, E., Michaud, P., Joussein, E., Peyratout, C., Smith, A., Arrii-Clacens, S., Clacens, J.M. & Rossignol, S., 2010. Silica fume as porogent agent in geo-materials at low temperature. *Journal of the European Ceramic Society,* 30(7), pp. 1641-1648.

Rees, C.A., Provis, J.L., Lukey, G.C. & van Deventer, J.S.J., 2007. In Situ ATR-FTIR Study of the Early Stages of Fly Ash Geopolymer Gel Formation. *Langmuir,* 23(17), pp. 9076-9082.

Sedmale, G., Korovkins, A., Seglins, V. & Lindina, L., 2013. Application of chemical trated illite clay for development of ceramics products. In: G.A. László, ed. *Iop Conf Ser-Mat Sci.* Miskolc-Lillafüred, Hungary: IOP Publishing, p. 012056.

Seiffarth, T., Hohmann, M., Posern, K. & Kaps, C., 2013. Effect of thermal pre-treatment conditions of common clays on the performance of clay-based geopolymeric binders. *Applied Clay Science,* 73, pp. 35-41.

Shinoda, T.O., Makoto; Izumi, Yusuke, 1995. Proposed Models of Mesopore Structures in Sulfuric Acid-Treated Montmorillonites and K10. *Chemistry Letters,* 24(7), pp. 495-496.

Singh, P.S., Bastow, T. & Trigg, M., 2005. Structural studies of geopolymers by 29Si and 27Al MAS-NMR. *J Mater Sci,* 40(15), pp. 3951-3961.

Škvára, F., Šmilauer, V., Hlaváček, P., Kopecký, L. & Cilova, Z., 2012. A weak alkali bond in (N, K)–A–S–H gels: evidence from leaching and modeling. *Ceram Silik,* 56(4), pp. 374-382.

Sperberga, I., Sedmale, G., Stinkulis, G., Zeila, K. & Ulme, D., 2011. Comparative study of illite clay and illite-based geopolymer products. In: K. Niihara, T. Ohji & Y. Sakka, eds. *3rd International Congress on Ceramics (ICC3).* Osaka, Japan: IOP Publishing, p. 222027.

Tchadjie, L.N. & Ekolu, S.O., 2018. Enhancing the reactivity of aluminosilicate materials toward geopolymer synthesis. *J Mater Sci,* 53(7), pp. 4709-4733.

Thompson, J., 1984. 29Si and 27Al nuclear magnetic resonance spectroscopy of 2: 1 clay minerals. *Clay Miner,* 19, pp. 229-236.

Tironi, A., Trezza, M.A., Scian, A.N. & Irassar, E.F., 2013. Assessment of pozzolanic activity of different calcined clays. *Cement and Concrete Composites,* 37, pp. 319-327.

Van der Marel, H.W. & Beutelspacher, H., 1976. *Atlas of infrared spectroscopy of clay minerals and their admixtures.* Amsterdam; New York: Elsevier Scientific Publishing Company.

Van Jaarsveld, J.G.S., van Deventer, J.S.J. & Lukey, G.C., 2002. The effect of composition and temperature on the properties of fly ash- and kaolinite-based geopolymers. *Chemical Engineering Journal,* 89(1–3), pp. 63-73.

Van Olphen, H., 1963. *An introduction to clay colloid chemistry for clay technologists, geologists, and soil scientists.* New York; London: Interscience.

Varadwaj, G.B.B., Rana, S. & Parida, K., 2013. Cs salt of Co substituted lacunary phosphotungstate supported K10 montmorillonite showing binary catalytic activity. *Chemical Engineering Journal,* 215–216, pp. 849-858.

Verburg, K. & Baveye, P., 1994. Hysteresis in the binary exchange of cations on 2: 1 clay minerals: a critical review. *Clays and Clay minerals,* 42(2), pp. 207-220.

Viani, A., Gualtieri Alessandro, F. & Artioli, G., 2002. The nature of disorder in montmorillonite by simulation of X-ray powder patterns. *Am Mineral.* Pp. 966-975.

Wagner, J.F., 2013. Chapter 9 – Mechanical Properties of Clays and Clay Minerals. In: F. Bergaya & G. Lagaly, eds. *Handbook of Clay Science.* 2nd ed. Amsterdam: Elsevier, pp. 347-381.

Walkley, B., San Nicolas, R., Sani, M.-A., Gehman, J.D., van Deventer, J.S.J. & Provis, J.L., 2016. Phase evolution of Na2O-Al2O3-SiO2-H2O gels in synthetic aluminosilicate binders. *Dalton Transactions,* 45(13), pp. 5521-5535.

Weng, L. & Sagoe-Crentsil, K., 2007. Dissolution processes, hydrolysis and condensation reactions during geopolymer synthesis: Part I—Low Si/Al ratio systems. *J Mater Sci,* 42(9), pp. 2997-3006.

Willoughby, D., Gross, K., Ingles, O., Silva, S. & Spiers, V.M., 1968. The identification of reaction products in alkali-stabilized clays by electron microscopy, X-ray and electron diffraction. In: 4th Australian Road Research Board Conference 1968. Aust. Road Res. Board pp. 1386-1408.

Xu, H. & Van Deventer, J.S.J., 2000. The geopolymerisation of alumino-silicate minerals. *International Journal of Mineral Processing,* 59(3), pp. 247-266.

Yip, C.K., Lukey, G.C. & van Deventer, J.S.J., 2005. The coexistence of geopolymeric gel and calcium silicate hydrate at the early stage of alkaline activation. *Cement and Concrete Research,* 35(9), pp. 1688-1697.

Yokoyama, S., Kuroda, M. & Sato, T., 2005. Atomic force microscopy study of montmorillonite dissolution under highly alkaline conditions. *Clays and Clay Minerals,* 53(2), pp. 147-154.

Zhang, L., 2013. Production of bricks from waste materials – A review. *Construction and Building Materials,* 47, pp. 643-655.

Zhang, Z., Provis, J.L., Reid, A. & Wang, H., 2014. Fly ash-based geopolymers: The relationship between composition, pore structure and efflorescence. *Cement and Concrete Research,* 64, pp. 30-41.

Appendix

In the main set of experiments, an acid-washed K10 montmorillonite was used as one of the clay precursors in alkali activation. As already described in the main text of the article, the acid-washing process is known to affect surface area and interlayer cation state. Additional experiments were undertaken to ensure that the reaction products were not affected by acid washing the K10 montmorillonite, and therefore that the comparison between the alkali activation behaviour of the K10 montmorillonite and the untreated illite was valid.

In this supplementary set of experiments, alkali activation was carried out on an untreated bentonite, containing montmorillonite as the major mineral phase. The activation behaviour was compared with that of the K10 montmorillonite. Additional experiments involving cation saturation were also carried out on the K10 montmorillonite to determine whether changes in d-value in the alkali-activated samples were due to interlayer cation exchange or other factors.

5.6 Introduction

In the main set of experiments, an acid-washed K10 montmorillonite was used as one of the clay precursors in alkali activation. As already described in the main text of the article, the acid-washing process is known to affect surface area and interlayer cation state. Additional experiments were undertaken to ensure that the reaction products were not affected by acid washing the K10 montmorillonite, and therefore that the comparison between the alkali activation behaviour of the K10 montmorillonite and the untreated illite was valid.

In this supplementary set of experiments, alkali activation was carried out on an untreated bentonite, containing montmorillonite as the major mineral phase. The activation behaviour was compared with that of the K10 montmorillonite. Additional experiments involving cation saturation were also carried out on the K10 montmorillonite to determine whether changes in d-value in the alkali-activated samples were due to interlayer cation exchange or other factors.

5.7 Experimental

5.7.1 Materials

The untreated montmorillonite-containing precursor used was a Fluka/Honeywell Bentonite (product no. 285234). BET surface area was measured as 24.9 m^2g^{-1}, however, this does not include the interlayer interface areas, which are accessible when the clay undergoes swelling in moisture (Christidis, 2011). Oxide composition was measured by EDX and is given in Table 5-4. For the cation saturation, a 1.1 M aqueous solution of sodium chloride was prepared using reagent grade sodium chloride (Sigma-Aldrich, product no. 31434) and distilled water. For the standard synthesis route, a 1.1 M aqueous solution of sodium chloride was prepared using sodium chloride flakes (Sigma-Aldrich, product no. 57653).

Table 5-4: Oxide composition of Bentonite (Fluka/Honeywell 285234), measured by EDX.

Oxide	**Al_2O_3**	**CaO**	**Fe_2O_3**	**K_2O**	**MgO**	**Na_2O**	**SO_3**	**SiO_2**	**Total**
Bentonite %wt. (std error)	19.78 (0.09)	1.70 (0.03)	6.95 (0.28)	0.47 (0.02)	2.12 (0.03)	1.81 (0.02)	0.55 (0.03)	66.63 (0.2)	100

5.7.2 Experimental procedures

Two main routes were used to make samples: the standard synthesis route as described in the main article, and cation saturation. A summary of the main variables for the additional samples is given in Table 5-5.

Table 5-5: Summary of main variables for additional samples, for 25 g of clay precursor.

Sample name	**Precursor**	**Method**	**Solution**	**Water : clay mass ratio**
Bent-1Na:Al	Bentonite	Standard synthesis	NaOH (6.4 M)	0.6
Bent-Na-exchange	Bentonite	Cation saturation	NaCl (1.1 M)	10.0
Mont-NaCl	K10 Montmorillonite	Standard synthesis	NaCl (1.1 M)	0.8
Mont-1Na:Al	K10 Montmorillonite	Standard synthesis	NaOH (6.4 M)	0.6
Mont-Na-exchange	K10 Montmorillonite	Cation saturation	NaCl (1.1 M)	10.0
Mont-control-exchange	K10 Montmorillonite	Cation saturation	Water	10.0

Alkali activation of the bentonite for sample Bent-1Na:Al was performed in the same manner as for the Na:Al = 1 sample of K10 montmorillonite. 25 g of clay was mixed with sufficient 6.4 M NaOH solution to achieve a wet mix with workability at the plastic limit. The standard synthesis procedure was also adapted for the sample Mont-NaCl by using a 1.1 M NaCl solution with K10 Montmorillonite.

Cation saturation was performed to provide an excess of Na^+ in conditions similar to those in the synthesis process, but without alkalinity. 25 g of clay was dispersed in 250 ml of 1.1 M aqueous sodium chloride solution in a round-bottomed flask, mixed by magnetic stirrer and heated under reflux to 80°C using an oil bath. A concentration of 1.1 M was chosen, as this was the lowest concentration of NaOH solution used in the series of activation of K10 montmorillonite in the main experiments. The saturation process was run for 6 hours, before the flask was removed and placed in an ice bath to cool. The K10 montmorillonite sample, Mont-Na-exchange, was dried by filtration through a Buchner funnel using a Fisher Qualitative filter paper, and then left to air dry. Due to its water adsorption and swelling properties, a Rotovap R-114 with acetone was used to remove excess water from the bentonite sample, Bent-Na-exchange, at 40°C, and then left to air dry. Control saturation for sample Mont-control-exchange was also performed using the same process, but with distilled water instead of a sodium chloride solution.

pH testing was performed to confirm that the high level of NaOH added was sufficient to overcome any residual acidity from the acid washing. For both K10 Montmorillonite and Bentonite, 2.5 g of clay was added to 25 ml of 1M NaOH solution in a round-bottomed flask, mixed by magnetic stirrer and heated under reflux to 80°C using an oil bath. The pH was measured before addition of clay, and then 1 hour and 24 hours after the addition of the clay.

5.7.3 Characterisation methods

XRD was used as already described, to measure the °2θ value of the 001 montmorillonite reflection in each sample, and then calculate the d-value in Å. The 001 basal reflection was analysed in order to elucidate the extent of interlayer cation exchange in alkali activation of montmorillonite, and determine the influence of interlayer cation exchange on plasticity behaviour. Patterns were corrected for sample height difference by calibration to the theoretical position of the quartz 101 reflection at 26.7 °2θ. SEM, BET, FTIR, TGA and plasticity measurements were also used as already described.

5.8 Results

5.8.1 Interlayer cation exchange behaviour

Each treatment of the K10 montmorillonite precursor resulted in different shifts in the 001 reflection peak centre of the montmorillonite phase (Figure 5-13 and Table 5-6). Whilst the 001 reflection in the precursor had a peak centre at 6.1 °2θ (calculated from the Le Bail refinement of the pattern) corresponding to a d-value of 14.4 Å, the control-saturated sample had a more well-defined reflection at 6.0 °2θ, and d-value of 14.7 Å. Na-saturation decreased the apparent d-value to 13.1 Å, whilst alkali activation resulted in a larger decrease to 11.6 Å.

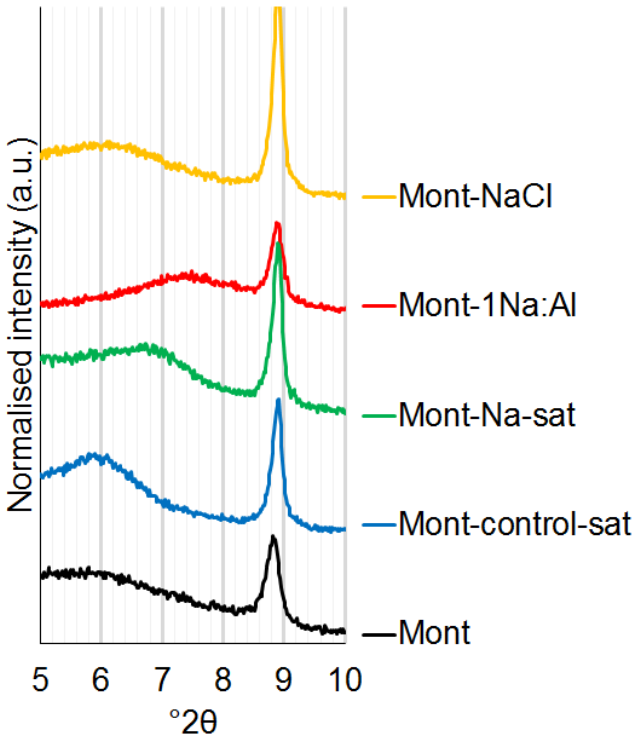

Figure 5-13: XRD patterns showing the position of the 001 reflection for the K10 montmorillonite precursor and after different processing routes.

Table 5-6: °2θ positions of the 001 montmorillonite reflection centre for the K10 montmorillonite precursor and after different processing.

Sample	001 reflection centre (°2θ)	d-value (Å)
Mont-NaCl	6.1	14.4
Mont-1Na:Al	7.6	11.6
Mont-Na-sat	6.7	13.1
Mont-control-sat	6.0	14.7
Mont	6.1	14.4

Plastic limit measurements for the K10 montmorillonite precursor, Na-saturated sample and activated sample are provided in Figure 5-14. After Na-saturation, there was a decrease in plastic limit, and after alkali activation there was a larger decrease, possibly because of some of the clay mineral being dissolved by the alkali activator. This trend was observed for both K10 montmorillonite and bentonite, although the decreases were greater for Bentonite.

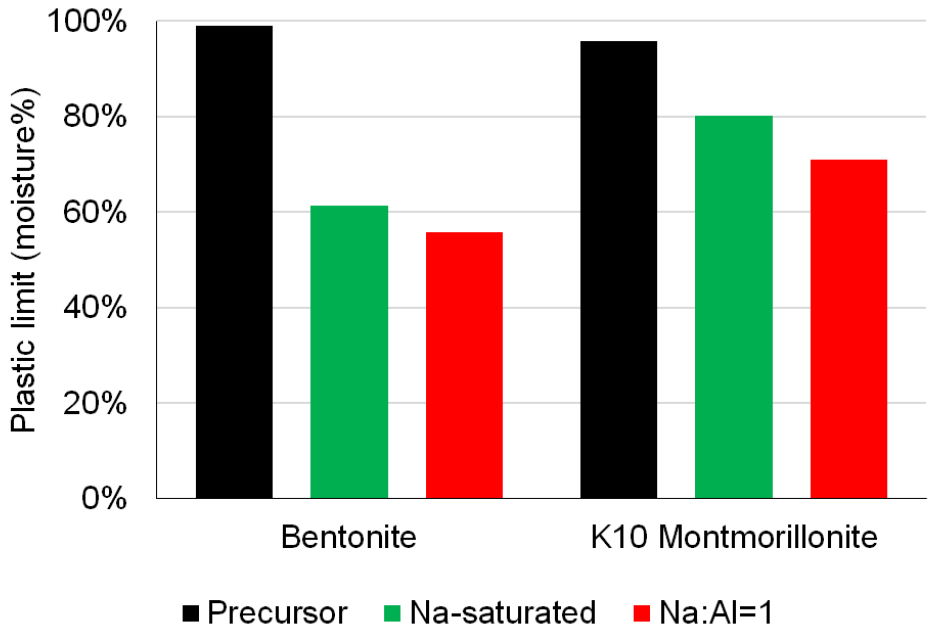

Figure 5-14: Plastic limit values for the Bentonite and K10 montmorillonite precursors, Na-saturated samples and alkali-activated samples.

5.8.2 Alkali activation behaviour of Bentonite and K10 Montmorillonite

Figure 5-15 gives XRD patterns for the precursors and activated samples of both K10 montmorillonite and bentonite. Both precursors contained quartz and muscovite as minor phases. K10 montmorillonite also contained microcline; bentonite also contained cristobalite and an albite. In the pH testing, the addition of K10 montmorillonite to 1 M NaOH solution resulted in a small decrease in pH within 1 hour, whereas there was no change for the addition of bentonite. The 0.3 reduction in pH was not anticipated to have a major effect on reaction products for the K10 montmorillonite.

The 001 reflection of montmorillonite was a lot broader and weaker in the K10 montmorillonite than the bentonite, which suggested greater disorder resulting from the acid treatment. In the activated samples, no major new crystalline phases were formed from either clay. There was also some evidence of a background shift in the XRD pattern in the 20 – 35 °2θ region in both activated clays, which is associated with geopolymer formation (Duxson *et al.*, 2007).

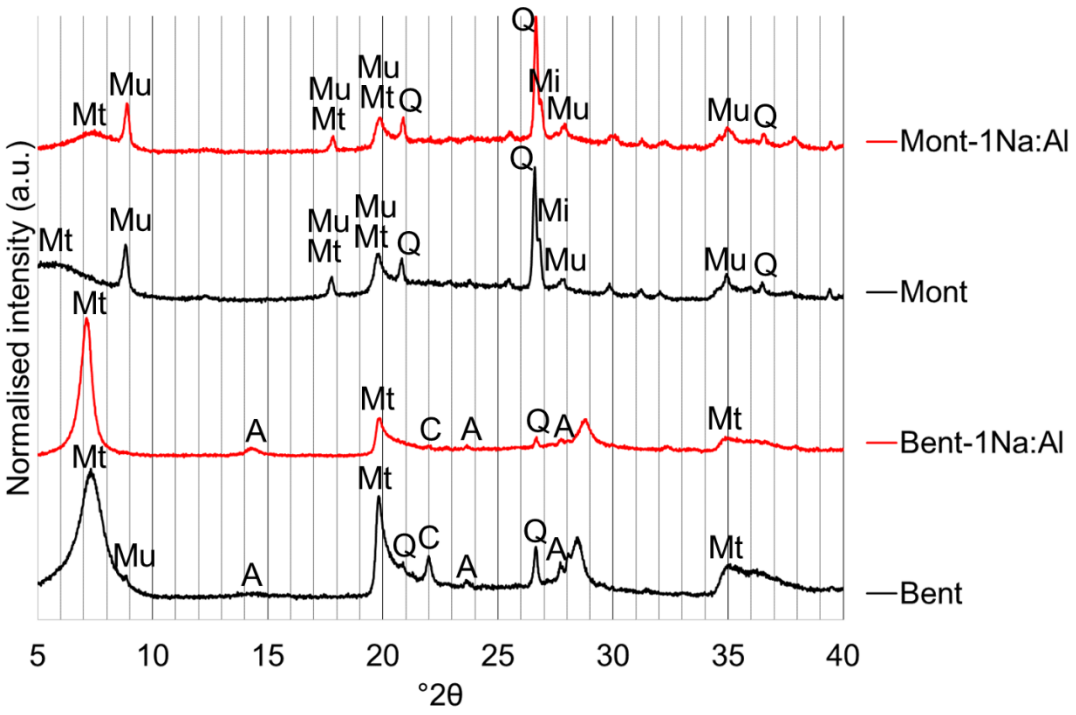

Figure 5-15: XRD patterns of precursors and alkali-activated samples of K10 montmorillonite and bentonite.

SEM images of the control and activated samples are shown in Figure 5-16. Both precursors had a plate-like morphology. After activation, there was a clear change in morphology in both clays. A granular structure was formed in bentonite, whilst a more continuous structure was formed in K10 montmorillonite.

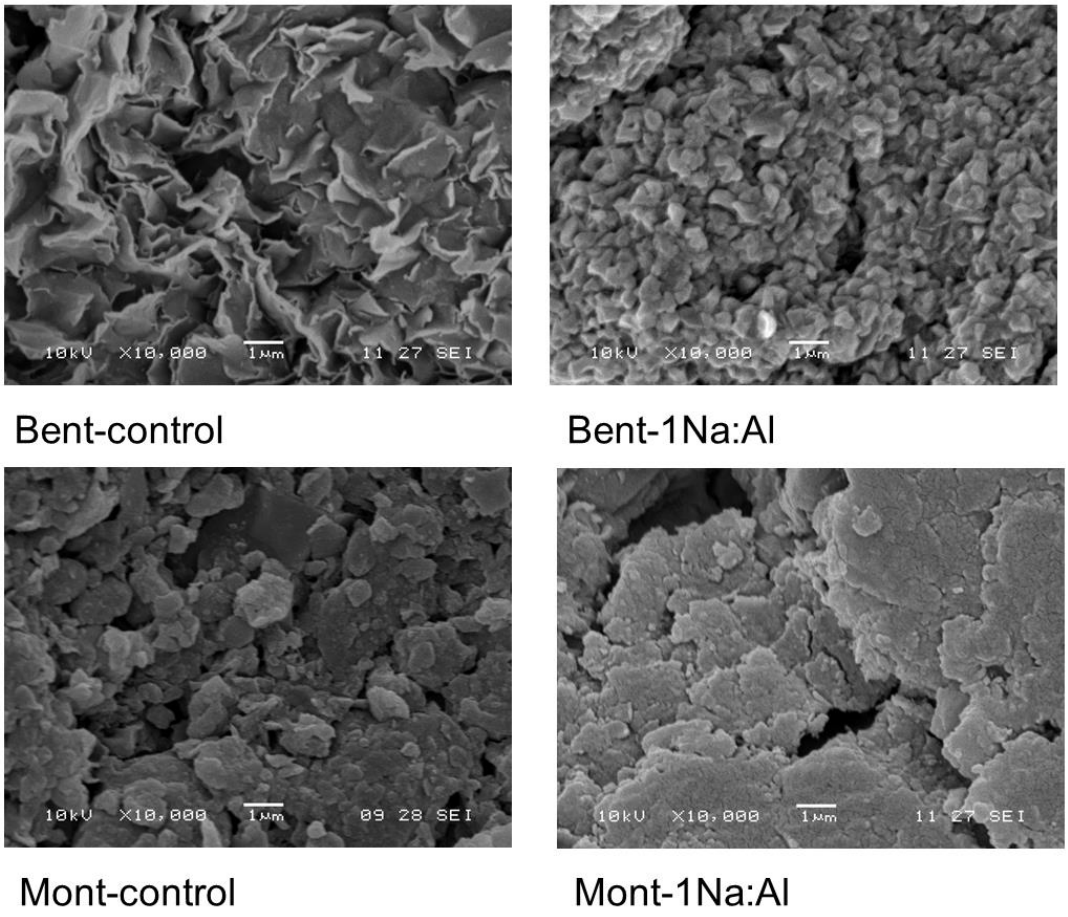

Figure 5-16: SEM images of control and activated samples of K10 montmorillonite and bentonite.

TG and dTG spectra for the precursors and activated samples of both clays are given in Figure 5-17. MS data is presented at the end of this Appendix. In the precursors of both clays, peak mass loss from surface adsorbed moisture was at around 100°C. The montmorillonite dehydroxylation peak in bentonite was well-defined at ~680°C, whereas in K10 montmorillonite it was much broader and centred at ~580°C. This temperature difference suggested that the montmorillonite phase in the bentonite had mainly cis-vacant octahedral sheets, whereas in the K10 montmorillonite it had mainly trans-vacant octahedral sheets (Drits *et al.*, 1995). The broader peak in the K10 montmorillonite would be expected from the amorphisation resulting from the acid activation process, yielding a range of activation energies for dehydroxylation.

There were no other large peaks in the dTG pattern, indicating that there was a small proportion of impurity phases in both precursors. The mass loss in the region of 200 – 1000°C was 4.5% for K10 montmorillonite and 4.9% for bentonite. These values are within, or close to, the range of theoretical dehydroxylation mass loss for montmorillonites of 4.7 – 4.9wt% (Christidis, 2011). This suggested that montmorillonite was the majority phase in both precursors.

After activation, both displayed similar changes in the profile of the dTG spectrum. The montmorillonite peak was reduced in intensity, whilst a series of broad peaks emerged in the range 100 – 500°C.

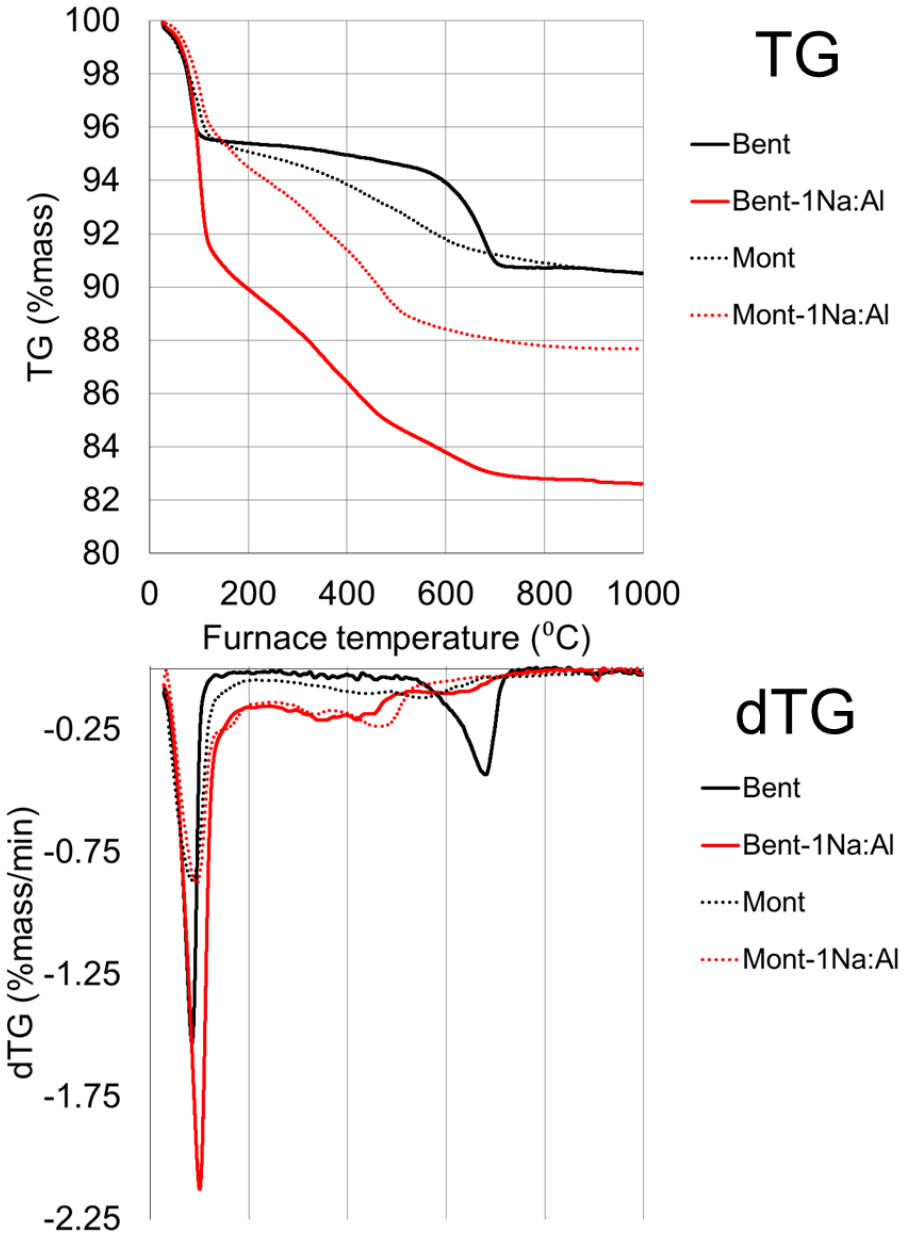

Figure 5-17: TG and dTG spectra of precursors and activated samples of K10 montmorillonite and bentonite.

The FTIR spectra of precursors and activated samples are given in Figure 5-18. The centre of the Si-O-T band was at 1031 cm^{-1} for the K10 montmorillonite and 999 cm^{-1} for the bentonite. The profile of the spectrum was broader and less well-resolved in the K10 montmorillonite compared to the bentonite, which suggested greater disorder in the material.

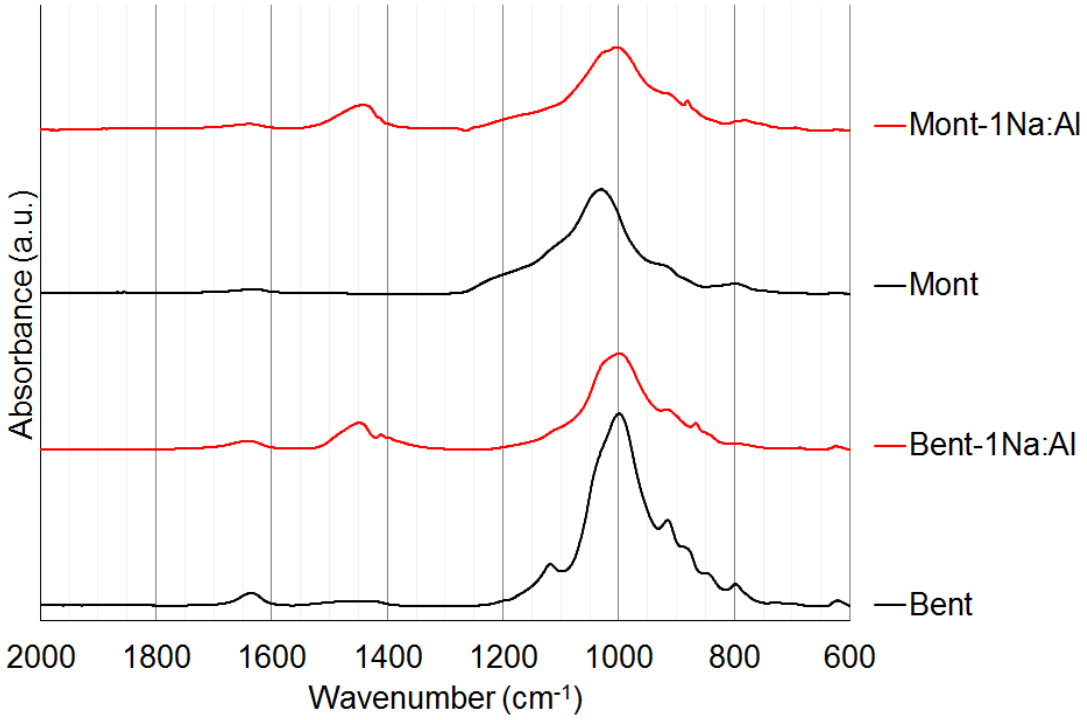

Figure 5-18: FTIR spectra of precursors and activated samples of K10 montmorillonite and bentonite.

In the activated samples, the centre of the Si-O-T band changed to 1003 cm^{-1} for the K10 montmorillonite and 999 cm^{-1} for the bentonite. Carbonate bands formed at ~1450 cm^{-1}, and the overall profile of the spectrum in the 1200 – 800 cm^{-1} region was similar. Full tables of band attributions are included here for the activated montmorillonite and illite series as described in the main article (Table 5-7, Table 5-8).

Table 5-7: Indexed absorption bands in montmorillonite series' FTIR spectra. Wavenumbers given are from the montmorillonite precursor's spectrum for montmorillonite phase bands, and from the Mont-1.5Na:Al spectrum for geopolymer phase bands. ⊥ = stretching vibration, ∥ = bending vibration. Rounded to nearest whole wavenumber.

Band	Wavenumber (cm^{-1})	Intensity	Phase	Reference
Si-O-Al	695	vw	Montmorillonite	(Van der Marel and Beutelspacher, 1976)
Si-O-Al	696	vw	Montmorillonite	(Van der Marel and Beutelspacher, 1976)
Si-O	779	w	Geopolymer	(Barbosa *et al.*, 2000)
Si-O (⊥)	799	w	Quartz / Montmorillonite	(Monteiro *et al.*, 2014; Van der Marel and Beutelspacher, 1976)
C-O	880	m / sh	Carbonate	(Barbosa *et al.*, 2000)
Al-OH-Al (∥)	920	m / sh	Montmorillonite	(Russell and Fraser, 1994)
Si-O-T (⊥)	995	vs	Geopolymer	(Lee and van Deventer, 2003; Rees *et al.*, 2007)
Si-O-Si (⊥)	1031	vs	Montmorillonite	(Van der Marel and Beutelspacher, 1976)
C-O	1441	m	Carbonate	(Barbosa *et al.*, 2000)
O-H (∥)	1629	vw	Montmorillonite	(Farmer, 1974; Russell and Fraser, 1994; Van der Marel and Beutelspacher, 1976)
O-H (∥)	1644	w	Geopolymer	(Barbosa *et al.*, 2000)

Table 5-8: Indexed absorption bands in the illite series' FTIR spectra. Wavenumbers given are from the illite precursor's spectrum for illite phase bands, and from the ILL-0.75Na:Al spectrum for altered illite bands. ⊥ = stretching vibration, ∥ = bending vibration. Rounded to nearest whole wavenumber.

Band	Wavenumber (cm^{-1})	Intensity	Phase	Reference
Si-O-Al	695	vw	Illite	(Van der Marel and Beutelspacher, 1976)
Si-O (⊥)	778	w	Quartz	(Van der Marel and Beutelspacher, 1976)
Si-O (⊥)	798	w	Quartz / Illite	(Van der Marel and Beutelspacher, 1976)
Si-O-Al	827	w	Illite	(Russell and Fraser, 1994)
C-O	880	m	Carbonate	(Barbosa *et al.*, 2000)
Al--O-H	901	m / sh	Illite	(Van der Marel and Beutelspacher, 1976)
Al--O-H	912	m / sh	Illite	(Van der Marel and Beutelspacher, 1976)
Si-O-Al	987	vs	Illite	(Russell and Fraser, 1994; Van der Marel and Beutelspacher, 1976)
Si-O-Al	999	vs	Altered illite	(Russell and Fraser, 1994; Van der Marel and Beutelspacher, 1976)
Si-O-Si (⊥)	1080	m / sh	Illite	(Russell and Fraser, 1994; Van der Marel and Beutelspacher, 1976)
Si-O-Si (⊥)	1089	m / sh	Illite	(Russell and Fraser, 1994; Van der Marel and Beutelspacher, 1976)
Si-O	1163	w / sh	Illite	(Russell and Fraser, 1994; Van der Marel and Beutelspacher, 1976)
C-O	1436	s	Carbonate	(Barbosa *et al.*, 2000)
O-H (∥)	1652	vw	Illite	(Van der Marel and Beutelspacher, 1976)

5.9 Discussion

5.9.1 Changes in basal spacing in K10 montmorillonite

The d-value measured from the position of the 001 reflection in PXRD is the sum of the layer thickness and the interlayer distance. The interlayer distance is determined by the interlayer cations and the extent of interlayer hydration. The interlayer hydration is in turn influenced by layer charge, interlayer cation species, relative humidity and any Brownian swelling between particles (Brigatti *et al.*, 2013).

The K10 montmorillonite precursor underwent cation exchange for Na^+ when an excess of Na^+ is supplied in solution. This was shown by the decrease in d-value in the Na-saturated sample relative to the control-saturated sample. The measured values for the control-saturated (14.7 Å) and Na-saturated (13.1 Å) samples are similar to the values measured by Ferrage et al. for a Ca-saturated montmorillonite (15.02 Å) and a Na-saturated montmorillonite (12.45 Å) respectively, at 40% humidity (Ferrage *et al.*, 2005).

The profile of the 001 reflection in the precursor was much broader compared to samples in which it has subsequently been wetted and dried. This could be due to rehydration-dehydration effects. It is possible that the precursor was flash-dried, which may give different drying behaviour to the typical processing route used in this study, which is wetting and then drying in an 80°C oven or in ambient conditions.

There was a greater decrease in d-value in the alkali-activated samples than in the Na-saturated sample. This shift was the same for all the alkali-activated K10 montmorillonite samples. Comparing the samples prepared with NaCl solutions, Mont-Na-exchange and Mont-NaCl, there was a large d-value decrease for the former but not the latter. This shows that cation exchange of Na in K10 montmorillonite occurs when liquid:solid ratio is high. When the liquid:solid ratio is low, only limited Na exchange appears to occur. Comparing the samples prepared at low liquid:solid ratio using the standard synthesis method, Mont-1Na:Al and Mont-NaCl, there was a large d-value decrease for the former but only a small decrease in the latter. As already stated, the lack of 001 reflection shift in the Mont-NaCl sample suggests that Na-exchange does not occur to a large extent under the standard synthesis conditions. However, there was still a large 001 reflection shift in the Mont-1Na:Al sample. It would therefore seem that the large decrease in d-spacing for the alkali-activated K10 montmorillonite samples is caused by something other than only Na-exchange. Determination of the exact mechanism of this phenomenon is beyond the scope of this study, but some suggestions are briefly described here.

Ca, K and Mg were present in minor quantities in the K10 montmorillonite precursor. Exchange for Ca and Mg would be consistent with the d-value of the precursor, so even if they did participate in exchange, this would not explain the shift. Interlayer saturation with K would be expected to provide a decrease of similar magnitude, but it is believed that low quantity of K present is from the limited muscovite present rather than in in the montmorillonite interlayer. The muscovite is not believed to have undergone a large extent of dissolution during the synthesis process.

The interlayer spacing of the alkali-activated samples agrees well with the 0% r.h. values of Ca- and Mg-smectites, which have a similar d-value to the precursor (Ferrage *et al.*, 2005). Negligible change in d-spacing was observed after storage in these conditions up to 12 months. The observed behaviour seems to be the opposite of a pillaring synthesis, in that the interlayer spacing is permanently reduced – possibly by permanent dehydration. The formation of geopolymer may have 'sealed' the montmorillonite in its dehydrated state during curing. Given the small extent of transformation for the lower values of Na:Al, this explanation seems unsatisfactory. However, given the residual acidity shown by the pH testing, this phenomenon could be associated with a neutralisation reaction occurring between layers.

There is some similarity between the alkali activation process used here and the procedures used in making pillared clays – both use NaOH to produce Al oligomers. However, in NaOH solutions the dominant Al oligomer is $[Al(OH)_4]^-$ (Weng and Sagoe-Crentsil, 2007; Weng *et al.*, 2005), and does not include the anions required to obtain typical pillaring species (Vicente *et al.*, 2013).

Unreacted NaOH in the activated samples could act as a local desiccant, dehydrating the montmorillonite layers. However, given the storage conditions, any residual NaOH may have already reached equilibrium hydration, negating any desiccating potential.

The decrease in plastic limit observed for the Na-saturated K10 Montmorillonite sample agreed with previous experimental results (Bain, 1971). However, when the precursor was mixed with sodium hydroxide solution, the reduction in plastic limit was unlikely to be due to Na-exchange at these low liquid:solid ratios, as previously shown. The even lower plastic limit measured for this is therefore likely to be due to the partial dissolution of particles. Partial dissolution would decrease the solid:liquid mass ratio, therefore acting as a plasticizing process.

5.9.2 Comparison of the K10 montmorillonite and Bentonite precursors

From the characterisation carried out, it was shown that both precursors contain montmorillonite clay mineral as the majority phase.

The biggest difference between them is in stacking and swelling behaviour. This was evident visually in the large amount of swelling of the bentonite clay during the control saturation process, which was not observed for the K10 montmorillonite. This difference is likely to arise because the K10 montmorillonite's ability to form stacks, and therefore to swell, had been disrupted by the effect of the acid washing treatment. This interpretation is supported by the measurements of the BET nitrogen adsorption. The stacking behaviour of the bentonite meant that under vacuum the interlayer spaces in stacks collapsed, meaning a much smaller surface area was measured than would be available in an excess of water. For the K10 montmorillonite, the lack of stacking behaviour meant that all available surface area was accessible to N_2 molecules under vacuum. The difference in dehydroxylation temperatures shows a difference in structure within the montmorillonite's octahedral sheets, but this is not believed to be a significant factor in the dissolution process.

5.9.3 Activation behaviour of the K10 montmorillonite and Bentonite precursors

After activation, in both clays there was an emergence of a new morphology in the microstructure, an absence of strong crystalline peaks in XRD, as well as a characteristic background shift. There was also a notable reduction in friability. The collective evidence therefore suggests that a geopolymer phase was formed in both activated clays.

5.10 Conclusions

It is unlikely that a large extent of Na-interlayer exchange of the K10 montmorillonite occurred during the alkali-activation synthesis route, due to the low liquid:solid ratio. The decrease in d-value of the montmorillonite phase during synthesis is therefore thought to be caused by a different mechanism, which has not yet been confirmed.

The two montmorillonite-containing precursors had several differences, in particular their degree of crystalline disorder, and stacking and swelling behaviour. In terms of alkali activation behaviour – the focus of investigation of the main article – behaviour is not identical but is similar for both precursors. The characterisation evidence suggests that a geopolymer was formed in both activated samples. This therefore shows that despite the acid activation process, the reaction products from alkali activation of K10 montmorillonite is similar to that of the untreated bentonite. Therefore, it is valid for a comparison to be made between the activation of K10 montmorillonite and untreated illite in the main article.

5.11 Mass spectrometry data

The mass spectrometry (MS) data that was collected alongside the thermogravimetric (TG) data is presented here for the following sample series from both the main article and Appendix:

- Mont and activated Mont (Figure 5-19)
- ILL and activated ILL (Figure 5-20)
- Bent and activated Bent (Figure 5-21)

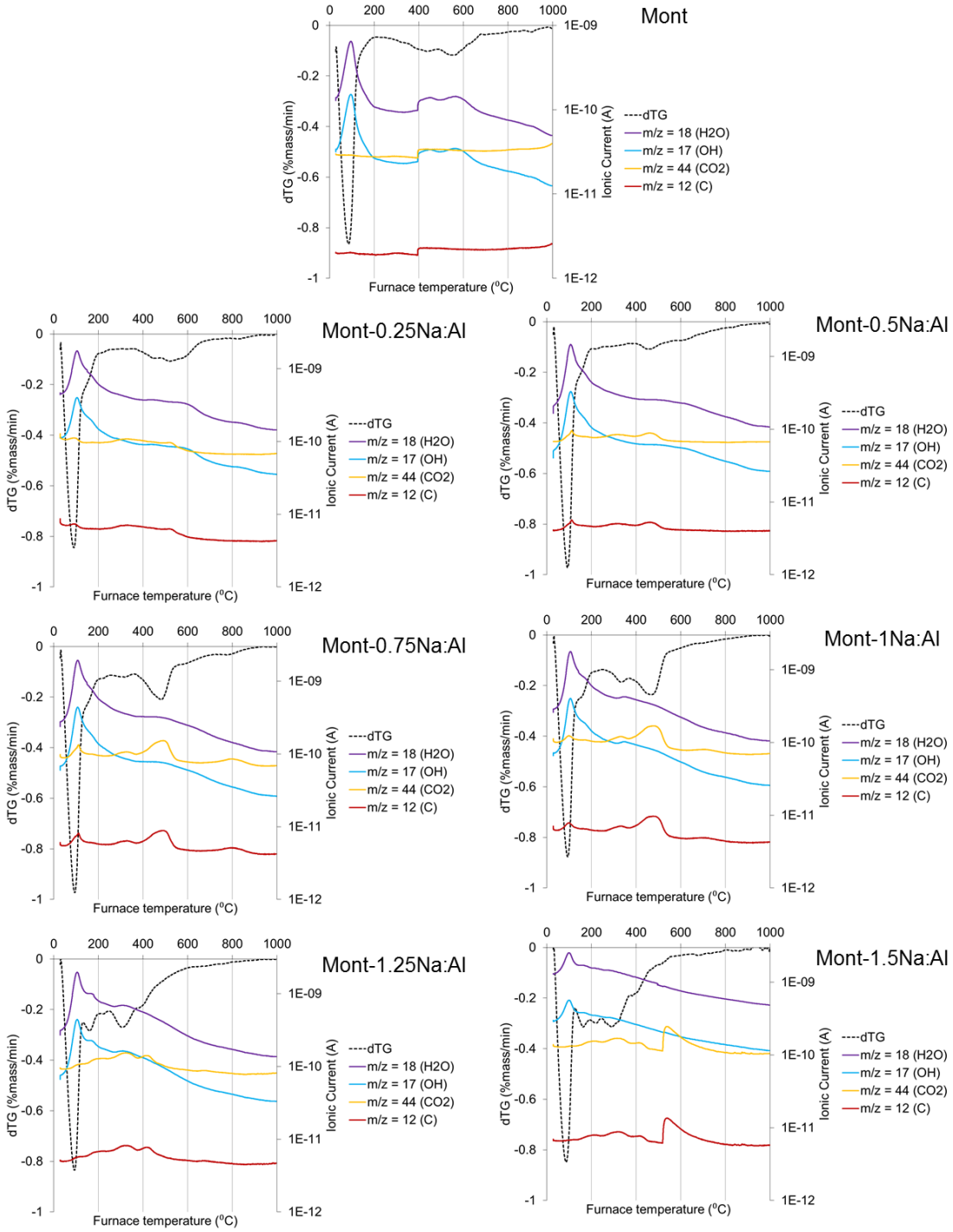

Figure 5-19: MS and dTG data for Mont and activated Mont samples.

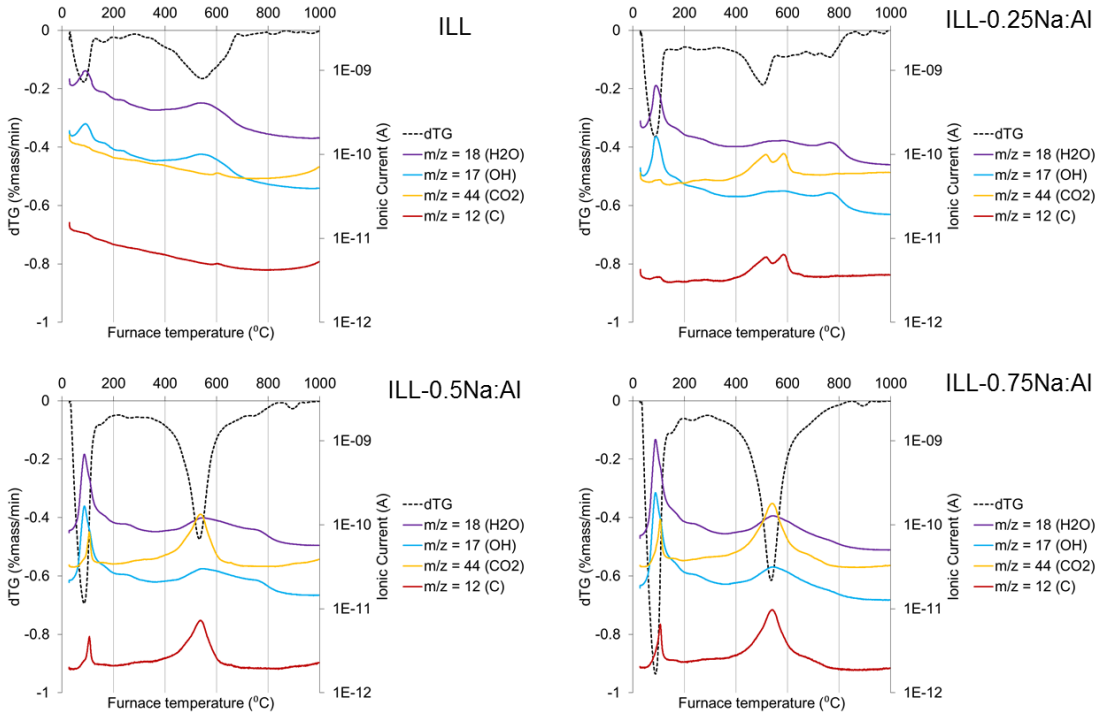

Figure 5-20: MS and dTG data for ILL and activated ILL samples.

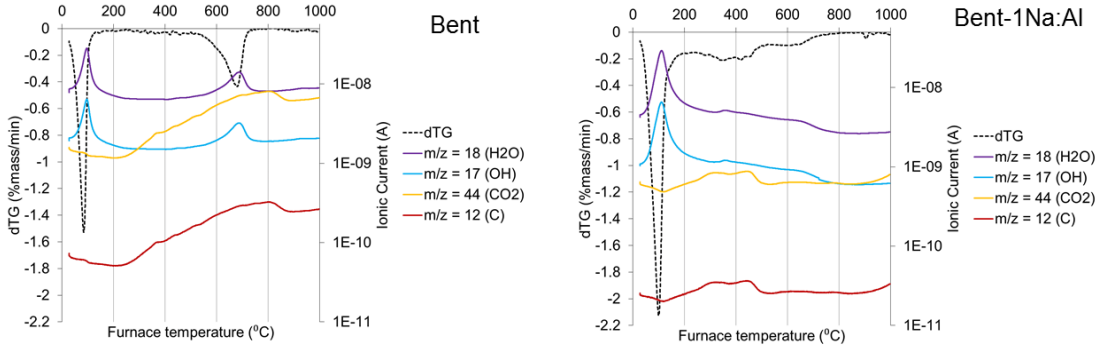

Figure 5-21: MS and dTG data for Bent and Bent-1Na:Al

References

Bain, J., 1971. A plasticity chart as an aid to the identification and assessment of industrial clays. *Clay Miner,* 9(1), pp. 1-17.

Barbosa, V.F.F., MacKenzie, K.J.D. & Thaumaturgo, C., 2000. Synthesis and characterisation of materials based on inorganic polymers of alumina and silica: sodium polysialate polymers. *International Journal of Inorganic Materials,* 2(4), pp. 309-317.

Brigatti, M.F., Galán, E. & Theng, B.K.G., 2013. Chapter 2 – Structure and Mineralogy of Clay Minerals. In: F. Bergaya & G. Lagaly, eds. *Handbook of Clay Science.* 2nd ed. Amsterdam: Elsevier, pp. 21-81.

Christidis, G.E., 2011. *Advances in the characterization of industrial minerals.* London: The Mineralogical Society of Great Britain and Ireland.

Drits, V., Besson, G. & Muller, F., 1995. An improved model for structural transformation of heat-treated aluminous dioctahedral 2: 1 layer silicates. *Clays and Clay Minerals,* 43(6), pp. 718-731.

Duxson, P., Fernández-Jiménez, A., Provis, J.L., Lukey, G.C., Palomo, A. & van Deventer, J.S.J., 2007. Geopolymer technology: the current state of the art. *J Mater Sci,* 42(9), pp. 2917-2933.

Farmer, V.C., 1974. *Infrared spectra of minerals.* London: Mineralogical society.

Ferrage, E., Lanson, B., Sakharov, B.A. & Drits, V.A., 2005. Investigation of smectite hydration properties by modeling experimental X-ray diffraction patterns: Part I. Montmorillonite hydration properties. *Am Mineral,* 90(8-9), pp. 1358-1374.

Lee, W.K.W. & van Deventer, J.S.J., 2003. Use of Infrared Spectroscopy to Study Geopolymerization of Heterogeneous Amorphous Aluminosilicates. *Langmuir,* 19(21), pp. 8726-8734.

Monteiro, A., Jarrais, B., Rocha, I.M., Pereira, C., Pereira, M.F.R. & Freire, C., 2014. Efficient immobilization of montmorillonite onto cotton textiles through their functionalization with organosilanes. *Applied Clay Science,* 101, pp. 304-314.

Rees, C.A., Provis, J.L., Lukey, G.C. & van Deventer, J.S.J., 2007. In Situ ATR-FTIR Study of the Early Stages of Fly Ash Geopolymer Gel Formation. *Langmuir,* 23(17), pp. 9076-9082.

Russell, J.D. & Fraser, A.R., 1994. Infrared methods. In: M.J. Wilson, ed. *Clay Mineralogy: Spectroscopic and Chemical Determinative Methods.* Dordrecht: Springer Netherlands, pp. 11-67.

Van der Marel, H.W. & Beutelspacher, H., 1976. *Atlas of infrared spectroscopy of clay minerals and their admixtures.* Amsterdam; New York: Elsevier Scientific Publishing Company.

Vicente, M.A., Gil, A. & Bergaya, F., 2013. Chapter 10.5 – Pillared Clays and Clay Minerals. In: F. Bergaya & G. Lagaly, eds. *Handbook of Clay Science.* 2nd ed. Amsterdam: Elsevier, pp. 523-557.

Weng, L. & Sagoe-Crentsil, K., 2007. Dissolution processes, hydrolysis and condensation reactions during geopolymer synthesis: Part I—Low Si/Al ratio systems. *J Mater Sci,* 42(9), pp. 2997-3006.

Weng, L., Sagoe-Crentsil, K., Brown, T. & Song, S., 2005. Effects of aluminates on the formation of geopolymers. *Materials Science and Engineering: B,* 117(2), pp. 163-168.

Chapter 6 - Alkali activation of clay mixtures

In this chapter, the alkali activation behaviour of binary and ternary mixtures of kaolinite, montmorillonite and illite, the most common clay minerals in soils, is investigated. The rule of mixtures approach is used to build on the understanding developed in Chapters 4 and 5 for the alkali activation of the three clay minerals as individuals.

This chapter has been revised following suggestions from the examiners, so the article presented here has minor differences compared to the article in review.

Declaration of authorship

This declaration concerns the article entitled:									
Phase formation behaviour in alkali activation of clay mixtures									
Publication status (tick one)									
draft manuscript		**Submitted**		**In review**	✓	**Accepted**		**Published**	
Publication details (reference)	Marsh, A., Heath, A., Patureau, P., Evernden, M., Walker, P. (under review). “Phase formation behaviour in alkali activation of clay mixtures.”								
Candidate’s contribution to the paper (detailed, and also given as a percentage).	The candidate predominantly executed the… Formulation of ideas: A.Marsh (80%) developed the idea for this study, with suggestions and guidance given by the co-authors (20%) (i.e. supervisors). Design of methodology: A.Marsh (80%) developed the methodology for this study, with suggestions and guidance given by the co-authors (20%) (i.e. supervisors). Experimental work: A.Marsh undertook the majority of experimental work and analysis (80%), with input from co-authors (20%). Presentation of data in journal format: A.Marsh (100%) undertook all formatting.								
Statement from Candidate	This paper reports on original research I conducted during the period of my Higher Degree by Research candidature.								
Signed							**Date**	30/10/2018	

Published as Marsh, A, Heath, A, Patureau, P, Evernden, M & Walker, P 2019, 'Phase formation behaviour in alkali activation of clay mixtures', Applied Clay Science, vol. 175, pp. 10-21 and available online via: https://doi.org/10.1016/j.clay.2019.03.037

Phase formation behaviour in alkali activation of clay mixtures

Abstract

Alkali-activated soils have potential as precursors for low carbon, low cost construction materials. There is a lack of fundamental understanding around how soil composition influences alkali activation behaviour, especially for uncalcined soils. The types and relative amounts of clay minerals can vary greatly throughout real soils across the world. Since clays are typically the dominant reactive aluminosilicate constituent in soils, it is desirable to understand how the types and relative amounts of clay minerals influence reaction products in alkali activation. In this study, mixtures of kaolinite, montmorillonite and illite precursors were activated with sodium hydroxide solutions. By comparing with extrapolations of cross-characterisation from the behaviour of individual clays, it was shown that phase formation behaviour deviated from an ideal rule of mixtures model. Instead, there was a hierarchy between the clays in influencing reaction products: kaolinite and montmorillonite dominated illite. This study demonstrates that the viability of a given soil for alkali activation depends not only on the total amount of clay, but the types and relative amounts of clay minerals present. In order to unlock the potential of alkali-activated soils, more understanding is needed of the role of the different components in soil.

6.1 Introduction

Alkali activated materials have become a promising candidate as low carbon construction materials (Davidovits, 2011; Provis, 2014).Their low curing temperature of typically 100 °C or less, and absence of carbon-releasing chemical changes during precursor preparation, gives them the potential for better environmental performance than Portland cement based materials (Heath *et al.*, 2014; Khale and Chaudhary, 2007). The principle of the alkali activation reaction is to transform an aluminosilicate precursor into an alkali aluminosilicate phase by the addition of an alkaline activating solution, mixing and curing (Duxson *et al.*, 2007a). The exact alkali aluminosilicate phase produced in this reaction depends on several compositional and processing factors, most importantly, the Si:Al ratio of the dissolved precursor (Duxson *et al.*, 2007b; Weng and Sagoe-Crentsil, 2007). It is usually intended to form an amorphous gel phase, also known as a geopolymer, as this possesses good strength, durability and other desirable properties (Liew *et al.*, 2016). It is also possible to form crystalline products, typically members of the zeolite family (Criado *et al.*, 2007). Crystalline products are more likely to form at lower Si:Al ratios while geopolymer phases are more likely to form at higher Si:Al ratios (Buchwald *et al.*, 2011; Duxson *et al.*, 2007b), as discussed later.

Within this emerging category of materials, alkali-activated soils have significant potential because subsoil is a widely available resource, available at very low environmental cost (Diop and Grutzeck, 2008). In the application of soil stabilisation for construction blocks, the alkali aluminosilicate product fulfils the function of the stabilising phase (Murmu and Patel, 2018). By being stronger and less expandable than the clay mineral precursors it replaces, it improves the strength and durability of the soil. However, a significant barrier to adoption is a lack of understanding of how soil composition influences the alkali activation reaction.

Soils are composed of clay minerals, unreactive quartz, and other associated minerals typically in minor quantities (Dixon and Weed, 1989). The most common clay minerals in soils are kaolinite, montmorillonite and illite, with allophane and halloysite less common (Reeves *et al.*, 2006). The dissolution of aluminosilicates in a concentrated alkaline solution determines the ultimate extent of alkali aluminosilicate phase formation (Xu and Van Deventer, 2000). Of the aluminosilicate phases in soils, clays are typically the most soluble component, more so than other common minerals such as quartz (Autef *et al.*, 2012; Tchakoute *et al.*, 2015) and muscovite (Zografou, 2015).

Previous studies have investigated the effect of aluminosilicate precursor and activating solution composition on geopolymer formation (Pacheco-Torgal *et al.*, 2008).

However, this is generally done using an aluminosilicate precursor of roughly fixed stoichiometric composition (usually metakaolin) and varying the chemical ratio of the liquor by adding additional soluble Si (Duxson *et al.*, 2007b; Duxson *et al.*, 2005). This is not the same as supplying silicates solely from mineral precursors, as such minerals' behaviours are likely to differ based on dissolution rates (Bauer and Berger, 1998; Xu and Van Deventer, 2000) and particle size effects (Weng *et al.*, 2005). Although it is well-established that clays are more reactive when calcined, the energy cost of this step gives a strong incentive to investigate the activation of un-calcined clays (MacKenzie, 2009).

The alkali activation behaviour of individual clays kaolinite (Liew *et al.*, 2016), montmorillonite (Belviso *et al.*, 2017; Seiffarth *et al.*, 2013) and illite (Belviso *et al.*, 2017; El Hafid and Hajjaji, 2015; Seiffarth *et al.*, 2013; Sperberga *et al.*, 2011) have previously been investigated. However, almost all previous studies on montmorillonite and illite have used their calcined state. Whilst kaolinite (Liew *et al.*, 2016), real soils (Lemougna *et al.*, 2014), and blends of uncalcined real soils and other materials such as metakaolin (Omar Sore *et al.*, 2018) are popular for studies, there has been much less attention on the alkali activation of individual clays, and in particular, controlled mixtures of clays. Soils around the world contain clays in different amounts (Abe *et al.*, 2006; Nickovic *et al.*, 2012), notwithstanding other minor minerals. Improving our fundamental understanding of how mixtures of clays react under alkali conditions is crucial to determining whether alkali activated soils can be widely used and reliable construction materials.

Given the strong influence of processing conditions, including curing temperature (Hounsi *et al.*, 2013; Muñiz-Villarreal *et al.*, 2011), curing time (Diop and Grutzeck, 2008), solid:liquid ratio (Alshaaer *et al.*, 2002; Heah *et al.*, 2012; Liew *et al.*, 2012) and activating solution concentration (Hounsi *et al.*, 2014), it is difficult to make comparisons between previous studies. A useful practical constraint on processing conditions is for the consistency of the wet mix to be approximately at the plastic limit, making it compatible with extrusion, an established brickmaking process (Maskell *et al.*, 2013). This study builds on previous experiments on the alkali activation of individual clays under conditions compatible with extrusion, for which the same processing constraints are used here (Marsh *et al.*, 2018a; Marsh *et al.*, 2018b).

A small number of previous studies have used a systematic approach for understanding the alkali activation behaviour of clay mixtures. Richardson et al. (1986) showed that binary and ternary mixtures of kaolinite, montmorillonite and illite activated using aqueous NaOH solution produced reaction products of combinations of sodalite, cancrinite and nepheline. However, no mention of geopolymers or amorphous phases

was made, and since only XRD characterisation was used, this gives an incomplete picture of the activated systems. In addition, very short curing times (less than 30 minutes) microwave curing was used, giving limited comparability with other systems. Buchwald et al. (2011) showed that for solutions of aluminium and silicon, geopolymer formation was favoured for systems with Si:Al > 1.5, with geopolymers and zeolites co-existing in some systems. This is a valuable contribution to fundamental understanding, but there is still a gap to consider the effects of the mineralogy and composition of real aluminosilicate precursors.

In this study, a Rule of Mixtures (RoM) approach was used to investigate how phase formation behaviour in alkali activation differed for mixtures of clays, compared to the activation of the constituent clays individually. The RoM approach has been used to evaluate a range of properties for material mixtures including elastic modulus (Marom *et al.,* 1978) and glass transition temperature (Couchman, 1978), as well as to evaluate phase formation in material mixtures (Donald and Davies, 1978). Mixtures of the common clay minerals kaolinite, montmorillonite and illite were activated with NaOH solutions, in order to determine to their phase formation behaviour in comparison with the clays as individuals.

6.2 Experimental

6.2.1 Materials

Imerys Speswhite kaolin (mined from Cornwall, U.K.), K10 montmorillonite (Sigma-Aldrich, product no. 69866-1KG) and Clay Minerals Society IMt-2 (Silver Hill) illite were used as the precursor clays. Chemical compositions were determined by energy dispersive X-rays (JEOL SEM6480LV with Oxford INCA X-Act SDD X-ray detector) at an accelerating voltage of 20 kV, a chamber pressure of between 10 – 30 Pa, a Si wafer as a standard, and measuring 4 scan areas per sample. The precursor powders were mounted on a sticky carbon tab on top of an aluminium stub, and were not coated. Standard errors in composition were calculated from the variation in values between the different area scans for each sample. Specific surface area was determined using the BET method (Brunauer *et al.*, 1938) using a Micromeritics 3-Flex. The precursor powders (1 g of kaolinite, 0.2 g of K10 Montmorillonite, and 1 g of Illite) were degassed under vacuum conditions at 150°C for 14 h, before testing.

The kaolinite (Kao), montmorillonite (Mont) and illite (ILL) precursor clays have previously been characterised (Marsh *et al.*, 2018a; Marsh *et al.*, 2018b), but will briefly be restated here. The XRD pattern of the kaolinite precursor gave kaolinite clay mineral (Powder Diffraction File (PDF)# 01-079-1570) as the major phase, with muscovite (PDF# 01-084-1304) and quartz (PDF# 00-046-1045) present as minor phases (Figure 6-1), as expected from a Cornish mixed hydrothermal and residual deposit (Murray and Keller, 1993). The XRD pattern of the montmorillonite precursor showed it contained montmorillonite clay mineral (PDF# 00-013-0135) as the major phase, along with muscovite, quartz and minor amounts of microcline (PDF# 00-019-0932) and kaolinite (Figure 6-1). The refined basal spacing of 14.4 Å suggested it was a Ca-montmorillonite (Ferrage *et al.*, 2005). The XRD pattern of the illite showed it contained illite clay mineral (PDF# 00-026-0911) as the major phase, with quartz, microcline and kaolinite present as minor phases (Gailhanou *et al.*, 2007) (Figure 6-1). Previous studies on this source clay identified the illite clay mineral to be mostly of the 1M/1Md polytype (Haines and van der Pluijm, 2008).

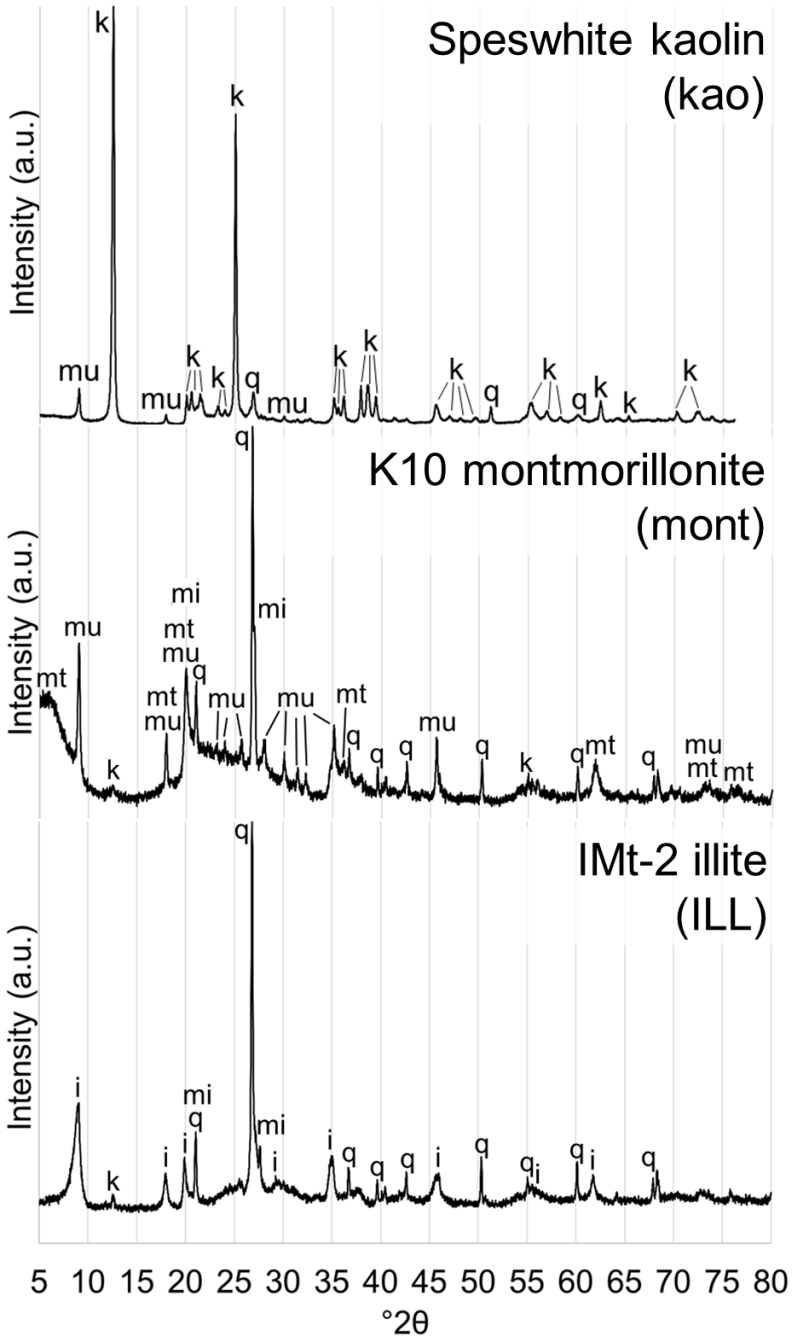

Figure 6-1: XRD patterns of the clay precursors.

The kaolinite precursor contained minor amounts of iron, potassium and magnesium (Table 6-1) and these were not considered to have a major effect on the reactions and products under the conditions in this study. BET specific surface area was 11.9 m^2g^{-1}. The montmorillonite precursor contained minor amounts of iron, potassium, magnesium, sodium, sulphur and titanium (Table 6-1). BET specific surface area was 265.8 m^2g^{-1}. The illite precursor contained minor amounts of iron, potassium, magnesium and titanium (Table 6-1). BET specific surface area was 19.5 m^2g^{-1}.

The precursor clays were activated using sodium hydroxide pellets of >98% purity (Sigma-Aldrich, product no. 06203).

Table 6-1: Chemical composition of clay precursors in oxide wt%, after LOI removed.

Oxide (wt.%)	Al_2O_3	CaO	Fe_2O_3	K_2O	MgO	Na_2O	SiO_2	SO_3	TiO_2	Total
Speswhite kaolin (std error)	40.11 (0.15)	0.00	0.95 (0.06)	2.06 (0.09)	0.04 (0.04)	0.00	56.83 (0.15)	0.00	0.00	100
K10 Montmorillonite (std error)	13.53 (0.66)	0.47 (0.14)	4.53 (1.05)	1.56 (0.22)	1.67 (0.11)	0.03 (0.03)	77.60 (2.12)	0.12 (0.07)	0.49 (0.02)	100
Imt-2 illite (std error)	20.80 (0.34)	0.00	8.32 (0.38)	8.67 (0.18)	2.28 (0.06)	0.00	59.14 (0.26)	0.00	0.78 (0.06)	100

6.2.2 Synthesis procedure

Using the same procedure as used in a previous study (Marsh *et al.*, 2018b), the masses of clays, water and NaOH for each sample (Table 6-2) were specified so that all samples had two characteristics. Firstly, all samples had the same Na:Al molar ratio (chosen to be 1), and secondly, the wet mix consistency of all samples was at the plastic limit. This was done by initially undertaking Atterberg plastic limit measurements (Wagner, 2013) for the clay minerals over a range of sodium hydroxide solutions. The exception to this condition is activated illite – due to its lower plastic limit, the maximum Na:Al ratio that could be achieved was 0.75 without exceeding the saturation limit of $NaOH_{(aq.)}$ at room temperature. The plastic limits of the clay mixtures were extrapolated from the plastic limit behaviour of the individual clays.

Table 6-2: Compositions of the clay mixtures made in each series. Clay contents given in wt%.

Series	Sample	Kao content (%mass)	Mont content (%mass)	ILL content (%mass)	[NaOH] molarity	NaOH solution : clay mass ratio
Kao-Mont	100Kao-0Mont	100%	n/a	n/a	16.1	0.73
	90Kao-10Mont	90%	10%	n/a	15.0	0.73
	50Kao-50Mont	50%	50%	n/a	10.7	0.75
	10Kao-90Mont	10%	90%	n/a	7.2	0.77
	0Kao-100Mont	0%	100%	n/a	6.4	0.77
Mont-ILL	100Mont-0ILL	n/a	100%	0%	6.4	0.77
	50Mont-50ILL	n/a	50%	50%	12.2	0.61
	0Mont-100ILL	n/a	0%	100%	19.7	0.39
ILL-Kao	100ILL-0Kao	0%	n/a	100%	19.7	0.39
	50ILL-50Kao	50%	n/a	50%	18.9	0.59
	0ILL-100Kao	100%	n/a	0%	16.1	0.73
Kao-Mont-ILL	33Kao-33Mont-33ILL	33%	33%	33%	13.6	0.65

The chosen combinations of clay mixtures were activated by adding a sodium hydroxide solution. Solutions of different concentrations were prepared by adding sodium hydroxide pellets to distilled water, mixed with a magnetic stirrer (Stuart UC152 heat-stir) for a minimum of 2 hours until fully dissolved and then allowed to cool. The clays were pre-dried in a 105°C oven, and left to cool. The constituent clays were then dry-mixed together using the magnetic stirrer for 5 minutes. Varying amounts of activating solutions were added in the quantities presented in Table 6-2. Each wet mixture of activating solution and clay mixture was mixed by hand for 3 minutes, providing a consistent and well-distributed mixture. The consistency of the samples allowed them to be compacted by hand into 18mm x 36mm cylindrical Teflon moulds by tamping with a glass rod in three layers for each sample, using 25 blows for each layer. Samples were cured in an air atmosphere in an 80°C oven for 24 hours in their moulds. For each composition, a control sample was made in addition to an activated sample. Distilled water was used instead of sodium hydroxide solution, such that the consistency of the wet mix was still at the plastic limit. The control samples were then mixed and cured in the same manner as the activated samples.

Samples 50Kao-50Mont, 50ILL-50Kao and 33Kao-33Mont-33ILL did not fully dry with curing, so were forcibly dried in a vacuum desiccator for 72 hours. After demoulding, samples were aged for 28 days in a controlled environment of 20 ± 0.5°C and 50 ± 2.5% relative humidity. An air atmosphere was intentionally used for both curing and ageing, to provide conditions representative of industrial brickmaking processes.

6.2.3 Characterisation methods

The set of characterisations were done at 28 ± 2 days ageing time, and (with the exception of SEM imaging) were performed on powders prepared from the cured samples. These were ground by hand, having been wetted with isopropanol to avoid damaging the clay mineral crystal structures (Moore and Reynolds, 1997). Powders were ground until there was no further discernible reduction in particle size, and so were comparable between samples. Any variation in particle size of the ground powders was not expected to have any noticeable effect on characterisation results. For XRD and FTIR, all characterisation was carried out on powder samples stored for at least 24 hours at 50% relative humidity, to allow for equal hydration states.

Powder X-ray diffraction (XRD) was undertaken with a Bruker D8 Advance instrument using monochromatic CuKα1 L3 (λ = 1.540598 Å) X-radiation and a Vantec superspeed detector. A step size of 0.016 °(2θ) and step duration of 0.3 seconds were used. Phase identification was performed using Bruker EVA software, using reference patterns from the Joint Committee on Powder Diffraction Standards (JCPDS) database.

Patterns were corrected for sample height shift by calibrating to the most intense quartz reflection (101) at 26.6 °(2θ), and normalised to the most intense peak in each pattern.

For each of the activated clay mixtures, a Rule of Mixtures (RoM) XRD pattern was calculated and plotted, to compare with the measured pattern. The RoM XRD patterns were calculated by proportionally summing the raw data of the XRD patterns for the constituent activated clays. For example, the calculated RoM pattern for activated 50Kao-50Mont was generated by summing together the activated Kao pattern at 50% intensity, and the activated Mont pattern at 50% intensity. The calculated pattern was then normalised in the same way as for the measured patterns. As XRD intensity is affected by particle orientation and other factors, this is not considered an exact prediction but was used to make a very rough comparison between each clay mixture's measured pattern, and what would be expected from a RoM model. This method gave good agreement to the measured pattern when comparing the control mixtures of clays. Due to the limitations of the XRD preparation techniques used, it was not possible to make quantitative comparisons. However, for the purpose of identifying differences in phases formed and any large differences in the quantities of phases formed, this method was deemed acceptable.

Scanning electron microscope (SEM) imaging was used to characterise phase size and morphology, using a JEOL SEM6480LV in secondary electron mode with an accelerating voltage (AV) of 10 kV. Bulk specimens were sputter coated with gold for 3 min. All images were taken >2 mm away from the edge to minimise edge effects. Because the SEM used a tungsten filament, an AV of 10 kV was selected as an optimal balance between the tendencies towards a noisy image at lower AV, and lower resolution at higher AV. Unpolished samples were used to enable easier distinction of particle morphology in the microstructures, and also given the friability of some of the samples.

Fourier Transform Infrared Spectroscopy (FTIR) was performed to characterise molecular bonding, using a Perkin-Elmer Frontier with a diamond Attenuated Total Reflectance (ATR) head. Spectra were collected over a range of 4000-600 cm^{-1} using a resolution of 4 cm^{-1} and 5 scans per spectrum. Corrections were made for ATR and background using Perkin-Elmer Spectrum software, and each spectra was normalised relative to its most intense band. RoM spectra were calculated for the clay mixtures using the same method described for the RoM XRD patterns.

6.3 Results

6.3.1 Visual inspection

A range of colour and form was observed in the cured samples (Figure 6-2). The influence of ≥50% montmorillonite was strong, giving distinctive angled shrinkage cracking. The reasons for the distinctive form of these shrinkage cracks are not yet known, but these were consistent with similar cracks previously observed in alkali activation of this montmorillonite clay (Marsh et al., 2018a). There was a clear band of darker colour at the top of the 33Kao-33Mont-33ILL sample, and to a lesser extent, some darkening at the top of the 50ILL-50Kao sample. These phenomena are likely to be associated with the one-dimensional flow of soluble matter to the top of the sample, given that a mould with one open end was used.

Figure 6-2: Photos of the cured activated mixed clay samples.

6.3.2 XRD

In the figures for XRD, for purposes of clarity given the number of patterns shown, only the main reflections for the clay minerals and reflections for product phases are indexed. In general, most of the reflections above 15 °2θ correspond to unreactive phases. Full indexation of reflections in the precursors' patterns is given in Figure 6-1.

6.3.2.1 Kao-Mont series

Firstly considering the individual clays at each end of this series, alkali activation of kaolinite and montmorillonite under these conditions has already been shown to form a 8:2:2 hydrosodalite (Marsh *et al.*, 2018b) – a member of the sodalite and zeolite families – and a geopolymer (Marsh *et al.*, 2018a) respectively. 90Kao-10Mont formed the same hydrosodalite phase (PDF# 00-042-0215) and a small amount of

hydroxycancrinite (PDF# 00-046-1457) (Figure 6-3a). 50Kao-50Mont formed a trace amount of hydrosodalite and a small amount of thermonatrite ($Na_2CO_3 \cdot H_2O$) (PDF# 00-008-0448). 10Kao-90Mont formed a small amount of thermonatrite as the only crystalline product phase, but experienced a background shift in the 20 – 35 °2θ region (Figure 6-3b) indicative of geopolymer formation (Duxson *et al.,* 2007a), whilst retaining a large amount of unreacted montmorillonite.

Amongst the activated samples, kaolinite was still present in all mixes originally containing kaolinite. Montmorillonite was still present in mixtures with ≥ 50% montmorillonite in the starting mix. It was not detectable in 90Kao-10Mont, but was only faintly detectable in the control sample. The montmorillonite 001 reflection consistently shifted from 5.9 to 7.3 °2θ after activation, corresponding to a decrease of d-value from 14.4 to 11.6 Å. For this particular montmorillonite clay, this phenomenon is due to a combination of interlayer cation exchange for the Na in solution, as well as other possible effects associated with alkali activation (Marsh *et al.,* 2018a). Muscovite was present in all samples, with no significant change in °2θ position, as expected from previous work by Zografou (2015).

In summary, hydrosodalite formed in mixtures with ≥90% kaolinite, but not for samples with <50% kaolinite. Hydroxycancrinite formed in 90Kao-10Mont, but in no others. A geopolymer hump seemed to form in samples with ≥50% montmorillonite, but was a more subtle change for 50Kao-50Mont (Figure 6-3b).

The RoM patterns were broadly correct in predicting the product phases formed, but were not consistent over the whole series. For 90Kao-10Mont the RoM model predicted hydrosodalite as a major product phase, while in the measured pattern, a small amount of hydroxycancrinite was formed in addition to hydrosodalite. For 50Kao-50Mont, hydrosodalite was predicted as a major phase, whereas only a trace amount was formed. For 90Mont-10Kao, it was correctly predicted that a large amount of montmorillonite remained unreacted, but the prediction that a minor amount of hydrosodalite would form could not be confirmed from the XRD pattern.

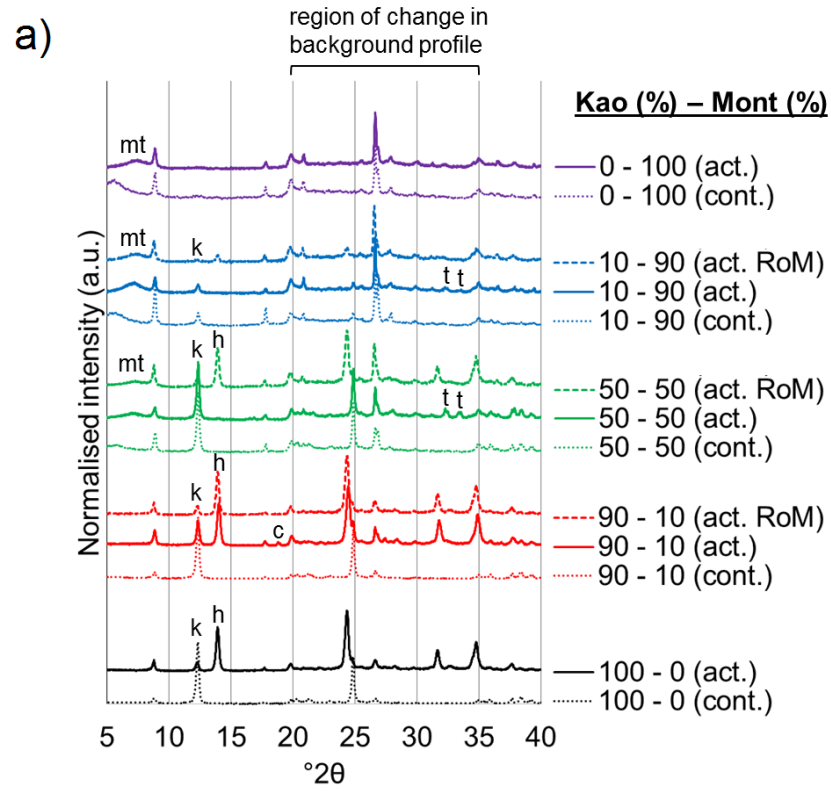

Precursor clay minerals: **k** = kaolinite; **mt** = montmorillonite.
Product phases: **c** = hydroxycancrinite; **h** = hydrosodalite; **t** = thermonatrite.

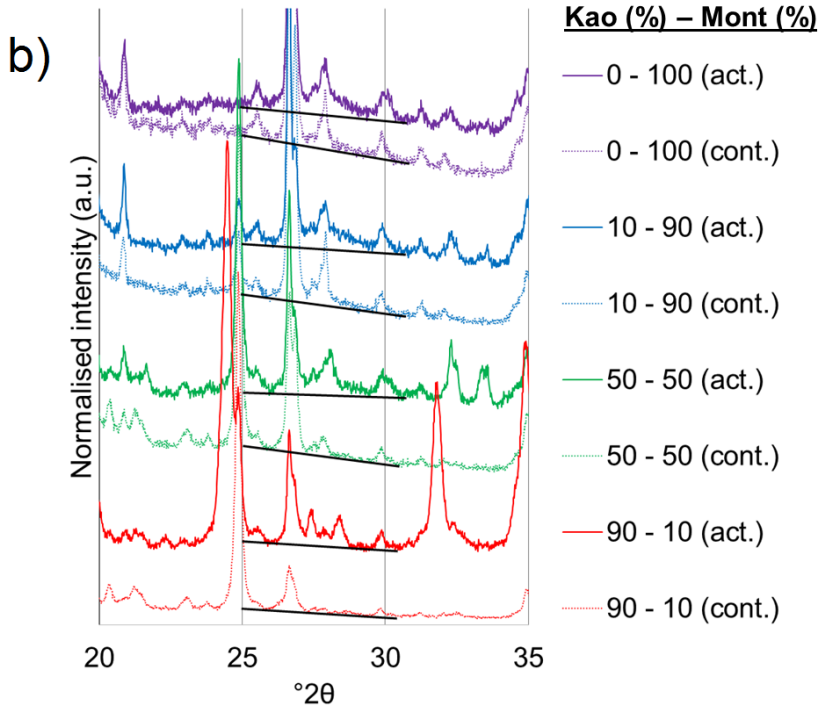

Figure 6-3: Kao-Mont series: a) XRD patterns of control (cont.) samples, compared with measured (act.) and RoM calculated (act. RoM) patterns of the activated samples. b) XRD patterns for a selection of samples for the range 20 – 35 °2θ. Lines have been drawn to illustrate the changes in the backgrounds of the patterns from 25 – 30 °2θ.

6.3.2.2 Mont-ILL series

Firstly considering the individual clays at each end of this series, alkali activation of montmorillonite and illite under these conditions has already been shown to form a geopolymer and altered illite respectively (Marsh *et al.*, 2018a). 50Mont-50ILL formed a small amount of thermonatrite ($Na_2CO_3 \cdot H_2O$) as the only new crystalline phase (Figure 6-4). Montmorillonite shifted its 001 reflection position as already observed in the previous series. The trace kaolinite impurity, evident by the reflection at 12.5 °2θ in the control sample's pattern, appeared to be consumed. However, there was no evidence for formation of a hydrosodalite reflection, as observed for consumption of trace kaolinite in 0Mont-100ILL. The illite reflections at 9 and 18 °2θ overlapped with those of the muscovite impurity in the montmorillonite precursor. These reflections appeared to decrease in intensity, but the reflections at 20 °2θ were maintained, which could suggest this was partly an orientation effect. In each measured pattern, a large amount of clay precursor was still present, as shown in the 5 – 10 °2θ region.

The RoM model matched well with the measured pattern. The only difference was the prediction of a trace amount of hydrosodalite, which was not observed in the measured pattern of 50Mont-50ILL. Given that both the product phases from individual activated montmorillonite and illite did not appear as new crystalline reflections, this alone was not conclusive. However, the background profiles of the measured and RoM patterns were broadly similar.

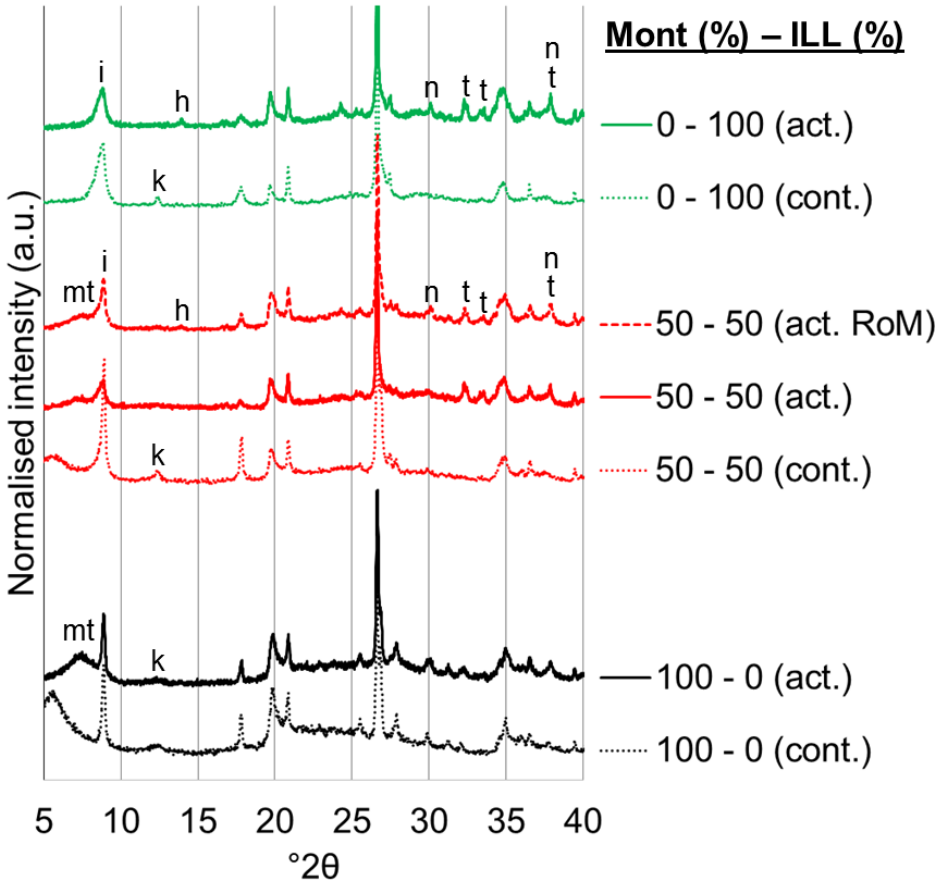

Precursor clay minerals: **i** = illite; **k** = kaolinite; **mt** = montmorillonite.
Product phases: **h** = hydrosodalite; **n** = natrite; **t** = thermonatrite.

Figure 6-4: Mont-ILL series: XRD patterns of control (cont.) samples, compared with measured (act.) and RoM calculated (act. RoM) patterns of the activated samples.

6.3.2.3 ILL-Kao series

Firstly considering the individual clays at each end of this series, alkali activation of illite and kaolinite under these conditions has already been shown to form altered illite (Marsh *et al.*, 2018a) and 8:2:2 hydrosodalite (Marsh *et al.*, 2018b) respectively. In 50ILL-50Kao, hydrosodalite was the major crystalline reaction product with a trace amount of hydroxycancrinite (Figure 6-5). All the kaolinite in the precursor seemed to be consumed, but unreacted illite was still present. However, as previously stated, the 001 reflection overlapped with that of the muscovite, which undergoes very limited dissolution in alkali solutions.

The RoM pattern correctly predicted that hydrosodalite was the dominant product phase for 50ILL-50Kao sample. However, it predicted a minor amount of kaolinite phase would remain in the 50% mixture, whilst the measured pattern showed only a trace amount. It also failed to predict the formation of a trace amount of hydroxycancrinite.

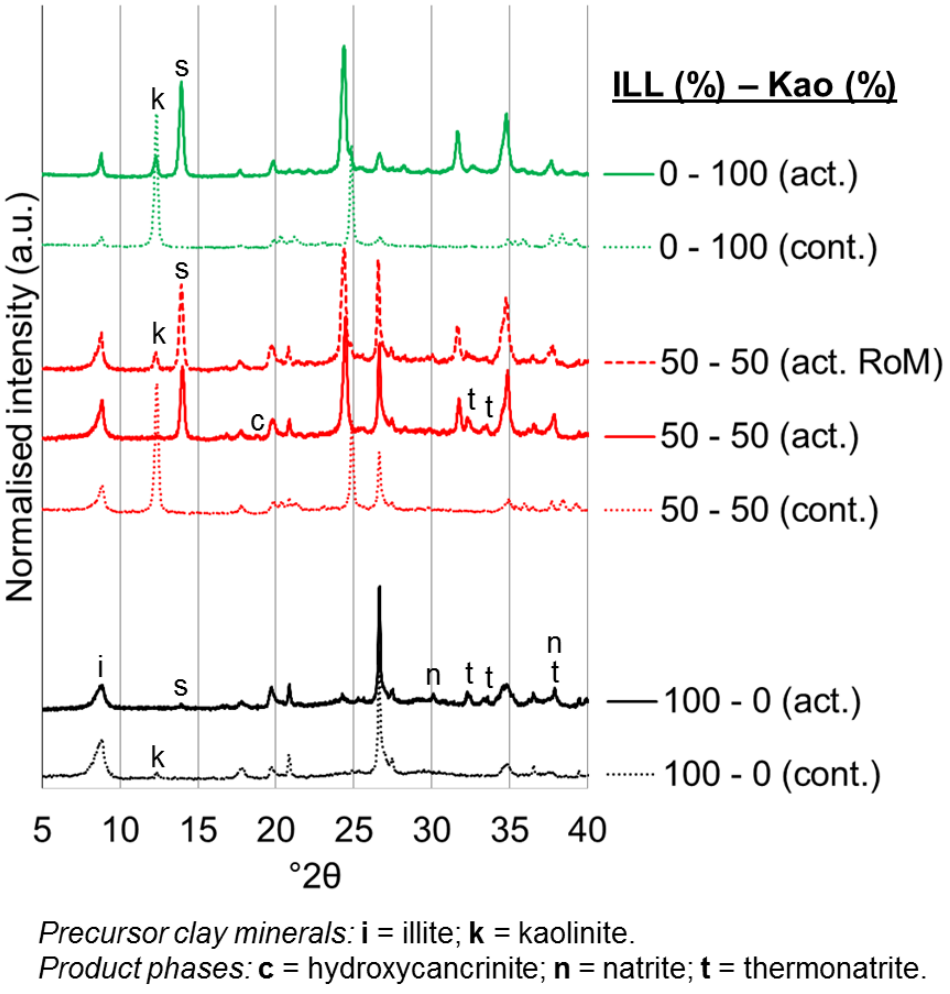

Precursor clay minerals: **i** = illite; **k** = kaolinite.
Product phases: **c** = hydroxycancrinite; **n** = natrite; **t** = thermonatrite.

Figure 6-5: ILL-Kao series: XRD patterns of control (cont.) samples, compared with measured (act.) and RoM calculated (act. RoM) patterns of the activated samples.

6.3.2.4 Kao-Mont-ILL

In the mix of all three clay precursors, hydrosodalite was formed as the major crystalline product phase (Figure 6-6). There was some evidence of a shift in background profile towards higher angles in the 20 – 35 °2θ region. Some kaolinite and montmorillonite was consumed, with some left as a remnant. The overlap of the first two illite reflections with those of muscovite made it difficult to discern whether the intensity of these had decreased after activation. The RoM model was correct in predicting hydrosodalite as the main reaction product, as well as a small change in the background profile in the 20 – 25 °2θ region.

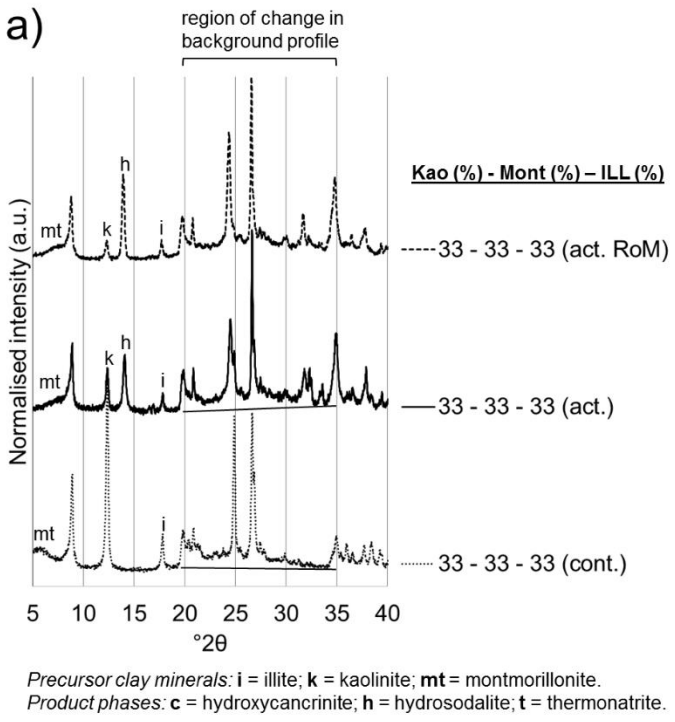

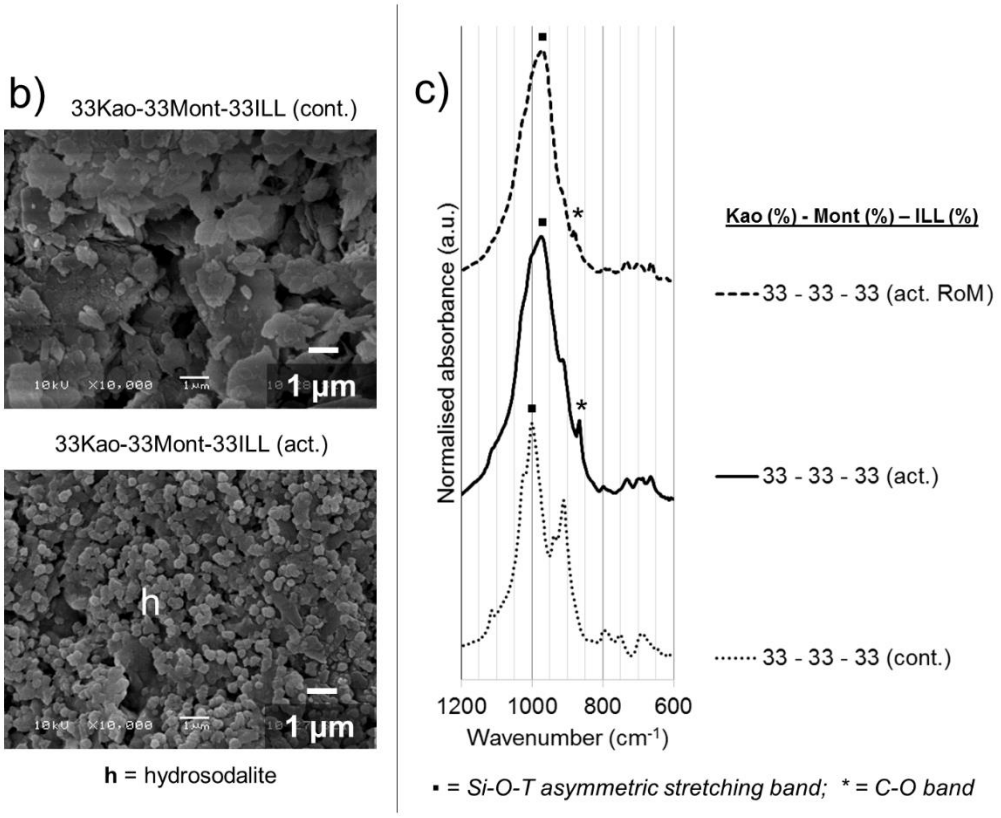

Figure 6-6: Combined results for the Kao-Mont-ILL series: a) XRD pattern of the control (cont.) sample, compared with measured (act.) and RoM calculated (act. RoM) patterns of the activated sample. Lines have been drawn to illustrate the changes in the backgrounds of the patterns from 20 – 35 °2θ. b) SEM images, comparing the cont. and act. samples. c) FTIR spectrum of the cont. sample, compared with act. and act. RoM spectra of the activated sample.

6.3.3 SEM

6.3.3.1 Kao-Mont series

Small, spheroidal particles were observed to have formed in 100Kao-0Mont and 90Kao-10Mont, typically with size of 250 - 500 nm and an irregular morphology (Figure 6-7). It was known from the XRD results that a large amount of hydrosodalite had formed in both of these samples. Given that these spheroidal particles had a morphology similar to that expected from hydrosodalites (Moloy et al., 2016), they were attributed as hydrosodalite. The amount of hydrosodalite formed was less for 50Kao-50Mont than for the samples with >50% kaolinite, with a corresponding increase in unreacted kaolinite. For 10Kao-90Mont, there was a large quantity of new particles with irregular morphology and particle size of around 250 nm, with more of a connected structure between particles. At 0% kaolinite (100% montmorillonite), the new particles were semi-continuous. Both of these microstructural characteristics have previously been observed in geopolymer systems (Duxson *et al.*, 2005). Given that no hydrosodalite or other crystalline phase was present in the XRD pattern for the 10% kaolinite sample, it was inferred that the new particles observed in both 10Kao-90Mont and 0Kao-100Mont samples were part of a geopolymer phase.

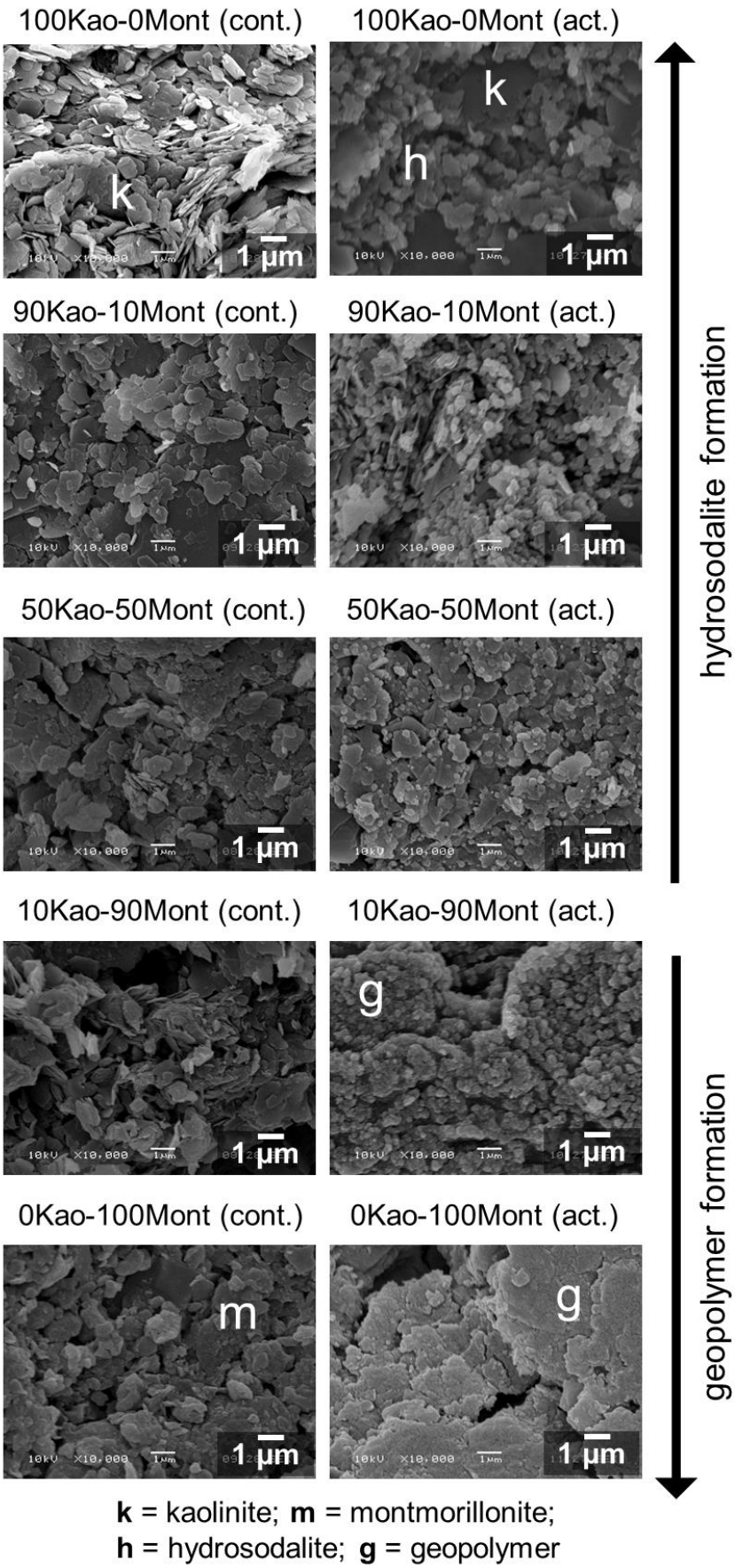

Figure 6-7: Kao-Mont series: SEM images comparing the control (cont.) and activated (act.) samples for each mixture.

6.3.3.2 Mont-ILL series

In 50Mont-50ILL, the microstructure was made of irregular particles of 100-500 nm, sometimes showing connectedness (Figure 6-8).This is different to the microstructures of both 100Mont-0ILL, a semi-continuous geopolymer, and 0Mont-100ILL, an altered illite with a distinctive arrangement of particles. Given that the XRD pattern revealed no crystalline product phase, and that geopolymers have been observed to have similar particle morphologies (Duxson *et al.*, 2005), this new microstructure was also believed to be a geopolymer. This was similar to the microstructure of the 10Kao-90Mont sample, also believed to be a geopolymer for the same reasons.

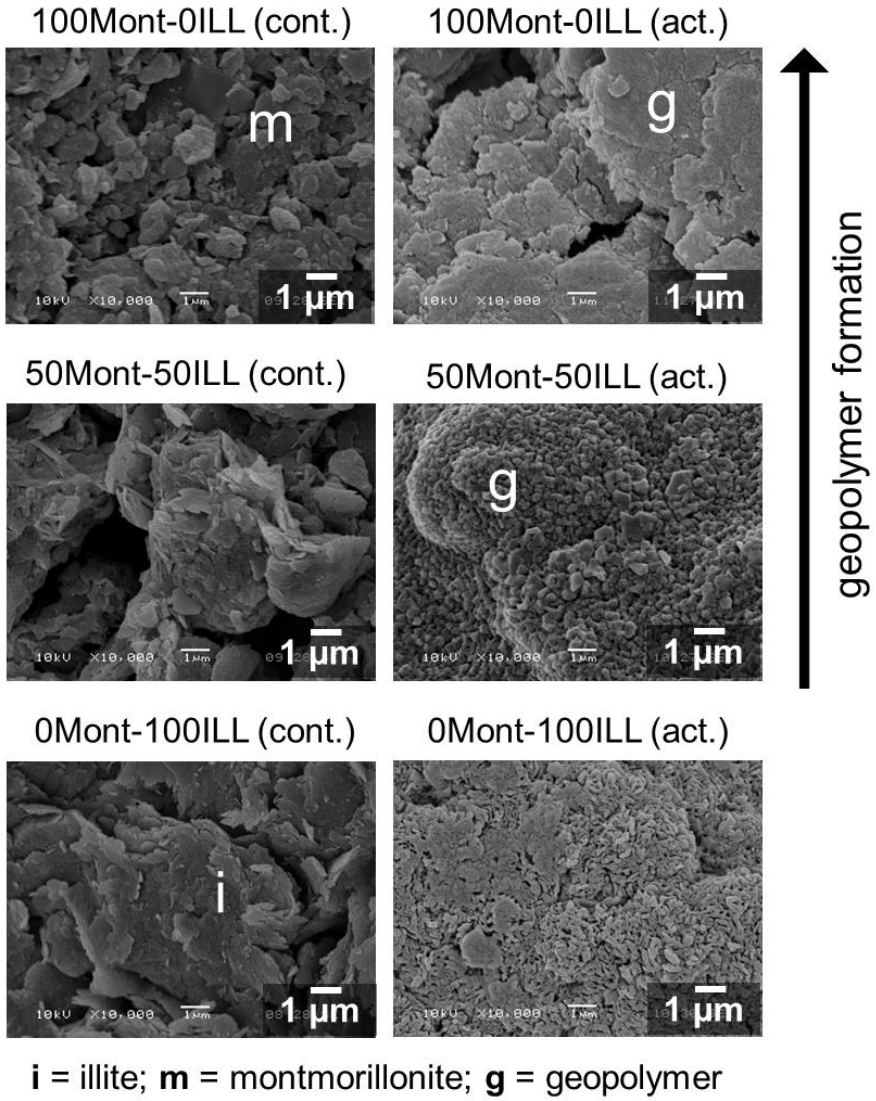

Figure 6-8: Mont-ILL series: SEM images comparing the control (cont.) and activated (act.) samples for each mixture.

6.3.3.3 ILL-Kao series

In 50ILL-50Kao, the microstructure was made of irregular particles of size 250-500 nm (Figure 6-9). Given that the control sample contained clay particles of similar dimensions, the change in appearance after activation was not dramatic. Some unreacted clay particles were still present in the activated sample. Given that the XRD pattern for 50ILL-50Kao showed that a large amount of hydrosodalite was present, and that these new particles had a morphology similar to that expected from hydrosodalites (Moloy et al., 2016), they were attributed as hydrosodalite. The modified microstructure seen in 100ILL-0Kao wasn't observed in 50ILL-50Kao.

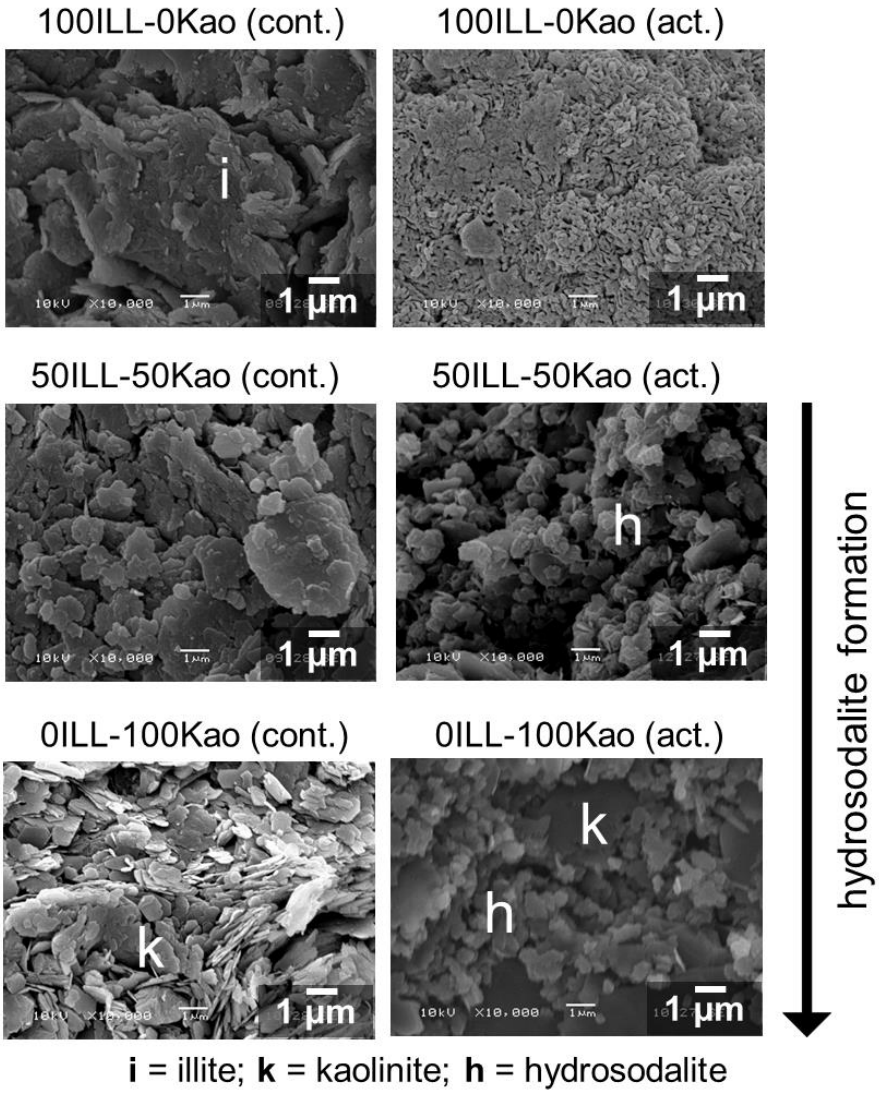

Figure 6-9: ILL-Kao series: SEM images comparing the control (cont.) and activated (act.) samples for each mixture.

6.3.3.4 Kao-Mont-ILL

The 33Kao-33Mont-33ILL sample contained a microstructure made of fine particles of size ~300 nm (Figure 6-6). Unreacted clay particles were present too. The XRD pattern for this sample showed hydrosodalite to be the crystalline reaction product, and these particles were similar to those observed in 100Kao-90Mont and 90Kao-10Mont, both of which contained a large amount of hydrosodalite (Figure 6-7). Therefore, these fine particles in this sample were also attributed to hydrosodalite.

6.3.4 FTIR

The most intense bands in the FTIR spectra were observed between 950 – 1080 cm^{-1}. This region is dominated by the Si-O-Si and Si-O-T bands of the clay mineral precursor phases and alkali aluminosilicate product phases respectively.

The dominant band in each of the precursor clay minerals is the Si-O-Si stretching vibration in the 970 – 1070 cm^{-1} region (Farmer, 1974; Madejova and Komadel, 2001). The dominant band in both of the crystalline product phases, hydrosodalite and hydroxycancrinite, is an asymmetric T-O-T stretching vibration in the region of 980 – 1000 cm^{-1} (Flanigen *et al.*, 1974; Henderson and Taylor, 1977; Mikuła *et al.*, 2015). In a geopolymer, it is an Si-O-T asymmetric stretching vibration (Rees *et al.*, 2007b), the position of which depends on the Si:Al composition of the gel (Roy, 1990), the number of non-bridging oxygens and the extent of activation (Fernández-Jiménez and Palomo, 2005; Lee and van Deventer, 2003; Rees *et al.*, 2007a).

Outside of this main region of interest, quartz has bands at Si-O stretching vibrations at around 778 and 798 cm^{-1} (Van der Marel and Beutelspacher, 1976). In the cured samples' spectra, carbonate bands are often seen in alkali-activated systems, with a C-O bands at around 880 cm^{-1} (Barbosa *et al.*, 2000).

6.3.4.1 Kao-Mont series

There were two clear groupings amongst the activated samples' FTIR spectra in this series (Figure 6-10). The main Si-O-T band region of 1200 – 800 cm^{-1} was similar between 100Kao-0Mont and 90Kao-10Mont, with a single band with a centre at ~965 cm^{-1}, indicating hydrosodalite formation. For the three other spectra for samples with ≥50% Mont, the main band area was broader with the band centres at higher wavenumbers in the region of 995 – 1005 cm^{-1} indicating geopolymer formation. In this latter group, a carbonate band emerged at ~870 cm^{-1}.

Behaviour in the lower wavenumber region supported this interpretation. For 100Kao-0Mont and 90Kao-10Mont, bands emerged at ~663 and ~732 cm^{-1} attributed to hydrosodalite T-O-T symmetric stretching modes (Henderson and Taylor, 1977). In the

other three spectra, no narrow new bands were formed in this region. This discounted the possibility of formation of nanocrystalline zeolitic phases in large amounts, with the emergence of a weak broad hump in this region suggesting geopolymer formation instead (Rees *et al.*, 2007a).

The RoM spectra for activated 90Kao-10Mont and 10Kao-90Mont matched well with the measured spectra. However, for activated 50Kao-50Mont, there were clear differences in the RoM and measured spectra. The RoM spectrum's profile was broader, and the Si-O-T main band peak was at a lower wavenumber (968 cm^{-1}) than for the measured spectrum (1004 cm^{-1}). Given the association between a negative shift of the main Si-O-T band and formation of alkali aluminosilicate product phases (Prud'homme *et al.,* 2013), the difference in Si-O-T band wavenumber suggests that a smaller extent of transformation occurred in the 50Kao-50Mont mixture than was expected from the behaviour of the individual clays.

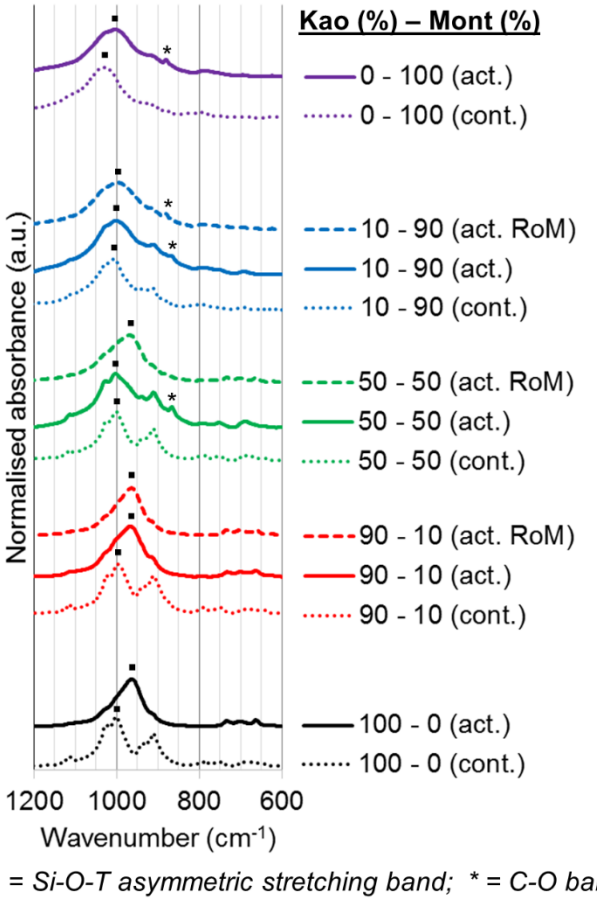

Figure 6-10: Kao-Mont series: FTIR spectra of the control (cont.) samples, compared with measured (act.) and RoM calculated (act. RoM) spectra of the activated samples.

6.3.4.2 Mont-ILL series

The end members of this series behaved differently after activation (Figure 6-11). The dominant band in 100Mont-0ILL shifted from 1031 cm^{-1} to a lower wavenumber at 1003 cm^{-1} after activation, indicating geopolymer formation, whereas the dominant band in 0Mont-100ILL shifted from 987 cm^{-1} to a slightly higher wavenumber at 994 cm^{-1}. For 50Mont-50ILL, the dominant band shifted from 1004 cm^{-1} to a slightly lower wavenumber at 992 cm^{-1} after activation and no narrow zeolitic bands emerged in the 650 – 750 cm^{-1} region. Given the microstructural changes observed in the SEM images, this also supported the interpretation that a geopolymer was formed in 50Mont-50ILL. A carbonate band emerged at 866 cm^{-1}. The RoM spectrum for activated 50Mont-50ILL matched well with the measured spectrum.

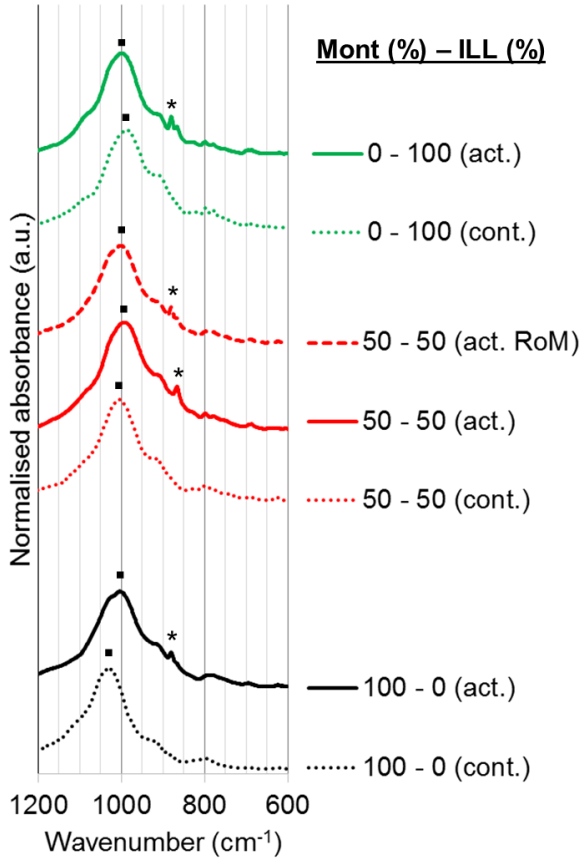

Figure 6-11: Mont-ILL series: FTIR spectra of the control (cont.) samples, compared with measured (act.) and RoM calculated (act. RoM) spectra of the activated samples.

6.3.4.3 ILL-Kao series

In the spectrum of the activated 50ILL-50Kao sample, the dominant band moved to a lower wavenumber at 968 cm^{-1} and Si-O-T symmetric stretching bands emerged at 664 and 735 cm^{-1} (Figure 6-12).These observations supported the evidence of the XRD pattern that a hydrosodalite is the dominant reaction product. A carbonate band emerged at 866 cm^{-1}. The RoM spectrum for activated 50ILL-50Kao matched well with the measured spectrum.

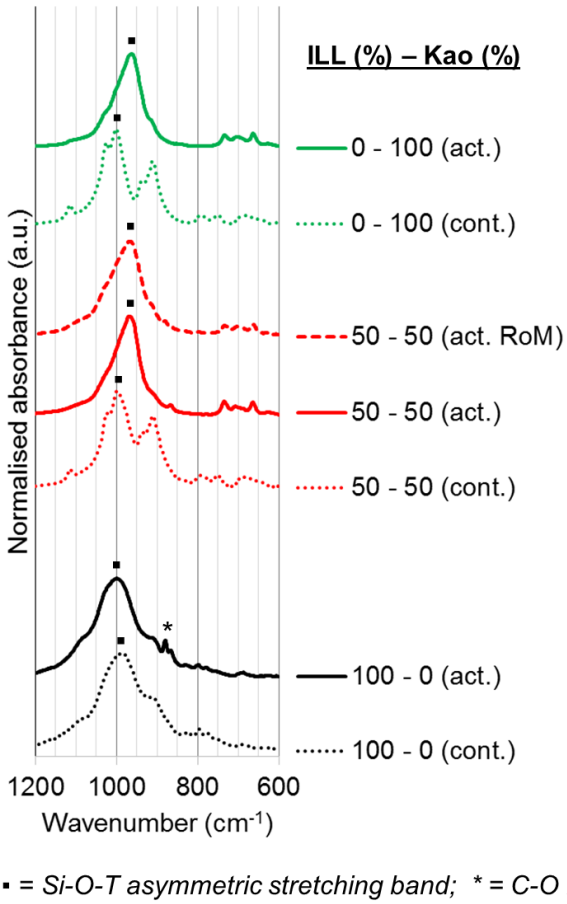

▪ = *Si-O-T asymmetric stretching band;* * = *C-O band*

Figure 6-12: ILL-Kao series: FTIR spectra of the control (cont.) samples, compared with measured (act.) and RoM calculated (act. RoM) spectra of the activated samples.

6.3.4.4 Kao-Mont-ILL

After activation, the dominant band centre in the 33Kao-33Mont-33ILL spectrum shifted from 1000 cm^{-1} to 975 cm^{-1} and Si-O-T symmetric stretching bands emerged at 664 and 732 cm^{-1} (Figure 6-6). Hydrosodalite was known to be present from the XRD patterns, but a geopolymer phase may have also formed. The observed shift of the Si-O-T band centre may support this - the band centre was at a higher wavenumber than inactivated samples which contained hydrosodalite as the primary reaction product (100Kao-0Mont and 50ILL-50Kao), but lower than in activated samples which contained a geopolymer as the primary reaction product (0Kao-100Mont and 10Kao-

90Mont). An intermediate value of wavenumber for the Si-O-T band could therefore indicate the presence of a geopolymer phase as well as hydrosodalite. As with other samples, carbonate bands emerged at 866 and 1451 cm^{-1}.

For all the clays and clay mixtures except illite and 50Kao-50Mont, there was a decrease in wavenumber of the main Si-O-T band after activation.

6.3.4.5 Changes in wavenumber position of dominant band

As previously used in studies investigating the variables of time (Essaidi *et al.*, 2014), alkali source and calcination temperature (Prud'homme *et al.*, 2013), the position of the dominant Si-O-T band in the sample can help understand product phases formed in alkali activation. As previously stated, the main region of interest is from approximately 950 – 1080 cm^{-1}, as this is dominated by the Si-O-Al and Si-O-Si bands of the precursor and product phases. There was large variation in wavenumber of the dominant band between precursor samples, and between activated samples. There was also significant variation between samples in the change in Si-O-T band wavenumber after activation (Figure 6-13). In most, but not all cases, alkali activation resulted in a decrease in wavenumber position of the dominant band, as a result of more Si-O-Al bonds in the aluminosilicate framework (Fernández-Jiménez and Palomo, 2005). The extent of shift for geopolymer formation was less than the 40 cm^{-1} observed by Prud'homme et al. (2013), as might be expected since those experiments used calcined clays. However, for 50Kao-50Mont and 0Mont-100ILL / 100ILL-0Kao, there is a positive shift. No explanation of this positive shift has been yet found in the literature.

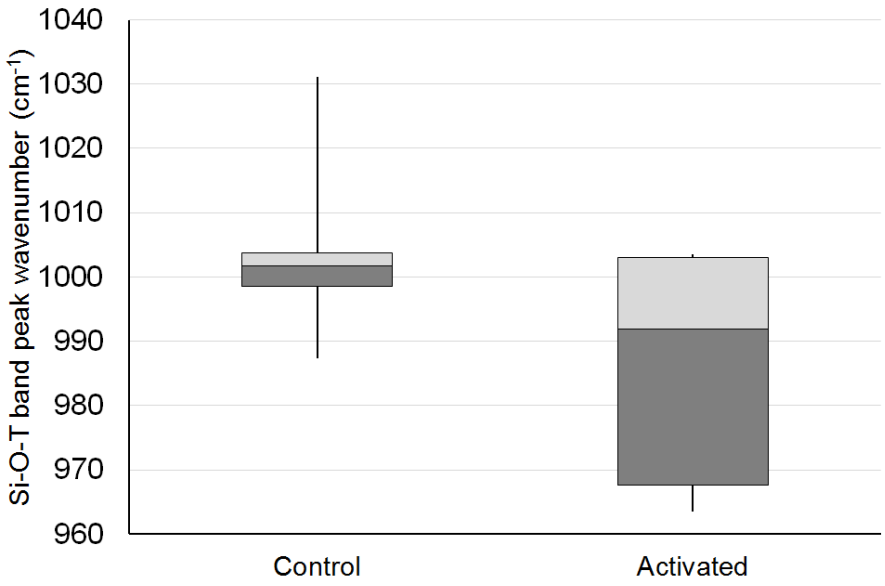

Figure 6-13: The distribution of wavenumbers for the Si-O-T band peak centre for control and activated samples. The centre-line of each box is the median value; the edges of each box are the first and third quartile values, and the lines extend to the maximum and minimum values.

6.4 Discussion

6.4.1 Evaluation of phase formation

Mixtures of clays are complex to characterise, even without alkali activation. Furthermore, given the amorphous nature of the geopolymer phase, it is important to use multiple characterisation methods to provide corroborating evidence. It has previously been shown that in the alkali activation of clays, different reaction products can coexist, including different zeolitic phases (Barrer and Mainwaring, 1972) and a zeolite with a geopolymer (Heller-Kallai and Lapides, 2007). Due to the multiple phases present, the amorphous character of geopolymers and the presence of some phases in small amounts, it is not possible to state the phase composition of the activated systems with complete certainty. Nonetheless, a summary of phases observed in the activated samples, as well as the phases predicted from the RoM model, is given in Table 6-3.

Table 6-3: A summary of the product phases observed through characterisation for the activated clay mixtures, and the product phases expected from the rule of mixtures model. Phases marked with a ? indicate less certainty.

Series	Sample	Phases observed	Phases expected from RoM model
Kao-Mont	90Kao-10Mont	Hydrosodalite Hydroxycancrinite	Hydrosodalite Geopolymer
	50Kao-50Mont	Hydrosodalite Geopolymer?	Hydrosodalite Geopolymer
	10Kao-90Mont	Geopolymer	Geopolymer Hydrosodalite
Mont-ILL	50Mont-50ILL	Geopolymer	Geopolymer Altered illite
ILL-Kao	50ILL-50Kao	Hydrosodalite Hydroxycancrinite	Hydrosodalite Altered illite
Kao-Mont-ILL	33Kao-33Mont-33ILL	Hydrosodalite Geopolymer?	Hydrosodalite Geopolymer Altered illite

The trends observed here suggest that the wavenumber of the Si-O-T FTIR band could be a useful indicator for the alkali aluminosilicate phase formed in a given system of uncalcined clay mixtures, as has previously been shown for fly ash (Fernández-Jiménez and Palomo, 2005) and calcined clays (Prud'homme *et al.*, 2013). However, given the inconsistencies within the series here, it should not be relied on as a standalone method, but should be supported with complementary characterisation techniques. This is especially important for uncalcined clay mixtures. Given the coexistence of crystalline and amorphous phases, as well as the significant amount of unreacted precursors, phase identification is more complex and less certain than for simpler, more reactive systems such as metakaolin.

Regarding carbonate phase formation (not included in Table 6-3 for concision), a C-O band was detected in all of the samples where carbonates had been identified from the XRD pattern. In 0Kao-100Mont, a C-O band was detected, but no carbonate phase was identified in the XRD pattern. These two observations suggest two further insights. Firstly, that in most - if not all - of these systems there is an excess of Na available, which carbonates when not consumed during the reaction. And secondly, that the presence of carbonates in these systems cannot reliably be detected solely using XRD.

6.4.2 Performance of the rule of mixtures (RoM) model

For alkali-activated soils to be a viable construction technology, the phase formation behaviour needs to be predictable. As previously described, a rule of mixtures predictive model provides a useful basis for describing the phase formation behaviour of the clay mixtures.

For the Kao-Mont series in general, the RoM XRD patterns overpredicted the propensity of hydrosodalite formation. It predicted a large quantity of hydrosodalite for 50Kao-50Mont when only a trace amount was formed, and a minor quantity for 90Mont-10Kao when none was detected. It also did not predict the formation of a minor amount of hydroxycancrinite for 90Kao-10Mont. For the Mont-ILL series, the RoM pattern matched the measured pattern well, but since the expected transformations do not yield strongly crystalline signals, it is difficult to verify the accuracy of this. For the ILL-Kao series, the RoM model underestimated the extent of kaolinite consumption and hydrosodalite formation for 50ILL-50Kao. As in the Kao-Mont series, it also did not predict formation of hydroxycancrinite.

The formation of hydroxycancrinite is of special interest as it did not form in any of the activated individual clays. Favourable conditions for formation of hydroxycancrinite are typically at high concentrations of activating solution and higher temperatures, such as 200°C (Querol *et al.*, 2002). For clay precursors, Barrer and Mainwaring (1972) formed hydroxycancrinite from alkali activation of metakaolin, under conditions of >100 °C and < 1 M $NaOH_{(aq.)}$.The addition of soluble silicate was found to discourage its formation. This seems to contradict the observations made here that hydroxycancrinite only formed in mixtures of 50% kaolinite in combination with 50% of a 2:1 clay. The presence of a 2:1 clay would be expected to provide additional Si. Cancrinite has been formed from kaolinite, but this required the presence of certain sodium salts for synthesis at 80°C, or else temperatures of ~400°C (Barrer *et al.*, 1968). No previous studies have shown the formation of hydroxycancrinite from uncalcined clay minerals in the <100°C temperature range without a hydrothermal process involved.

The RoM FTIR spectra generally agreed well with the measured spectra, with the exception of 50Kao-50Mont. Here, the wavenumber of the Si-O-T band was higher in the measured pattern than in the RoM spectrum, suggesting that a smaller extent of transformation to alkali aluminosilicate reaction products occurred than expected. This agreed with the observation from the measured and RoM XRD patterns for 50Kao-50Mont, in that less hydrosodalite was formed than expected. Therefore, the evaluation of the FTIR RoM spectra is in broad agreement with the evaluation of the XRD RoM patterns.

Comparing the phases observed in the activated clay mixtures to those predicted by the RoM model, there is some degree of disagreement for nearly all of the mixtures. The RoM model is not consistently correct in predicting the phases and quantities formed in the alkali activation of mixtures of clays. This suggests there are hierarchies in the dissolution and subsequent reactivity of these clays and in determining the product phases formed. Given that consistent curing conditions were used for all compositions, the deviation from RoM behaviour is likely to be due to the conditions in the Al- and Si-rich pore solution favouring the production of different phases (Buchwald *et al.*, 2011), and possibly the influence of the precursor minerals.

6.4.3 Dominance relations between clays in determining product phase formation

Given that the behaviour of the clay mixtures deviated from a rule of mixtures (RoM) model, this can be used as a baseline to consider the dominance relations between the clays under the activation conditions used in this study. Dominance relations are evaluated here in two areas of interest – precursor reactivity, and product phase formation. For example, in an alkali-activated clay mixture of A and B, if more of clay mineral A reacts and less of clay mineral B reacts (compared to the baseline behaviour in the RoM model), then clay mineral A could be said to be dominant in terms of reactivity. In the same mixture, if more of the product phase associated with clay mineral B forms than the product phase associated with clay mineral A (again, compared to the RoM model), then clay B could be said to be dominant in terms of determining product phase formation in the mixture. Predicting the suitability of aluminosilicate precursors for alkali activation is acknowledged to be difficult even for individual minerals (Xu and Van Deventer, 2000), let alone for mixtures of minerals. The approach used here is not a quantitative method of evaluation, but is helpful in developing an empirical understanding of how such mixtures behave in alkali activation. In the following section, the constituent clay minerals' reactivity and influence on phase formation in the different mixtures are evaluated in this way.

In the Kao-Mont series as a whole, less kaolinite was consumed than expected from the RoM model, and less hydrosodalite was formed than expected. From the behaviour of the 50Kao-50Mont sample, montmorillonite seemed to be more reactive than kaolinite, given how much of each was consumed in the reaction. On the other hand, the characterisation evidence suggested that more hydrosodalite (the product phase associated with kaolinite) had formed than geopolymer (the product phase associated with montmorillonite). Thus, over the Kao-Mont series as a whole, montmorillonite was dominant in terms of reactivity, but kaolinite was dominant in determining phase formation.

In the Mont-ILL series, there was evidence of a geopolymer (the product phase associated with montmorillonite) but not of altered illite (the product associated with illite) in 50Mont-50ILL. Given the overlap between the illite reflections and the muscovite impurity reflections in this XRD pattern, it was not possible to compare the relative extents of reaction of the montmorillonite and illite. So, for the Mont-ILL series, one can only say that montmorillonite dominated illite in determining phase formation.

In the ILL-Kao series, the RoM model underestimated both the extent of kaolinite consumption and the extent of hydrosodalite formation (the product phase associated with kaolinite) in 50ILL-50Kao. At the same time, no microstructural features similar to those in 100ILL-0Kao were observed in the SEM images of 50ILL-50Kao. So, for the ILL-Kao series, kaolinite dominated illite both in reactivity and in determining product phase formation.

The validity of this interpretation can be checked against 33Kao-33Mont-33ILL, as this mixture includes the three constituent clay minerals together. As summarised in Table 6-3, the XRD pattern and SEM images showed hydrosodalite to be present, with no evidence of the microstructure characteristic of altered illite. There was possibly a background hump indicative of a geopolymer in the XRD pattern, with the position of the dominant T-O-T band in the FTIR spectrum suggesting a possible mix of geopolymer and hydrosodalite. These observations broadly agree with the dominance relations established from the three binary series of clay mixtures.

These dominance relations have been evaluated for these specific clay precursors, under the alkali activation conditions used in this study. The chemistry and mineralogy of the clay minerals is highly influential in determining their reactivity and product phase formation. However, it is unlikely to be the case that these are inherent, irrevocable qualities of the clay minerals. It is conceivable that these dominance relations could change depending on other factors influencing dissolution, such as available surface area (Tchadjie and Ekolu, 2018), and phase formation, such as curing temperature,

curing time and concentration of NaOH activating solution (Abdullahi *et al.,* 2017; Johnson and Arshad, 2014).

Nonetheless, this finding has implications for the application of alkali-activated clays and soils in construction. The expansive behaviour of soils containing montmorillonite means they are typically avoided in earth construction. However, given that montmorillonite influences phase formation towards geopolymers, the presence of montmorillonite could be beneficial in alkali-activated soil materials, if enough of the montmorillonite can be consumed. Illite is much less expansive, so is normally considered acceptable in soil construction. In isolation, its alkaline activation behaviour is problematic, although could be useful when present as a minor component with other clay minerals. Although these dominance relations were established for un-calcined clays, and without using additional soluble silicates, it is an important step in improving the fundamental understanding of the behaviour of alkali-activated soils.

6.5 Conclusions

Through investigating the alkali activation of binary series of clay mixtures, it has been shown that there was a hierarchy between the clay minerals kaolinite, montmorillonite and illite in determining the product phases in a clay mixture. Montmorillonite and kaolinite both dominated illite. Montmorillonite seemed to be more reactive than kaolinite, but kaolinite had a stronger influence in determining reaction products. Hydroxycancrinite was formed in some binary mixtures, which was not a reaction product from any of the individual clays under these conditions. These findings suggest that knowing which clay minerals are present can help predict the general phase formation; but, neither the relative amounts of phases formed, nor the type of phases formed, can be fully predicted. The systematic method employed in this study has enabled a useful bridge to be made between the study of individual clays and complex soil systems.

Acknowledgements

This study was supported by the EPSRC Centre for Decarbonisation of the Built Environment (dCarb) [grant number EP/L016869/1] and a University of Bath Research Scholarship. All data created during this research are openly available from the University of Bath data archive at https://doi.org/10.15125/BATH-00563

References

Abdullahi, T., Harun, Z. & Othman, M.H.D., 2017. A review on sustainable synthesis of zeolite from kaolinite resources via hydrothermal process. *Advanced Powder Technology,* 28(8), pp. 1827-1840.

Abe, S.S., Masunaga, T., Yamamoto, S., Honna, T. & Wakatsuki, T., 2006. Comprehensive assessment of the clay mineralogical composition of lowland soils in West Africa. *Soil Science & Plant Nutrition,* 52(4), pp. 479-488.

Alshaaer, M., Cuypers, H. & Wastiels, J., 2002. Stabilisation of kaolinitic soil for construction purposes by using mineral polymerisation technique. In: M. Resheidat, ed. *Proceedings of the 6th International Conference on Concrete Technology for Developing Countries.* Amman, Jordan, pp. 1085-1092.

Autef, A., Joussein, E., Gasgnier, G. & Rossignol, S., 2012. Role of the silica source on the geopolymerization rate. *Journal of Non-Crystalline Solids,* 358(21), pp. 2886-2893.

Barbosa, V.F.F., MacKenzie, K.J.D. & Thaumaturgo, C., 2000. Synthesis and characterisation of materials based on inorganic polymers of alumina and silica: sodium polysialate polymers. *International Journal of Inorganic Materials,* 2(4), pp. 309-317.

Barrer, R., Cole, J. & Sticher, H., 1968. Chemistry of soil minerals. Part V. Low temperature hydrothermal transformations of kaolinite. *Journal of the Chemical Society A: Inorganic, Physical, Theoretical*, pp. 2475-2485.

Barrer, R.M. & Mainwaring, D.E., 1972. Chemistry of soil minerals. Part XIII. Reactions of metakaolinite with single and mixed bases. *Journal of the Chemical Society, Dalton Transactions,* (22), pp. 2534-2546.

Bauer, A. & Berger, G., 1998. Kaolinite and smectite dissolution rate in high molar KOH solutions at 35° and 80°C. *Applied Geochemistry,* 13(7), pp. 905-916.

Belviso, C., Cavalcante, F., Niceforo, G. & Lettino, A., 2017. Sodalite, faujasite and A-type zeolite from 2:1 dioctahedral and 2:1:1 trioctahedral clay minerals. A singular review of synthesis methods through laboratory trials at a low incubation temperature. *Powder Technology,* 320, pp. 483-497.

Brunauer, S., Emmett, P.H. & Teller, E., 1938. Adsorption of gases in multimolecular layers. *Journal of the American chemical society,* 60(2), pp. 309-319.

Buchwald, A., Zellmann, H.D. & Kaps, C., 2011. Condensation of aluminosilicate gels—model system for geopolymer binders. *Journal of Non-Crystalline Solids,* 357(5), pp. 1376-1382.

Couchman, P.R., 1978. Compositional Variation of Glass-Transition Temperatures. 2. Application of the Thermodynamic Theory to Compatible Polymer Blends. *Macromolecules,* 11(6), pp. 1156-1161.

Criado, M., Fernández-Jiménez, A. & Palomo, A., 2007. Alkali activation of fly ash: Effect of the SiO2/Na2O ratio: Part I: FTIR study. *Microporous and Mesoporous Materials,* 106(1), pp. 180-191.

Davidovits, J., 2011. *Geopolymer chemistry and applications.* 3rd ed. Saint-Quentin: Institut Geopolymere.

Diop, M.B. & Grutzeck, M.W., 2008. Low temperature process to create brick. *Construction and Building Materials,* 22(6), pp. 1114-1121.

Dixon, J.B. & Weed, S.B., 1989. *Minerals in Soil Environments.* 2nd ed. Madison, WI: Soil Science Society of America.

Donald, I.W. & Davies, H.A., 1978. Prediction of glass-forming ability for metallic systems. *Journal of Non-Crystalline Solids,* 30(1), pp. 77-85.

Duxson, P., Fernández-Jiménez, A., Provis, J.L., Lukey, G.C., Palomo, A. & van Deventer, J.S.J., 2007a. Geopolymer technology: the current state of the art. *J Mater Sci,* 42(9), pp. 2917-2933.

Duxson, P., Mallicoat, S.W., Lukey, G.C., Kriven, W.M. & van Deventer, J.S.J., 2007b. The effect of alkali and Si/Al ratio on the development of mechanical properties of metakaolin-based geopolymers. *Colloids and Surfaces A: Physicochemical and Engineering Aspects,* 292(1), pp. 8-20.

Duxson, P., Provis, J.L., Lukey, G.C., Mallicoat, S.W., Kriven, W.M. & van Deventer, J.S.J., 2005. Understanding the relationship between geopolymer composition, microstructure and mechanical properties. *Colloids and Surfaces A: Physicochemical and Engineering Aspects,* 269(1), pp. 47-58.

El Hafid, K. & Hajjaji, M., 2015. Effects of the experimental factors on the microstructure and the properties of cured alkali-activated heated clay. *Applied Clay Science,* 116–117, pp. 202-210.

Essaidi, N., Samet, B., Baklouti, S. & Rossignol, S., 2014. The role of hematite in aluminosilicate gels based on metakaolin. *Ceramics Silikati,* 58(1), pp. 1-11.

Farmer, V.C., 1974. *Infrared spectra of minerals.* London: Mineralogical society.

Fernández-Jiménez, A. & Palomo, A., 2005. Mid-infrared spectroscopic studies of alkali-activated fly ash structure. *Microporous and Mesoporous Materials,* 86(1), pp. 207-214.

Ferrage, E., Lanson, B., Sakharov, B.A. & Drits, V.A., 2005. Investigation of smectite hydration properties by modeling experimental X-ray diffraction patterns: Part I. Montmorillonite hydration properties. *Am Mineral,* 90(8-9), pp. 1358-1374.

Flanigen, E.M., Khatami, H. & Szymanski, H.A., 1974. Infrared Structural Studies of Zeolite Frameworks. *Molecular Sieve Zeolites-I.* AMERICAN CHEMICAL SOCIETY, pp. 201-229.

Gailhanou, H., van Miltenburg, J.C., Rogez, J., Olives, J., Amouric, M., Gaucher, E.C. & Blanc, P., 2007. Thermodynamic properties of anhydrous smectite MX-80, illite Imt-2 and mixed-layer illite–smectite ISCz-1 as determined by calorimetric methods. Part I: Heat capacities, heat contents and entropies. *Geochimica et Cosmochimica Acta,* 71(22), pp. 5463-5473.

Haines, S.H. & van der Pluijm, B.A., 2008. Clay quantification and Ar–Ar dating of synthetic and natural gouge: Application to the Miocene Sierra Mazatán detachment fault, Sonora, Mexico. *Journal of Structural Geology,* 30(4), pp. 525-538.

Heah, C.Y., Kamarudin, H., Mustafa Al Bakri, A.M., Bnhussain, M., Luqman, M., Khairul Nizar, I., Ruzaidi, C.M. & Liew, Y.M., 2012. Study on solids-to-liquid and

alkaline activator ratios on kaolin-based geopolymers. *Construction and Building Materials,* 35, pp. 912-922.

Heath, A., Paine, K. & McManus, M., 2014. Minimising the global warming potential of clay based geopolymers. *Journal of Cleaner Production,* 78, pp. 75-83.

Heller-Kallai, L. & Lapides, I., 2007. Reactions of kaolinites and metakaolinites with NaOH—comparison of different samples (Part 1). *Applied Clay Science,* 35(1–2), pp. 99-107.

Henderson, C. & Taylor, D., 1977. Infrared spectra of anhydrous members of the sodalite family. *Spectrochimica Acta Part A: Molecular Spectroscopy,* 33(3-4), pp. 283-290.

Hounsi, A.D., Lecomte-Nana, G., Djétéli, G., Blanchart, P., Alowanou, D., Kpelou, P., Napo, K., Tchangbédji, G. & Praisler, M., 2014. How does Na, K alkali metal concentration change the early age structural characteristic of kaolin-based geopolymers. *Ceramics International,* 40(7, Part A), pp. 8953-8962.

Hounsi, A.D., Lecomte-Nana, G.L., Djétéli, G. & Blanchart, P., 2013. Kaolin-based geopolymers: Effect of mechanical activation and curing process. *Construction and Building Materials,* 42, pp. 105-113.

Johnson, E.B.G. & Arshad, S.E., 2014. Hydrothermally synthesized zeolites based on kaolinite: A review. *Applied Clay Science,* 97-98, pp. 215-221.

Khale, D. & Chaudhary, R., 2007. Mechanism of geopolymerization and factors influencing its development: a review. *J Mater Sci,* 42(3), pp. 729-746.

Lee, W.K.W. & van Deventer, J.S.J., 2003. Use of Infrared Spectroscopy to Study Geopolymerization of Heterogeneous Amorphous Aluminosilicates. *Langmuir,* 19(21), pp. 8726-8734.

Lemougna, P.N., Madi, A.B., Kamseu, E., Melo, U.C., Delplancke, M.P. & Rahier, H., 2014. Influence of the processing temperature on the compressive strength of Na activated lateritic soil for building applications. *Construction and Building Materials,* 65, pp. 60-66.

Liew, Y.M., Heah, C.Y., Mohd Mustafa, A.B. & Kamarudin, H., 2016. Structure and properties of clay-based geopolymer cements: A review. *Progress in Materials Science,* 83, pp. 595-629.

Liew, Y.M., Kamarudin, H., Mustafa Al Bakri, A.M., Bnhussain, M., Luqman, M., Khairul Nizar, I., Ruzaidi, C.M. & Heah, C.Y., 2012. Optimization of solids-to-liquid and alkali activator ratios of calcined kaolin geopolymeric powder. *Construction and Building Materials,* 37, pp. 440-451.

MacKenzie, K.J.D., 2009. Utilisation of non-thermally activated clays in the production of geopolymers. In: J.L. Provis & J.S.J. Van Deventer, eds. *Geopolymers: Structure, Processing, Properties and Industrial Applications.* Pp. 296-316.

Madejova, J. & Komadel, P., 2001. Baseline studies of the clay minerals society source clays: infrared methods. *Clays and Clay Minerals,* 49(5), pp. 410-432.

Marom, G., Fischer, S., Tuler, F.R. & Wagner, H.D., 1978. Hybrid effects in composites: conditions for positive or negative effects versus rule-of-mixtures behaviour. *J Mater Sci,* 13(7), pp. 1419-1426.

Marsh, A., Heath, A., Patureau, P., Evernden, M. & Walker, P., 2018a. Alkali activation behaviour of un-calcined montmorillonite and illite clay minerals. *Applied Clay Science,* 166, pp. 250-261.

Marsh, A., Heath, A., Patureau, P., Evernden, M. & Walker, P., 2018b. A mild conditions synthesis route to produce hydrosodalite from kaolinite, compatible with extrusion processing. *Microporous and Mesoporous Materials,* 264, pp. 125-132.

Maskell, D., Heath, A. & Walker, P., 2013. Laboratory scale testing of extruded earth masonry units. *Materials & Design,* 45, pp. 359-364.

Mikuła, A., Król, M. & Koleżyński, A., 2015. The influence of the long-range order on the vibrational spectra of structures based on sodalite cage. *Spectrochimica Acta Part A: Molecular and Biomolecular Spectroscopy,* 144, pp. 273-280.

Moloy, E.C., Liu, Q. & Navrotsky, A., 2006. Formation and hydration enthalpies of the hydrosodalite family of materials. *Microporous and Mesoporous Materials,* 88(1), pp. 283-292.

Muñiz-Villarreal, M.S., Manzano-Ramírez, A., Sampieri-Bulbarela, S., Gasca-Tirado, J.R., Reyes-Araiza, J.L., Rubio-Ávalos, J.C., Pérez-Bueno, J.J., Apatiga, L.M., Zaldivar-Cadena, A. & Amigó-Borrás, V., 2011. The effect of temperature on the geopolymerization process of a metakaolin-based geopolymer. *Materials Letters,* 65(6), pp. 995-998.

Murmu, A.L. & Patel, A., 2018. Towards sustainable bricks production: An overview. *Construction and Building Materials,* 165, pp. 112-125.

Murray, H.H. & Keller, W.D., 1993. Kaolins, Kaolins and Kaolins. In: H.H. Murray, W.M. Bundy & C.C. Harvey, eds. *Kaolin Genesis and Utilization.* Clay Minerals Society.

Nickovic, S., Vukovic, A., Vujadinovic, M., Djurdjevic, V. & Pejanovic, G., 2012. High-resolution mineralogical database of dust-productive soils for atmospheric dust modeling. *Atmospheric Chemistry and Physics,* 12(2), pp. 845-855.

Omar Sore, S., Messan, A., Prud'homme, E., Escadeillas, G. & Tsobnang, F., 2018. Stabilization of compressed earth blocks (CEBs) by geopolymer binder based on local materials from Burkina Faso. *Construction and Building Materials,* 165, pp. 333-345.

Pacheco-Torgal, F., Castro-Gomes, J. & Jalali, S., 2008. Alkali-activated binders: A review. Part 2. About materials and binders manufacture. *Construction and Building Materials,* 22(7), pp. 1315-1322.

Provis, J.L., 2014. Geopolymers and other alkali activated materials: why, how, and what? *Mat. Struct.,* 47(1), pp. 11-25.

Prud'homme, E., Autef, A., Essaidi, N., Michaud, P., Samet, B., Joussein, E. & Rossignol, S., 2013. Defining existence domains in geopolymers through their physicochemical properties. *Applied Clay Science,* 73, pp. 26-34.

Querol, X., Moreno, N., Umaña, J.C., Alastuey, A., Hernández, E., López-Soler, A. & Plana, F., 2002. Synthesis of zeolites from coal fly ash: an overview. *International Journal of Coal Geology,* 50(1), pp. 413-423.

Rees, C.A., Provis, J.L., Lukey, G.C. & van Deventer, J.S.J., 2007a. Attenuated Total Reflectance Fourier Transform Infrared Analysis of Fly Ash Geopolymer Gel Aging. *Langmuir,* 23(15), pp. 8170-8179.

Rees, C.A., Provis, J.L., Lukey, G.C. & van Deventer, J.S.J., 2007b. In Situ ATR-FTIR Study of the Early Stages of Fly Ash Geopolymer Gel Formation. *Langmuir,* 23(17), pp. 9076-9082.

Reeves, G.M., Sims, I. & Cripps, J.C., 2006. *Clay materials used in construction.* London: Geological Society.

Richardson, C.K., Markuszewski, R., Durham, K.S. & Bluhm, D.D., 1986. Effect of Caustic and Microwave Treatment on Clay Minerals Associated with Coal. *Mineral Matter and Ash in Coal.* American Chemical Society, pp. 513-523.

Roy, B.N., 1990. Infrared Spectroscopy of Lead and Alkaline-Earth Aluminosilicate Glasses. *Journal of the American Ceramic Society,* 73(4), pp. 846-855.

Seiffarth, T., Hohmann, M., Posern, K. & Kaps, C., 2013. Effect of thermal pre-treatment conditions of common clays on the performance of clay-based geopolymeric binders. *Applied Clay Science,* 73, pp. 35-41.

Sperberga, I., Sedmale, G., Stinkulis, G., Zeila, K. & Ulme, D., 2011. Comparative study of illite clay and illite-based geopolymer products. In: K. Niihara, T. Ohji & Y. Sakka, eds. *3rd International Congress on Ceramics (ICC3).* Osaka, Japan: IOP Publishing, p. 222027.

Tchadjie, L.N. & Ekolu, S.O., 2018. Enhancing the reactivity of aluminosilicate materials toward geopolymer synthesis. *J Mater Sci,* 53(7), pp. 4709-4733.

Tchakoute, H.K., Rüscher, C.H., Djobo, J.N.Y., Kenne, B.B.D. & Njopwouo, D., 2015. Influence of gibbsite and quartz in kaolin on the properties of metakaolin-based geopolymer cements. *Applied Clay Science,* 107, pp. 188-194.

Van der Marel, H.W. & Beutelspacher, H., 1976. *Atlas of infrared spectroscopy of clay minerals and their admixtures.* Amsterdam; New York: Elsevier Scientific Publishing Company.

Weng, L. & Sagoe-Crentsil, K., 2007. Dissolution processes, hydrolysis and condensation reactions during geopolymer synthesis: Part I—Low Si/Al ratio systems. *J Mater Sci,* 42(9), pp. 2997-3006.

Weng, L., Sagoe-Crentsil, K., Brown, T. & Song, S., 2005. Effects of aluminates on the formation of geopolymers. *Materials Science and Engineering: B,* 117(2), pp. 163-168.

Xu, H. & Van Deventer, J.S.J., 2000. The geopolymerisation of alumino-silicate minerals. *International Journal of Mineral Processing,* 59(3), pp. 247-266.

Zografou, A., 2015. *The use of china clay waste as a construction material using alkali-activated cement technology.* PhD, University of Bath.

Appendix

Additional experimental information is provided here regarding the quantities of water used to manufacture the samples (Table 6-4).

Table 6-4: Quantities of clay, water and NaOH used for sample manufacture.

Series	Sample	Mass of clay (g)	Mass of water (g)	Mass of NaOH (g)
Kao-Mont	100Kao-0Mont	25	10.4	7.8
	100Kao-0Mont (control)	50	18.0	0
	90Kao-10Mont	10	4.4	3.0
	90Kao-10Mont (control)	25	10.0	0
	50Kao-50Mont	10	5.1	2.4
	50Kao-50Mont (control)	10	6.5	0
	10Kao-90Mont	10	5.9	1.8
	10Kao-90Mont (control)	25	22.5	0
	0Kao-100Mont	25	15.3	4.1
	0Kao-100Mont (control)	50	48.0	0
Mont-ILL	100Mont-0ILL	25	15.3	4.1
	100Mont-0ILL (control)	50	48.0	0
	50Mont-50ILL	10	4.0	2.1
	50Mont-50ILL (control)	10	5.8	0
	0Mont-100ILL	25	4.8	1.7
	0Mont-100ILL (control)	25	4.8	0
ILL-Kao	100ILL-0Kao	25	4.8	1.7
	100ILL-0Kao (control)	25	4.8	0
	50ILL-50Kao	10	3.1	2.9
	50ILL-50Kao (control)	10	2.7	0
	0ILL-100Kao	25	10.4	7.8
	0ILL-100Kao (control)	50	18.0	0
Kao-Mont-ILL	33Kao-33Mont-33ILL	10	4.1	2.5
	33Kao-33Mont-33ILL (control)	12.5	6.2	0

Chapter 7 - Alkali activation of natural and synthetic soils

In this chapter, the alkali activation behaviour of natural and synthetic soils is investigated. The aim of this chapter is to understand the behaviour of non-clay components in soil in alkali activation. The use of synthetic soils, comprised of mixtures of the same individual clay mineral precursors used previously, builds on the understanding of clay mixtures developed in Chapter 6.

Declaration of authorship

This declaration concerns the article entitled:									
Influence of clay minerals and associated minerals in alkali activation of soils									
Publication status (tick one)									
draft manuscript	✓	**Submitted**		**In review**		**Accepted**		**Published**	
Publication details (reference)	Marsh, A., Heath, A., Patureau, P., Evernden, M., Walker, P. (in preparation). “Influence of clay minerals and associated minerals in alkali activation of soils”								
Candidate’s contribution to the paper (detailed, and also given as a percentage).	The candidate predominantly executed the… Formulation of ideas: A.Marsh (80%) developed the idea for this study, with suggestions and guidance given by the co-authors (20%) (i.e. supervisors). Design of methodology: A.Marsh (80%) developed the methodology for this study, with suggestions and guidance given by the co-authors (20%) (i.e. supervisors). Experimental work: A.Marsh undertook the majority of experimental work and analysis (80%), with input from co-authors (20%). Presentation of data in journal format: A.Marsh (100%) undertook all formatting.								
Statement from Candidate	This paper reports on original research I conducted during the period of my Higher Degree by Research candidature.								
Signed							**Date**	30/10/2018	

Influence of clay minerals and associated minerals in alkali activation of soils

Abstract

Alkali activation is promising for low environmental impact soil stabilisation. Given soils' complexity, there is a lack of fundamental understanding of the role different components play in their alkali activation behaviour. A novel method was developed to compare three natural soils with synthetic versions. Precursors and products were characterised by XRD, SEM, TGA and FTIR to explore the soils' alkali activation phase formation behaviour. It is shown that only the clay minerals will determine phase formation, whereas most associated minerals had negligible influence. The trade-off between Na:Al and NaOH concentration in mix design means lower plasticity soils are more suitable.

7.1 Introduction

Alkali-activated materials are a growing area of interest in construction material development, due to their versatility in using a range of precursors and their potential for low environmental impact (Provis, 2018a). One application for alkali activation is soil stabilisation (Hamzah *et al.*, 2015; Pourakbar and Huat, 2017; Sargent, 2015). Research in this area has concentrated on the route of indirect alkali activation – the addition of reactive aluminosilicates to a soil, which are then transformed to form a stabilising phase. Additions have included fly ash (Cristelo *et al.*, 2013), GGBS (Singhi *et al.*, 2016; Toda *et al.*, 2018), agricultural wastes (Arulrajah *et al.*, 2016; Kinuthia, 2016; Pourakbar *et al.*, 2017), metakaolin (Omar Sore *et al.*, 2018; Zhang *et al.*, 2013), volcanic ash (Miao *et al.*, 2017) and others (Sargent, 2015). The alternative route of direct alkali activation – transforming the clay minerals in soil, without the addition of external aluminosilicates – has been less explored. This route has the possible benefits of being more versatile in areas where there is not a readily available source of reactive aluminosilicate, negating the troublesome effects of some clays in soil (e.g. swelling clays), and still retaining improvements in embodied carbon (Dahmen *et al.*, 2018). There is also a general benefit of developing methods to understand the alkali activation behaviour of lower purity aluminosilicates. This is to enable a wider range of precursors to be used, and hence greater impact of alkali-activated materials (Gharzouni *et al.*, 2016; McIntosh *et al.*, 2015; Provis, 2018b). Previous research in direct alkali activation of clays and soils has mostly focussed either on relatively simple systems such as metakaolin (Rahier *et al.*, 1996) and kaolinite (van Jaarsveld *et al.*, 2002), with only a small number of studies on more complex natural soils (Boutterin and Davidovits, 1988; Diop and Grutzeck, 2008; Lassinantti Gualtieri *et al.*, 2015; Lemougna *et al.*, 2014; Obonyo *et al.*, 2014). The objectives of these studies have typically been to understand the effect of alkali activator and curing variables on the reaction, or simply the strength of the end products. This approach has been valuable in gaining an understanding of the fundamentals of the alkali activation process, as well as an empirical understanding of the range of these variables which typically give optimal results. However, in order to determine the feasibility of alkali-activated soils as a scalable technology, it is necessary to determine which compositional factors are important in making a given soil well-suited for activation, and which are not. This requires a more systematic approach to considering the influence of both the clay minerals in the reaction (Marsh *et al.*, under review), and the influence of associated minerals in soils, some of which are known to be reactive in alkali activation. This has been done to some extent for common clay mineral deposits (Zibouche *et al.*, 2009), but without isolating the effect of clay minerals other than kaolin.

The composition of sub-soils can be considered to consist of clay minerals, associated minerals (i.e. naturally occurring non-clay minerals) (Bergaya and Lagaly, 2013; Guggenheim and Martin, 1995) and some amount of organic compounds present in humic substances (Dixon and Weed, 1989). Soils with low organic content are used for stabilised soil materials, as this is a general requirement in earth building (Jagadish, 2007). The composition of soils can vary greatly between different locations, as well as varying with depth in a single location (Dixon and Weed, 1989). The direct alkali activation behaviour of the common clay minerals is still being investigated, but a basic understanding of their behaviour as individuals (Marsh *et al.*, 2018a; Marsh *et al.*, 2018b) and in mixtures (Marsh *et al.*, under review) has already been established under comparable processing conditions. In contrast, as a group, common associated minerals – especially in the context of soil systems – are less well understood.

The aim of this study is to investigate the relative influence of clay minerals and associated minerals in determining the direct alkali activation behaviour of soils. By using multi-component systems to close the gap between laboratory studies and real conditions, it is intended to gain a better understanding for a direct application in construction. This is the first known attempt to isolate the effect of associated minerals in soil on alkali activation using this approach.

7.2 Materials and Methods

7.2.1 Materials

Natural soils were used from: Bristol, U.K.; Bengaluru, India, and Khartoum, Sudan. The particle size distribution (Figure 7-1) was measured by a combination of wet-sieving, to measure particle grading from 2 mm – 63 µm, and hydrometer testing, to measure particle grading < 63 µm by using the principle of Stokes' Law to measure particle size by the time taken for particles to fall out of suspension in water (BSI, 1990). All three soils were fine-grained under the USCS terminology, with Bristol as a lean clay (CL) (Maskell, 2013), Bengaluru as a lean clay (CL) and Khartoum as an intermediate clay (CI) (Balila, 2017). Regarding colour, Bristol was brown, Bengaluru red and Khartoum brown-grey. Calcination is a common processing step in alkali activation of clay minerals, as it generally improves reactivity by the dehydroxylation of clay minerals – in particular, the conversion of kaolinite to metakaolin. In this study, it was chosen not to use calcination for two reasons. Firstly, because it increases the environmental impact of the precursor (Habert and Ouellet-Plamondon, 2016). Secondly, because the ideal calcination temperature depends on the type and nature of clay minerals present (Hollanders *et al.*, 2016), and in soils with different clay minerals choosing a single calcination temperature would be difficult.

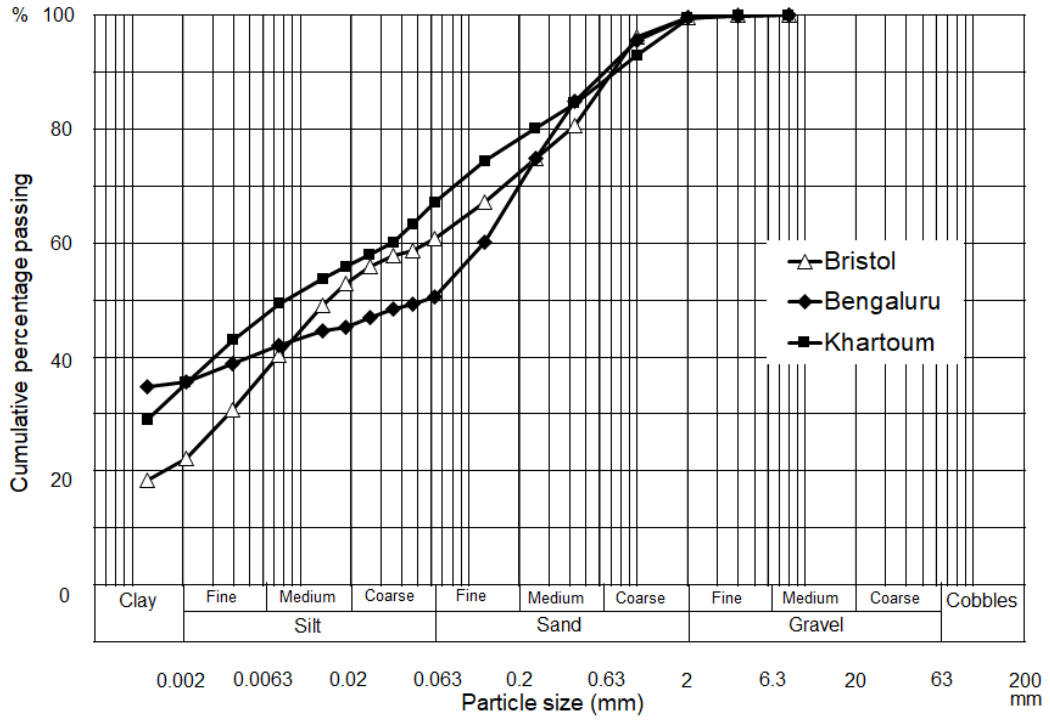

Figure 7-1: The particle size distribution of the three natural soils.

To manufacture synthetic soils, Imerys Speswhite kaolin (mined from Cornwall, U.K.), K10 montmorillonite (Sigma-Aldrich, product no. 69866-1KG) and Clay Minerals Society Imt-2 (Silver Hill) illite were used as precursor clays. Builders' fine quartz sand was used as an inert aggregate, sieved to <425 μm and washed clean with distilled water. This contained quartz, with a trace amount of calcite. Chemical compositions of the natural and synthetic soils were determined by energy dispersive X-rays (JEOL SEM6480LV with Oxford INCA X-Act SDD X-ray detector) at an accelerating voltage of 20 kV, a chamber pressure of 30 Pa, a Si wafer as a standard, and measuring ≥ 3 scan areas per sample. The soil powders were mounted on a sticky carbon tab on top of an aluminium stub, and were not coated. Specific surface areas were measured using the BET method (Brunauer *et al.*, 1938) using a Micromeritics 3-Flex. 2 g of each precursor powder were degassed ex-situ in a N_2 atmosphere under atmospheric pressure at 250°C for ≥ 70 h, and then degassed in-situ under vacuum at 250°C for 14 h.

The natural and synthetic soils' chemical compositions are given in Table 7-1. In order to ensure consistency, the soils were ground by hand in isopropanol until they passed through a 425 μm sieve. The natural and synthetic soils' specific surface areas are given in Table 7-2. The precursors were activated using sodium hydroxide pellets of >98% purity (Sigma-Aldrich, product no. 06203).

Table 7-1: Chemical composition of the natural (nat) and synthetic (syn) soils in oxide wt%.

Soil	Al_2O_3	CaO	CuO	Fe_2O_3	K_2O	MgO	MnO	Na_2O	SiO_2	SO_3	TiO_2	Total
Bristol-nat	22.85	1.29	0.34	9.75	4.84	1.16	0.00	0.25	57.76	0.39	1.37	100.00
Bengaluru-nat	24.05	0.38	0.08	12.10	1.21	0.26	0.00	0.00	60.73	0.08	1.11	100.00
Khartoum-nat	11.60	11.45	0.17	10.36	1.12	2.46	0.41	0.64	60.20	0.30	1.30	100.00
Bristol-syn	32.93	0.44	0.00	2.36	2.98	0.37	0.00	0.00	60.71	0.06	0.13	100.00
Bengaluru-syn	37.65	0.52	0.13	1.62	2.49	0.14	0.00	0.00	57.45	0.00	0.00	100.00
Khartoum-syn	16.63	0.50	0.00	3.93	2.09	1.00	0.00	0.00	75.28	0.00	0.57	100.00

Table 7-2: Specific surface areas of the natural (nat) and synthetic (syn) soils in oxide wt%.

Soil	Specific surface area (m^2g^{-1})
Bristol-nat	17.6
Bengaluru-nat	33.7
Khartoum-nat	36.9
Bristol-syn	14.0
Bengaluru-syn	6.7
Khartoum-syn	42.0

7.2.2 Synthesis procedure

The phase compositions of the natural Bristol (Maskell, 2013) and Khartoum (Balila, 2017) soils had been previously quantified. The Bengaluru soil was found to contain kaolinite as the only clay mineral, the mass proportion of which was assumed to be the same as the clay fraction (<2 μm particle size). Using this information about the phase compositions of the natural soils (Table 7-3), synthetic soils were prepared. The compositions of the synthetic soils were determined in order to have the same types and proportions of clay minerals as each respective natural soil - but, instead of the associated minerals found in the natural soils, the remaining mass was made up with quartz sand as a filler. Using these proportions of clay minerals and quartz sand, the synthetic soils were prepared to have compositions given in Table 7-3. These were made by adding the constituent ingredients together in a beaker, then dry-mixing for 5 minutes with a magnetic stirrer (Stuart UC152 heat-stir). Their chemical compositions are given in Table 7-1.

*Table 7-3: Compositions of natural (nat) and synthetic (syn) soils used. *Natural associated minerals are assumed not to participate in the reaction.*

Sample	Kaolinite (%)	Montmorillonite (%)	Illite (%)	Natural associated minerals* (%)	Inert filler sand (%)
Bristol-nat	31	3	13	53	0
Bristol-syn	31	3	13	0	53
Bengaluru-nat	36	0	0	64	0
Bengaluru-syn	36	0	0	0	64
Khartoum-nat	4	18	3	75	0
Khartoum-syn	4	18	3	0	75

As previously described (Marsh *et al.*, 2018b), the compositions in Table 7-4 were determined to provide samples of a predetermined Na:Al ratio (chosen to be 1), whilst maintaining the wet mix workability at the plastic limit. In order to be consistent about calculating the reactive moles of Al, a working assumption was made that only the clay minerals would react in alkali activation. Therefore, molar quantities of Al in each soil were calculated from the clay contents and generic structural formulae of the clay minerals. To model workability behaviour, Atterberg plastic limit measurements (Wagner, 2013) were undertaken for each of the natural soils over a range of sodium hydroxide solution concentrations (BSI, 1990), shown in Figure 7-2. The behaviour matched well for the synthetic soils too.

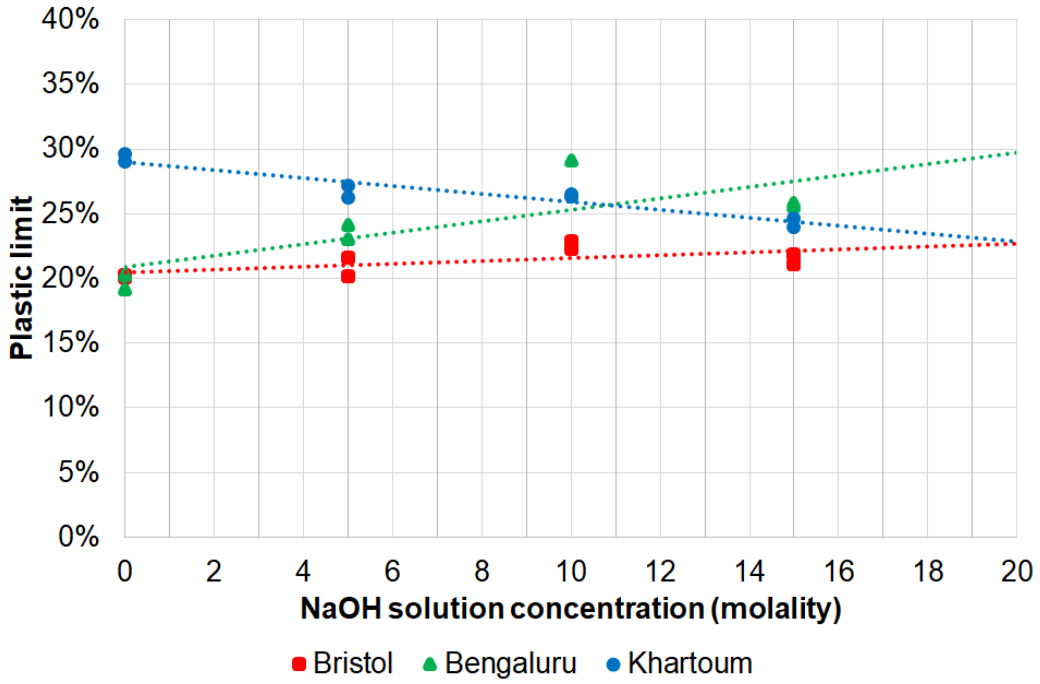

Figure 7-2: Variation in plastic limit with sodium hydroxide solution concentration for the three natural soils.

The soil samples were activated by adding an aqueous sodium hydroxide solution. Solutions of different concentrations were prepared by adding sodium hydroxide pellets to distilled water, mixing with a magnetic stirrer (Stuart UC152 heat-stir) for a minimum of 2 h until fully dissolved and then allowing to cool. Varying quantities of activating solutions were added to 20 g of each soil, as given in Table 7-4. Each mixture of activating solution and soil was mixed by hand for 3 minutes, providing a consistent and well-distributed mixture. The high viscosity of the samples allowed them to be compacted by hand into 18 mm x 36 mm cylindrical Teflon moulds by tamping with a glass rod in three layers for each sample, using 25 blows for each layer. Samples were cured in an air atmosphere in an 80 °C oven for 24 h in their moulds. After curing, activated samples in the Bristol and Bengaluru soil series were not fully dried so required further drying, by storing for 48 h in a vacuum dessicator. This phenomenon of slow drying has previously been observed in other alkali-activated clay-based systems (Marsh *et al.*, 2018a). After demoulding, samples were aged for 28 days in a controlled environment of 20 ± 0.5°C and 50 ± 2.5% relative humidity. An air atmosphere was intentionally used for both curing and ageing, to provide conditions representative of industrial brickmaking processes. A control sample was made for each composition, by adding distilled water and then mixing and curing in the same manner.

Due to the experimental constraints of plastic limit consistency and Na:Al = 1, the NaOH solution was a lower concentration for Khartoum (4.1 M) than for the other soils (10.2 M and 13.2 M) (Table 7-4). Therefore, to test whether the difference in behaviour was due to a lower concentration, activation of the Khartoum soils was repeated using

a 10 M NaOH activating solution whilst maintaining the plastic limit condition, and hence giving an Na:Al molar ratio > 1. These results are included in an Appendix.

Table 7-4: Composition of activating solutions used for 20g of dry soil, for the control (cont) and activated (act) samples.

Sample	Water (g)	NaOH (g)	[NaOH] (molarity)
Bristol-nat-cont	4.04	n/a	n/a
Bristol-nat-act	4.41	2.56	13.2
Bristol-syn-cont	4.04	n/a	n/a
Bristol-syn-act	4.41	2.56	13.2
Bengaluru-nat-cont	3.94	n/a	n/a
Bengaluru-nat-act	5.13	2.23	10.2
Bengaluru-syn-cont	3.94	n/a	n/a
Bengaluru-syn-act	5.13	2.23	10.2
Khartoum-nat-cont	5.86	n/a	n/a
Khartoum-nat-act	5.54	0.94	4.1
Khartoum-syn-cont	5.86	n/a	n/a
Khartoum-syn-act	5.54	0.94	4.1

7.2.3 Characterisation methods

The set of characterisations was performed at 28 ±2 days ageing time, and (with the exception of SEM imaging) was done using powders prepared from the cured samples. These were ground by hand, having been wetted with isopropanol to avoid damaging the clay minerals' crystal structures (Moore and Reynolds, 1997). For XRD and TGA, powders were ground until there was no further discernible reduction in particle size, and so were comparable between samples. Any variation in particle size of the ground powders was not expected to have any noticeable effect on characterisation results. For FTIR, due to the constraints on particle size when making measurements in reflection mode, and the wider particle size distribution in soils compared to clays, powders were ground until they passed through a 75 μm sieve.

Powder X-ray diffraction (XRD) analysis was performed to identify phases with a Bruker D8 Advance instrument using monochromatic CuKα1 L3 (λ = 1.540598 Å) X-radiation and a Vantec superspeed detector. A step size of 0.016 °(2θ) and step duration of 0.3 seconds were used. Powder samples were prepared using the pressed glass slide method. Patterns were corrected for sample height shift by calibrating to the most intense quartz reflection (101) at 26.6 °(2θ), and normalised to the most intense reflection in each respective pattern. Phase identification was done using Bruker EVA software, using reference patterns from the Joint Committee on Powder Diffraction Standards (JCPDS) database.

Fourier Transform Infrared Spectroscopy (FTIR) was done to characterise molecular bonding, using a Perkin-Elmer Frontier with a diamond Attenuated Total Reflectance (ATR) head. For FTIR, powder samples were ground further until they passed through a 75 µm sieve. Spectra were collected over a range of 4000 – 600 cm^{-1} using a resolution of 4 cm^{-1} and 5 scans per spectrum. Corrections were made for ATR and background using Perkin-Elmer Spectrum software. Spectra were normalised to the most intense band in each respective spectrum.

Scanning electron microscope (SEM) imaging was used to characterise phase size and morphology, using a JEOL SEM6480LV in secondary electron mode with an accelerating voltage (AV) of 10 kV. Because the SEM used a tungsten filament, an AV of 10 kV was selected as an optimal balance between the tendencies towards a noisy image at lower AV, and lower resolution at higher AV. Unpolished samples were used to enable easier distinction of particle morphology in the microstructures, and also given the friability of some of the samples. Bulk specimens were sputter coated with gold for 3 minutes. All images were taken of regions in the bulk of the specimen, >2 mm away from the edge.

7.3 Results

7.3.1 Macroscopic behaviour

No unusual curing shrinkage or expansion defects were observed in any of the samples after curing (Figure 7-3). The difference in colour between the natural and synthetic clays is mostly attributable to the presence of iron compounds (Dixon and Weed, 1989). Most of the soils did not undergo any changes of colour after activation. Exceptions included: the Bristol natural soil darkened slightly; the Khartoum synthetic soil turned a shade of brown, and both the Bengaluru real soil and the Bristol synthetic soil had a strip of darker material at the top (i.e. the open end of the mould).

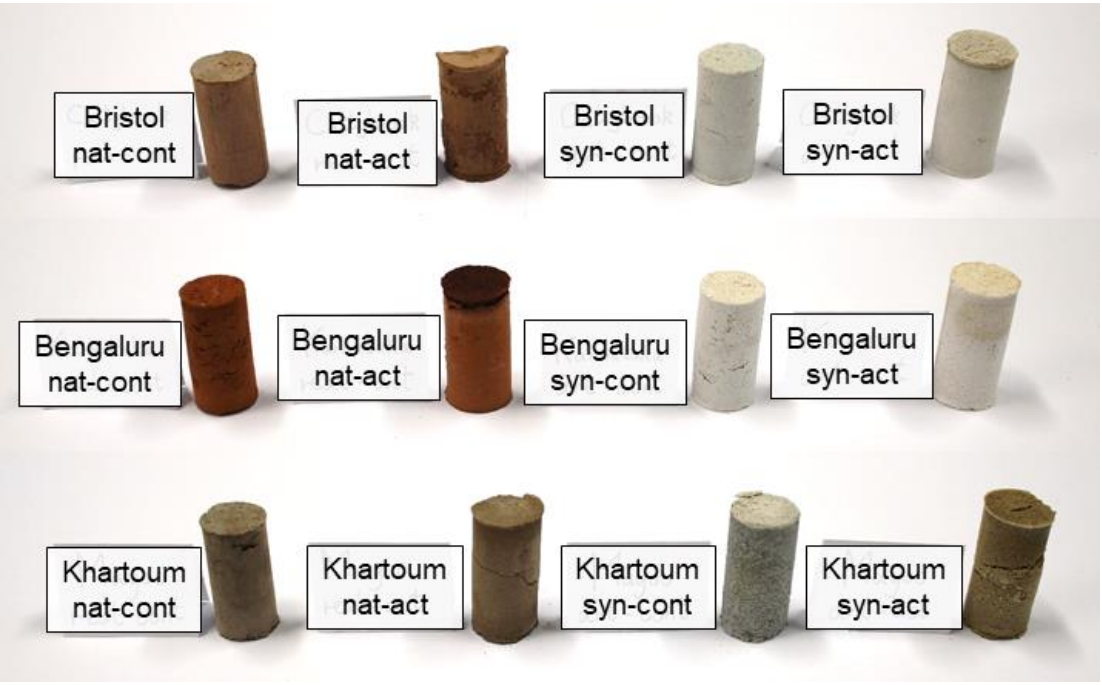

Figure 7-3: Photos of cured control and activated samples.

7.3.2 XRD

7.3.2.1 Precursors

The indexing of the Bristol and Khartoum natural soils was based on the quantitative analysis undertaken on these soils in previous studies (Balila, 2017; Maskell, 2013). XRD patterns were also measured for the <2 µm fraction of the soils, separated using a sedimentation technique (Stucki, 2013). Regarding iron oxide/hydroxide compounds, only hematite was identified in Bristol-nat and Bengaluru-nat (Figure 7-4). Both these soils demonstrated a noticeable response to an applied magnetic field, as expected (Stucki *et al.*, 1987). The Khartoum-nat soil demonstrated a weak response. Given the brown/grey colour, it may contain a small amount of fine goethite which was not detectable in XRD due to small size and low crystallinity (Kuhnel *et al.*, 1975; Stucki *et al.*, 1987).

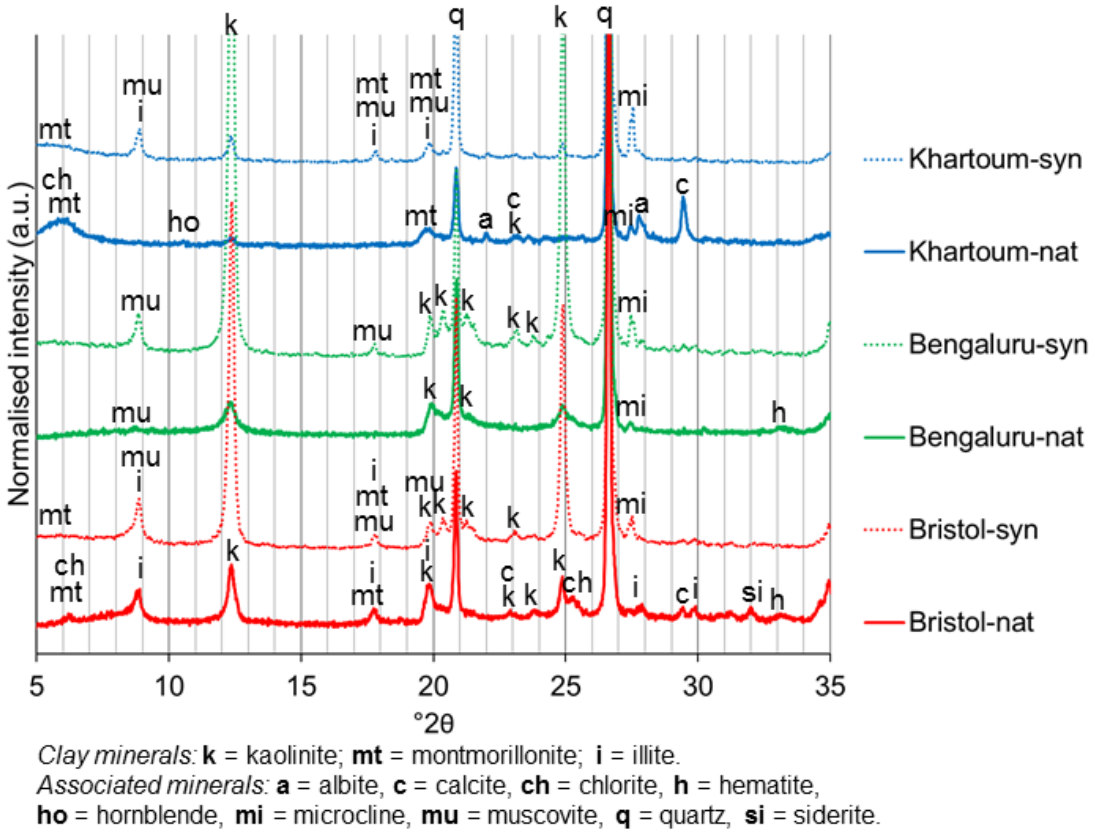

Figure 7-4: Indexed XRD patterns of the natural and synthetic soils.

In the Bristol natural soil, the clay phases present (listed in order of most to least abundant) were kaolinite (Powder Diffraction File (PDF)# 01-079-1570), illite (PDF# 00-026-0911) and montmorillonite (PDF# 00-013-0135), with quartz (PDF# 00-046-1045), hematite (PDF# 00-033-0664), a chlorite (PDF# 01-085-2163), calcite (PDF# 00-005-0586) and siderite (PDF# 00-029-0696) also present. In the synthetic soil, the same

clay phases were present, with quartz, muscovite (PDF# 01-084-1304) and microcline (PDF# 00-019-0932) present as impurities.

In the Bengaluru natural soil, kaolinite was the only clay mineral present, with quartz, hematite, microcline and a mica phase also present. The mica phase was assigned as muscovite, given that the underlying geology of the area was granitic. In the synthetic soil, kaolinite was the sole clay phase, with quartz, microcline and muscovite present as impurities. The broader profile of the kaolinite reflections is likely due to weathering in lateritic soils (Kaze *et al.*, 2017; Kuhnel *et al.*, 1975).

In the Khartoum natural soil, the clay phases present (listed in order of most to least abundant) were montmorillonite, kaolinite and illite, with quartz, microcline, a chlorite (PDF# 01-074-1137), albite (PDF# 00-009-0466), calcite and hornblende (PDF# 01-071-1060) also present. Given the high iron content of this soil (Table 7-1), at least one iron oxide or hydroxide phase was also expected to be present. Although reflections for these could not identified in the measured pattern, this might expected as its reflections are generally weak due to its small size of typically 10 – 100 nm (Stucki *et al.*, 1987), and also given the number of other phases' reflections in the pattern. In the synthetic soil, the same clay phases were present, with quartz, microcline and muscovite present as impurities. The d-values of the 001 montmorillonite peak were 14.7 and 14.5 Å for the natural and synthetic soils respectively. This suggests their interlayer cations were Ca^{2+} and/or Mg^{2+} (Ferrage *et al.*, 2005).

In the following figures, only the main reflections for the clay minerals and reflections for product phases are indexed. This is done for purposes of clarity, given the number of associated mineral phases, and their general lack of observed reactivity.

7.3.2.2 Bristol Soils

In the natural soil, activation resulted in emergence of new reflections attributed to hydrosodalite $Na_6[AlSiO_4]_6 \cdot 4H_2O$ (PDF# 00-042-0216)(Figure 7-5). For the clay minerals: there was a reduction in intensity of the kaolinite reflections; the illite reflections did not seem not to decrease, and the montmorillonite reflection was too weak to discern any change, especially given its overlap with a chamosite reflection. No notable changes were observed for any of the associated minerals' reflections.

In the synthetic soil, activation also resulted in emergence of new reflections attributed to basic hydrosodalite $Na_8[AlSiO_4]_6(OH)_2 \cdot 4H_2O$ (PDF# 00-041-0009). For the clay minerals there was: a reduction in intensity of the kaolinite reflections; the illite/muscovite reflections seemed to reduce in intensity, and again the montmorillonite reflection was too weak to discern any change. With regard to the minor phases, microcline's strongest reflections seemed also to reduce in intensity relative to the strongest quartz reflection.

Although particle orientation may have some influence, the intensity is less and the breadth is greater of the kaolinite 001 reflection (12.4 °2θ) in the natural soil compared to the synthetic soil. This could be due to particle-size broadening, suggesting that the kaolinite clay mineral phase may have a much smaller average crystallite size in the natural soil, although it is possible strain broadening could contribute too (Moore and Reynolds, 1997).

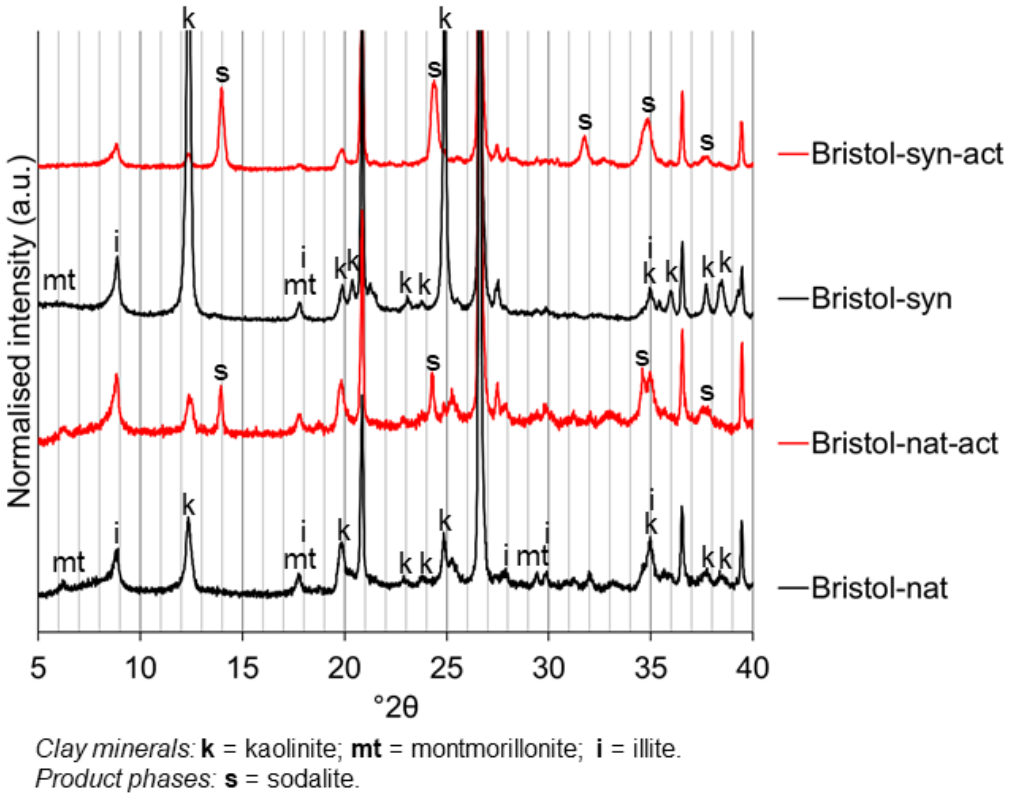

Figure 7-5: XRD patterns of the precursors and activated samples of the natural and synthetic Bristol soils

7.3.2.3 Bengaluru Soils

In the natural soil, activation resulted in emergence of new reflections attributed to the hydrosodalite $Na_6[AlSiO_4]_6 \cdot 4H_2O$ (PDF# 00-042-0216) (Figure 7-6). The reflections of kaolinite, the sole clay mineral present, decreased in intensity after activation. With regard to other phases, the weak reflection of hematite at 33.2 °2θ is still present after activation, whilst the main reflection of muscovite at 8.9 °2θ is too weak to be conclusive.

In the synthetic soil, activation resulted in emergence of new reflections also attributed to the hydrosodalite $Na_6[AlSiO_4]_6 \cdot 4H_2O$ (PDF# 00-042-0216). The reflections of kaolinite decreased in intensity after activation. The muscovite 002 and 004 reflections at 8.9 and 17.8 °2θ seemed to decrease relative to the most intense quartz reflection.

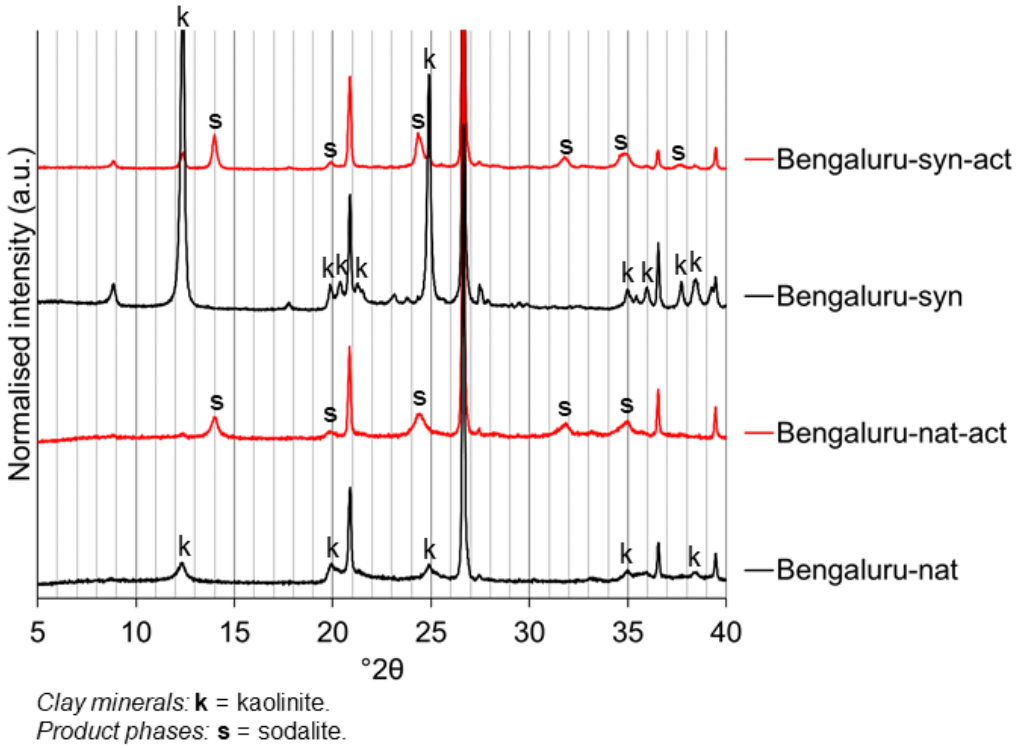

Figure 7-6: XRD patterns of the precursors and activated samples of the natural and synthetic Bengaluru soils.

7.3.2.4 Khartoum Soils

In the natural soil, activation resulted in no visible formation of crystalline product phases (Figure 7-7). For the clay minerals, there was a shift of the montmorillonite 001 reflection from 5.9 to 7.3 °2θ, and hence a decrease in d-value from 15.0 to 12.1 Å. This shift has previously been attributed partly to interlayer cation exchange of Na^{+} for Ca^{2+}/Mg^{2+}, and partly to the activation process itself (Marsh *et al.*, 2018a). This interpretation was consistent with a noticeable decrease in plastic limit when NaOH concentration was increased (Figure 7-2), which is typical of Ca^{2+} montmorillonite (Bain, 1971). The 001 reflection became broader after activation, making it unclear whether there was any change in overall intensity. The kaolinite 001 reflection (12.4 °2θ) did not undergo any noticeable change, and the illite reflections were too weak to say anything conclusive. No notable changes were observed for any of the associated minerals' reflections.

In the synthetic soil, activation also resulted in no visible formation of crystalline product phases. For the clay minerals, there were also the effects of cation exchange and activation process on montmorillonite, which underwent a shift of the 001 reflection from 5.6 to 7.2 °2θ, and hence a decrease in d-value from 15.8 to 12.3 Å. The montmorillonite 001 reflection also seemed to undergo a decrease in intensity. The kaolinite and illite/muscovite reflections seemed to decrease in intensity in comparison to the main quartz reflection. With regard to minor phases, the microcline reflection at 27.5 °2θ seemed to undergo a decrease in intensity.

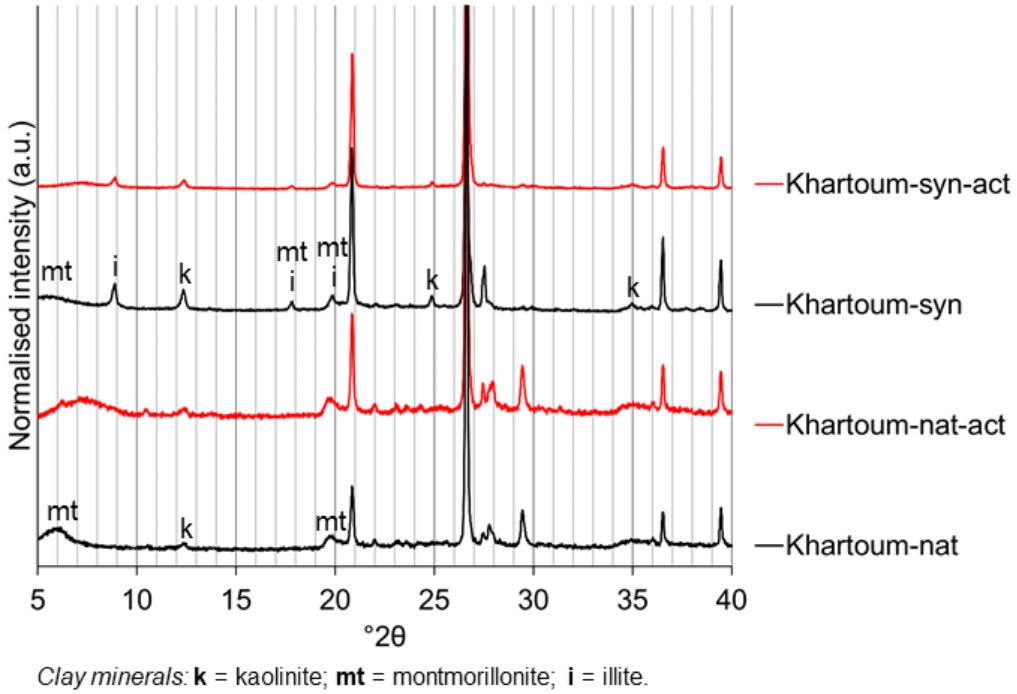

Figure 7-7: XRD patterns of the precursors and activated samples of the natural and synthetic Khartoum soils.

7.3.3 SEM

7.3.3.1 Bristol Soils

The micron-scale clay platelets were clearly visible in the images of both the natural and synthetic control samples (Figure 7-8). In the activated natural soil, there were still a large number of clay particles visible, and also new particles of typical size ~0.5 µm. These were attributed to the hydrosodalite phase identified in the XRD pattern. In the activated synthetic soil, only a small number of clay particles were still present. The microstructure was dominated by new particles of typical size ~0.2 µm, attributed to the hydrosodalite phase identified in the XRD pattern.

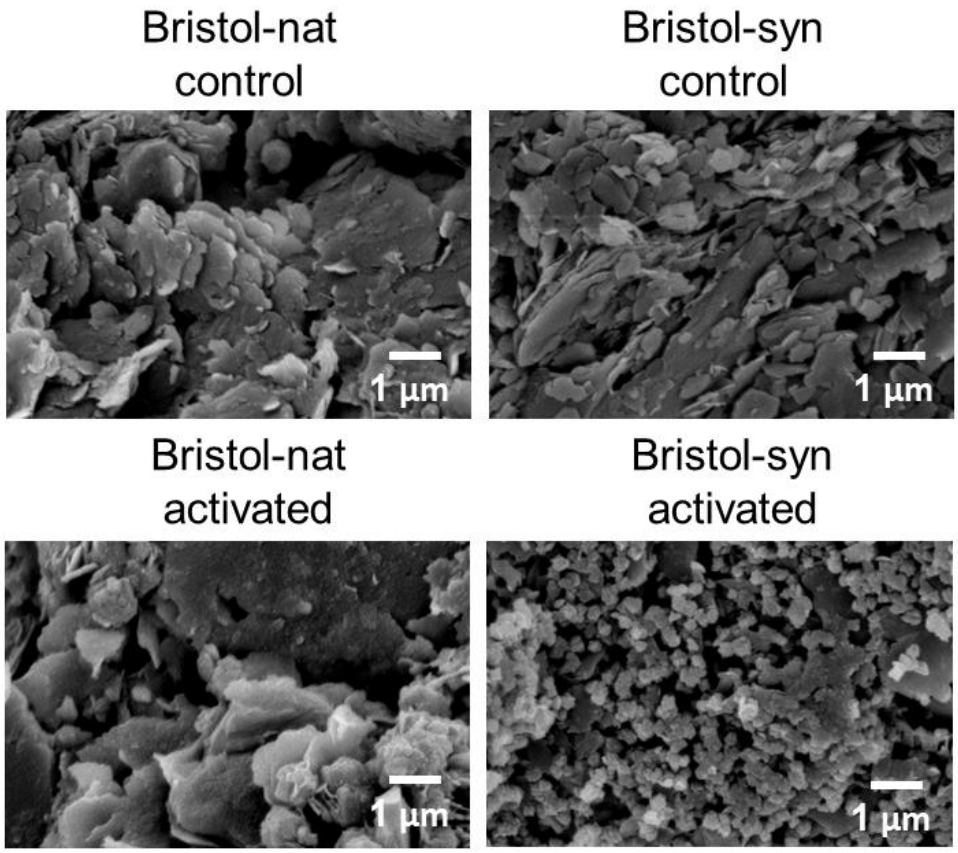

Figure 7-8: SEM images of control and activated samples of the natural and synthetic Bristol soils.

7.3.3.2 Bengaluru Soils

The micron-scale clay platelets are clearly visible in the image of the synthetic control sample (Figure 7-9). In the image of the natural control sample, the scale of the particles was much finer, typically <0.1 µm. This observation agrees with the BET SSA values given in Section 7.2.1, which were significantly higher for the natural control soil.

In the activated natural soil, the microstructural features were of a similar scale to the control sample. This made differences in phase morphology inconclusive, although the size distribution of fine particles increased from <0.1 µm to 0.1 – 0.2 µm. This difference in particle size distribution was attributed to the transformation of kaolinite into a hydrosodalite phase, as identified in the XRD pattern. In the activated synthetic soil, a small number of clay particles were still present. The microstructure was dominated by new particles of typical size ~0.3 µm, attributed to the hydrosodalite phase identified in the XRD pattern.

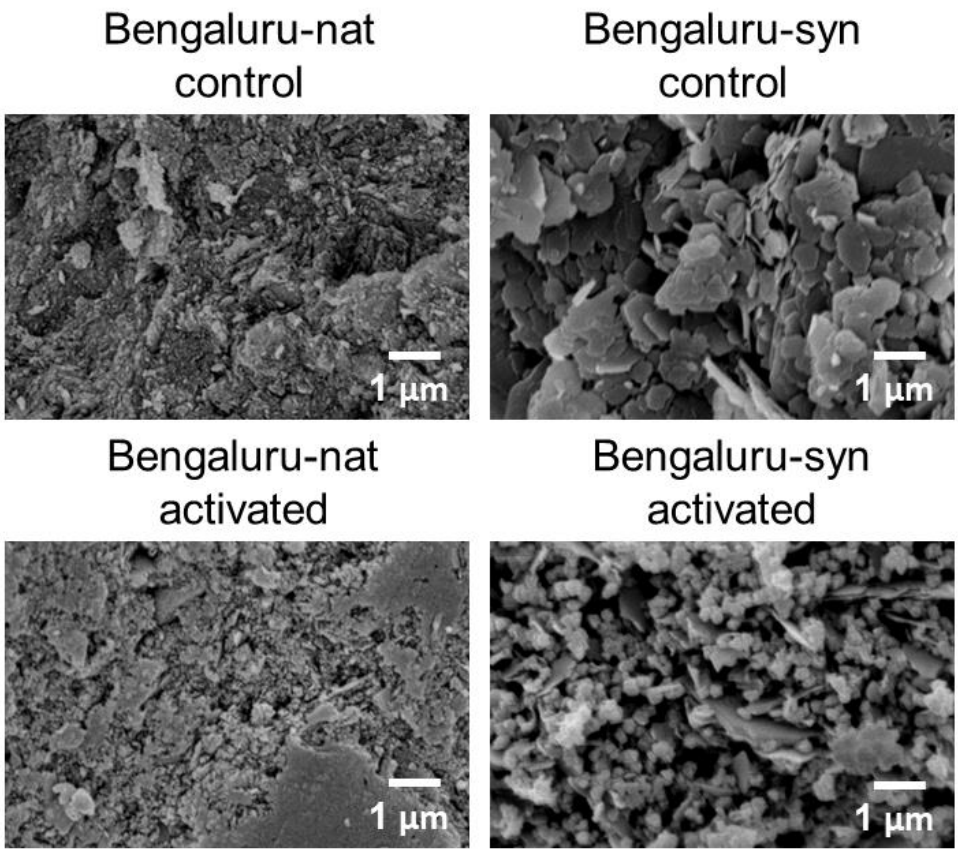

Figure 7-9: SEM images of control and activated samples of the natural and synthetic Bengaluru soils.

7.3.3.3 Khartoum Soils

The micron-scale clay platelets were clearly visible in the images of both the natural and synthetic control samples (Figure 7-10). In the image of the activated natural soil, the edges of the platy particles appeared with ragged edges, suggestive of the edge-dominated dissolution mechanism of these clays in alkaline solutions (Bauer and Berger, 1998; Köhler *et al.*, 2003). No new microstructural features were observed. In the image of the activated synthetic soil, irregular particles of typical size ~0.5 µm were evenly distributed in the microstructure. This was similar to the microstructure previously observed for an activated mixture of 90% montmorillonite and 10% kaolinite clays (Marsh *et al.*, under review). These are unlikely to be individual zeolitic particles – they do not exhibit the expected angular morphology, and given that no zeolitic reflections were observed in the XRD patterns, they are too large to be x-ray amorphous zeolites (Jacobs *et al.*, 1981). This suggests these could be either a poorly linked geopolymer phase or carbonate precipitates.

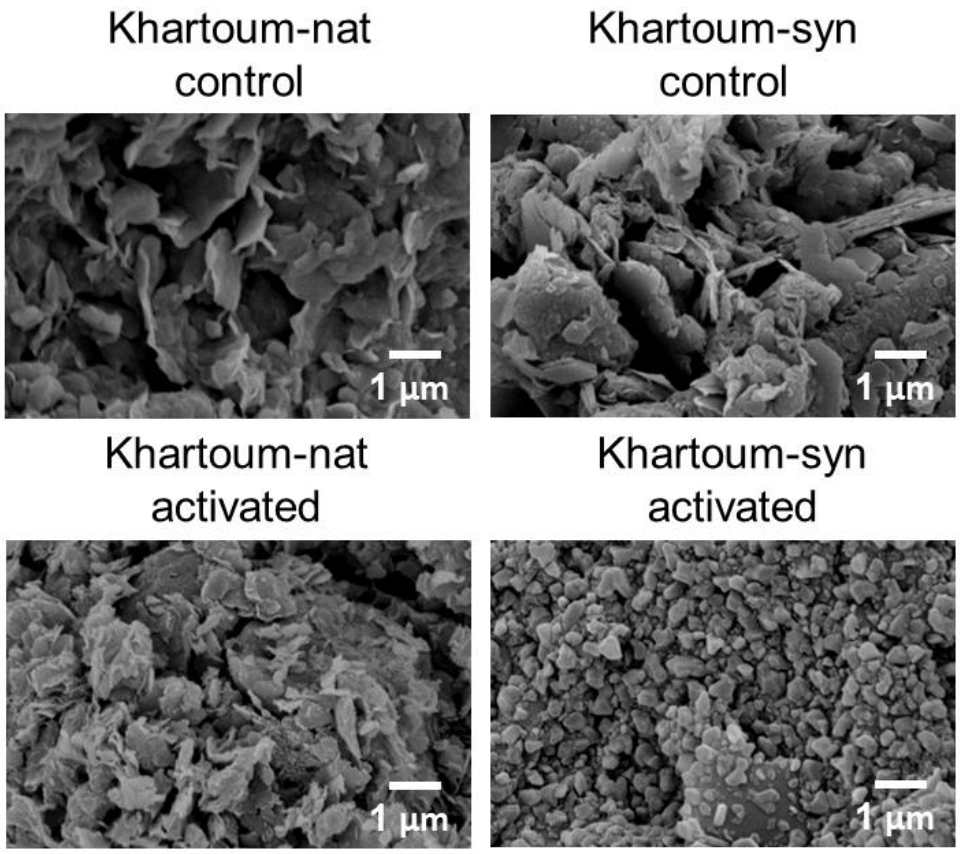

Figure 7-10: SEM images of control and activated samples of the natural and synthetic Khartoum soils.

7.3.4 FTIR

The range 2000 – 600 cm^{-1} is displayed, as this is range of most interest given it contains the stretching bands of the aluminosilicate phases.

7.3.4.1 Bristol Soils

There were no significant differences between the FTIR spectra of the natural and synthetic soils' control samples (Figure 7-11). The same bands were present, albeit with small differences in relative intensity. The position of the dominant Si-O-Si stretching vibration was slightly higher for the synthetic soil (1006 cm^{-1}) than the natural soil (1000 cm^{-1}).

The changes in the dominant aluminosilicate band were similar for both natural and synthetic soils, with a broadening and shift to lower wavenumbers (984 and 979 cm^{-1} respectively). Broad carbonate bands, likely composed of several superimposed bands emerged for both soils centred at ~1450 cm^{-1}, along with another individual band at 850 – 865 cm^{-1}. These were more intense for the natural soil.

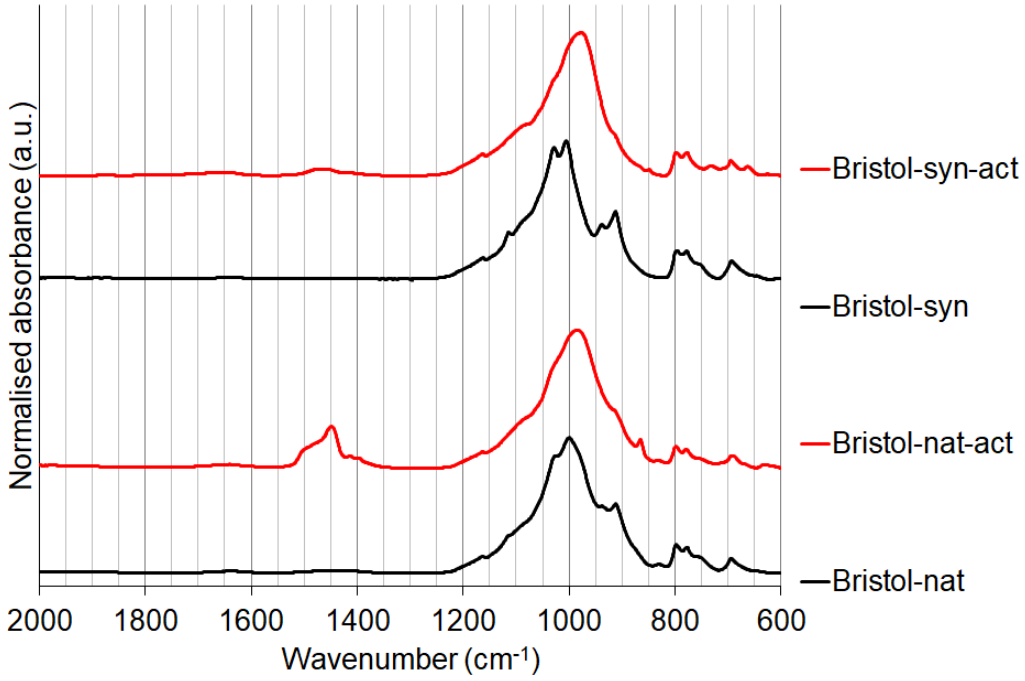

Figure 7-11: FTIR spectra of precursor and activated samples of the natural and synthetic Bristol soils.

7.3.4.2 Bengaluru Soils

There were no significant differences between the FTIR spectra of the natural and synthetic soils' control samples (Figure 7-12). The same bands were present, albeit with small differences in relative intensity. The position of the dominant Si-O-Si stretching vibration was slightly higher for the synthetic soil (1006 cm^{-1}) than the natural soil (1004 cm^{-1}).

The changes in the dominant aluminosilicate band were similar for both natural and synthetic soils, with a broadening and shift to lower wavenumbers (976 and 979 cm^{-1} respectively). A very weak, broad carbonate band emerged in the synthetic soil, centred at 1476 cm^{-1}.

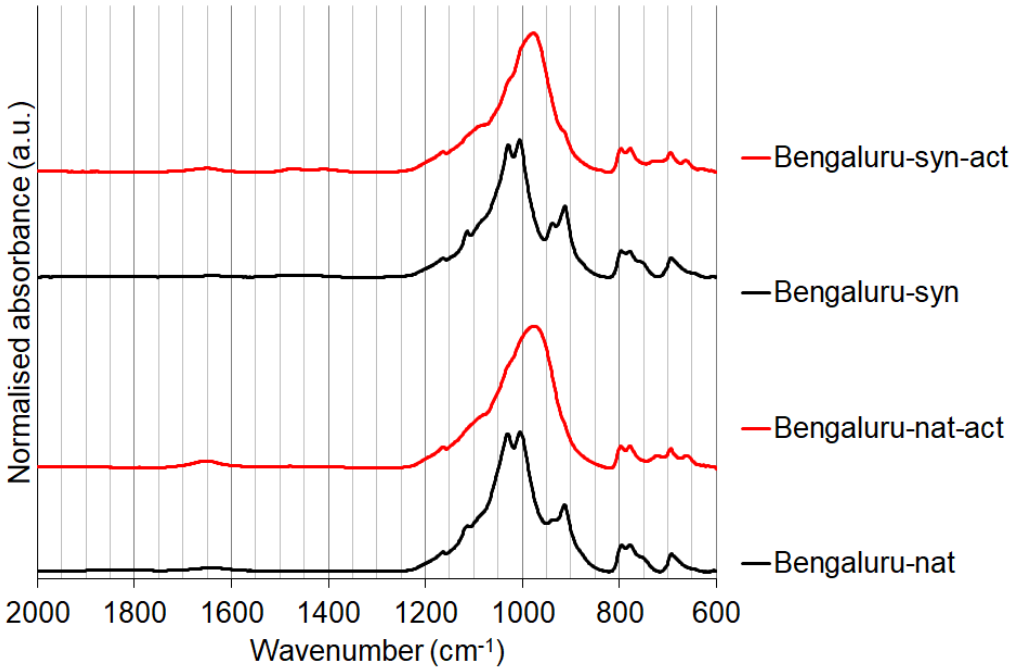

Figure 7-12: FTIR spectra of control and activated samples of the natural and synthetic Bengaluru soils.

7.3.4.3 Khartoum Soils

Due to larger differences in relative intensity between the different aluminosilicate bands in the control samples' spectra, the position of the dominant Si-O-Si stretching vibration was significantly lower in the natural soil (1003 cm^{-1}) than in the synthetic soil (1032 cm^{-1}) (Figure 7-13). Carbonate bands at ~1450 cm^{-1} and 873 cm^{-1} were only present in the natural soil's control spectrum, attributed to calcite.

The changes in the dominant aluminosilicate band were similar for both natural and synthetic soils, undergoing broadening but also a very small shift in wavenumbers compared to the other soils (1004 and 1031 cm^{-1} respectively). The calcite carbonate bands remained present for the natural soil, and weaker carbonate bands emerged in the same locations for the synthetic soil. A broad carbonate band, also centred at ~1450 cm^{-1}, emerged for the synthetic artificial soil after activation, along with another individual band at ~865 cm^{-1}.

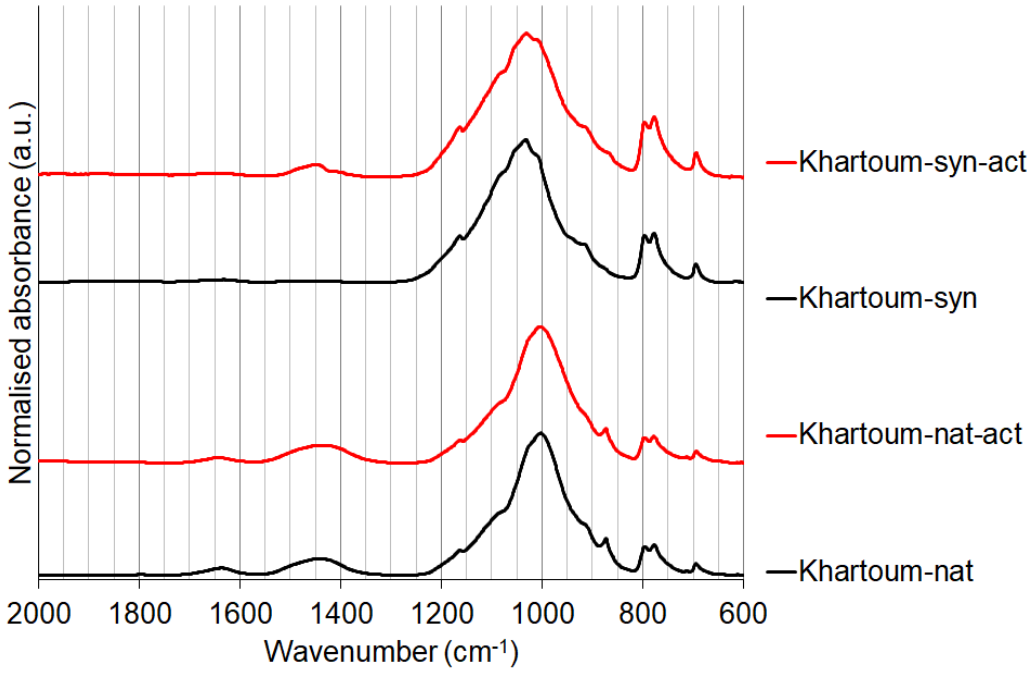

Figure 7-13: FTIR spectra of control and activated samples of the natural and synthetic Khartoum soils.

7.3.5 TGA

Most of the minerals known to be present in the soils undergo some form of mass loss event in the temperature range tested, as follows (Smykatz-Kloss, 1974; Ulery and Drees, 2008). Clay minerals can be distinguished by their dehydroxylation temperatures, which typically lie within the range of 450 – 750 °C. For the silicates and other aluminosilicates, dehydroxylation typically occurs in a higher range. The exceptions are quartz and microcline, which do not contain hydroxyl groups. For the carbonates, decomposition typically occurs from 700 – 960 °C. For the iron oxides and hydroxides, some only undergo decomposition rather than structural changes. These specificities make TG and dTG curves particularly helpful for confirming the identity of minerals in soil.

As shown in the FTIR results (Section 7.3.4), it is likely that due to efflorescence, small amounts of sodium carbonate phases were present in the activated soils which were not detected in the XRD patterns. The phases most likely to be present are natrite (Na_2CO_3), thermonatrite ($Na_2CO_3 \cdot H_2O$) and trona ($Na_3H(CO_3)_2 \cdot 2H_2O$). For the latter two compounds, dehydration and/or partial carbon loss can occur < 300 °C, to form natrite (Nikulshina *et al.*, 2008; Smykatz-Kloss, 1974). Full decomposition of natrite occurs above 840 °C (Newkirk and Aliferis, 1958).

Due to the complex phase composition of these soils and the possibilities of overlapping loss peaks, it was not always possible to provide a complete indexing of the dTG curves. dTG peaks will be described either by their peak centre if well-resolved, or approximate temperature range if not.

7.3.5.1 Bristol Soils

In the dTG curves of the natural / synthetic precursor soils (Figure 7-14), the mass loss events were attributed to the following phases: 102 / 92 °C to the loss of surface adsorbed water from clay minerals; the largest magnitude peaks at 490 / 507 °C to the dehydroxylation of kaolinite and montmorillonite; 645 °C to the dehydroxylation of illite in the natural soil (Földvári, 1991; Smykatz-Kloss, 1974). In the natural soil, the small peak at 309 °C was assigned to the dehydration of hydrate phases associated with hematite (Rodulfo-Baechler *et al.*, 2004), and the peak at 644 °C to decomposition of calcite (Criado and Ortega, 1992). In the synthetic soil, the shoulder at 656 °C could possibly have been due to a trace amount of calcite in the sand addition. The major dTG loss peaks expected from the other associated minerals were either overlapping with the larger clay minerals' peaks, or not of large enough magnitude to be assigned with confidence. The overall mass loss was slightly greater for the natural precursor soil (-7.0 %) than for the artificial one (-4.9 %).

In the activated samples of both the natural and artificial soils, there was a large decrease in the magnitude of the kaolinite dTG peak, in agreement with the consumption of kaolinite shown in the XRD patterns (Figure 7-5). In the activated natural soil, broad peaks emerged at 212, 315 and 394 °C, which overlapped in the 100 – 400 °C region. The magnitude of the 89 °C surface adsorbed moisture peak increased greatly. In the activated synthetic soil, there was also a large decrease in magnitude of the kaolinite dTG peak. New, broad peaks emerged at 160 °C and elsewhere within the 100 – 400 °C region. There was also a large increase of the surface adsorbed moisture peak at 102 °C.

The new peaks in the 100 – 400 °C region for both activated samples were attributed to the respective hydrosodalites identified in the XRD patterns. Peaks in this region are indicative of hydrosodalites, with the loss temperature and number of the dTG peaks corresponding to H_2O and/or OH loss from the β-cages (Engelhardt *et al.*, 1992). The clear difference in the profile of the dTG curves in this region would therefore be expected from the formation of a basic and non-basic hydrosodalite. The increase in surface-adsorbed moisture loss at ~100 °C was also attributed to the presence of hydrosodalites.

In both activated soils, the dTG intensity increased in the 700 – 1000 °C region. This could partly be attributed to the decomposition of natrite (Na_2CO_3), but only in the range of >840 °C. In the TG curves, overall mass loss increased after activation for both soils but to a greater extent for the natural soil (2.1 %) than for the synthetic soil (0.7 %).

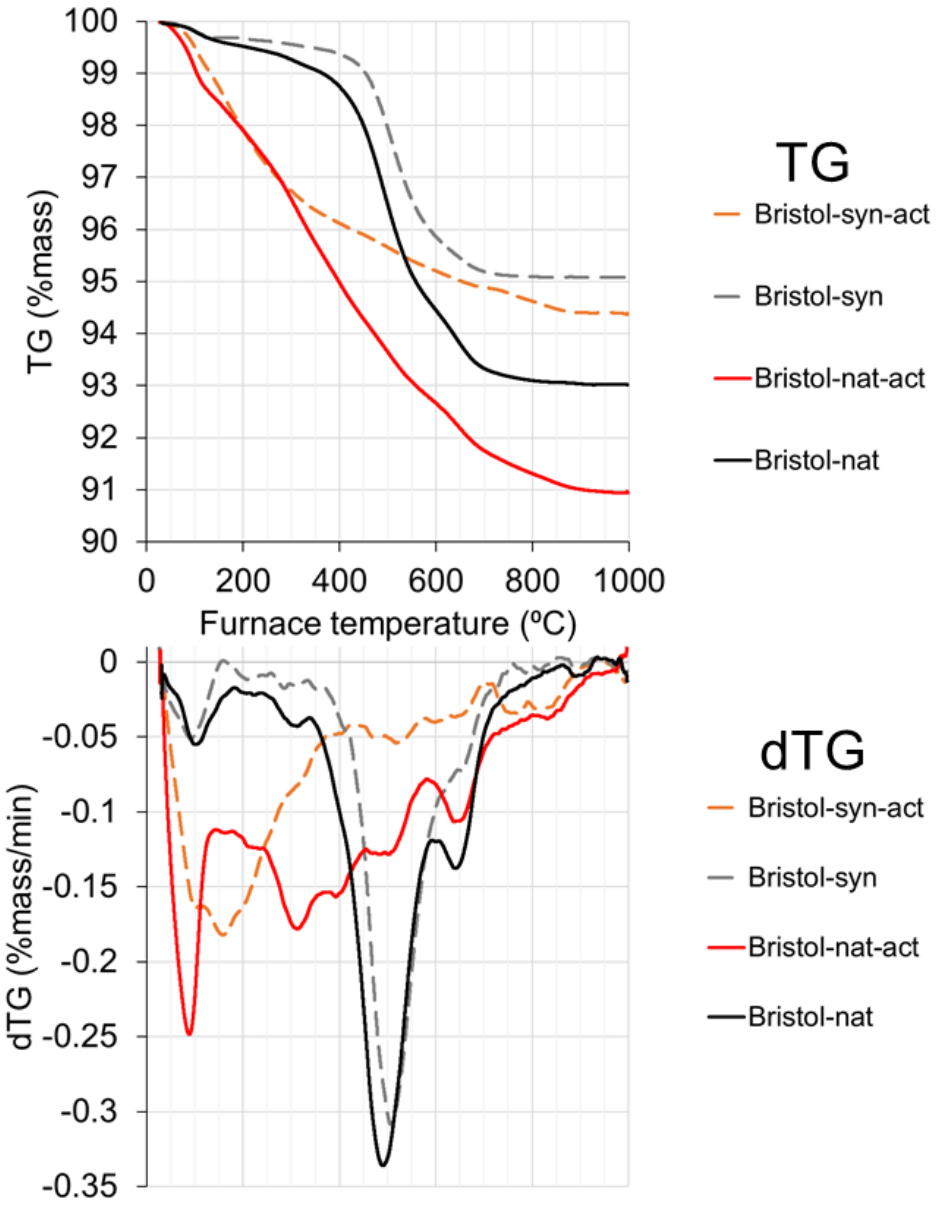

Figure 7-14: TGA and dTG spectra of control and activated samples of the natural and synthetic Bristol soils.

7.3.5.2 Bengaluru Soils

In the dTG curves of the natural / synthetic precursor soils (Figure 7-15), the mass loss events were attributed to the following phases: 87 / 105 °C to the loss of surface adsorbed water from clay minerals; the largest magnitude peaks at 458 / 508 °C to the dehydroxylation of kaolinite (Földvári, 1991; Smykatz-Kloss, 1974). In the natural soil, the small peak at 289 °C was assigned to the dehydration of hydrate phases associated with hematite (Rodulfo-Baechler *et al.*, 2004). In the synthetic soil, the shoulder at 618 °C could possibly have been due to a trace amount of calcite in the sand addition. The overall mass loss was slightly greater for the natural precursor soil (-6.8 %) than for the artificial one (-5.2 %).

In the activated samples of both the natural and artificial soils, there was a large decrease in the magnitude of the kaolinite dTG peak, in agreement with the consumption of kaolinite shown in the XRD patterns (Figure 7-6). In the activated natural soil, broad peaks emerged at 198 and 287 °C. The magnitude of the 111 °C surface adsorbed moisture peak increased greatly. The hematite peak was still present after activation. In the activated synthetic soil, a new peak emerged at 197 °C, with another possibly in the overlapping region from 100 – 200 °C. There was also a large increase of the surface adsorbed moisture peak.

The new peaks in the 100 – 200 °C range were attributed to the non-basic hydrosodalite identified in the XRD patterns (Figure 7-6). The broad similarity in number and locations of loss peaks in this temperature range between the activated soils is in agreement with the observation that the same type of hydrosodalite was formed in both samples. The increase in surface-adsorbed moisture loss was also attributed to the presence of hydrosodalites.

In the activated synthetic soil, minor, broad peaks also emerged at 658 and 759 °C. In contrast, there was negligible change for the activated natural soil in this temperature range. In the TG curves, overall mass loss did not change after activation for the real soil, but decreased a slight amount for the synthetic soil.

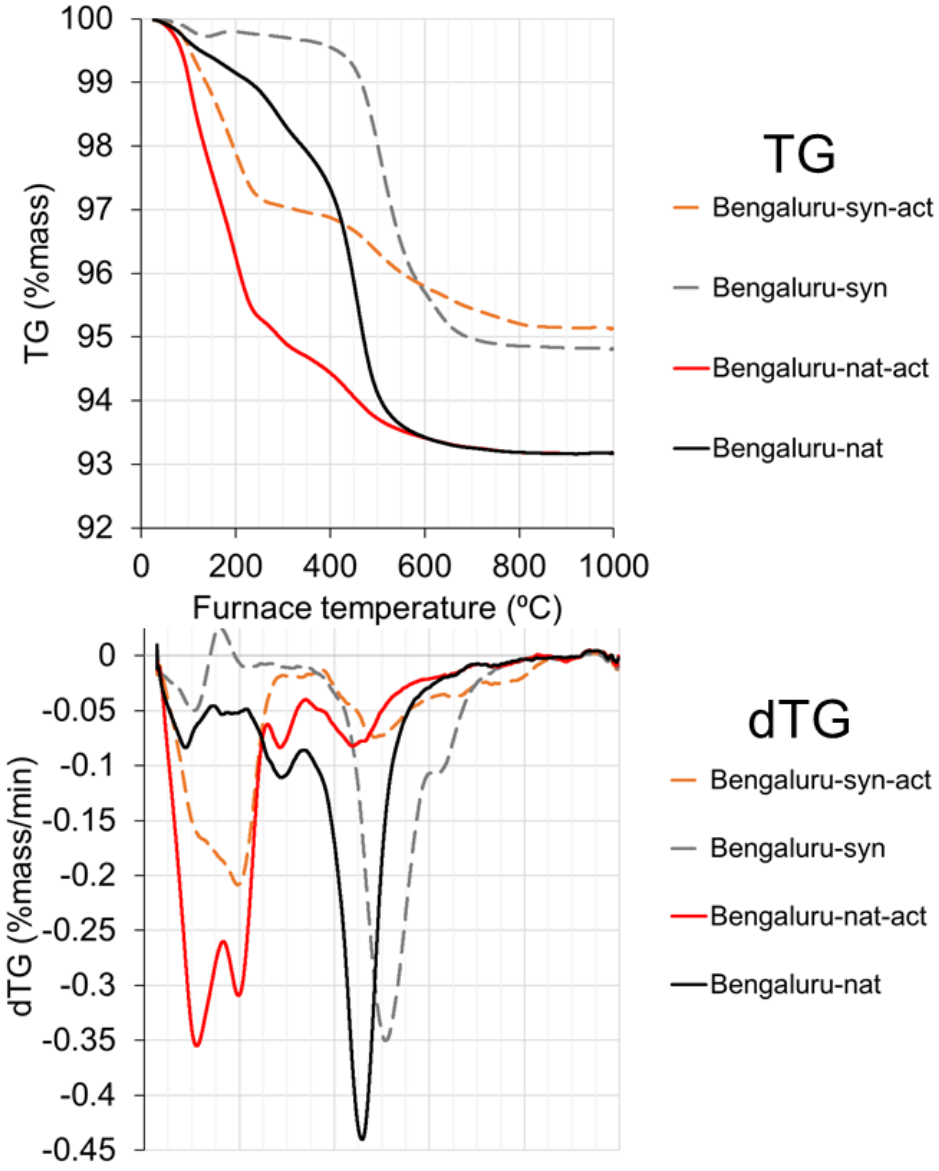

Figure 7-15: TGA and dTG spectra of control and activated samples of the natural and synthetic Bengaluru soils.

7.3.5.3 Khartoum Soils

In the dTG curves of the natural / synthetic precursor soils (Figure 7-16), the mass loss events were attributed to the following phases: 88 / 78 °C to the loss of surface adsorbed water from clay minerals; the largest magnitude peaks at 471 / 496 °C to the dehydroxylation of montmorillonite (Földvári, 1991; Smykatz-Kloss, 1974). Both these dehydroxylation temperatures are in the lower end of the range for montmorillonites, suggesting that both had a trans-vacant octahedral sheet structure (Drits *et al.*, 1995; Wolters and Emmerich, 2007). In the natural soil only, mass loss peak attributions were: 285 °C to the dehydration of hydrate phases associated with hematite (Rodulfo-Baechler *et al.*, 2004); 696 °C to the decomposition of calcite (Criado and Ortega, 1992). The montmorillonite dehydroxylation peak at 471 °C exhibited a shoulder on the lower temperature side – after activation, a peak was visible at 421 °C. This peak could be the dehydroxylation of goethite (FeOOH) (Smykatz-Kloss, 1974), a common iron compound in soils (Stucki *et al.*, 1987). However, it was not possible to confirm this attribution through XRD due to the fine size distribution and low crystallinity of iron compounds in soil, as previously described in Section 7.3.2.1. In the synthetic soil only, the peak at 656 °C could have been due to decomposition of a trace amount of calcite in the sand addition. The overall mass loss was greater for the natural precursor soil (-10.0 %) than for the artificial one (-2.5 %).

In the activated natural soil, there was a decrease in magnitude of the montmorillonite dehydroxylation peak at 471 °C. In the activated synthetic soil, there seemed to be a decrease in magnitude of the equivalent peak at 496 °C. In the activated natural soil, there was almost no change in the surface adsorbed moisture peak, whereas in the synthetic activated soil there was a large increase in magnitude of the equivalent peak.

In the activated natural soil, a new minor peak emerged at 774 °C. The calcite peak, and possible hematite and goethite peaks, were still present after activation. In the synthetic activated soil there was negligible change in the 750 – 1000 °C range, but there was a broad increase in magnitude from 170 – 400 °C. From a previous study on a montmorillonite system (Marsh *et al.*, 2018a), this phenomenon is associated with geopolymer formation. In the TG curves, overall mass loss decreased (-0.7%) for the natural soil, but increased for the synthetic soil (1.5 %).

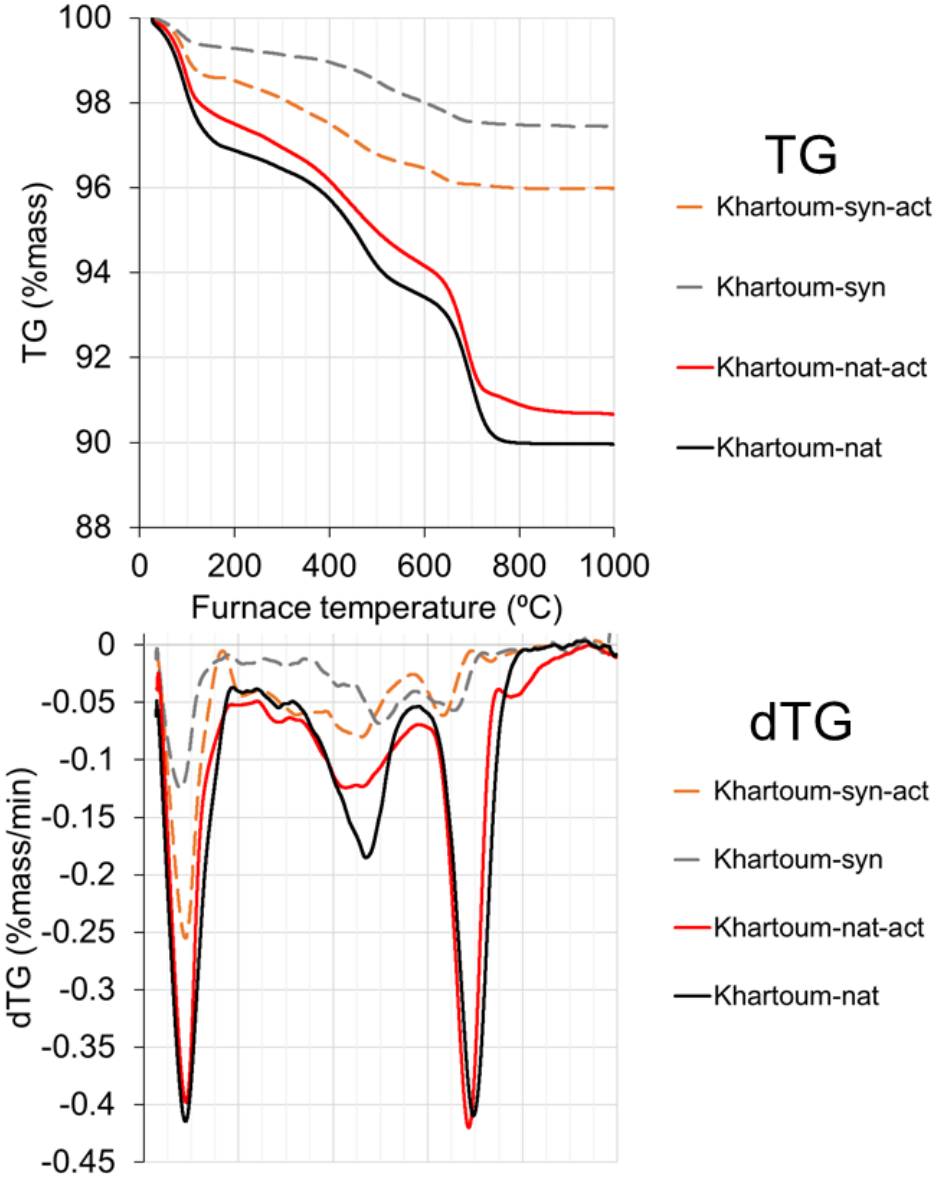

Figure 7-16: TGA and dTG spectra of control and activated samples of the natural and synthetic Khartoum soils.

7.4 Discussion

7.4.1 Phase formation for natural and synthetic soils

There were both similarities and differences between the phases formed in the natural and synthetic versions of each soil, as summarised in Table 7-5.

Table 7-5: Summary table showing phases formed from activation of the natural and synthetic soils.

Soil	Natural	Synthetic
Bristol	hydrosodalite	basic hydrosodalite
Bengaluru	hydrosodalite	hydrosodalite
Khartoum	geopolymer	none

As expected for a kaolinite dominated soil (Marsh *et al.*, 2018b), for the Bristol soils, hydrosodalite was formed as the reaction product in both the natural and synthetic soils. However, different hydrosodalities were formed in each of the soils: a non-basic hydrosodalite $Na_6[AlSiO_4]_6 \cdot 4H_2O$ in the natural soil, and a basic hydrosodalite $Na_8[AlSiO_4]_6(OH)_2 \cdot 4H_2O$ in the synthetic soil. The existence of different product phases is supported by differences in the TGA and FTIR signals, as already described in Sections 7.3.5.1 and 7.3.4.1. The difference in the scale of the clay phases, predominantly kaolinite, was negligible between the two precursor soils, as already shown from the BET specific surface area and SEM results in Sections 7.2.1 and 7.3.3.1. Previous studies on the synthesis of zeolites from kaolinite have shown that phase formation is sensitive to temperature, time, alkaline solution concentration and Si:Al ratio (Abdullahi *et al.*, 2017; Barrer *et al.*, 1968). It is therefore likely that this difference is either due to slight differences in the mineralogy of the kaolinite, or very minor variations in the processing and curing conditions.

For the Bengaluru soils, exactly the same hydrosodalite phase was formed in both the natural and synthetic soils, the non-basic hydrosodalite $Na_6[AlSiO_4]_6 \cdot 4H_2O$. The hydrosodalite particles formed were much finer in the activated natural soil, as already described in the SEM results in Section 7.3.3.2. In the precursor, the kaolinite particles were much smaller, and specific surface area much higher as already described in Sections 7.3.3.2 and 7.2.1. It is likely that the finer kaolinite particles offered a higher spatial density of nucleation sites, thus resulting in the formation of more, finer hydrosodalite particles.

For the Khartoum soils, no crystalline product phases were formed in either the natural or synthetic soils. A change of microstructure was observed in the SEM images which could have been a geopolymer (Section 7.3.3.3), but the evidence was not conclusive given there was no large observed negative shift of the Si-O-T FTIR band after

activation (Section 7.3.4.3). It is therefore likely that a small amount of poorly linked geopolymer N-A-S-H or (N,C)-A-S-H phase formed in the synthetic soil, but not for the natural soil. However, the results included in the Appendix show some evidence for geopolymer formation in both natural and synthetic soils when using 10 M NaOH. This suggests that in the lower concentration activation of the natural soil, geopolymer formation was retarded, but not prevented, relative to the synthetic soil.

In summary, in spite of the differences in particle size and the absence of minor non-clay minerals in the synthetic soils, the phase formation behaviour was generally similar between the natural and synthetic soils, albeit with non-clay components having a retarding effect in Khartoum-syn.

7.4.2 Evaluation of clay minerals in activation

In addition to characterising overall phase formation, the purpose of this study was to determine the relative influence of clay minerals and associated minerals in alkaline activation behaviour of soils.

The Bristol natural soil had a slightly larger specific surface area than the synthetic soil (17.6 to 14.0 m^2g^{-1}), but the difference in particle size distribution as seen from the SEM images was negligible (Figure 7-8). The Bengaluru natural soil had a significantly larger specific surface area and finer particle size than the synthetic soil (33.7 to 6.7 m^2g^{-1}), also seen in the SEM images (Figure 7-9). The kaolinite dTG mass loss peak was 50 °C lower for the natural soil than the synthetic soil, which is consistent with smaller particle size (Suraj *et al.*, 1997). Accumulation of iron in kaolinite during pedogenic processes can make them more reactive by increasing disorder (Obonyo *et al.*, 2014). The decrease in intensity of the kaolinite 001 peak after activation was similar for the natural and synthetic soils, suggesting that the clays had similar reactivity and hence that the kaolinite in the natural soil had low iron accumulation and was still relatively ordered. The Khartoum natural soil had a similar surface area to the synthetic soil (36.9 to 42.0 m^2g^{-1}), and seemed similar in terms of size from the SEM images (Figure 7-10). Furthermore, the montmorillonite dehydroxylation temperatures suggested that the montmorillonite clay minerals in both soils had a trans-vacant octahedral sheet structure (Section 7.3.5.3). The sheet structure of montmorillonites is known to influence some behaviours such as dehydroxylation mechanism (Drits *et al.*, 1995; Wolters and Emmerich, 2007), and also pozzolanic reactivity (Hollanders *et al.*, 2016). It was therefore desirable for getting an overall match between the clay minerals in the real and synthetic soils that both montmorillonite precursors had a trans-vacant structure. However, wavenumber of the Si-O-T FTIR band was ~30 cm^{-1} lower for the natural soil (Figure 7-13), and the dTG peak for montmorillonite dehydroxylation occurred at ~30 °C lower in the natural soil (Figure 7-16). For the purpose of this

exercise, the clay minerals in the synthetic soils were deemed to be suitable comparison points for those in the natural soils.

A previous study (Marsh *et al.*, under review) investigated the alkali activation products of different clay mixtures under the same processing conditions used here. These are useful comparison systems, as they can be considered as simplified soil systems. The mixtures closest to the soils, and their phase formation behaviours, were: for Bengaluru, 100%Kao forming hydrosodalite; for Bristol, 50%Kao-50%ILL forming hydrosodalite and a minor amount of hydroxycancrinite, and for Khartoum, 90%Mont-10%Kao forming a geopolymer. These make an overall good agreement with the phases formed in the respective soils here. This is in agreement with the findings of the previous section, and supports the argument that phase formation behaviour is predominantly determined by the clay minerals.

7.4.3 Evaluation of associated minerals in activation

The associated minerals found in the natural soils included quartz, hematite, chlorite, siderite, muscovite, microcline, albite, calcite and hornblende. The synthetic soils were designed to match the natural soils in terms of clay content, but would not feature any of the minor phases found in the natural soils. In practice it was not possible to fully avoid these, since the precursor clays used for the synthetic soils contained small amounts of quartz, muscovite and microcline. Therefore, the behaviour of the associated minerals in all of the soil systems will be evaluated. The associated minerals can be categorised into two groups: firstly, silicate/aluminosilicate phases that might contribute directly to the alkali activation reaction through dissolution and donation of aluminium and/or silicon species (quartz, chlorite, muscovite, microcline, albite, hornblende); secondly, other phases which do not contain aluminium or silicon, but which might influence the system in other ways (hematite, siderite, calcite).

In the first group of aluminosilicate/silicate minerals, quartz is the most common associated mineral in soils, and typically the largest component of the silt and sand size fractions, albeit with a size distribution dependent on weathering conditions (Dixon and Weed, 1989). Given that quartz consistently has the most intense reflections in the XRD patterns (Figure 7-4), this is likely the case for all the precursor soils used here. It is therefore difficult to say whether any minor dissolution of quartz occurred, although quartz remained the largest peak after activation for all soils. However, given the curing conditions used (Lucas *et al.*, 2011), and the presence of more reactive minerals, it is unlikely that anything more than a minor amount of quartz dissolution occurred.

Feldspars are the second most common associated mineral in soils (Dixon and Weed, 1989), and include the alkali feldspar (including microcline) and plagioclase (including

albite) sub-groups. Microcline's most intense XRD reflection seemed to undergo a decrease in intensity after activation in all the synthetic soils (Figure 7-5, Figure 7-6, Figure 7-7), but not in Bengaluru-nat, the only natural soil in which microcline was present (Figure 7-6). Albite was present in the precursor of Khartoum-nat, but did not undergo any noticeable decrease (Figure 7-7). In comparison with previous studies, Xu and van Deventer (2000) found that aluminosilicates with a ring structure – including feldspars – had a lower extent of dissolution than minerals with framework or chain structures. The same researchers later activated uncalcined albite and microcline, and found that both formed a geopolymer when in a mixture with kaolinite (Xu and Van Deventer, 2002). In comparison, Feng et al. (2012) found that albite in isolation had little ability to form a geopolymer phase when activated in its uncalcined or calcined state, albeit without additional silicate. No hard conclusions can be drawn on the exact extent of participation of feldspars in these specific systems, except that there seems to be variation between feldspars, and that they do not have a deleterious effect on overall phase formation behaviour.

Amongst micas, muscovite is a common minor component in soils (Dixon and Weed, 1989). Muscovite was present in all the synthetic soils (through its presence in the kaolinite precursor), and also in Bengaluru-nat. Noticing changes in muscovite reflections in the XRD patterns of Bristol-syn and Khartoum-syn was not feasible, as they overlapped with the other 2:1 phyllosilicates montmorillonite and/or illite. In the Bengaluru soils, kaolinite was the sole clay mineral, and hence did not overlap (Figure 7-6). In Bengaluru-nat, the intensity of the muscovite reflection was too weak to discern any change with confidence, whereas in Bengaluru-syn, there seemed to be a clear decrease. It is within reason that this change could be partly explained by orientation effects.

Chlorites are unstable in soil environments, but can be found as an inherited mineral (Dixon and Weed, 1989). In Bristol-nat both the reflections at 6.2 and 25.2 °2θ were retained after activation (Figure 7-5). In Khartoum-nat, the reflection at 6.2 °2θ was also retained after activation. In Khartoum-nat, the only soil containing a hornblende, the main reflection at 10.5 °2θ was retained (Figure 7-7).

In the second group of non-aluminosilicate/silicate minerals, iron compounds are found to some extent in nearly all soils, with goethite (α-FeOOH), hematite (α-Fe_2O_3) and magnetite (Fe_3O_4) the most widespread (Dixon and Weed, 1989). Their size distribution is in the <2 μm clay fraction (Stucki *et al.*, 1987). The presence of iron phases in lateritic soils is of additional interest because of their known surface hardening effect under conditions of wetting and drying cycles (Alexander and Cady, 1962; Lassinantti Gualtieri *et al.*, 2015). Iron compounds were only found in the natural soils. As shown in

Table 7-1, iron oxide composition differed by up to 10 wt.% between the natural and synthetic soils. Hematite was present in Bristol-nat and Bengaluru-nat, with possibly a small amount of goethite present in Khartoum-nat as described in Section 7.3.2.1. Hematite's main reflection at 33.2 °2θ seemed to decrease in intensity after activation in both Bristol-nat and Karnatak-nat. Hematite has low solubility in alkaline solutions, but does increase with concentration (Ishikawa *et al.*, 1997). Siderite was only present in Bristol-nat, and its main reflection at 32.0 °2θ decreased in intensity after activation. The iron phase (likely goethite) in Khartoum-nat was too fine and/or disordered to confirm its presence or detect any changes after activation. From previous studies, the role played by iron in alkali activation depends on the phase it is present in. Iron can be included within a geopolymer gel if it is available in solution during the polymerisation process, and hence in a reactive form, as shown for ferric nitrate solution and freshly precipitated ferric (oxy)hydroxide (Perera *et al.*, 2007), as well as augite (Lemougna *et al.*, 2013). However, if the iron is held in an unreactive form, including ferran forsterite (Lemougna *et al.*, 2013) or hematite (Essaidi *et al.*, 2014), this iron does not participate, or can have a slight retardation effect. The effect of unreacted iron on strength is debated, with some studies suggesting it has little effect (Lemougna *et al.*, 2014) and others suggesting it is deleterious (Obonyo *et al.*, 2014). Due to the complexity of these systems and the objectives, checking for elemental incorporation within the product phases is beyond the scope of this study. In summary, hematite did not prevent the formation of zeolitic phases in Bristol-nat and Bengaluru-nat, but the influence of the iron compound in the Khartoum-nat (likely goethite) may have contributed to a retarding effect on geopolymer formation. This is in broad agreement with previous studies.

Calcite is a common mineral in soils and many other deposits. Calcite is present in Bristol-nat and Khartoum-nat (Figure 7-4). Its main reflection at 29.4 °2θ is not reduced in either soil. This is in agreement with the dTG spectra, in which the calcite mass loss peak does not appreciably change after activation in both soils (Figure 7-14, Figure 7-16). Calcite can participate in dissolution and geopolymer formation to some extent, although reported effects on strength have been mixed (Cwirzen *et al.*, 2014; Yip *et al.*, 2008). Ca^{2+} ions can fulfil the charge-balancing role in the aluminosilicate polymer framework (Garcia-Lodeiro *et al.*, 2015), but the overall effect on alkali aluminosilicate phase formation depends on activating solution concentration (Yip *et al.*, 2005), and quantity of soluble Ca in the system (Garcia-Lodeiro *et al.*, 2011). In this case it seems that the calcite underwent negligible dissolution, likely due to the presence of more reactive phases.

Organic matter in sub-soils is typically present as humus, a general term given to a variety of unidentifiable organic substances (Dixon and Weed, 1989). Organic compounds generally act as retardants in the setting of Portland cement (Paria and Yuet, 2006), but their effect in alkali activation is not well-investigated so far. NaOH is commonly used to extract organic matter from soils undergoing testing (Schnitzer and Schuppli, 1989). The evidence so far suggests that adsorption onto mineral surface sites has an inhibiting effect for dissolution of both kaolinite (Chin and Mills, 1991) and smectite-illite (Claret *et al.*, 2002), as well as binding free Ca in solution (Toda *et al.*, 2018). However, as stated previously, soils with low organic content are used for stabilised soil materials, as this is a general requirement in earth building (Jagadish, 2007).

With regards to the associated minerals found in the synthetic soils, the coarse size of the added quartz (sieved to >63μm) made appreciable dissolution unlikely. Muscovite was generally observed to be unreactive. The exception was microcline, which consistently seemed to undergo a reduction in intensity, but only in the synthetic soils. With regards to the associated minerals found in the natural soils, quartz, microcline, albite, muscovite, chlorite, hornblende and calcite were likely to have made a negligible contribution, whilst the iron compounds hematite and siderite underwent an appreciable degree of dissolution.

7.4.4 Implications for practical adoption

If a soil has a high plastic limit there is a trade-off between NaOH concentration and Na:Al molar ratio whilst maintaining mix workability at the plastic limit. As shown for Khartoum-nat, when a system molar ratio of Na:Al = 1 was used, the NaOH concentration was insufficient for a reaction to occur. When a 10 M NaOH solution was used, a product phase was formed but the Na:Al molar ratio far exceeded the ideal value of 1. This means there was an excess of Na in the system available to form soluble carbonates in the form of surface efflorescence, which poses practical difficulties in leaching and even potential for surface damage (Allahverdi *et al.*, 2015). This study has shown that there is a trade-off in mix design between NaOH concentration and Na:Al molar ratio. As a result of this trade-off, although the mineralogy of montmorillonite-rich soils may be conducive to successful alkali activation, the practical production constraints make them unfeasible to use in their natural form using NaOH as the sole activator. However, there is still strong potential for alkali-activated soil systems, albeit using a range of activators, reactive precursors and/or admixtures. The increased understanding of the fundamental behaviours developed in this study will assist the development of such systems. In future, it would be valuable to measure the mechanical properties of these systems for comparison

with conventional construction materials. However, to give accurate data, larger samples should be used. This was not possible with the limited amounts of these clays and soils available for this study. A contribution to this aim has been carried out in a follow-up study (Chapter 8).

7.5 Conclusions

Clay minerals have been shown to be the primary determinants of phase formation in alkali-activated soils. In zeolite-forming soil systems, the scale and type of zeolite particles formed were influenced by clay particle size, mineralogy and possibly processing conditions. In contrast, through the innovative use of synthetic soil systems, it was shown that most associated minerals had little or no influence in the reaction. Regarding iron compounds, hematite did not prevent zeolite formation in two of the soil systems, but iron compounds did seem to have a retarding effect on geopolymer formation in the montmorillonite-rich soil. There is a trade-off in mix design between Na:Al molar ratio and NaOH concentration. Given this, in addition to clay mineralogy, it is the plastic limit which determines if a given soil is suitable for alkali activation.

Acknowledgements

Thanks are given to Prof. BVV Reddy, Indian Institute of Science, and Dr. Amal Balila, University of Reading, for providing the Bengaluru and Khartoum soils respectively. Thanks are given to Ms. Preethi Krishnamurthy for providing additional information about the Bengaluru Soil. This study was supported by the EPSRC Centre for Decarbonisation of the Built Environment (dCarb) [grant number EP/L016869/1], a University of Bath Research Scholarship and the UKIERI project “Developing earth based building products utilising solid wastes”. All data created during this research are openly available from the University of Bath data archive at https://doi.org/10.15125/BATH-00565.

References

Abdullahi, T., Harun, Z. & Othman, M.H.D., 2017. A review on sustainable synthesis of zeolite from kaolinite resources via hydrothermal process. *Advanced Powder Technology,* 28(8), pp. 1827-1840.

Alexander, L.T. & Cady, J.G., 1962. *Genesis and hardening of laterite in soils.* Washington, D.C. : US Department of Agriculture.

Allahverdi, A., Najafi Kani, E., Hossain, K.M.A. & Lachemi, M., 2015. 17 – Methods to control efflorescence in alkali-activated cement-based materials. *Handbook of Alkali-Activated Cements, Mortars and Concretes.* Oxford: Woodhead Publishing, pp. 463-483.

Arulrajah, A., Kua, T.-A., Phetchuay, C., Horpibulsuk, S., Mahghoolpilehrood, F. & Disfani, M.M., 2016. Spent Coffee Grounds-Fly Ash Geopolymer Used as an Embankment Structural Fill Material. *Journal of Materials in Civil Engineering,* 28(5), p. 04015197.

Bain, J., 1971. A plasticity chart as an aid to the identification and assessment of industrial clays. *Clay Miner,* 9(1), pp. 1-17.

Balila, A., 2017. *Enhancing Strength and Durability of Adobe Bricks by Introducing Bio-inspired Stabilisers.* PhD, University of Reading.

Barrer, R., Cole, J. & Sticher, H., 1968. Chemistry of soil minerals. Part V. Low temperature hydrothermal transformations of kaolinite. *Journal of the Chemical Society A: Inorganic, Physical, Theoretical*, pp. 2475-2485.

Bauer, A. & Berger, G., 1998. Kaolinite and smectite dissolution rate in high molar KOH solutions at 35° and 80°C. *Applied Geochemistry,* 13(7), pp. 905-916.

Bergaya, F. & Lagaly, G., 2013. Chapter 1 – General Introduction: Clays, Clay Minerals, and Clay Science. In: F. Bergaya & G. Lagaly, eds. *Developments in Clay Science.* Elsevier, pp. 1-19.

Boutterin, C. & Davidovits, J., 1988. Geopolymeric Cross-Linking (LTGS) and Building materials. In: Geopolymer ‘ 88, 1988.

Brunauer, S., Emmett, P.H. & Teller, E., 1938. Adsorption of gases in multimolecular layers. *Journal of the American Chemical Society,* 60(2), pp. 309-319.

BSI, 1990. BS 1377-2:1990 Methods of test for soils for civil engineering purposes. Classification tests

Chin, P.-K.F. & Mills, G.L., 1991. Kinetics and mechanisms of kaolinite dissolution: effects of organic ligands. *Chemical Geology,* 90(3), pp. 307-317.

Claret, F., Bauer, A., Schäfer, T., Griffault, L. & Lanson, B., 2002. Experimental investigation of the interaction of clays with high-pH solutions: A case study from the Callovo-Oxfordian formation, Meuse-Haute Marne underground laboratory (France). *Clays and Clay Minerals,* 50(5), pp. 633-646.

Criado, J.M. & Ortega, A., 1992. A study of the influence of particle size on the thermal decomposition of CaCO3 by means of constant rate thermal analysis. *Thermochimica Acta,* 195, pp. 163-167.

Cristelo, N., Glendinning, S., Fernandes, L. & Pinto, A.T., 2013. Effects of alkaline-activated fly ash and Portland cement on soft soil stabilisation. *Acta Geotechnica,* 8(4), pp. 395-405.

Cwirzen, A., Provis, J.L., Penttala, V. & Habermehl-Cwirzen, K., 2014. The effect of limestone on sodium hydroxide-activated metakaolin-based geopolymers. *Construction and Building Materials,* 66, pp. 53-62.

Dahmen, J., Kim, J. & Ouellet-Plamondon, C.M., 2018. Life cycle assessment of emergent masonry blocks. *Journal of Cleaner Production,* 171, pp. 1622-1637.

Diop, M.B. & Grutzeck, M.W., 2008. Low temperature process to create brick. *Construction and Building Materials,* 22(6), pp. 1114-1121.

Dixon, J.B. & Weed, S.B., 1989. *Minerals in Soil Environments.* 2nd ed. Madison, WI: Soil Science Society of America.

Drits, V., Besson, G. & Muller, F., 1995. An improved model for structural transformation of heat-treated aluminous dioctahedral 2: 1 layer silicates. *Clays and Clay Minerals,* 43(6), pp. 718-731.

Engelhardt, G., Felsche, J. & Sieger, P., 1992. The hydrosodalite system Na6+ x [SiAlO4] 6 (OH) x. cntdot. nH2O: formation, phase composition, and de-and rehydration studied by 1H, 23Na, and 29Si MAS-NMR spectroscopy in tandem with thermal analysis, x-ray diffraction, and IR spectroscopy. *Journal of the American Chemical Society,* 114(4), pp. 1173-1182.

Essaidi, N., Samet, B., Baklouti, S. & Rossignol, S., 2014. The role of hematite in aluminosilicate gels based on metakaolin. *Ceramics Silikati,* 58(1), pp. 1-11.

Feng, D., Provis, J.L. & van Deventer, J.S.J., 2012. Thermal Activation of Albite for the Synthesis of One-Part Mix Geopolymers. *Journal of the American Ceramic Society,* 95(2), pp. 565-572.

Ferrage, E., Lanson, B., Sakharov, B.A. & Drits, V.A., 2005. Investigation of smectite hydration properties by modeling experimental X-ray diffraction patterns: Part I. Montmorillonite hydration properties. *Am Mineral,* 90(8-9), pp. 1358-1374.

Földvári, M., 1991. Measurement of different water species in minerals by means of thermal derivatography. In: W. Smykatz-Kloss & S.S.J. Warne, eds. *Thermal Analysis in the Geosciences.* Berlin, Heidelberg: Springer Berlin Heidelberg, pp. 84-100.

Garcia-Lodeiro, I., Palomo, A. & Fernández-Jiménez, A., 2015. 2 – An overview of the chemistry of alkali-activated cement-based binders. *Handbook of Alkali-Activated Cements, Mortars and Concretes.* Oxford: Woodhead Publishing, pp. 19-47.

Garcia-Lodeiro, I., Palomo, A., Fernández-Jiménez, A. & Macphee, D.E., 2011. Compatibility studies between N-A-S-H and C-A-S-H gels. Study in the ternary diagram Na2O–CaO–Al2O3–SiO2–H2O. *Cement and Concrete Research,* 41(9), pp. 923-931.

Gharzouni, A., Samet, B., Baklouti, S., Joussein, E. & Rossignol, S., 2016. Addition of low reactive clay into metakaolin-based geopolymer formulation: Synthesis, existence domains and properties. *Powder Technology,* 288, pp. 212-220.

Guggenheim, S. & Martin, R., 1995. Definition of clay and clay mineral: Joint Report of the AIPEA and CMS Nomenclature Committees. *Clay Miner,* 30(3), pp. 257-259.

Habert, G. & Ouellet-Plamondon, C., 2016. Recent update on the environmental impact of geopolymers. *RILEM Technical Letters,* 1, pp. 17-23.

Hamzah, H.N., Al Bakri Abdullah, M.M., Yong, H.C., Zainol, M.R.R.A. & Hussin, K., 2015. Review of soil stabilization techniques: Geopolymerization method one of the new technique. *Key Engineering Materials,* 660, pp. 298-304.

Hollanders, S., Adriaens, R., Skibsted, J., Cizer, Ö. & Elsen, J., 2016. Pozzolanic reactivity of pure calcined clays. *Applied Clay Science,* 132-133, pp. 552-560.

Ishikawa, K., Yoshioka, T., Sato, T. & Okuwaki, A., 1997. Solubility of hematite in LiOH, NaOH and KOH solutions. *Hydrometallurgy,* 45(1), pp. 129-135.

Jacobs, P.A., Derouane, E.G. & Weitkamp, J., 1981. Evidence for X-ray-amorphous zeolites. *Journal of the Chemical Society, Chemical Communications,* (12), pp. 591-593.

Jagadish, K., 2007. *Building with Stabilized Mud.* New Delhi: I.K. International Publishing House Pvt. Ltd.

Kaze, R.C., Beleuk à Moungam, L.M., Fonkwe Djouka, M.L., Nana, A., Kamseu, E., Chinje Melo, U.F. & Leonelli, C., 2017. The corrosion of kaolinite by iron minerals and the effects on geopolymerization. *Applied Clay Science,* 138, pp. 48-62.

Kinuthia, J.M., 2016. 9 – Unfired clay materials and construction. *Nonconventional and Vernacular Construction Materials.* Woodhead Publishing, pp. 251-272.

Köhler, S.J., Dufaud, F. & Oelkers, E.H., 2003. An experimental study of illite dissolution kinetics as a function of ph from 1.4 to 12.4 and temperature from 5 to 50°C. *Geochimica et Cosmochimica Acta,* 67(19), pp. 3583-3594.

Kuhnel, R., Roorda, H. & Steensma, J., 1975. The crystallinity of minerals – a new variable in pedogenetic processes: a study of goethite and associated silicates in laterites. *Clays and Clay Minerals,* 23(5), pp. 349-354.

Lassinantti Gualtieri, M., Romagnoli, M., Pollastri, S. & Gualtieri, A.F., 2015. Inorganic polymers from laterite using activation with phosphoric acid and alkaline sodium silicate solution: Mechanical and microstructural properties. *Cement and Concrete Research,* 67, pp. 259-270.

Lemougna, P.N., MacKenzie, K.J.D., Jameson, G.N.L., Rahier, H. & Chinje Melo, U.F., 2013. The role of iron in the formation of inorganic polymers (geopolymers) from volcanic ash: a 57Fe Mössbauer spectroscopy study. *J Mater Sci,* 48(15), pp. 5280-5286.

Lemougna, P.N., Madi, A.B., Kamseu, E., Melo, U.C., Delplancke, M.P. & Rahier, H., 2014. Influence of the processing temperature on the compressive strength of Na activated lateritic soil for building applications. *Construction and Building Materials,* 65, pp. 60-66.

Lucas, S., Tognonvi, M.T., Gelet, J.L., Soro, J. & Rossignol, S., 2011. Interactions between silica sand and sodium silicate solution during consolidation process. *Journal of Non-Crystalline Solids,* 357(4), pp. 1310-1318.

Marsh, A., Heath, A., Patureau, P., Evernden, M. & Walker, P., 2018a. Alkali activation behaviour of un-calcined montmorillonite and illite clay minerals. *Applied Clay Science,* 166, pp. 250-261.

Marsh, A., Heath, A., Patureau, P., Evernden, M. & Walker, P., 2018b. A mild conditions synthesis route to produce hydrosodalite from kaolinite, compatible with extrusion processing. *Microporous and Mesoporous Materials,* 264, pp. 125-132.

Marsh, A., Heath, A., Patureau, P., Evernden, M. & Walker, P., under review. Phase formation behaviour in alkali activation of clay mixtures. *Applied Clay Science*.

Maskell, D., 2013. *Development of Stabilised Extruded Earth Masonry Units.* PhD, University of Bath.

McIntosh, A., Lawther, S.E.M., Kwasny, J., Soutsos, M.N., Cleland, D. & Nanukuttan, S., 2015. Selection and characterisation of geological materials for use as geopolymer precursors. *Advances in Applied Ceramics,* 114(7), pp. 378-385.

Miao, S., Shen, Z., Wang, X., Luo, F., Huang, X. & Wei, C., 2017. Stabilization of Highly Expansive Black Cotton Soils by Means of Geopolymerization. *Journal of Materials in Civil Engineering,* 29(10), p. 04017170.

Moore, D.M. & Reynolds, R.C., 1997. *X-ray diffraction and the identification and analysis of clay minerals.* 2nd ed. Oxford: Oxford University Press.

Newkirk, A. & Aliferis, I., 1958. Drying and decomposition of sodium carbonate. *Analytical Chemistry,* 30(5), pp. 982-984.

Nikulshina, V., Ayesa, N., Gálvez, M.E. & Steinfeld, A., 2008. Feasibility of Na-based thermochemical cycles for the capture of CO2 from air—Thermodynamic and thermogravimetric analyses. *Chemical Engineering Journal,* 140(1), pp. 62-70.

Obonyo, E., Kamseu, E., Lemougna, P., Tchamba, A., Melo, U. & Leonelli, C., 2014. A Sustainable Approach for the Geopolymerization of Natural Iron-Rich Aluminosilicate Materials. *Sustainability,* 6(9), p. 5535-5553.

Omar Sore, S., Messan, A., Prud'homme, E., Escadeillas, G. & Tsobnang, F., 2018. Stabilization of compressed earth blocks (CEBs) by geopolymer binder based on local materials from Burkina Faso. *Construction and Building Materials,* 165, pp. 333-345.

Paria, S. & Yuet, P.K., 2006. Solidification–stabilization of organic and inorganic contaminants using portland cement: a literature review. *Environmental Reviews,* 14(4), pp. 217-255.

Perera, D.S., Cashion, J.D., Blackford, M.G., Zhang, Z. & Vance, E.R., 2007. Fe speciation in geopolymers with Si/Al molar ratio of ~2. *Journal of the European Ceramic Society,* 27(7), pp. 2697-2703.

Pourakbar, S., Asadi, A., Huat, B.B.K., Cristelo, N. & Fasihnikoutalab, M.H., 2017. Application of Alkali-Activated Agro-Waste Reinforced with Wollastonite Fibers in Soil Stabilization. *Journal of Materials in Civil Engineering,* 29(2), p. 04016206.

Pourakbar, S. & Huat, B.K., 2017. A review of alternatives traditional cementitious binders for engineering improvement of soils. *International Journal of Geotechnical Engineering,* 11(2), pp. 206-216.

Provis, J.L., 2018a. Alkali-activated materials. *Cement and Concrete Research*, 114, pp. 40-48.

Provis, J.L., 2018b. Alkali-Activation of Calcined Clays – Past, Present and Future. In: F. Martirena, A. Favier & K. Scrivener, eds. Calcined Clays for Sustainable Concrete, 2018 Dordrecht. Springer Netherlands, pp. 372-376.

Rahier, H., Van Mele, B., Biesemans, M., Wastiels, J. & Wu, X., 1996. Low-temperature synthesized aluminosilicate glasses. Part I Low-temperature reaction stoichiometry and structure of a model compound. *J Mater Sci,* 31(1), pp. 71-79.

Rodulfo-Baechler, S.M., González-Cortés, S.L., Orozco, J., Sagredo, V., Fontal, B., Mora, A.J. & Delgado, G., 2004. Characterization of modified iron catalysts by X-ray diffraction, infrared spectroscopy, magnetic susceptibility and thermogravimetric analysis. *Materials Letters,* 58(20), pp. 2447-2450.

Sargent, P., 2015. 21 – The development of alkali-activated mixtures for soil stabilisation. *Handbook of Alkali-Activated Cements, Mortars and Concretes.* Oxford: Woodhead Publishing, pp. 555-604.

Schnitzer, M. & Schuppli, P., 1989. THE EXTRACTION OF ORGANIC MATTER FROM SELECTED SOILS AND PARTICLE SIZE FRACTIONS WITH 0.5M NaOH AND 0.1M Na4P2O7 SOLUTIONS. *Canadian Journal of Soil Science,* 69(2), pp. 253-262.

Singhi, B., Laskar, A.I. & Ahmed, M.A., 2016. Investigation on Soil–Geopolymer with Slag, Fly Ash and Their Blending. *Arabian Journal for Science and Engineering,* 41(2), pp. 393-400.

Smykatz-Kloss, W., 1974. *Differential Thermal Analysis: Application and Results in Mineralogy.* Berlin; Heidelberg: Springer-Verlag Berlin Heidelberg

Stucki, J.W., 2013. Chapter 11 – Properties and Behaviour of Iron in Clay Minerals. In: F. Bergaya & G. Lagaly, eds. *Developments in Clay Science.* Elsevier, pp. 559-611.

Stucki, J.W., Goodman, B.A. & Schwertmann, U., 1987. *Iron in Soils and Clay Minerals* Springer.

Suraj, G., Iyer, C.S.P., Rugmini, S. & Lalithambika, M., 1997. The effect of micronization on kaolinites and their sorption behaviour. *Applied Clay Science,* 12(1), pp. 111-130.

Toda, K., Sato, H., Weerakoon, N., Otake, T., Nishimura, S. & Sato, T., 2018. Key Factors Affecting Strength Development of Steel Slag-Dredged Soil Mixtures. *Minerals,* 8(5), p. 174.

Ulery, A.L. & Drees, L.R., 2008. *Methods of Soil Analysis Part 5—Mineralogical Methods.* Madison, WI: Soil Science Society of America.

Van Jaarsveld, J.G.S., van Deventer, J.S.J. & Lukey, G.C., 2002. The effect of composition and temperature on the properties of fly ash- and kaolinite-based geopolymers. *Chemical Engineering Journal,* 89(1–3), pp. 63-73.

Wagner, J.F., 2013. Chapter 9 – Mechanical Properties of Clays and Clay Minerals. In: F. Bergaya & G. Lagaly, eds. *Handbook of Clay Science.* 2nd ed. Amsterdam: Elsevier, pp. 347-381.

Wolters, F. & Emmerich, K., 2007. Thermal reactions of smectites—Relation of dehydroxylation temperature to octahedral structure. *Thermochimica Acta,* 462(1), pp. 80-88.

Xu, H. & Van Deventer, J.S.J., 2000. The geopolymerisation of alumino-silicate minerals. *International Journal of Mineral Processing,* 59(3), pp. 247-266.

Xu, H. & Van Deventer, J.S.J., 2002. Geopolymerisation of multiple minerals. *Minerals Engineering,* 15(12), pp. 1131-1139.

Yip, C.K., Lukey, G.C. & van Deventer, J.S.J., 2005. The coexistence of geopolymeric gel and calcium silicate hydrate at the early stage of alkaline activation. *Cement and Concrete Research,* 35(9), pp. 1688-1697.

Yip, C.K., Provis, J.L., Lukey, G.C. & van Deventer, J.S.J., 2008. Carbonate mineral addition to metakaolin-based geopolymers. *Cement and Concrete Composites,* 30(10), pp. 979-985.

Zhang, M., Guo, H., El-Korchi, T., Zhang, G.P. & Tao, M.J., 2013. Experimental feasibility study of geopolymer as the next-generation soil stabilizer. *Construction and Building Materials,* 47, pp. 1468-1478.

Zibouche, F., Kerdjoudj, H., d'Espinose de Lacaillerie, J.-B. & Van Damme, H., 2009. Geopolymers from Algerian metakaolin. Influence of secondary minerals. *Applied Clay Science,* 43(3), pp. 453-458.

Appendix

7.6 Introduction

As described in the Synthesis Procedure section in the main article, mix compositions were designed for efficient production of an alkali aluminosilicate phase and compatibility with extrusion processing. To this end, two constraints were used for each soil system: the wet mix had plastic limit consistency, and the system molar ratio Na:Al = 1. Given the differences in plastic limit between the soils (Figure 7-2 in the main article), the NaOH solution had a lower concentration for Khartoum (4.1 M) than for Bristol (13.2 M) and Bengaluru (10.2 M) (Table 7-3 in the main article). After activation, it was observed that new microstructural features had formed in Khartoum-syn, believed to be a N-A-S-H or (N,C)-A-S-H geopolymer phase. In contrast, in Khartoum-nat there was no evidence of new phase formation, with clay particles showing evidence of only partial dissolution at their edges (Section 7.3.2.3 in the main article).

To test whether associated minerals were preventing the formation of a geopolymer phase, or just retarding it, activation of the Khartoum soils was repeated using a 10 M NaOH activating solution. This concentration was chosen as it is a similar value to those in the other soil systems, and because the optimal concentration range for alkali activation of uncalcined clays using NaOH solution is understood to be in the range of 8 – 12 M (Diop and Grutzeck, 2008; Heah *et al.*, 2013; Hounsi *et al.*, 2014; Lemougna *et al.*, 2014; Xu and Van Deventer, 2000). New mix compositions were designed to maintain the plastic limit condition whilst using a 10 M concentration. This broke the second constraint, giving a system Na:Al molar ratio greater than 1. These additional results are presented here, with attention given to the phase formation in the additional systems, and comparison between the 10 M and 4.1 M systems for both Khartoum-nat and Khartoum-syn.

7.7 Materials and Methods

The same precursors were used as described in the main article, using a soil mass of 20g for each mix. The activating solution quantities are given in Table 7-6. These quantities gave a Na:Al molar ratio of 2.4 in the activated systems.

Table 7-6: Composition of activating solutions used for 20g of dry soil.

Sample	Water (g)	NaOH (g)	[NaOH] molarity
Khartoum-nat-act10M	5.1	2.2	10.0
Khartoum-nat-act	5.5	0.9	4.1
Khartoum-syn-act10M	5.1	2.2	10.0
Khartoum-syn-act	5.5	0.9	4.1

The same preparation procedures and characterisation methods were used as described in the main article.

7.8 Results

7.8.1 Macroscopic behaviour

There were no major changes in form or appearance between the 10 M and original 4.1 M activated samples of either natural or synthetic Khartoum soils (Figure 7-17). There was slightly more colour contrast between the top and rest of the cylinders for the 10 M samples. Unlike for the original 4.1 M samples, no major cracks developed in demoulding the 10 M activated cylinders, indicating potentially improved binding.

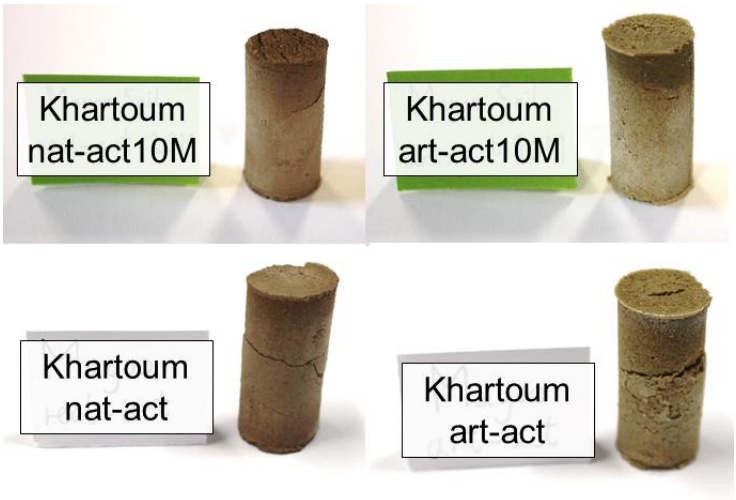

Figure 7-17: Photos of the 10 M and original 4.1 M activated samples of the natural and synthetic Khartoum soils.

7.8.2 XRD

In the 10 M activated samples new reflections emerged, attributed to a small amount of hydrosodalite phase (Figure 7-18). Given the small number of clearly visible reflections, it was not possible to index this with complete confidence, but was believed to be the non-basic hydrosodalite $Na_6[AlSiO_4]_6 \cdot 4H_2O$ (PDF# 00-042-0216). These were accompanied by a large reduction in intensity of the kaolinite reflections. With regards to the associated minerals, no large changes were observed relative to the original 4.1 M activated samples. The only small difference of note is the variability of the intensity of the microcline reflections at 27.5 °2θ, which suggests this may have been more to do with orientation than consumption. In Khartoum-nat, there was a decrease in intensity of the calcite peak at 29.4 °2θ.

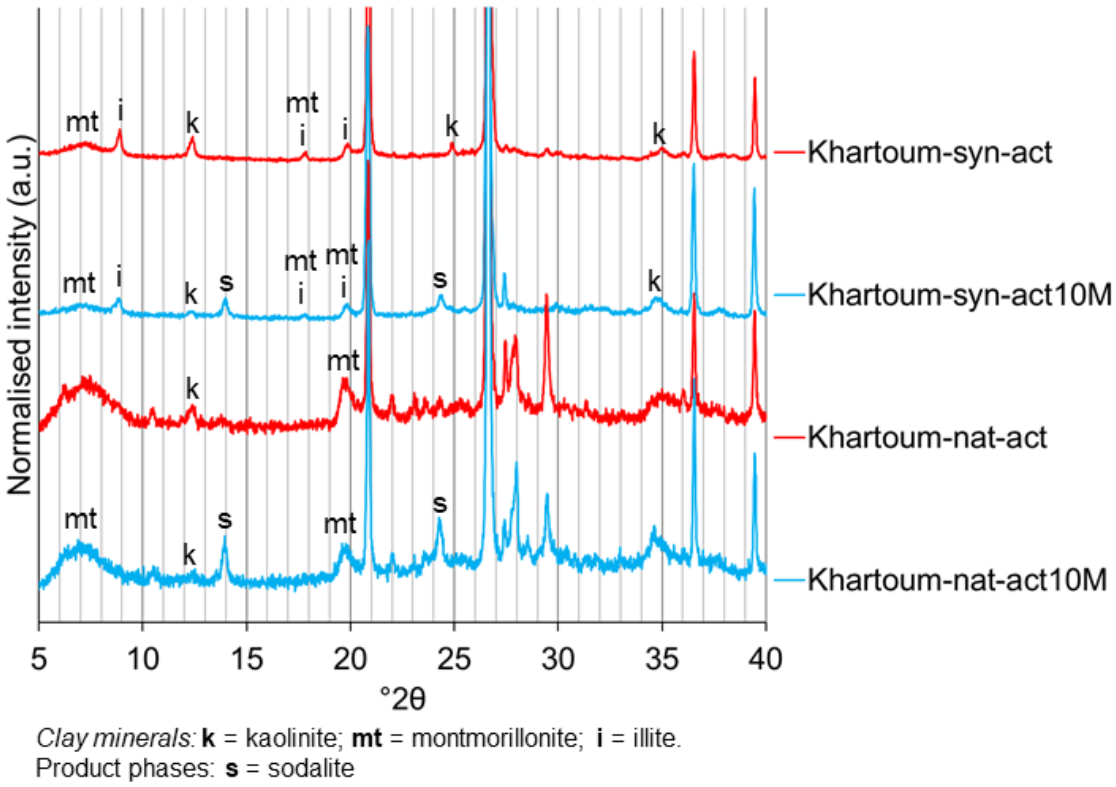

Figure 7-18: XRD patterns of the 10 M and original 4.1 M activated samples of the natural and synthetic Khartoum soils.

7.8.3 SEM

In the 10 M activated sample of Khartoum-nat (Figure 7-19), the same ragged clay particles were present as with the original 4.1 M activated sample but new particles appeared to be present, of particle size <500 µm. In the 10 M activated sample of Khartoum-syn (Figure 7-19), the microstructure was dominated by irregular particles, which seemed to be more connected and with a wider size distribution than in the original 4.1 M activated synthetic sample.

In both the natural and synthetic soils, there seemed to be changes in the SEM images for the 10 M activated sample relative to the original 4.1 M activated sample, although some overall similarities in microstructure were maintained.

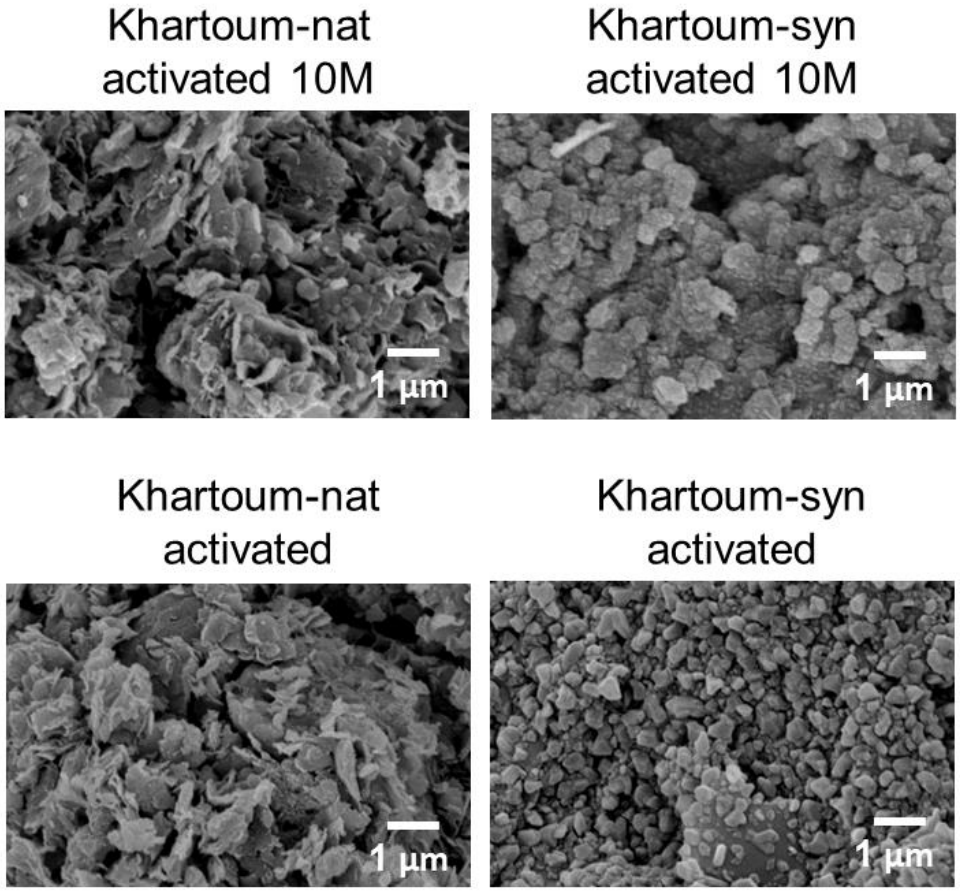

Figure 7-19: SEM images of the 10 M and original 4.1 M activated samples of the natural and synthetic Khartoum soils.

7.8.4 FTIR

Some similar changes were observed for both natural and synthetic soils for 10 M activation relative to the original 4.1 M activation (Figure 7-20). In Khartoum-syn, the 10 M NaOH activation led to a small positive shift in wavenumber of the Si-O-T band peak, from 1031 to 1035 cm^{-1}. However, the profile of this band clearly changed with a more prominent shoulder on the lower wavenumber side. In Khartoum-nat, there was a negative shift in wavenumber of the Si-O-T band peak, from 1004 to 988 cm^{-1}. This was especially striking, since the wavenumber position in the precursor was 1003 cm^{-1}. This suggested that an alkali aluminosilicate product had formed after 10 M activation, but not after the original 4.1 M activation.

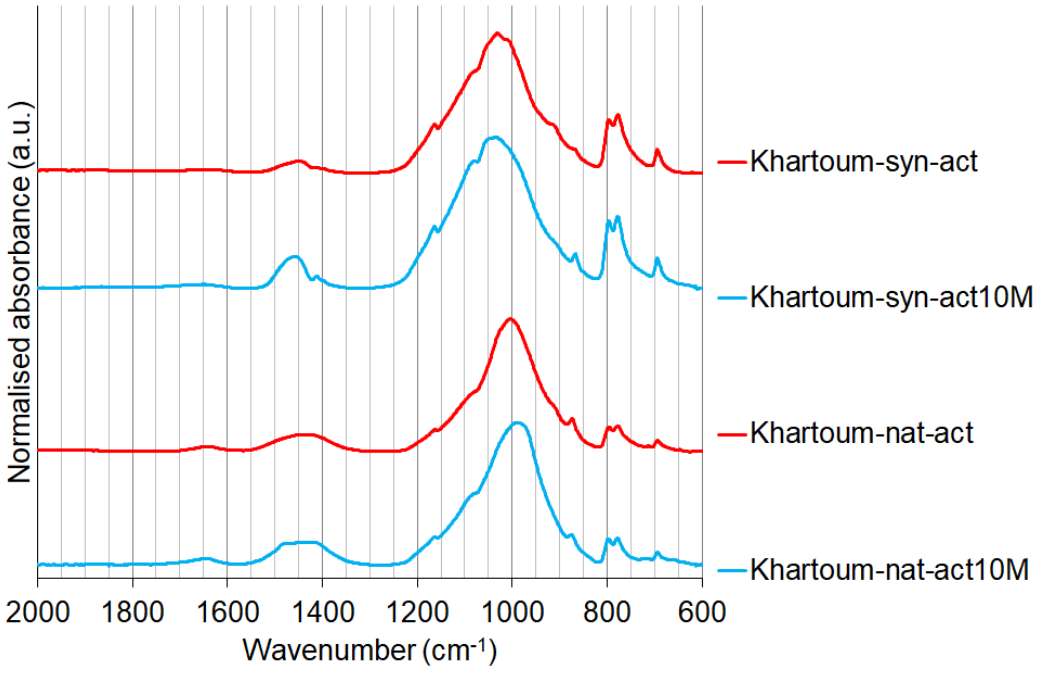

Figure 7-20: FTIR spectra of the 10 M and original 4.1 M activated samples of the natural and synthetic Khartoum soils.

7.8.5 TGA

In the TGA and dTG spectra (Figure 7-21), the same features were present in the 10 M and original 4.1 M activated samples, but these were more pronounced in the 10 M samples. Several changes were common to both soils with the increase to 10 M. Overall mass loss increased by 3.0% for both. There was an increase in the surface-adsorbed moisture dTG peak (centre at 83 °C), and an increase in the background signal to form a plateau between 150 – 350 °C, which is associated with geopolymer formation (Marsh *et al.*, 2018). This was in agreement with the FTIR results, which suggested a geopolymer phase had formed in Khartoum-syn-act10M.

Regarding clay minerals, no large changes were visible for Khartoum-syn-act10M. In Khartoum-nat-act10M there was overlap with the positions of the dTG peaks and the plateau region between 150-350 °C. Regarding associated minerals, there was a noticeable decrease in intensity of the calcite dTG peak (centre at 661 °C) for Khartoum-nat, in agreement with the XRD observations.

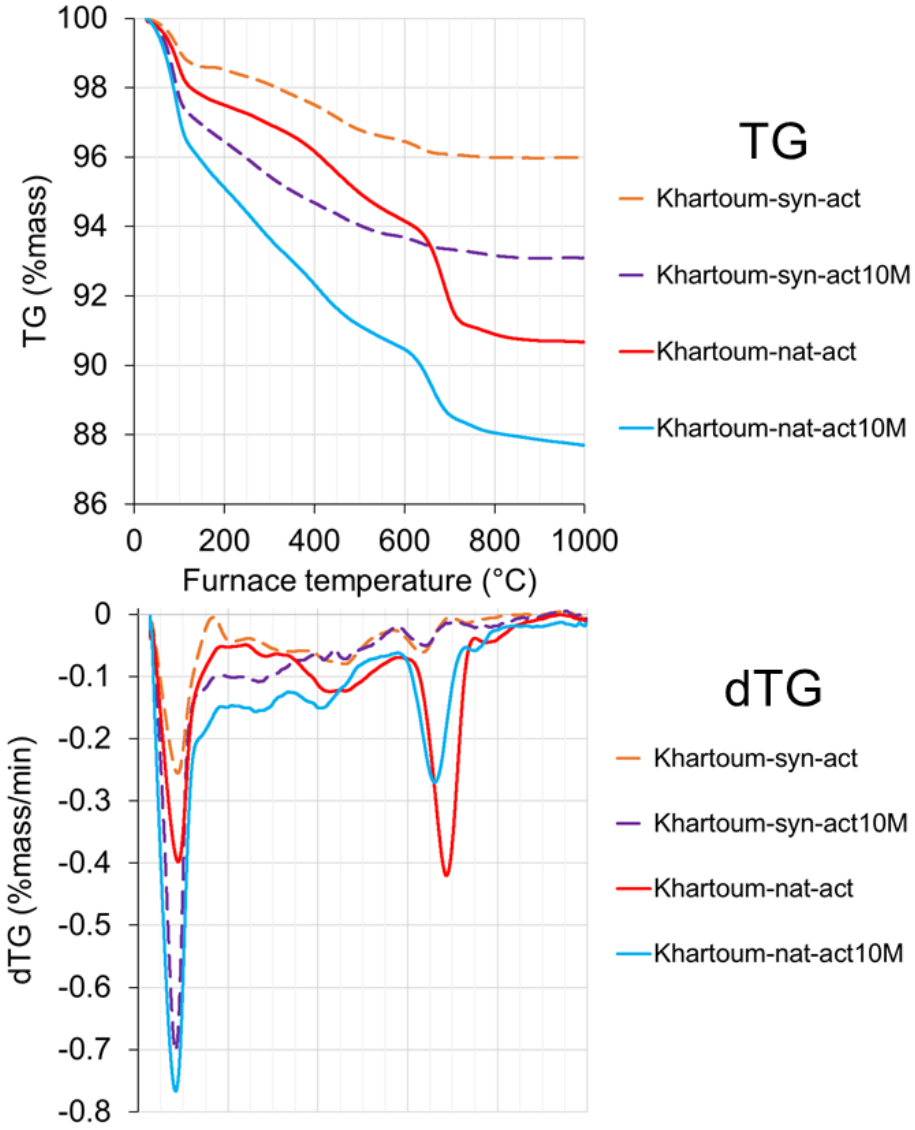

Figure 7-21: TG and dTG spectra of the 10 M and original 4.1 M activated samples of the natural and synthetic Khartoum soils.

7.9 Discussion

Apart from the fact that kaolinite was consumed in the 10 M activated samples, behaviour of the clay minerals was largely the same in the 10 M and original 4.1 M activated samples. Regarding the associated minerals, this was also largely the same, with the exception of some degree of calcite consumption in Khartoum-syn as described in the XRD and TGA results. The discussion will then focus on the kaolinite and phase formation behaviour.

When 10 M activation was used, kaolinite was consumed and hydrosodalite formed in both the natural and synthetic soils. This was not observed for the original 4.1 M activated samples. Both soils contained just 4 wt.% kaolinite, and the XRD patterns showed that not all kaolinite was consumed (Figure 7-18). Therefore it seems likely that the changes observed in the different characterisation techniques were not wholly due to hydrosodalite formation, and that geopolymer formation also occurred in both soils, but this is more difficult to quantitatively identify. As mentioned in the main article, a useful comparison system is from a study on the activation of controlled mixtures of clays under the same processing conditions (Marsh *et al.*, under review). The clay mineral composition of the Khartoum soil falls between those of the systems 90%Mont-10%Kao, 50%Mont-50%Kao and 33%Kao-33%Mont-33%ILL. From these compositions, at comparable NaOH concentrations, both a geopolymer and a hydrosodalite would be expected to form. The participation of kaolinite only at higher concentration is also in agreement with the cited study which suggested that montmorillonite reacts preferentially to kaolinite under these processing conditions (Marsh *et al.*, under review). Whereas in the original 4.1 M activated samples only a geopolymer was formed for Khartoum-syn, in the 10 M activated samples both a geopolymer and a hydrosodalite formed in Khartoum-nat and Khartoum-syn. This therefore suggests that whilst the associated minerals in Khartoum-nat may have prevented geopolymer formation at 4.1 M, a geopolymer was successfully formed at 10 M, meaning that the associated minerals in Khartoum-nat may have a retarding rather than an inhibiting effect on geopolymer formation.

7.10 Conclusions

These results show evidence for geopolymer and hydrosodalite formation in both natural and synthetic soils using 10 M NaOH. This suggests that in the lower concentration activation of the natural soil, geopolymer formation was retarded, but not prevented, relative to the synthetic soil.

7.11 Mass spectrometry data

The mass spectrometry (MS) data that was collected alongside the thermogravimetric (TG) data is presented here for the following sample series from both the main article and Appendix:

- Bristol soils (control and activated) (Figure 7-22)
- Bengaluru soils (control and activated) (Figure 7-23)
- Khartoum soils (control and activated) (Figure 7-24)
- Khartoum soils (activated with 10 M NaOH) (Figure 7-25)

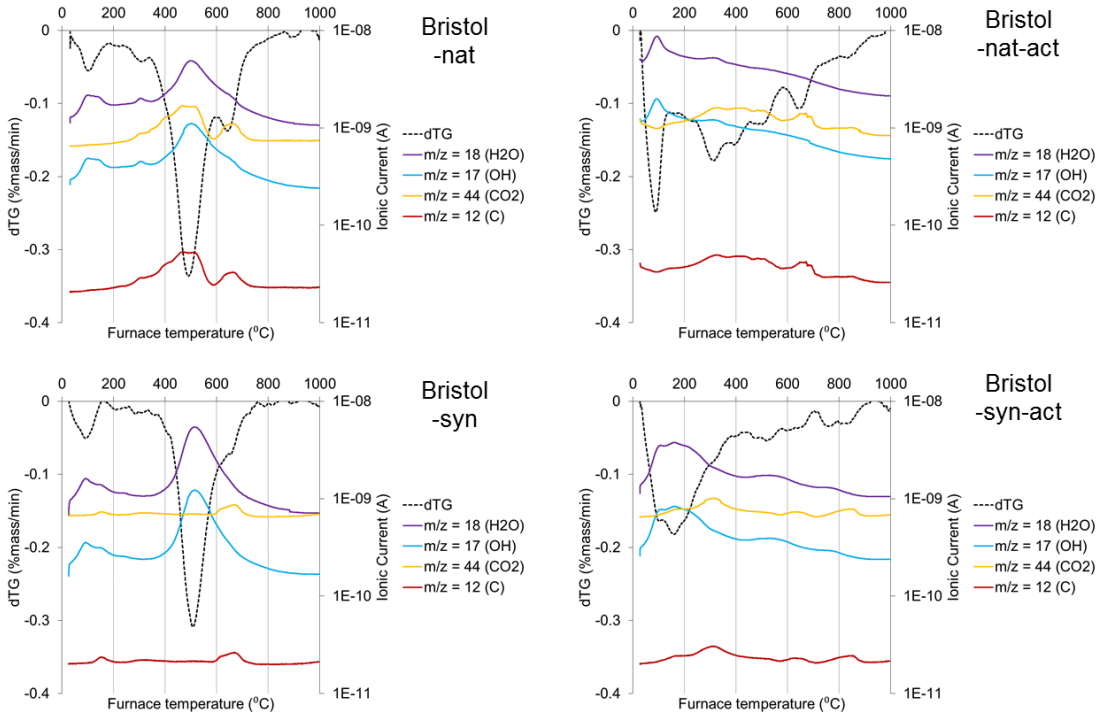

Figure 7-22: MS and dTG data for Bristol soil samples.

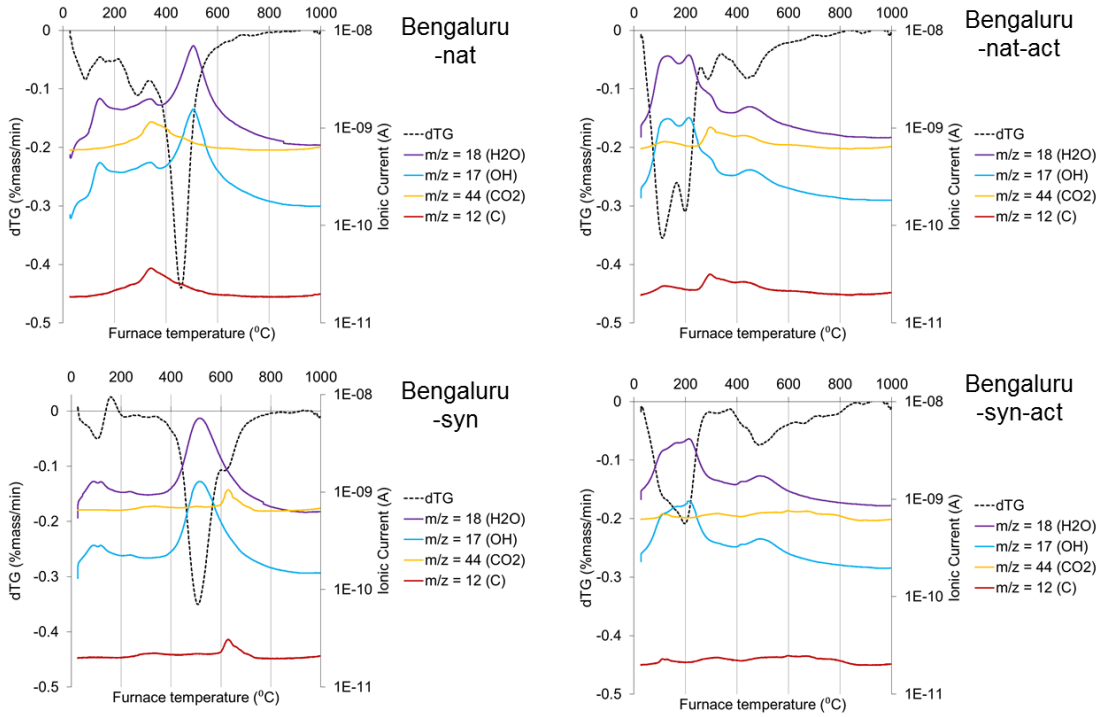

Figure 7-23: MS and dTG data for Bengaluru soil samples.

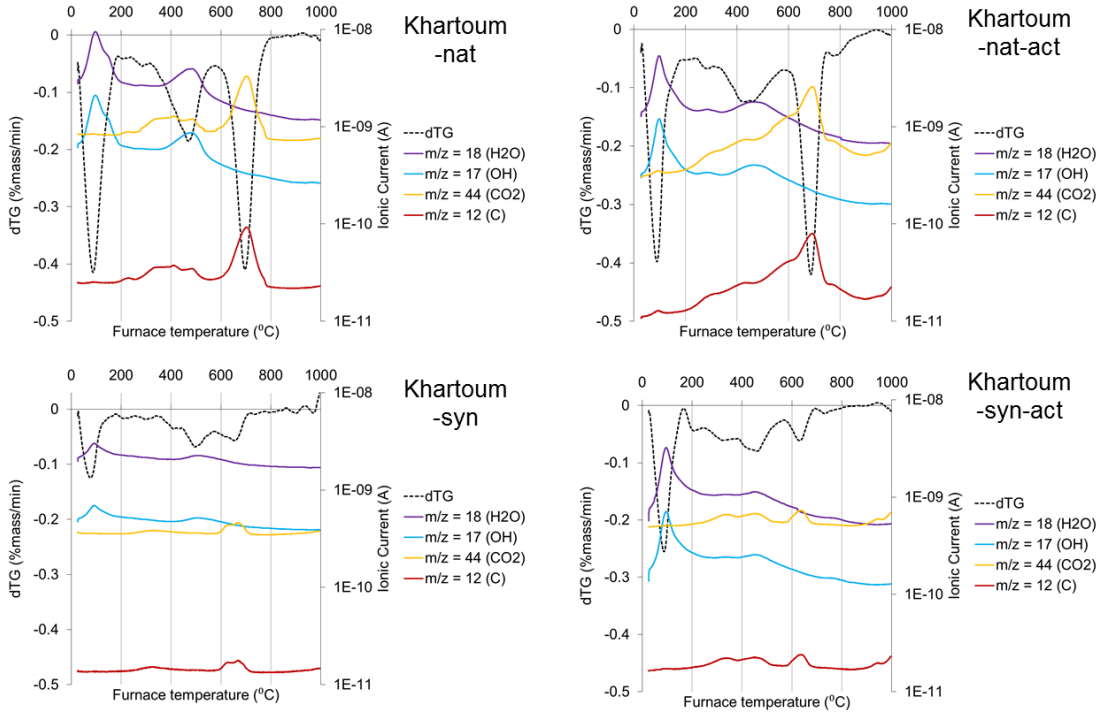

Figure 7-24: MS and dTG data for Khartoum soil samples.

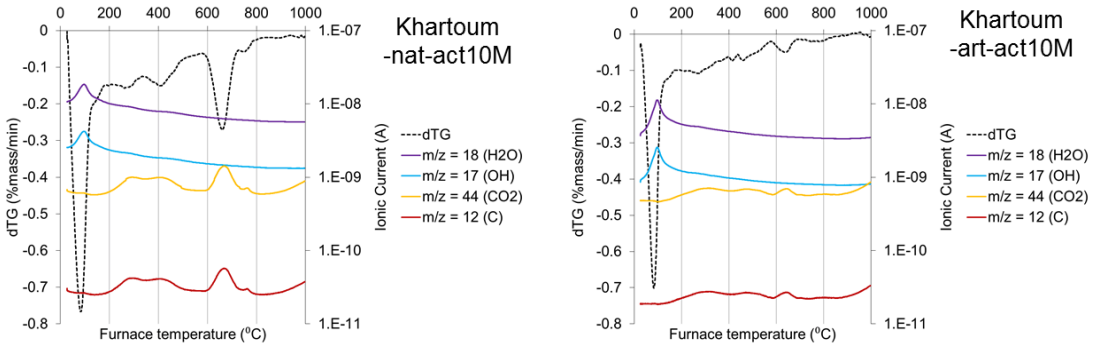

Figure 7-25: MS and dTG data for Khartoum soil samples activated with 10M NaOH.

References

Diop, M.B. & Grutzeck, M.W., 2008. Low temperature process to create brick. *Construction and Building Materials,* 22(6), pp. 1114-1121.

Heah, C.Y., Kamarudin, H., Mustafa Al Bakri, A.M., Bnhussain, M., Luqman, M., Khairul Nizar, I., Ruzaidi, C.M. & Liew, Y.M., 2013. Kaolin-based geopolymers with various NaOH concentrations. *Int J Miner Metall Mater,* 20(3), pp. 313-322.

Hounsi, A.D., Lecomte-Nana, G., Djétéli, G., Blanchart, P., Alowanou, D., Kpelou, P., Napo, K., Tchangbédji, G. & Praisler, M., 2014. How does Na, K alkali metal concentration change the early age structural characteristic of kaolin-based geopolymers. *Ceramics International,* 40(7, Part A), pp. 8953-8962.

Lemougna, P.N., Madi, A.B., Kamseu, E., Melo, U.C., Delplancke, M.P. & Rahier, H., 2014. Influence of the processing temperature on the compressive strength of Na activated lateritic soil for building applications. *Construction and Building Materials,* 65, pp. 60-66.

Marsh, A., Heath, A., Patureau, P., Evernden, M. & Walker, P., 2018. Alkali activation behaviour of un-calcined montmorillonite and illite clay minerals. *Applied Clay Science,* 166, pp. 250-261.

Marsh, A., Heath, A., Patureau, P., Evernden, M. & Walker, P., under review. Phase formation behaviour in alkali activation of clay mixtures. *Applied Clay Science*.

Xu, H. & Van Deventer, J.S.J., 2000. The geopolymerisation of alumino-silicate minerals. *International Journal of Mineral Processing,* 59(3), pp. 247-266.

Chapter 8 - Alkali activation of soil blocks

In this chapter, the alkali activation behaviour of soil blocks is investigated. The aim of this chapter is to understand the effects on alkali activation behaviour of scaling-up samples to block size and addition of inert aggregate. The same Bengaluru soil as used in Chapter 7 is used as the precursor, building on the understanding of the behaviour of this soil developed in that chapter.

This research was undertaken on a research placement at the Indian Institute of Science, Bangalore, as part of the project “Developing earth based building products utilising solid wastes”, funded by UKIERI.

Declaration of authorship

This declaration concerns the article entitled:									
Scale-up effects in alkali-activated soil blocks									
Publication status (tick one)									
draft manuscript	✓	**Submitted**		**In review**		**Accepted**		**Published**	
Publication details (reference)	Marsh, A., Heath, A., Krishnamurthy, P.R., Reddy, B.V.V., Patureau, P., Evernden, M., Walker, P. (in preparation). "Scale-up effects in alkali-activated soil blocks"								
Candidate's contribution to the paper (detailed, and also given as a percentage).	The candidate predominantly executed the… Formulation of ideas: A.Marsh (80%) developed the idea for this study, with suggestions and guidance given by the co-authors (20%) (i.e. supervisors). Design of methodology: A.Marsh (80%) developed the methodology for this study, with suggestions and guidance given by the co-authors (20%) (i.e. supervisors). Experimental work: A.Marsh undertook the majority of experimental work and analysis (80%), with input from co-authors (20%). Presentation of data in journal format: A.Marsh (100%) undertook all formatting.								
Statement from Candidate	This paper reports on original research I conducted during the period of my Higher Degree by Research candidature.								
Signed						**Date**	30/10/2018		

Scale-up effects in alkali-activated soil blocks

Abstract

Alkali activation is a novel method of soil stabilisation, which could be used for the production of compressed blocks for walling materials. Given that much of the fundamental research into the chemical behaviour of this process has been done for small specimens, there is a knowledge gap over the potential effects of increasing specimen size. In this study, blocks were made from a mix of soil, sand and NaOH solution using a manual block press. Their phase composition and microstructure were investigated using powder XRD and SEM; drying behaviour and compressive strength were also measured. No major microstructural or phase differences were found between the central and edge regions of the blocks. Longer curing time had little effect on phase formation and microstructure, but resulted in increased compressive strength. There are no fundamental chemical issues obstructing the scale-up of this stabilisation method, but further research should focus on the measurement of properties in line with building standards and eliminating hazards in the manufacturing process.

8.1 Introduction

Soil and soil-based materials can be used in a variety of construction methods, categorised into three groups: structural, monolithic and blockwork (Houben and Guillaud, 1994). Alkali-activated soils are most suited to blockwork, as it allows the material to be cured at elevated temperatures, which cannot be done for the other two groups. Within the blockwork group, there are several manufacturing methods for producing blocks (Houben and Guillaud, 1994). Pressed blocks are an appropriate method for alkali-activated soils, for several reasons. They minimise handling of the wet mix (compared to hand-moulding methods), which is favourable given their alkalinity at that stage of the process. The use of static compaction to produce a block of target density gives strength from the removal of voids in the soil mix as well as a more uniform appearance and dimensions (Reddy, 2015), making it more competitive with fired block specimens and concrete blocks. The manual block press is well-suited for in-situ production of walling blocks, especially in developing countries, due to its ease of operation and maintenance (Jagadish, 2007).

Investigation of the fundamental chemical behaviour of alkali-activated soils and clays has typically been done using small specimens, such as 18 mm x 36 mm cylinders, due to the cost of some precursors and the small amounts of material required for characterisation. In contrast, the manual block press can make blocks of different sizes, but typically ranges between 305 x 143 x 100 mm and 230 x 108 x 100 mm (Jagadish, 2007). The scaling up of alkali activation reactions is not a trivial aspect in the development of this technology. With respect to soil, care needs to be taken with regards to drying shrinkage when using larger individual elements in wall construction. Drying shrinkage puts limitations of the types of soil, speed of drying and potentially size of individual elements used in some earth building techniques (Houben and Guillaud, 1994). With regards to alkali activation, care needs to be taken with regards to moisture transport and heating effects. Shrinkage-induced cracking can occur in clay-based geopolymer systems, depending on the aggregate content (Kuenzel *et al.*, 2014). Although rapid or flash-setting is generally only an issue in systems containing a high amount of soluble Ca (Chindaprasirt *et al.*, 2012; Lee and van Deventer, 2002), setting time is also reduced by using higher curing temperatures (Rovnaník, 2010). The dissolution and phase formation processes for both geopolymers (Granizo and Blanco, 1998; Zhang *et al.*, 2012) and zeolites (Petrova and Kirov, 1995) are exothermic. Consequently, for larger mix volumes there is the potential for reaction-generated heat to build up, reducing setting times (Antoni *et al.*, 2016), and potentially altering the microstructure. Unlike cement and hydraulic lime stabilisation, commonly used stabilising agents which undergo a hydration reaction, the formation of a geopolymer

does not involve net consumption of water. Instead, water is a reaction medium which is temporarily consumed during the dissolution stage and released during the condensation stage (Duxson *et al.*, 2007; Weng and Sagoe-Crentsil, 2007), before removal from gel pores during drying (Mastali *et al.*, 2018). Therefore a balance is required to have enough water to facilitate the reaction, but not so much to create excessive porosity in the final gel (Provis *et al.*, 2010; Zuhua *et al.*, 2009). The plate-like morphology of clay particles gives them a higher demand for water than other aluminosilicate precursors such as fly ash or GGBS (Mastali *et al.*, 2018; Provis *et al.*, 2010). This makes them less well-suited for cast concrete, but more conducive to brickmaking processes such as extrusion (Maskell *et al.*, 2014) or manual compaction (Diop and Grutzeck, 2008). Zeolite formation under these conditions also begins with water-mediated dissolution and then precipitation from solution (Byrappa and Adschiri, 2007). The number of water and hydroxyl groups present in the β-cage of the product phase is dependent on the exact synthesis conditions used (Engelhardt *et al.*, 1992). For both geopolymers and zeolites, the availability of sufficient water for the formation process is a key requirement. Another concern is efflorescence. This can occur in cementitious materials in general, but is a particularly acute problem in alkali-activated materials (Allahverdi *et al.*, 2015). These are all practical, macro-scale considerations which depend on an understanding of micro-scale reactions.

The comparison between different alkali-activated systems is often difficult due to the large number of variables in composition and processing. Investigation of the effects of scaling-up in isolation is a neglected area of research, at least in the public domain. In this study, a well-characterised precursor soil - whose alkali activation behaviour has already been characterised at small scale - has been activated at block scale using similar composition and processing conditions. The aim of this study was to investigate any variations in phase formation and microstructure between the centre and edge regions in a block, and what implications these have for its development as a viable construction material.

8.2 Materials and Methods

8.2.1 Materials

The soil used is from Bengaluru, India. Its chemical and phase composition has previously been described in Marsh et al. (in preparation), but will briefly be restated here. It had a clay fraction of 36%, and kaolinite was the sole clay mineral. Other phases present were quartz, hematite, microcline and muscovite (Figure 8-1). The chemical composition is given in Table 8-1. A quartzitic river sand, known to contain no more than 5 wt% of clay, fine silt or organic impurities (Gourav and Reddy, 2018) in line with the standard IS:2116-1980 (BIS, 1980), was used as aggregate. The sand was sieved to < 4.75 mm before use. NaOH pellets (>97.5% purity, Thomas Baker) were mixed with water to make a 12 M NaOH solution.

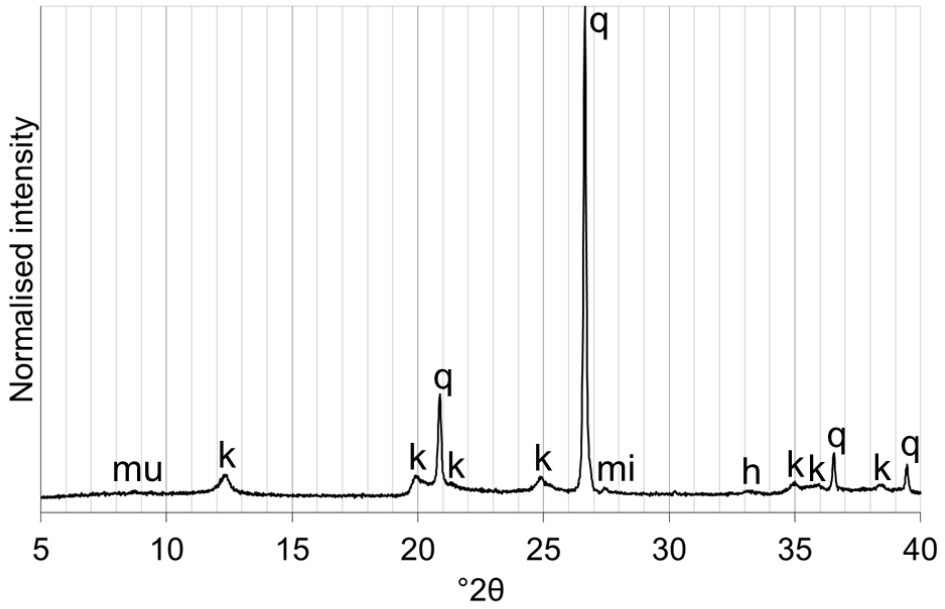

Figure 8-1: Indexed XRD pattern of the soil precursor used.

Table 8-1: Chemical composition of the Bengaluru soil in oxide wt.%.

	Al_2O_3	CaO	CuO	Fe_2O_3	K_2O	MgO	SiO_2	SO_3	TiO_2	Total
Bengaluru soil	24.05	0.38	0.08	12.10	1.21	0.26	60.73	0.08	1.11	100.00

8.2.2 Manufacturing procedure

A 50% aggregate mix was chosen in order to reduce the overall clay content in the mix to 18%, within the recommended range of clay content for cement stabilised soil blocks (Walker and Stace, 1997). At higher clay contents, the clay clumps together and does

not mix well at this scale. The mix quantities are given in Table 8-2. For the quantity and concentration of NaOH solution, and assuming kaolinite to be the only reactive aluminium-containing phase in the soil, this gave a molar ratio of Na:Al = 0.86.

Table 8-2: Mix proportions for control and activated block specimens

Mix parameter	Control	Activated
Soil mass (kg)	20.00	20.00
Sand mass (kg)	20.00	20.00
Water mass (kg)	4.00	3.59
NaOH dry mass (kg)	0	1.92
Solution molarity (M)	n/a	12

The water mass values used here are proportionally lower to the mass of dry components than those used in the manufacture of smaller samples. This is partly due to the use of 50% aggregate, but also because of the difference between the extrusion and static compaction processing methods. For extrusion, soil is required to have plastic consistency in order to achieve flow; but for static compaction, it is better for soil to have a more brittle consistency. For the manual block press using static compaction, it is desired for the soil to have the optimum moisture content for this compaction method in order to achieve for maximum dry density under the given compaction force.

The steps in the block specimen manufacture process are shown in Figure 8-2. The NaOH solution was mixed and left, covered to dissolve and cool overnight. The soil and sand were added together as a 40 kg batch in a 90 kg capacity pan-mixer and dry-mixed at a speed of 27 rpm for 2 minutes. The water or NaOH solution was slowly added, and then wet-mixed for a further 3 minutes. Any residual lumps were broken up by hand, and the mixture was covered with sacks to reduce drying out. A reverse toggle manual block press developed by the Department of Civil Engineering at the Indian Institute of Science was used (Reddy, 2015), to produce block specimens of dimensions 230 x 110 x 70 mm. A fixed mass of 3.64 kg of wet mix was used for each block specimen, to achieve a target density of 1.83 gcm^{-3} under static compaction, which is within the recommended range of 1.80 - 1.85 gcm^{-3} (Jagadish, 2007).

Figure 8-2: Stages in block specimen manufacture: a) mixing the soil, sand and activating solution, b) breaking up any remnant lumps in the wet mix, c) weighing out a set amount of wet mix for each block specimen, d) filling the mould with the wet mix, e) compacting the block specimen, f) releasing the block specimen from the mould.

Once pressed, the block specimens were placed into an 80°C oven, and cured for either 24 hours or 120 hours. One activated block specimen was not oven cured, for comparison. The naming conventions for each sample are given in Table 8-3. After heat curing, the specimens were left to age indoors in atmospheric conditions, with all doors to the room left open during the daytime for a high air change rate. In the ageing period, average outdoor temperature was 22.6°C (ranging from 19.6 - 27.6°C) and average outdoor relative humidity was 82% (ranging from 59 - 98%). Data is from Bangalore weather station (USAF #432950) (National Centers for Environmental Information, 2018).

Table 8-3: Details for each sample and its abbreviation

Sample abbreviation	Control or activated	Curing time	Location in block
Cont-24h-e	Control	24 hours	Edge
Cont-24h-c	Control	24 hours	Centre
Act-24h-e	Activated	24 hours	Edge
Act-24h-c	Activated	24 hours	Centre
Act-120h-e	Activated	120 hours	Edge
Act-120h-c	Activated	120 hours	Centre
Act-0h-e	Activated	0 hour	Edge

8.2.3 Characterisation and measurements

To compare behaviour in the centre and edge of the block specimens, material was obtained from the central 50 mm region as well as the 5 mm border at the edge of the block specimens. To prepare powder for characterisation, material was dry-ground in a ceramic pestle and mortar, and sieved through a 300 μm sieve, to remove the large sand aggregate particles.

Powder X-ray diffraction (XRD) patterns were taken with a Bruker D8 Advance diffractometer using Cu Kα (λ = 1.54060 Å) X-radiation using a step size of 0.02 °(2θ). For the precursor soil and act-120h samples, a different Bruker D8 Advance diffractometer was used with monochromatic CuKα (λ = 1.540598 Å) X-radiation and a step size of 0.016 °(2θ). Patterns were corrected for specimen height shift by calibrating to the most intense quartz reflection (101) at 26.6 °(2θ), and normalised to the most intense reflection in each respective pattern. Phase identification was done using Bruker EVA software.

Scanning electron microscope (SEM) imaging was used to characterise phase size and morphology, using a JEOL SEM6480LV in secondary electron mode with an accelerating voltage (AV) of 10 kV. Bulk specimens were sputter coated with gold for 3 minutes.

Unconfined compressive strength (UCS) testing was done at 7 ±1 days ageing time, using a TUN600 Universal Testing Machine. At least four block specimens were tested for each series. The frogs on both sides of each block specimen were filled in with a mix of Plaster of Paris and <1.18 mm sieved sand to create a level surface.

The mass change behaviour of the block specimens was measured after curing, and after 7 days ageing time. Average values and standard deviations were calculated for ≥4 measurements for each series.

8.3 Results

8.3.1 XRD

XRD patterns comparing the cont-24h, act-24h and act-120h specimens are given in Figure 8-3. In the control specimens, the phases present were kaolinite, albite, quartz, muscovite and microcline. For simplicity of viewing, where associated minerals (i.e. quartz, albite, muscovite and microcline) have been indexed in the control specimen patterns, these have not been indexed again in the activated specimen patterns. There was some variation in the intensity of the 002 microcline reflection at 27.5 °2θ between patterns – however, there was no consistent difference between the control and activated samples. This variation has been previously observed in alkali-activated soil systems (Marsh *et al.*, in preparation), and is likely due to orientation effects.

In all of the act-24h and act-120h block specimens, a hydrosodalite phase was formed. This is a known transformation from kaolinite under these processing conditions (Marsh *et al.*, 2018). The kaolinite was not fully consumed in any of the activated block specimens as evidenced by the residual kaolinite peaks. The peak profiles of all the hydrosodalite reflections were broad, suggesting the crystallites were small and/or highly strained (Burton *et al.*, 2009). There were small differences in the peak positions of the 310 (32.6 – 32.9 °2θ) and 222 (34.9 - 35.1 °2θ) reflections between the act-24h and act-120h specimens. This likely means that the cage contents of the hydrosodalite phases were slightly different, with different amounts of water and/or hydroxyl groups in the β-cage (Engelhardt *et al.*, 1992). The peaks were too broad to conclusively assign a specific hydrosodalite phase. Overall, no large differences were observed between the patterns from centre and edge regions in any of these block specimens.

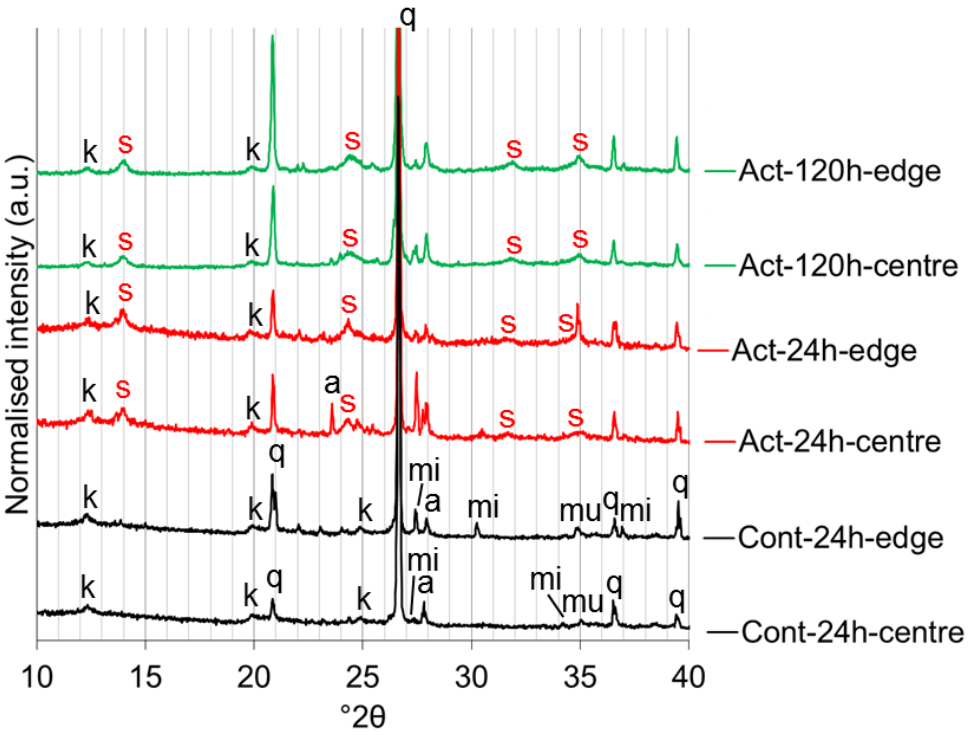

Precursor phases: ***a*** *= albite;* ***k*** *= kaolinite;* ***mi*** *= microcline;* ***mu*** *= muscovite;* ***q*** *= quartz*
Product phases: ***s*** *= sodalite*

Figure 8-3: XRD patterns of the centre and edge regions of cont-24h, act-24h and act-120h block specimens.

XRD patterns from the edge regions of the cont-24h, act-0h and act-24h blocks are compared in Figure 8-4. Also included is a pattern from some of the surface efflorescence collected from the act-0h block specimen after 5 days ageing, as shown in Figure 8-9. No hydrosodalite was formed in the act-0h block specimen. The efflorescence was composed of thermonatrite ($Na_2CO_3 \cdot H_2O$), one of several possible efflorescence phases in alkali-activated materials (Allahverdi *et al.*, 2015), along with other phases from the act-0h block specimen. The thermonatrite was likely formed by atmospheric carbonation of residual NaOH in the presence of water.

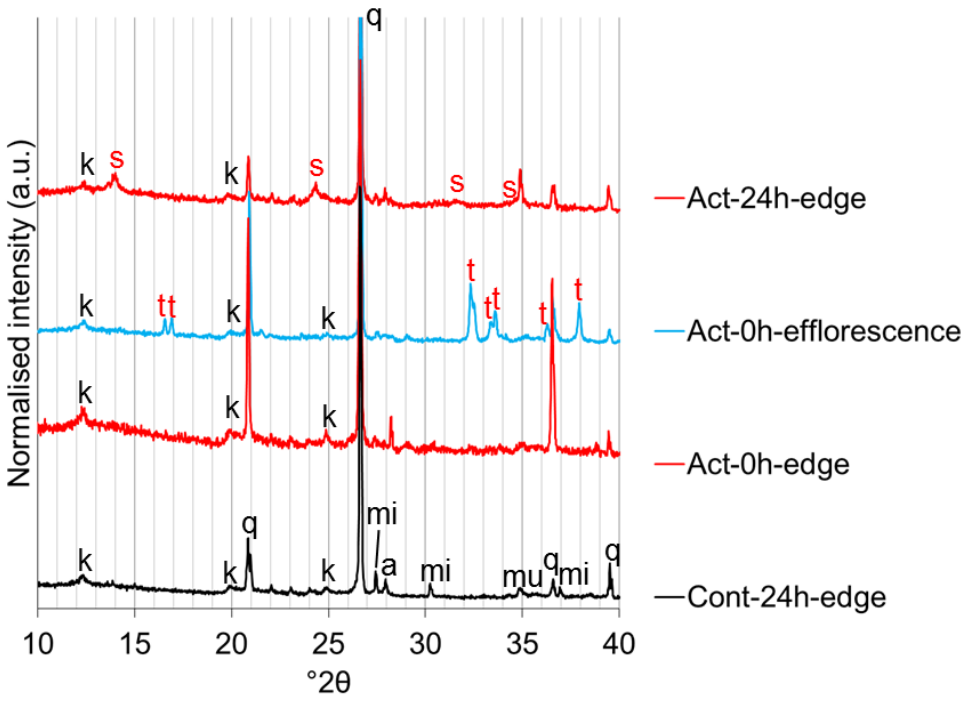

Precursor phases: ***a*** *= albite;* ***k*** *= kaolinite;* ***mi*** *= microcline;* ***mu*** *= muscovite;* ***q*** *= quartz*
Product phases: ***s*** *= sodalite,* ***t*** *= thermonatrite*

Figure 8-4: XRD patterns showing different behaviour in the edge region of the block specimens for different levels of activation and curing time.

8.3.2 SEM

SEM images of the centre and edge regions of the cont-24h, act-24h and act-120h block specimens are given for low (Figure 8-5) and high (Figure 8-6) magnifications. At low magnification (Figure 8-5), the large quartz aggregate particles were visible in some of the images, with areas of soil in between. Fine scale cracking between the large quartz aggregate particles and the soil was observed in the activated block specimens, but not in the control block specimen. This is consistent with observations of drying-induced micro-cracking in alkali-activated metakaolin-sand mixes (Kuenzel *et al.*, 2014). At high magnification (Figure 8-6), the microstructural features were consistently fine, typically <1 μm, but also with some very fine particles <200 nm. In the control specimens, out of the phases known to be present from the XRD analysis, kaolinite, hematite and possibly quartz are known to be present at these size scales (Dixon and Weed, 1989). In the activated specimens, it is known from the XRD analysis that the same phases are still there, in addition to hydrosodalite. As described in Section 8.3.1, hydrosodalite could be expected to be present at a very fine scale. Comparing the scale of microstructural features at high magnification in the block specimens, there were no significant differences between the control and activated specimens, the 24 h and 120 h cured specimens, nor between the centre and edge regions.

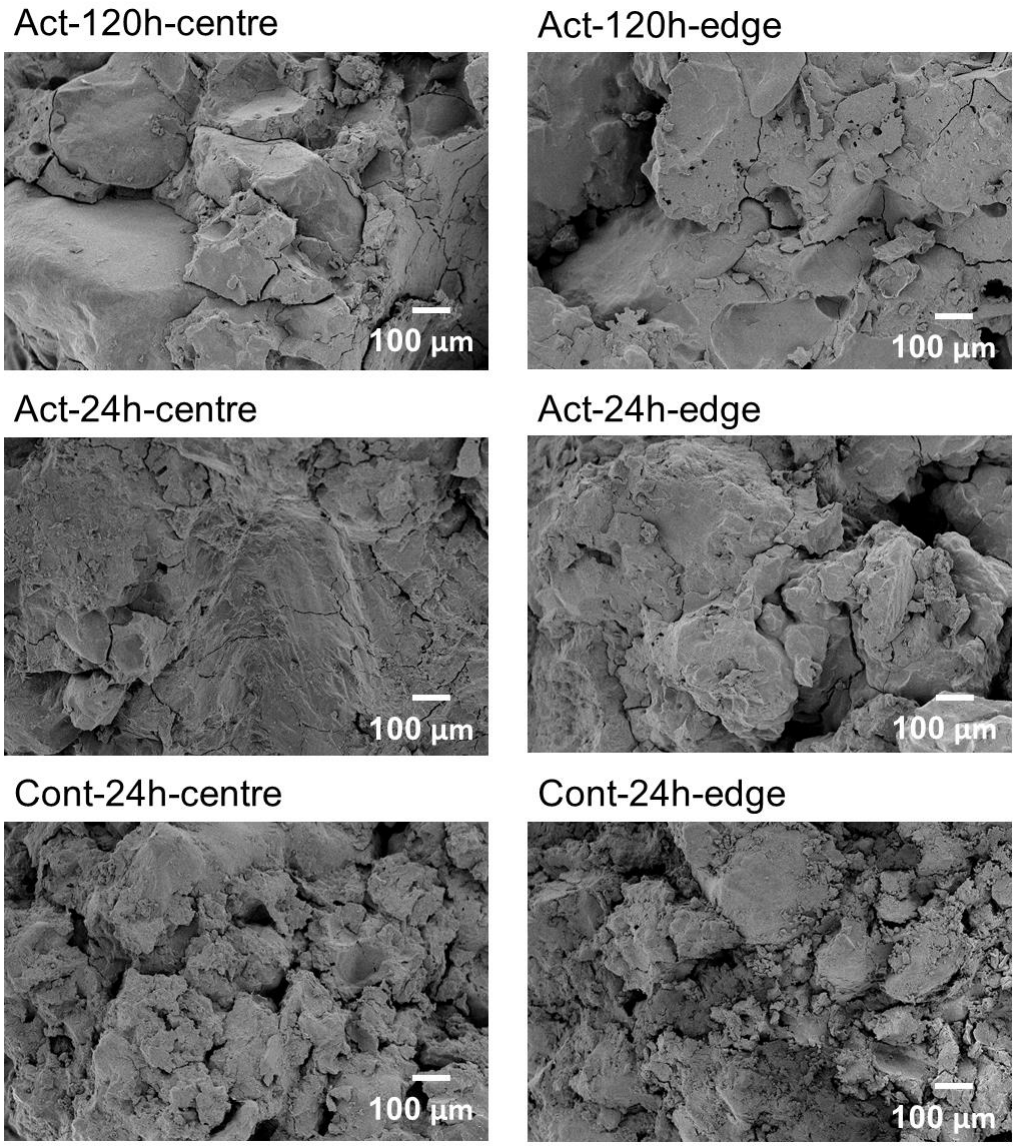

Figure 8-5: SEM images of centre and edge regions of cont-24h, act-24h and act-120h block specimens at 100x magnification.

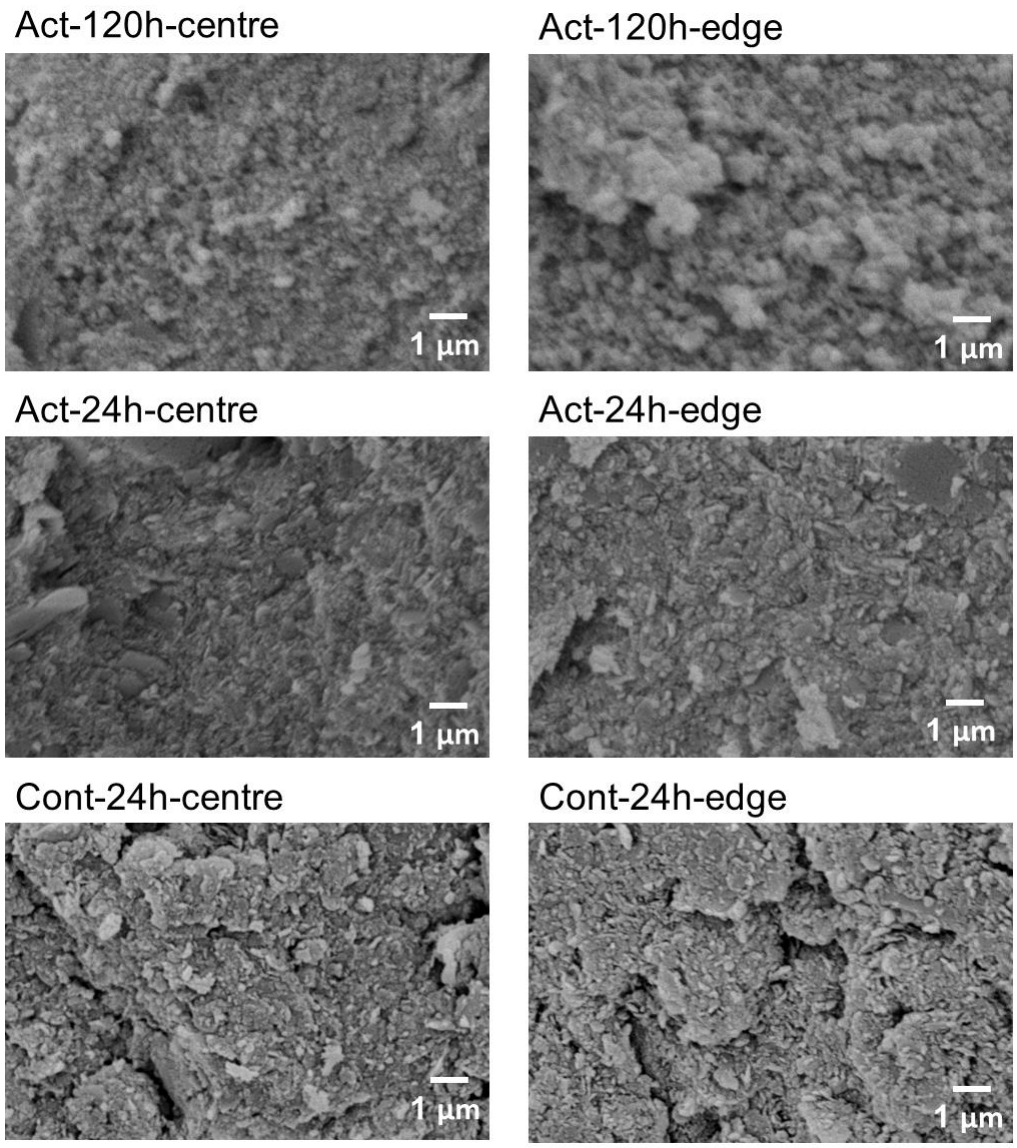

Figure 8-6: SEM images of centre and edge regions of cont-24h, act-24h and act-120h block specimens at 10,000x magnification.

8.3.3 Drying behaviour

The changes in mass of the control and activated block specimens with ageing time are given in Figure 8-7. Within the 24h cured block specimens, there was a clear difference between the control and activated block specimens. The control blocks continuously decreased in mass up to 7 days ageing, whereas the activated block specimens maintained an approximately constant mass. This could have been be due to: a) the formation of a surface barrier preventing moisture loss; b) atmospheric reactions that resulted in mass gain which offset any mass loss from drying, or c) re-adsorption of moisture from the atmosphere. No chemical hydration reactions were expected, given the chemical and phase composition of the precursors. Within the 120h cured block specimens, both the control and activated block specimens underwent a small increase in mass. This suggests that during the longer curing time, all excess moisture from mixing was driven off, and on return to atmospheric conditions underwent moisture re-adsorption (McGregor *et al.*, 2014).

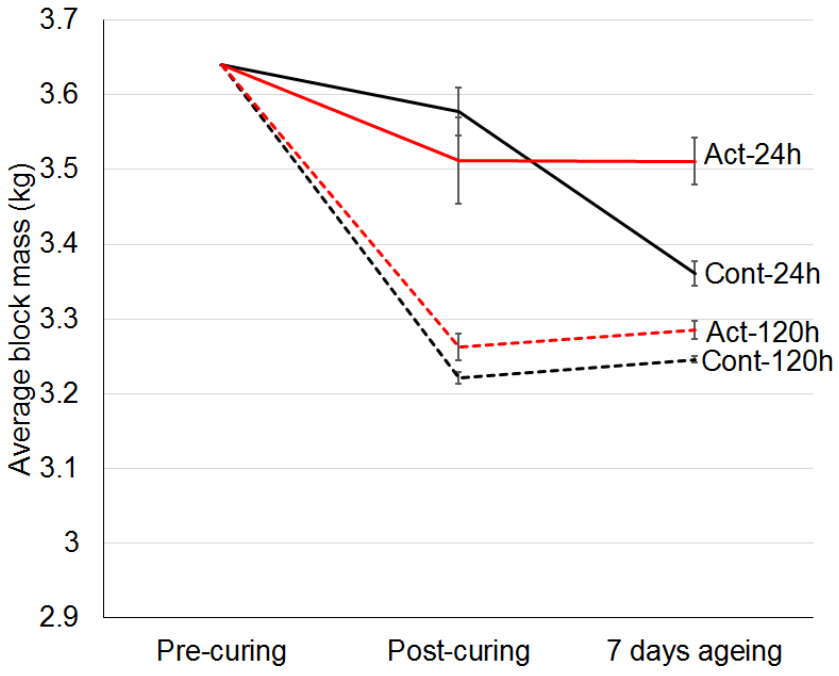

Figure 8-7: Changes in block specimen mass at different stages in the ageing process.

Immediately after demoulding, the control and activated block specimens looked nearly identical in appearance as shown in Figure 8-8. With increasing ageing time, the act-0h block specimen formed a profusion of white efflorescence as shown in Figure 8-9, forming needle-like crystals. This was extreme, but some minor efflorescence was also observed for some of the act-24h block specimens by 4 days of ageing.

Figure 8-8: Comparison of the control (left) and activated (right) block specimens immediately after compaction and demoulding.

Figure 8-9: The act-0h block specimen after demoulding (0 days), and after 1 and 5 days ageing.

8.3.4 UCS

Air dry UCS results for control and activated block specimens at 24 and 120h curing times are shown in Figure 8-10. Both control block specimens had low strength of <1 MPa. The act-24h block specimens had a slightly higher average strength than the cont-24h blocks, but this was smaller than the standard error. In contrast, the act-120h block specimens had a far higher average strength of 10.7 MPa. All block specimens failed with the 'hourglass' failure pattern, which is a valid mode of failure in compression (BSI, 2009).

Values for moisture content, bulk density and dry density for the block specimens at testing are given in Table 8-4. The moisture content at testing for the activated block specimens were higher than for the control block specimens, and the dry density was lower for the activated block specimens. Act-120h, which had by far the highest failure strength, also had the lowest dry density of all the block series tested. This indicated that the reason for the greater strength was not due to a smaller void proportion.

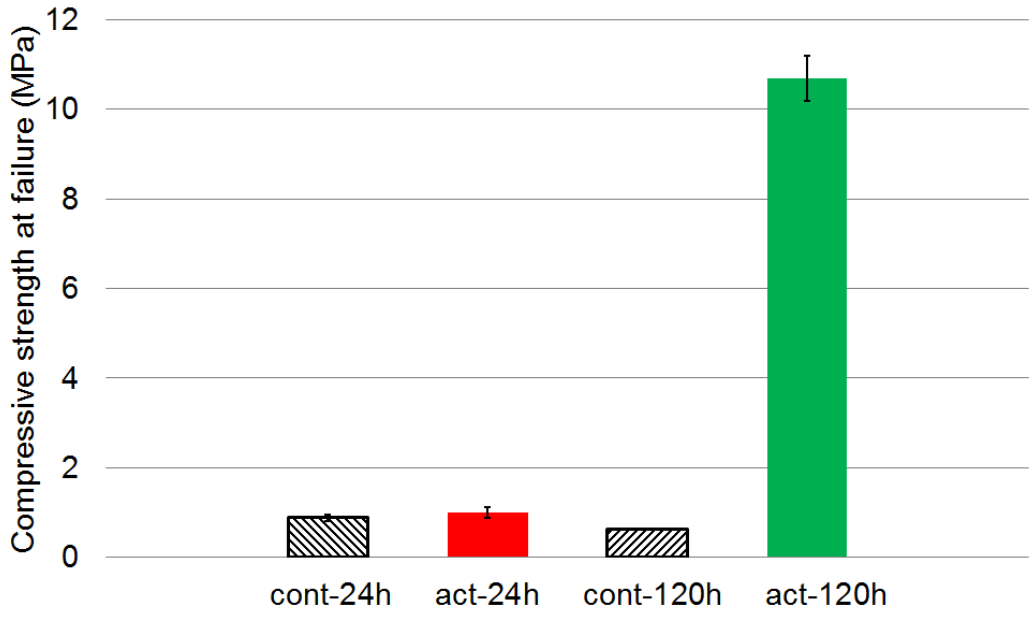

Figure 8-10: Air dry UCS results for control and activated block specimens at 24 and 120h curing times.

Table 8-4: Moisture content, bulk density, dry density and average dimensions for the block specimens at testing.

	Cont-24h	**Act-24h**	**Cont-120h**	**Act-120h**
Moisture content (%)	3.6%	9.5%	2.1%	4.1%
Bulk density (gcm^{-3})	1.96	1.99	1.86	1.83
Dry density (gcm^{-3})	1.89	1.80	1.82	1.75
Average dimensions (mm)	227.0 x 108.3 x 69.8	229.8 x 109.0 x 70.5	228.4 x 108.8 x 70.2	230.0 x 109.8 x 71.0

8.4 Discussion

8.4.1 Microstructure and properties

As described in Sections 8.3.1 and 8.3.2, there were no large differences in phase composition or microstructure between the centre and edge regions. Any differences in the exact phase and size of the hydrosodalite reaction products are unlikely to result in any large differences in performance as a walling material. It is also noted that the microstructures and phase formation of the activated block specimens were very similar to that of a small block specimen made without aggregate, as described in Marsh et al. (in preparation). This suggests that the addition of inert aggregate, use of a larger mould size and lower moisture content did not result in any fundamental changes in the alkali activation process.

Regarding the effects of curing time, the mass change results in Section 8.3.3 show that 24h was not a sufficient time for the control block specimen to fully dry. This was consistent with the curing of small 18 x 36 mm cylinders of the same soil in Marsh et al. (in preparation). Although 24h was sufficient to cause an alkali activation reaction in the act-24h block specimens, the strength results described in Section 8.3.4 show that this did not result in a meaningful increase in strength. In contrast, the act-120h block specimens demonstrated a large increase in strength compared to cont-120h. This was despite the fact that the phase formation behaviour and microstructure was very similar for the act-24h and act-120h blocks, but this may be influenced by other larger-scale factors. In cement-stabilised soil block specimens, it has been shown that compressive strength increases linearly with cement content, and that strength is higher when clay content is lower (Walker and Stace, 1997). However, the XRD results show that there is unreacted kaolinite in both the act-24h and act-120h block specimens, and their peak intensities suggest there was not a large difference in the extent of reaction between the two. The lower moisture content at testing (also given in Section 8.3.4) for act-120h compared to act-24h could explain some of the strength difference (Champiré *et al.*, 2016), but may not fully explain such a large difference in behaviour. Other factors which can influence mechanical behaviour in alkali-activated and soil systems include: particle grading, compacted density, and the binding between the different phases. Although finely grained soils have been shown to have a lower void ratio and hence higher strength than coarse grained soils in cement-stabilised soil block specimens (Reddy and Latha, 2014), the same soil and sand was used in all block specimens tested.

Regarding compacted density, it was shown in Section 8.3.4 that the act-120h block specimens had the lowest dry density of all the samples tested and it was hypothesised

that this could be due to the hydrosodalite phase having a lower particle density than the original kaolinite. Additional experimentation was therefore undertaken to investigate the influence of the kaolinite to hydrosodalite phase transformation on density. Because it was difficult to isolate the kaolinite mineral from the actual soil, for the additional experimentation on particle density, high purity Imerys Speswhite kaolin was used, activated with NaOH solutions made with NaOH pellets of >98% purity (Sigma-Aldrich, product #06203). Particle density was measured by He gas displacement using a Micromeritics Accupyc 1330. Before measurement, powder samples were degassed at 150°C under vacuum for 1 h.

The particle density for a kaolinite precursor was 2.62 gcm^{-3}, which decreased to 2.32 gcm^{-3} after alkali activation at Na:Al = 1 (an 11% reduction) (Figure 8-11). In this system, it is known that a significant proportion of the kaolinite is transformed into hydrosodalite (Marsh *et al.*, 2018), and the measured particle density value agrees well with the theoretical value for hydrosodalite calculated from a structural model (Kendrick and Dann, 2004). The lower density of hydrosodalite arises from its cage-like structure, which forms interconnected pores of approximately 12 nm in size (Franus *et al.*, 2014). Given that kaolinite comprised 16.3 wt.% of the wet mix, and the transformation is associated with an 11% reduction in particle density, one would expect a bulk density reduction of approximately 1.9% in the activated block specimens (approximating that all kaolinite was transformed to hydrosodalite), compared to the control ones. This value of 1.9% reduction is less than the bulk density reductions observed between the activated and control samples (3.8-4.8%). An analysis of the sample dimensions (Table 8-4) showed that the control samples shrunk 2.9% (24 hr curing) and 2.7% (120 hr curing) relative to the activated samples. This was most likely due to drying shrinkage of the unstabilised control samples (Walker, 1995) which led to an increase in dry density as the volume decreased. This indicates that not only does the conversion of kaolin to hydrosodalite result in a decreased particle density, but it can also reduce the amount of drying shrinkage.

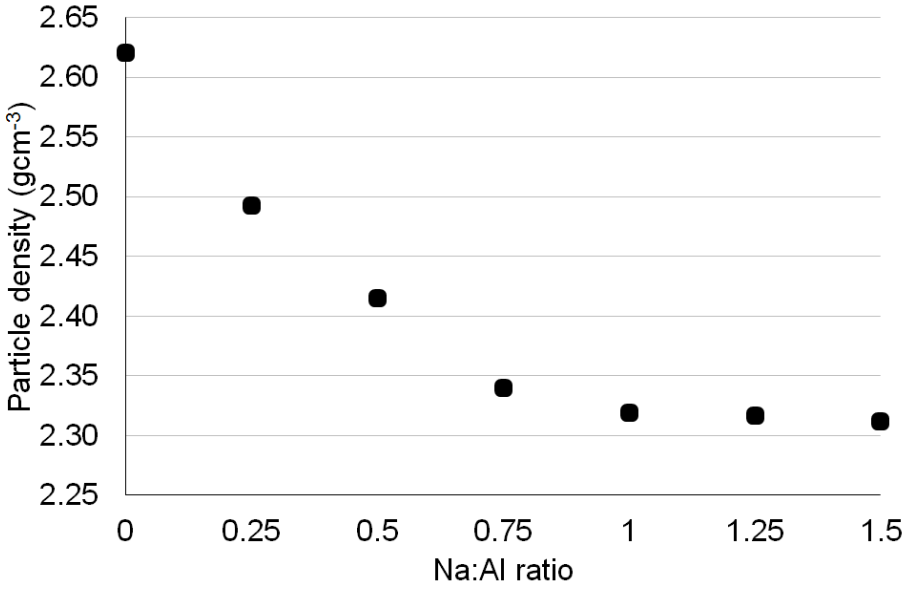

Figure 8-11: The variation of particle density with Na:Al ratio in an alkali-activated kaolinite system.

Now that some explanation of the changes in density has been given, the question still remains of what other factors could contribute to the large difference in strength between the act-120h and act-24h block specimens. Differences in interaction strength between the different phases at an atomic scale could also make a contribution. For a sodium silicate - quartz system, it has been shown that the curing temperature has an effect on the bonding mechanism between the sodium silicate phase and quartz particles, which then has a large effect on strength (Lucas *et al.*, 2011). Although the chemistry is different, it is a precedent which suggests that curing conditions could influence interaction between aggregate particles and a stabilising phase. In summary, the difference in strength between the act-24h and act-120h specimens is likely to be due to some combination of the effects of moisture content at testing, and the chemical and/or mechanical interaction between the product phase and aggregate. The size, morphology and crystallinity degree of the particles could have a minor effect as well.

Regarding the effects of ageing time, the most notable observation was the difference in mass change between the cont-24h and act-24h specimens in Section 8.3.3. Of the possible explanations for this difference, the existence of a surface barrier preventing moisture loss seems unlikely. The act-120h block specimens continued to lose more moisture during a longer curing time, so a preventative barrier could not have formed within the first 24h. For reactions that would increase mass, some minor efflorescence (thermonatrite) had formed on the act-24h specimens by 4 days ageing, as stated in Sections 8.3.1 and 8.3.3. Since the formation of thermonatrite consumes atmospheric CO_2, it would increase the mass of the specimen. However, it is not straightforward to determine the size of this contribution to the observed mass gain of act-24h with

ageing. As the act-0h-e XRD pattern in Figure 8-4 shows, even when thermonatrite dominates the specimen, its XRD peaks are not the dominant peaks. Therefore, moderate amounts of thermonatrite could be present in the act-24h specimen, but be undetected by XRD. The remaining possible explanation for this mass increase is the re-adsorption of moisture from the atmosphere. Alkali-activated soils have been shown to have an increased capacity for moisture adsorption (≤+2%) in the relative humidity range of 60-90%, i.e. the capillary condensation domain (McGregor *et al.*, 2014). This agrees well with thermogravimetric measurements in simple hydrosodalite-kaolinite systems, which give a similar value of +2% for the difference in surface-adsorbed moisture mass in hydrosodalite compared to kaolinite (Marsh *et al.*, 2018). Given this, the re-adsorption rate of act-24h would be expected to be higher than that of cont-24h. It is therefore likely that the observed mass change is due to a combination of moisture re-adsorption and some carbonation. This has consequence for these materials' performance as walling materials, as hygroscopic behaviour influences both strength and moisture buffering of the indoor environment (McGregor *et al.*, 2016).

8.4.2 Implications for practical adoption

The strength values for the act-120h block specimens are promising, as they demonstrated a large increase over the cont-120h block specimens. These would fulfil the strength requirements of 2.9 MPa for autoclaved aerated concrete (AAC) masonry blocks - this is a suitable comparison material for how earth materials could be used in construction (Heath *et al.*, 2012) - tested at 6% moisture content, under Part A of the UK Building Regulations (HM Government, 2013). There is some debate about what constitutes appropriate testing conditions, given that these should represent service conditions (Morel *et al.*, 2007). However, if such materials are to compete with fired bricks and concrete blocks in load-bearing walling, then saturated strength testing would be essential for any alkali-activated soil mix before use in construction. The Indian Standard for Stabilized Soil Blocks (IS 1725:2013) (BIS, 2013) demands a saturated compressive strength of ≥ 3.5 MPa, using the same testing procedure as used for fired clay bricks (IS 3495-1:1992) (BIS, 1992). More widely, it's recommended that a saturated compressive strength of 3 – 4 MPa is required for two storey construction, whilst 2.5 – 3 MPa is acceptable for single storey construction or non load bearing walls (Jagadish, 2007). Now that the phase formation behaviour of these blocks has been established, further testing would show whether they could meet the saturated strength requirements. However, this lies outside the scope of this study, given that such testing would benefit from firstly optimising the activating solution concentration for maximising strength and minimising efflorescence.

For hydrosodalite stabilisation, an increase in strength is accompanied by a decrease in density, as shown in the preceding section. This is the opposite trend observed for cement stabilisation (Reddy and Latha, 2014). Whilst dry density is determined by compaction force and moulding moisture content (Reeves *et al.*, 2006), in some circumstances a measurement of density change could be used to verify that the reaction has occurred. Regarding the influence on other engineering properties aside from strength, a decrease in bulk density is associated with an increase in thermal conductivity for earthen materials (Walker *et al.*, 2005). However, the scale of the decrease observed here would be unlikely to result in a significant change in thermal performance.

Another practical issue is the specific hazards of alkali activation in the construction process. The use of highly alkaline substances such as 12 M NaOH solution is routine in laboratory settings. This is safe, given the right precautions and protective measures. However, in many areas of the world where population growth and demand for housing is highest, protective measures on construction sites are often poorest. For the 40 kg soil-sand mix used in this study, direct handling of 4 litres of 12 M NaOH solution was required. Whilst other properties of a given soil mix, such as environmental impacts, depends on the exact amounts of solution used, in terms of health and safety, any exposure to such highly alkaline substances is a hazard. There have been efforts to find less hazardous substances in industry, but in publically available research, this is still a relatively neglected topic (Heath *et al.*, 2014).

8.5 Conclusions

In this investigation of the variation within alkali-activated soil block specimens, it was found that there were no major differences in phase formation or microstructure between the central and edge regions of the block specimens. Alkali activation resulted in a large increase in compressive strength after 120 hours of curing, but not after 24 hours. Although the addition of inert aggregate has been shown not to affect the fundamental reactions occurring in alkali activation, it could yet be the case that the interaction between the stabilising phase (in this system, a hydrosodalite) and the aggregate is an influential parameter on overall mechanical behaviour.

Acknowledgements

Thanks are given to the Masonry Laboratory, Department of Civil Engineering, for hosting A. Marsh on a research placement at the Indian Institute of Science. Thanks are also given to Mr. Nikhil, Mr. Nikhilash and Mr. Raghu for assistance with block specimen production, and to Mr. D Fosas De Pando for assistance with obtaining weather data. This study was supported by the EPSRC Centre for Decarbonisation of the Built Environment (dCarb) [grant number EP/L016869/1], a University of Bath Research Scholarship and the UKIERI project “Developing earth based building products utilising solid wastes”. All data created during this research are openly available from the University of Bath data archive at https://doi.org/10.15125/BATH-00564.

References

Allahverdi, A., Najafi Kani, E., Hossain, K.M.A. & Lachemi, M., 2015. 17 - Methods to control efflorescence in alkali-activated cement-based materials. *Handbook of Alkali-Activated Cements, Mortars and Concretes.* Oxford: Woodhead Publishing, pp. 463-483.

Antoni, Wijaya, S.W. & Hardjito, D., 2016. Factors affecting the setting time of fly ash-based geopolymer. In: J.E. Januarti & Antoni, eds. *Properties and Application of Geopolymers.* Surabaya, Indonesia: Trans Tech Publications, pp. 90-97.

BIS, 1980. IS:2116-1980 Specification for sand for masonry mortars. New Delhi: Bureau of Indian Standards.

BIS, 1992. IS 3495-1:1992. Methods of Tests of Burnt Clay Building Bricks. *Part 1. Determination of Compressive Strength.* New Delhi: Bureau of Indian Standards.

BIS, 2013. IS 1725:2013. Stabilized soil blocks used in general building construction - specification. New Delhi: Bureau of Indian Standards.

BSI, 2009. BS EN12390-3:2009. Testing hardened concrete. Part 3: Compressive strength of test specimens. London: BSI.

Burton, A.W., Ong, K., Rea, T. & Chan, I.Y., 2009. On the estimation of average crystallite size of zeolites from the Scherrer equation: A critical evaluation of its application to zeolites with one-dimensional pore systems. *Microporous and Mesoporous Materials,* 117(1), pp. 75-90.

Byrappa, K. & Adschiri, T., 2007. Hydrothermal technology for nanotechnology. *Progress in Crystal Growth and Characterization of Materials,* 53(2), pp. 117-166.

Champiré, F., Fabbri, A., Morel, J.-C., Wong, H. & McGregor, F., 2016. Impact of relative humidity on the mechanical behavior of compacted earth as a building material. *Construction and Building Materials,* 110, pp. 70-78.

Chindaprasirt, P., De Silva, P., Sagoe-Crentsil, K. & Hanjitsuwan, S., 2012. Effect of SiO2 and Al2O3 on the setting and hardening of high calcium fly ash-based geopolymer systems. *J Mater Sci,* 47(12), pp. 4876-4883.

Diop, M.B. & Grutzeck, M.W., 2008. Low temperature process to create brick. *Construction and Building Materials,* 22(6), pp. 1114-1121.

Dixon, J.B. & Weed, S.B., 1989. *Minerals in Soil Environments.* 2nd ed. Madison, WI: Soil Science Society of America.

Duxson, P., Fernández-Jiménez, A., Provis, J.L., Lukey, G.C., Palomo, A. & van Deventer, J.S.J., 2007. Geopolymer technology: the current state of the art. *J Mater Sci,* 42(9), pp. 2917-2933.

Engelhardt, G., Felsche, J. & Sieger, P., 1992. The hydrosodalite system Na6+ x [SiAlO4] 6 (OH) x. cntdot. nH2O: formation, phase composition, and de-and rehydration studied by 1H, 23Na, and 29Si MAS-NMR spectroscopy in tandem with thermal analysis, x-ray diffraction, and IR spectroscopy. *Journal of the American Chemical Society,* 114(4), pp. 1173-1182.

Franus, W., Wdowin, M. & Franus, M., 2014. Synthesis and characterization of zeolites prepared from industrial fly ash. *Environmental Monitoring and Assessment,* 186(9), pp. 5721-5729.

Gourav, K. & Venkatarama Reddy, B.V., 2018. Bond Development in Burnt Clay and Fly Ash-Lime-Gypsum Brick Masonry. *Journal of Materials in Civil Engineering,* 30(9), p. 04018202.

Granizo, M.L. & Blanco, M.T., 1998. Alkaline Activation of Metakaolin An Isothermal Conduction Calorimetry Study. *Journal of Thermal Analysis and Calorimetry,* 52(3), pp. 957-965.

Heath, A., Maskell, D., Walker, P., Lawrence, M. & Fourie, C., 2012. Modern earth masonry: structural properties and structural design. *The Structural Engineer,* 90(4), pp. 38-44.

Heath, A., Paine, K. & McManus, M., 2014. Minimising the global warming potential of clay based geopolymers. *Journal of Cleaner Production,* 78, pp. 75-83.

HM Government, 2013. The Building Regulations 2010. Structure: Approved Document A. Newcastle, U.K.: NBS.

Houben, H. & Guillaud, H., 1994. *Earth Construction: A comprehensive guide.* Rugby, U.K.: Practical Action Publishing.

Jagadish, K., 2007. *Building with Stabilized Mud.* New Delhi: I.K. International Publishing House Pvt. Ltd.

Kendrick, E. & Dann, S., 2004. Synthesis, properties and structure of ion exchanged hydrosodalite. *Journal of Solid State Chemistry,* 177(4–5), pp. 1513-1519.

Kuenzel, C., Li, L., Vandeperre, L., Boccaccini, A.R. & Cheeseman, C.R., 2014. Influence of sand on the mechanical properties of metakaolin geopolymers. *Construction and Building Materials,* 66, pp. 442-446.

Lee, W.K.W. & van Deventer, J.S.J., 2002. The effect of ionic contaminants on the early-age properties of alkali-activated fly ash-based cements. *Cement and Concrete Research,* 32(4), pp. 577-584.

Lucas, S., Tognonvi, M.T., Gelet, J.L., Soro, J. & Rossignol, S., 2011. Interactions between silica sand and sodium silicate solution during consolidation process. *Journal of Non-Crystalline Solids,* 357(4), pp. 1310-1318.

Marsh, A., Heath, A., Patureau, P., Evernden, M. & Walker, P., 2018. A mild conditions synthesis route to produce hydrosodalite from kaolinite, compatible with extrusion processing. *Microporous and Mesoporous Materials,* 264, pp. 125-132.

Marsh, A., Heath, A., Patureau, P., Evernden, M. & Walker, P., in preparation. Influence of clay minerals and associated minerals in alkali activation of soils.

Maskell, D., Heath, A. & Walker, P., 2014. Geopolymer stabilisation of unfired earth masonry units. In: K. Ghavami, N.P. Barbosa, U.T. Bezerra & A. Zhemchuzhnikov, eds. *14th International Conference on Non-Conventional Materials and Technologies for Sustainable Engineering* Joao Pessoa, Brazil: Trans Tech Publ, pp. 175-185.

Mastali, M., Kinnunen, P., Dalvand, A., Mohammadi Firouz, R. & Illikainen, M., 2018. Drying shrinkage in alkali-activated binders – A critical review. *Construction and Building Materials,* 190, pp. 533-550.

McGregor, F., Heath, A., Fodde, E. & Shea, A., 2014. Conditions affecting the moisture buffering measurement performed on compressed earth blocks. *Building and Environment,* 75, pp. 11-18.

McGregor, F., Heath, A., Maskell, D., Fabbri, A. & Morel, J.-C., 2016. A review on the buffering capacity of earth building materials. *Proceedings of the Institution of Civil Engineers - Construction Materials,* 169(5), pp. 241-251.

Morel, J.-C., Pkla, A. & Walker, P., 2007. Compressive strength testing of compressed earth blocks. *Construction and Building Materials,* 21(2), pp. 303-309.

National Centers for Environmental Information, 2018. Integrated Surface Database. National Oceanic and Atmospheric Administration.

Petrova, N. & Kirov, G.N., 1995. Zeolitization of glasses: a calorimetric study. *Thermochimica Acta,* 269-270, pp. 443-452.

Provis, J.L., Duxson, P. & van Deventer, J.S.J., 2010. The role of particle technology in developing sustainable construction materials. *Advanced Powder Technology,* 21(1), pp. 2-7.

Reddy, B., 2015. Design of a manual press for the production of compacted stabilized soil blocks. *Current Science (00113891),* 109(9).

Reddy, B.V.V. & Latha, M.S., 2014. Influence of soil grading on the characteristics of cement stabilised soil compacts. *Mat. Struct.,* 47(10), pp. 1633-1645.

Reeves, G.M., Sims, I. & Cripps, J.C., 2006. *Clay materials used in construction.* London: Geological Society.

Rovnaník, P., 2010. Effect of curing temperature on the development of hard structure of metakaolin-based geopolymer. *Construction and Building Materials,* 24(7), pp. 1176-1183.

Walker, P., Keable, R., Martin, J. & Maniatidis, V., 2005. *Rammed Earth: Design and Construction Guidelines.* Bracknell, U.K.: IHS BRE Press.

Walker, P. & Stace, T., 1997. Properties of some cement stabilised compressed earth blocks and mortars. *Mat. Struct.,* 30(9), pp. 545-551.

Walker, P.J., 1995. Strength, durability and shrinkage characteristics of cement stabilised soil blocks. *Cement and Concrete Composites,* 17(4), pp. 301-310.

Weng, L. & Sagoe-Crentsil, K., 2007. Dissolution processes, hydrolysis and condensation reactions during geopolymer synthesis: Part I—Low Si/Al ratio systems. *J Mater Sci,* 42(9), pp. 2997-3006.

Zhang, Z., Wang, H., Provis, J.L., Bullen, F., Reid, A. & Zhu, Y., 2012. Quantitative kinetic and structural analysis of geopolymers. Part 1. The activation of metakaolin with sodium hydroxide. *Thermochimica Acta,* 539(Supplement C), pp. 23-33.

Zuhua, Z., Xiao, Y., Huajun, Z. & Yue, C., 2009. Role of water in the synthesis of calcined kaolin-based geopolymer. *Applied Clay Science,* 43(2), pp. 218-223.

Chapter 9 - Conclusions and future research

In this chapter, the findings of this research will be drawn together to reflect on the original motivations of the research. Firstly, a short overview of the problem area and research motivations will be given. Secondly, the contributions to knowledge from Chapters 4-8 will be evaluated by answering the research questions concerning technical and overall viability. Thirdly, priorities for future research will be suggested. Lastly, a final evaluation of this research will be given.

9.1 Overview of problem area and research motivations

In Chapter 1, an introduction was given to the problem area of affordable and sustainable housing provision. A concise overview will be given here, to help provide context for interpreting the contributions to knowledge of this research.

There is currently a lack of adequate housing in urban areas of LEDCs. This situation is likely to be exacerbated in the coming decades as population growth rates are typically highest in these areas. Conventional materials used in housing construction include traditional materials such as unstabilised earth as well as fired brick and concrete block. None of these materials fulfil the multitude of requirements to provide adequate housing sustainably on the scale of units required. As a result, there is an urgent and as yet unmet demand for new construction materials. To be successful in this application, any new material must be practical, sustainable and affordable. Alkali-activated earth materials are an emerging material family that has the potential to fulfil this demand. By using soil as the main precursor, this has intrinsic advantages of low cost and low environmental impact. Alkali-activated materials have the potential to have lower environmental impact than Portland cement based materials due to their differences in chemistry. Alkali-activated earth materials could therefore become the next generation of stabilised earth materials, for which Portland cement is the stabilising agent typically used at present.

A review of the literature in Chapter 2 indicated there is a knowledge gap around which soil properties affect alkali activation, and that this is limiting the potential use of these materials. The motivation for this research is therefore to undertake fundamental investigation into the influence of soil composition on the alkali activation process. Through a better fundamental understanding of these systems, it is intended to improve understanding of the viability of alkali-activated earth materials for the application of walling materials for housing in LEDCs.

9.2 Technical viability of alkali-activated earth materials

By bringing together the findings of the preceding chapters, the specific research questions stated in Chapter 3 can now be answered. These are:

- What are the alkali activation potentials of kaolinite, montmorillonite and illite as individual clay minerals?
- What contribution do the non-clay minerals in soil make to alkali activation?
- Which soil compositions are most suited to stabilisation by alkali activation?
- Are alkali-activated soils a viable material to produce walling materials for sustainable, practical and affordable mass housing in LEDCs?

9.2.1 What is the alkali activation potential of the individual clay minerals?

As described in Chapters 4 and 5, the phase formation behaviour of the three most common clay minerals in soils has been characterised (Figure 9-1). When individually activated with NaOH solution under the conditions used in the testing, kaolinite forms a hydrosodalite as the main product, montmorillonite forms a N-A-S-H or (N,C)-A-S-H geopolymer and illite does not form a major product phase, but undergoes alteration.

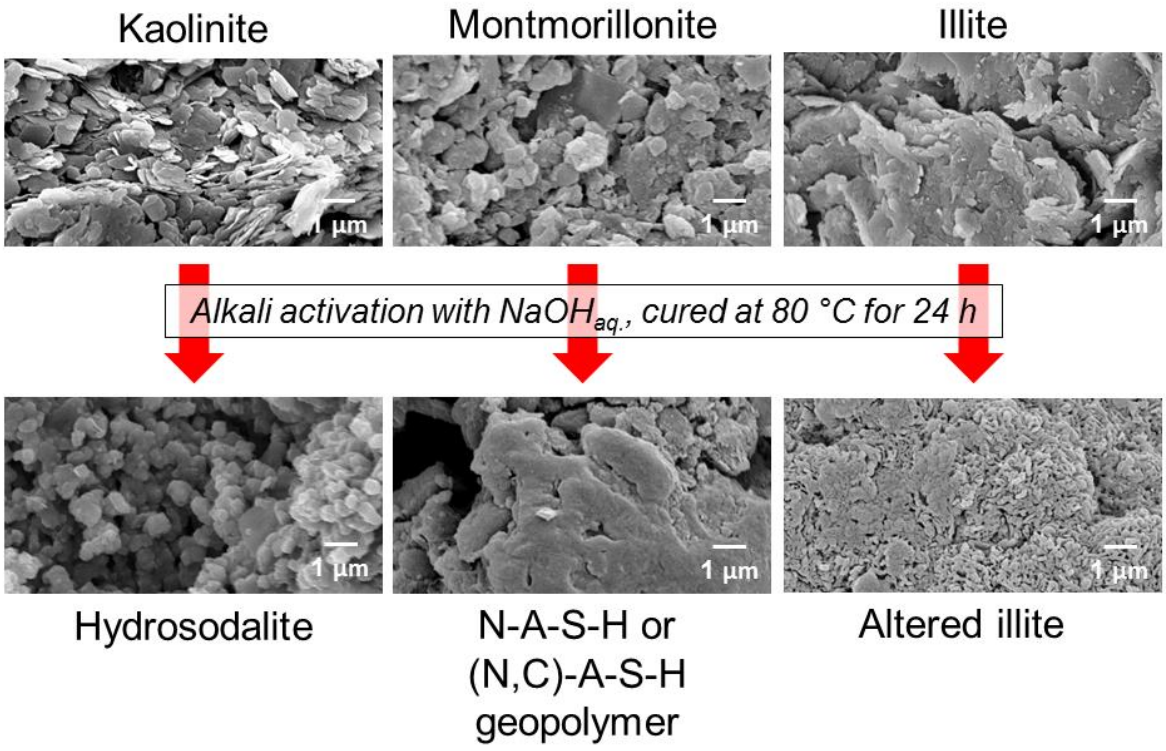

Figure 9-1: Summary of alkali activation reaction products from the clay minerals

The extent of hydrosodalite formation could be quantified, but geopolymer formation could not be accurately quantified. In both cases, the amount of product phase formed increased with Na:Al ratio. For all three of the clays tested and within the limits of the alkali contents used, not all of the clay was consumed; some amount was always left unreacted. These results also show that precursor Si:Al molar ratio is not the sole parameter in influencing what product phase is formed. Both montmorillonite and illite are 2:1 minerals, but only montmorillonite formed a geopolymer.

As described in Chapter 6, when mixtures of these clays are activated, there is a hierarchy between the clays in determining phase formation behaviour. Montmorillonite appears more reactive than kaolinite, but kaolinite has a stronger influence in determining reaction products. Montmorillonite and kaolinite both dominate illite. This shows that the alkali activation behaviour of clay mixtures (which is the case for many soils) has an extra degree of complexity, so that reaction products cannot be fully predicted from the clay mineral and activator composition alone.

9.2.2 What contribution do the non-clay minerals in soil make to alkali activation?

As described in Chapter 7, clay minerals are the primary determinants of alkali-activated product phase formation behaviour in soils. Most associated minerals had little or no influence on the reaction, although it appears that some additional minerals did produce a retarding effect on geopolymer formation in the Khartoum soil.

As described in Chapter 8, the introduction of an inert aggregate phase does not change the fundamental nature of the alkali activation reaction. However, there is evidence to suggest that the bonding between the soil and the aggregate could be an important determinant of block strength. Because clay minerals were the only major reactive phase present in the soils studied, the amount of NaOH required to achieve a system molar ratio of Na:Al = ~1 decreased with the higher amount of non-reactive material in the system (Table 9-1).

Table 9-1: Comparison of wt.% NaOH in the different systems, calculated by dividing dry weight of NaOH by the weight of dry components in the mix (i.e. soil and other minerals).

Sample	Kao-1Na:Al	Mont-1Na:Al	Bristol-nat-act	Bengaluru-nat-act	Bengaluru-block-act
Composition type	Clay	Clay	Soil	Soil	Soil + aggregate
Wt.% NaOH	31%	16%	13%	11%	5%

9.2.3 Which soil compositions are most suited to stabilisation by alkali activation?

For a soil to be suitable for an alkali-activated earth material, it must form a stabilising phase through alkali activation, as well as not being problematic if unreacted. These two conditions are both required as this research has shown that for all the clay minerals, transformation did not go to completion. More than very minor quantities of highly expansive clay minerals (such as montmorillonite) generally renders soils unsuitable for earth construction, as it can lead to excessive shrinkage cracking as well as expansion and strength loss when the moisture content increases. The findings in Chapters 4 to 8 can be drawn together to suggest broad guidelines (Table 9-2), based on clay mineralogy, from which soils can be deemed suitable or unsuitable for stabilisation by this method of alkali activation. Based on the findings presented in this work:

- Kaolinite-dominated soils are likely to work well, as they reliably form hydrosodalites.
- Montmorillonite-dominated soils are unlikely to work well. Although montmorillonite does form a geopolymer, there are associated dimensional changes and there is unreacted clay left. This means that its expansive properties are unlikely to be fully eliminated. Therefore it is unlikely to work well for external, load-bearing walling materials.
- Illite-dominated soils are also unlikely to work well. Illite does not form a useful product phase, so there is likely to be negligible benefit from this technique.

Table 9-2: Evaluation of technical suitability for soils whose properties are dominated by each of the most common clay minerals.

	Kaolinite	Montmorillonite	Illite
Suitable for alkali activation?	✓	✓	✗
Unlikely to be problematic if unreacted?	✓	✗	✓
Suitable for alkali-activated earth materials?	✓	✗	✗

For mixed soils, performance is likely to depend on the exact proportions of clay minerals. Minor amounts of montmorillonite and/or illite in a soil are likely to be acceptable.

In addition to clay mineralogy, guidelines can also be suggested for a suitable range of soils' plasticity. The two chemical constraints of 8 - 12 M NaOH concentration and a system Na:Al molar ratio = 1 together set processing limits on the plastic limits of soils. This is due to the interdependence of these three factors (Figure 9-2). If a soil is too plastic, then for Na:Al = 1, the NaOH solution will be too dilute, and dissolution will be insufficient. If a soil is too non-plastic, then the NaOH solution will exceed the saturation limit without achieving a Na:Al = 1. Only a soil having plasticity within the suitable range can meet these three requirements simultaneously.

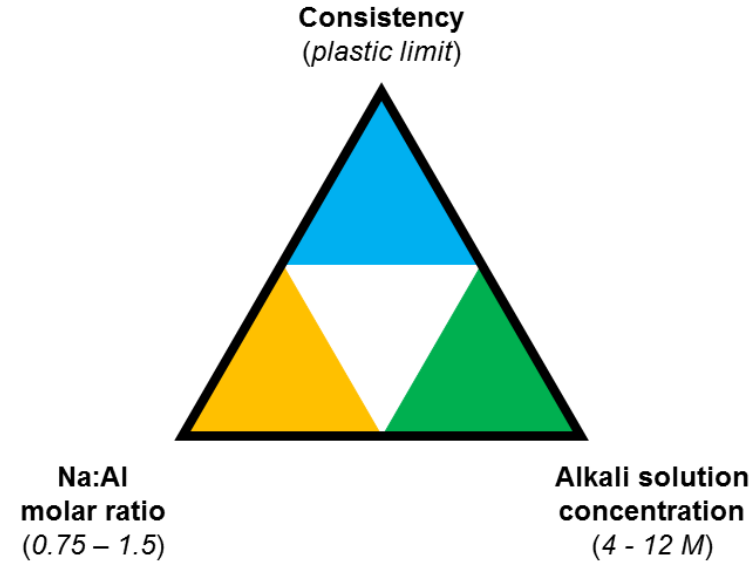

Figure 9-2: The interdependent factors influencing the chemistry and consistency of alkali-activated soil mixes, with approximate recommended ranges given in brackets.

9.3 Overall viability of alkali-activated earth materials

The additional understanding of the technical viability summarised above can be used to re-evaluate the overall viability of these systems. This will be categorised along the three requirements for new materials described in Chapter 1: sustainability, practicality, and affordability.

9.3.1 Sustainability

In an alkali-activated earth material, the majority of the environmental impact is associated with the alkaline activator (Dahmen *et al.*, 2018). Therefore, the amount of activator required, as well as the environmental impact per unit mass of a given activator, is crucial to determining the overall impact of the system.

The findings of Chapter 4 and 5 showed that under the given consistency constraints, a molar ratio of Na:Al > 0.75 is required to get appreciable transformation of the clay minerals in soil. From the mass ratios of NaOH to precursor (Table 9-1), the amount of NaOH required would be in approximately the same range as the amount of cement required for cement stabilisation of 5 – 10 wt.% (Reddy and Gupta, 2006; Walker and Stace, 1997). The global warming potential (GWP) for NaOH is 2.2 $kgCO_{2eq}.kg^{-1}$, and for CEM1 Portland cement is 0.84 $kgCO_{2eq}.kg^{-1}$ (Habert *et al.*, 2011); that is, the GWP of NaOH is a factor of >2 higher than Portland cement. Therefore, using this specific mix design, alkali activation is not obviously an improvement on cement stabilisation in terms of environmental impact. However, there are several caveats in this figure. This estimate does not normalise for strength (Habert and Ouellet-Plamondon, 2016), and the values used are for cradle-to-gate, and hence do not account for any potential benefits from reductions in material transport from localised NaOH production. Most significantly, the GWP for NaOH is based on conventional production methods. There is great potential for reducing the impacts of NaOH production, both by developments in processing technology, and using waste streams such as coal seam gas brine (Simon *et al.*, 2014) and desalination brine (Du *et al.*, 2018). This has the potential to produce NaOH from a wide geographical spread of resources, reducing impacts from both transport of the NaOH as well as from averting the release or disposal of such waste streams (Du *et al.*, 2018).

Aside from embodied energy and carbon, the use of NaOH has additional environmental impacts, such as ecotoxicity (Habert and Ouellet-Plamondon, 2016; Heath *et al.*, 2014), which would likely be exacerbated in a loosely regulated environment. However, there are possible ways around some of these risks, such as

the use of CaO and Na_2CO_3 to form NaOH in-situ without direct handling required (Heath *et al.*, 2014; Wang *et al.*, 2018b).

9.3.2 Practicality

Earthen construction is an established construction method in many parts of the world. However, the use of alkaline activators is a novel aspect which would be unfamiliar to most builders. This is relevant to three particular issues: safety, simplicity and standards.

Regarding safety, it was shown in Chapters 5 and 6 that a molar ratio of Na:Al > 0.75 is needed to form an appreciable amount of stabilising phase. This corresponds to a NaOH concentration of ≥ 4 M, which is ≥ pH 14.6. As described in Chapter 8, manual block production involves a lot of handling. The handling of alkaline substances in construction is common practice; both freshly mixed cement and slaked lime are alkaline. These are weaker than alkali activating solutions, although depending on the soil, a lime-soil wet mix can reach a pH of <13 (Yong and Ouhadi, 2007). The stronger alkalinity of the activating solutions required could expose workers to unacceptable levels of risk in a loosely regulated environment (Davidovits, 2011). However, there is potential for processes to be developed which could avoid the direct handling of such highly alkaline solutions in this way. One method is the use of sodium silicate solutions, which are classified as irritant rather than corrosive for SiO_2:Na_2O > 1.45 (Davidovits, 2011), and are also therefore much easier to transport (Araya, 2018). Another is the in-situ reaction of Na_2CO_3 with $Ca(OH)_2$ to form NaOH and $CaCO_3$ (Heath *et al.*, 2014). Lastly, there is the option of manufacturing using the one-part geopolymer technique (Luukkonen *et al.*, 2018).

Regarding simplicity, this is one of the great benefits of Portland cement based materials which are currently favoured for construction. Concrete is very simple to mix for a block-scale application. Use of cement stabilisation has several guidelines, but is a fairly straightforward process. To assess if a soil is suitable, one needs to know the clay, silt and sand size fractions of the soil, whether it is expansive, and whether it contains > 0.5% of organic matter, salt or sulphates (Jagadish, 2007). Specifying the cement content to be used is straightforward, with 5-10 wt.% established as an acceptable range (Reddy and Gupta, 2006; Walker and Stace, 1997). In contrast, stabilisation by alkali activation is arguably a more elegant solution – using the resources that are already in the soil (i.e. the clay) to form a stabiliser, rather than bringing in another material wholesale. However, as shown in the technical findings of this research, it is important to know the type of clay minerals present in a soil in addition to the clay fraction. Clay fraction can be easily (if highly inaccurately)

measured on-site (Price and Heath, 2014), and accurately measured using a simple hydrometer test in a laboratory. In contrast, determining mineralogy is far more complex, time-consuming and resource-intensive. This adds an additional point of complexity relative to current stabilised earth-building techniques, such as cement stabilisation.

Regarding standards, it is recognised that a lack of suitable standards can be a barrier to the use of innovative construction materials (Pacheco-Torgal and Labrincha, 2013). There are ongoing efforts to develop relevant testing procedures and standards by both the alkali-activated materials (Ko *et al.*, 2014; Provis, 2018; Van Deventer *et al.*, 2012) and earthen materials communities (Vyncke *et al.*, 2018). Not all tests can be directly transferred from Portland-cement based or masonry materials (Abora *et al.*, 2014; Bernal *et al.*, 2012). As explained in the technical findings, this thesis has shown that zeolite and/or geopolymer stabilising phases can be formed depending on the clay mineralogy. It remains to be seen whether appropriate testing methods are the same for zeolite-stabilised soils and geopolymer-stabilised soils. Building regulations and standards are frequently not followed, usually because people lack the means to do so or they are not enforced for domestic buildings in this application (Okpala, 1992; Wekesa *et al.*, 2011). However, given the importance of user perception and the influential role of government housing projects (UN-CHS, 1993), this is still a relevant factor.

9.3.3 Affordability

Of the three requirements, affordability is arguably the most variable and most difficult to estimate. The issues are different for the two main ingredients in alkali-activated earth materials: the soil, and the NaOH activating solution.

As explained in the technical findings, this research has shown that kaolinite-dominated soils are likely to be well-suited for stabilisation by alkali activation. Kaolinite is a widespread clay mineral in soils (Figure 9-3), along with a large number of geological deposits (Ekosse, 2010). This makes it compatible with localised production in urban areas.

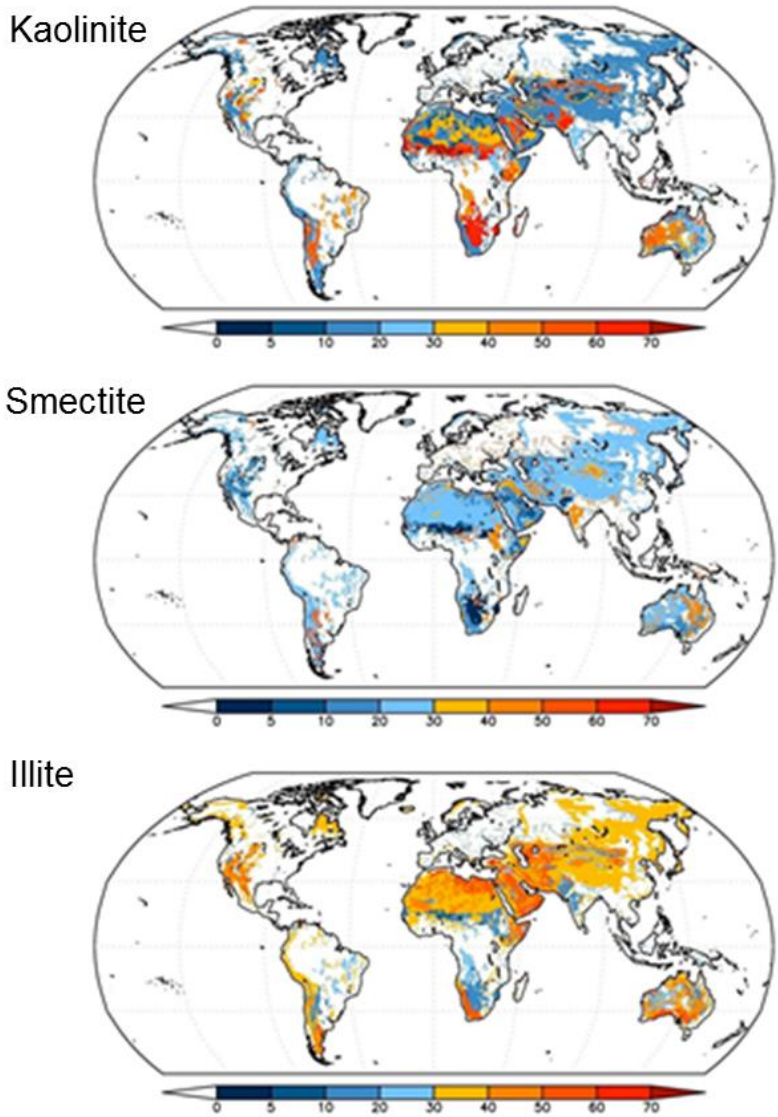

Figure 9-3: Maps showing the global distribution of kaolinite, smectite and illite in the clay fraction of soil. Adapted from Fig.1s of Nickovic et al. (2012) under a CC BY 3.0 license.

NaOH is a widely available industrial chemical with a global annual production of around 60 Mt/yr (Provis, 2018). It is currently more expensive than cement, but that could change depending on how the carbon-intensive cement industry is targeted by carbon emission reduction mechanisms, such as taxes or trading schemes (Duxson and Van Deventer, 2009). NaOH is mainly manufactured using the chlor-alkali process (Crook and Mousavi, 2016). Like cement production, this is an industrial process unsuited to small-scale, localised production. There are concerns about the scalability of NaOH production by the chlor-alkali-process, given that the world's demand for chlorine, the other product of this process, is not expected to increase (Provis, 2018). One alternative which would avoid chlorine production is production using trona ore, $Na_3(CO_3)(HCO_3)\cdot 2H_2O$, which has large resources and is scalable (Provis, 2018). A better alternative could be the use of industrial wastes, such as brines (Du *et al.*, 2018; Simon *et al.*, 2014), or agricultural wastes, such as plant ashes, in the activating

solution to displace the use of conventionally produced NaOH (Attwell, 2018). It is desirable to exploit a wide geographical range of resources, as transport can make up a disproportionately large part of material costs in this construction context (UN-CHS, 1993; Wells *et al.*, 1998). Using such waste streams would require further research to establish the technical viability, and would be locally specific, but could improve the affordability as well as the environmental impact of the activator.

9.4 Future research

There are several aspects of alkali-activated earth materials which would benefit from further research. These include further research to improve the fundamental understanding of these systems, as well as more applied research into how to optimise mix designs and use waste streams in the precursors.

Strength and durability is a commonly tested aspect of alkali-activated earth materials; but as described in Chapter 2, testing in a wet state is often not done. Wet testing is advisable if alkali-activated earth materials are ever to be considered as durable materials to replace fired brick and concrete block, as they need to be shown to meet the same demands of these conventional materials. The field would benefit from investigating the link between the type and quantity of a stabilising phase, and the resulting strength and durability. In addition, there needs to be a further understanding about the interaction between stabilising phases and aggregate or other inert particles in soils. There is also the potential to build on the experimental evidence so far by advancing the use of geochemical modelling to understand and predict the behaviour of these systems. This could use existing software such as PHREEQC (Wang *et al.*, 2018a).

A similar comment can be made for curing temperature and time. This is a commonly tested variable, and ranges have been established for some soils, as described in Chapter 2. However, there is not yet an understanding of how the individual clay minerals respond to curing temperature. There is also potential to investigate the viability of low cost solar curing methods, such as adapting designs for sludge drying beds (Kamil Salihoglu *et al.*, 2007).

As already mentioned in the preceding section, the majority of environmental impacts from these solutions arise from the activating solution. There is great scope to reduce this by developing industrial processes to extract NaOH or other alkaline activators from a variety of waste streams. Validation is needed so that these do not reduce the performance of the materials, as well as establishing how much refinement of the waste stream is required. There are precedents for obtaining soluble silicates from waste streams from research in supplementary silicates in Portland cement. This has partly been transferred to alkali-activated materials, particularly for rice husks (Kamseu *et al.*, 2017; Tong *et al.*, 2018). There is still scope to investigate a wider range of possible silica sources, and improving the simplicity, reliability and cost of the processing used. Adding soluble silicates will increase the Si:Al molar ratio and potentially increase strength and durability (Duxson *et al.*, 2007). Given that Na is required to balance the negative charge arising from Al substitution for Si in the N-A-S-

H gel framework (Barbosa *et al.*, 2000; Walkley *et al.*, 2018), a N-A-S-H product phase with a higher Si:Al molar ratio would contain a lower molar proportion of Al; hence, the total amount of Na required in the system would also be lower. Providing the extent of precursor dissolution is sufficient, the molar quantity of NaOH required in the activating solution would then be lower too, with subsequent possible benefits for environmental impact and cost.

One of the findings from this research has been an understanding of the need to control consistency whilst tailoring the chemical composition of the wet mix. This presents different issues for low plasticity and high plasticity soils. For low plasticity soils, the necessary quantity of activating solution is likely to make the wet mix wetter than desired. Such soils could be more suited to other earth-based construction techniques which benefit from a less viscous consistency, such as self-compacting earth concrete (Van Damme and Houben, 2017) or flowable earth concrete (Ouellet-Plamondon and Habert, 2016).

For high plasticity soils, admixtures may offer a route to reduce the amount of water required for plasticity, and hence obtain a suitable NaOH concentration without also getting an excess of Na in the system. Due to the deleterious effects of high pH on many superplasticizers used in Portland cement based materials (Palacios and Puertas, 2005), the development of appropriate superplasticizers for alkali-activated systems is still ongoing. However, in alkali-activated earth materials, there could be a wider range of options to control workability, such as by manipulating the flocculation behaviour of clay particles (Landrou *et al.*, 2016).

There is also potential to apply recent developments in hybrid or blended alkali-activated materials to earth based systems. By using a mid-range of soluble Ca, usually obtained by blending reactive aluminosilicate precursors with Portland cement clinker, some different combinations of C-A-S-H, N-A-S-H and C-S-H gels can be obtained (Garcia-Lodeiro *et al.*, 2015). This could still offer a lower environmental impact than a high Ca Portland cement based system, but with the advantages of room temperature curing. However, the viability of this would need to be investigated, given the lower reactivity of uncalcined clays than the precursors used so far in hybrid cements.

Finally, it would be highly beneficial to develop a less resource intensive way of measuring or accessing measurements of the clay mineralogy of soils worldwide. As shown in the technical findings of this research, it is the type of clay minerals, rather than just the size of the clay fraction in the soil, which determines alkali activation behaviour.

9.5 Overall evaluation

Alkali-activated earth materials are a promising construction material. This thesis has shown that in terms of technical viability, kaolinite-dominated soils are suitable for alkali activation, and are common around much of the world. However, in terms of overall viability, there remain many hurdles to be overcome; most importantly, making manufacture safe in loosely regulated environments, and easily determining the clay mineralogy of a given soil.

The findings in this thesis also make a valuable contribution to the understanding of clays and alkali activation as a whole. The scope of this research was intentionally limited to the chemical aspects of soil composition and alkali activation, and has successfully answered the research questions. This improved understanding also has the potential to help the design and development of other alkali-activated systems, such as the use of clays as supplementary cementitious materials. Aside from housing, this processing technique could be useful for other applications. For example, with montmorillonite, even if the reaction does not transform all of the montmorillonite, the in-situ replacement of it with a stabilising phase could be useful for specialist treatments of very expansive soils in certain situations. In other words, it could render some soils suitable for earth construction that are currently considered unsuitable.

The 20th century has been dominated by Portland cement based construction materials as a one size fits all solution. Future materials are likely to be more diverse, and more suited to local requirements and resources. Alkali-activated materials and earthen materials are both offering more sustainable alternatives to Portland cement based ones. As part of this smorgasbord of emergent materials, alkali-activated earth materials have potential to be used in some areas and applications. This will likely involve using different combinations of soils, activating solutions and reactive additives. The findings in this thesis have provided a valuable contribution in fundamental understanding to the further development of this material family.

References

Abora, K., Beleña, I., Bernal, S.A., Dunster, A., Nixon, P.A., Provis, J.L., Tagnit-Hamou, A. & Winnefeld, F., 2014. Durability and Testing – Chemical Matrix Degradation Processes. In: J.L. Provis & J.S.J. van Deventer, eds. *Alkali Activated Materials: State-of-the-Art Report, RILEM TC 224-AAM.* Dordrecht: Springer Netherlands, pp. 177-221.

Araya, A., 2018. PQ CuresilTM - Alkaline silicate activators for geopolymer" in "International Conference on Alkali Activated Materials and Geopolymers: Versatile Materials Offering High Performance and Low Emissions. In: J.L. Provis, C. Leonelli, W.M. Kriven, A.R. Boccaccini & A. Van Riessen, eds. *International Conference on Alkali Activated Materials and Geopolymers: Versatile Materials Offering High Performance and Low Emissions.* Tomar, Portugal: ECI Symposium Series.

Attwell, C., 2018. Hybrid concrete: Alternative future. In: J.L. Provis, C. Leonelli, W.M. Kriven, A.R. Boccaccini & A. Van Riessen, eds. *International Conference on Alkali Activated Materials and Geopolymers: Versatile Materials Offering High Performance and Low Emissions.* Tomar, Portugal: ECI Symposium Series.

Barbosa, V.F.F., MacKenzie, K.J.D. & Thaumaturgo, C., 2000. Synthesis and characterisation of materials based on inorganic polymers of alumina and silica: sodium polysialate polymers. *International Journal of Inorganic Materials,* 2(4), pp. 309-317.

Bernal, S.A., Provis, J.L., Brice, D.G., Kilcullen, A., Duxson, P. & van Deventer, J.S.J., 2012. Accelerated carbonation testing of alkali-activated binders significantly underestimates service life: The role of pore solution chemistry. *Cement and Concrete Research,* 42(10), pp. 1317-1326.

Crook, J. & Mousavi, A., 2016. The chlor-alkali process: A review of history and pollution. *Environmental Forensics,* 17(3), pp. 211-217.

Dahmen, J., Kim, J. & Ouellet-Plamondon, C.M., 2018. Life cycle assessment of emergent masonry blocks. *Journal of Cleaner Production,* 171, pp. 1622-1637.

Davidovits, J., 2011. *Geopolymer chemistry and applications.* 3rd ed. Saint-Quentin: Institut Geopolymere.

Du, F., Warsinger, D.M., Urmi, T.I., Thiel, G.P., Kumar, A. & Lienhard V, J.H., 2018. Sodium Hydroxide Production from Seawater Desalination Brine: Process Design and Energy Efficiency. *Environmental Science & Technology,* 52(10), pp. 5949-5958.

Duxson, P., Mallicoat, S.W., Lukey, G.C., Kriven, W.M. & van Deventer, J.S.J., 2007. The effect of alkali and Si/Al ratio on the development of mechanical properties of metakaolin-based geopolymers. *Colloids and Surfaces A: Physicochemical and Engineering Aspects,* 292(1), pp. 8-20.

Duxson, P. & Van Deventer, J.S.J., 2009. 17 - Commercialization of geopolymers for construction – opportunities and obstacles. In: J.L. Provis & J.S.J. van Deventer, eds. *Geopolymers.* Woodhead Publishing, pp. 379-400.

Ekosse, G.-I.E., 2010. Kaolin deposits and occurrences in Africa: Geology, mineralogy and utilization. *Applied Clay Science,* 50(2), pp. 212-236.

Garcia-Lodeiro, I., Palomo, A. & Fernández-Jiménez, A., 2015. 2 - An overview of the chemistry of alkali-activated cement-based binders. *Handbook of Alkali-Activated Cements, Mortars and Concretes.* Oxford: Woodhead Publishing, pp. 19-47.

Habert, G., d'Espinose de Lacaillerie, J.B. & Roussel, N., 2011. An environmental evaluation of geopolymer based concrete production: reviewing current research trends. *Journal of Cleaner Production,* 19(11), pp. 1229-1238.

Habert, G. & Ouellet-Plamondon, C., 2016. Recent update on the environmental impact of geopolymers. *RILEM Technical Letters,* 1, pp. 17-23.

Heath, A., Paine, K. & McManus, M., 2014. Minimising the global warming potential of clay based geopolymers. *Journal of Cleaner Production,* 78, pp. 75-83.

Jagadish, K., 2007. *Building with Stabilized Mud.* New Delhi: I.K. International Publishing House Pvt. Ltd.

Kamil Salihoglu, N., Pinarli, V. & Salihoglu, G., 2007. Solar drying in sludge management in Turkey. *Renewable Energy,* 32(10), pp. 1661-1675.

Kamseu, E., Beleuk à Moungam, L.M., Cannio, M., Billong, N., Chaysuwan, D., Melo, U.C. & Leonelli, C., 2017. Substitution of sodium silicate with rice husk ash-NaOH solution in metakaolin based geopolymer cement concerning reduction in global warming. *Journal of Cleaner Production,* 142, pp. 3050-3060.

Ko, L.S.-C., Beleña, I., Duxson, P., Kavalerova, E., Krivenko, P.V., Ordoñez, L.-M., Tagnit-Hamou, A. & Winnefeld, F., 2014. AAM Concretes: Standards for Mix Design/Formulation and Early-Age Properties. In: J.L. Provis & J.S.J. van Deventer, eds. *Alkali Activated Materials: State-of-the-Art Report, RILEM TC 224-AAM.* Dordrecht: Springer Netherlands, pp. 157-176.

Landrou, G., Brumaud, C., Winnefeld, F., Flatt, R. & Habert, G., 2016. Lime as an Anti-Plasticizer for Self-Compacting Clay Concrete. *Materials,* 9(5), p. 330.

Luukkonen, T., Abdollahnejad, Z., Yliniemi, J., Kinnunen, P. & Illikainen, M., 2018. One-part alkali-activated materials: A review. *Cement and Concrete Research,* 103, pp. 21-34.

Nickovic, S., Vukovic, A., Vujadinovic, M., Djurdjevic, V. & Pejanovic, G., 2012. High-resolution mineralogical database of dust-productive soils for atmospheric dust modeling. *Atmospheric Chemistry and Physics,* 12(2), pp. 845-855.

Okpala, D.C.I., 1992. Housing production systems and technologies in developing countries: a review of the experiences and possible future trends/prospects. *Habitat International,* 16(3), pp. 9-32.

Ouellet-Plamondon, C.M. & Habert, G., 2016. Self-Compacted Clay based Concrete (SCCC): proof-of-concept. *Journal of Cleaner Production,* 117, pp. 160-168.

Pacheco-Torgal, F. & Labrincha, J.A., 2013. The future of construction materials research and the seventh UN Millennium Development Goal: A few insights. *Construction and Building Materials,* 40, pp. 729-737.

Palacios, M. & Puertas, F., 2005. Effect of superplasticizer and shrinkage-reducing admixtures on alkali-activated slag pastes and mortars. *Cement and Concrete Research,* 35(7), pp. 1358-1367.

Price, N. & Heath, A., 2014. Quality control of earth construction in developing areas. *Proceedings of the Institution of Civil Engineers - Construction Materials,* 167(2), pp. 104-113.

Provis, J.L., 2018. Alkali-activated materials. *Cement and Concrete Research*, 114, pp. 40-48.

Reddy, B.V.V. & Gupta, A., 2006. Strength and Elastic Properties of Stabilized Mud Block Masonry Using Cement-Soil Mortars. *Journal of Materials in Civil Engineering,* 18(3), pp. 472-476.

Simon, A., Fujioka, T., Price, W.E. & Nghiem, L.D., 2014. Sodium hydroxide production from sodium carbonate and bicarbonate solutions using membrane electrolysis: A feasibility study. *Separation and Purification Technology,* 127, pp. 70-76.

Tong, K.T., Vinai, R. & Soutsos, M.N., 2018. Use of Vietnamese rice husk ash for the production of sodium silicate as the activator for alkali-activated binders. *Journal of Cleaner Production,* 201, pp. 272-286.

UN-CHS, 1993. Building materials for housing : Report of the executive director, United Nations Commission on Human Settlements. *Habitat International,* 17(2), pp. 1-20.

Van Damme, H. & Houben, H., 2017. Earth concrete. Stabilization revisited. *Cement and Concrete Research*.

Van Deventer, J.S.J., Provis, J.L. & Duxson, P., 2012. Technical and commercial progress in the adoption of geopolymer cement. *Minerals Engineering,* 29, pp. 89-104.

Vyncke, J., Kupers, L. & Denies, N., 2018. Earth as Building Material – an overview of RILEM activities and recent Innovations in Geotechnics. *MATEC Web Conf.,* 149, p. 02001.

Walker, P. & Stace, T., 1997. Properties of some cement stabilised compressed earth blocks and mortars. *Mat. Struct.,* 30(9), pp. 545-551.

Walkley, B., Rees, G.J., San Nicolas, R., van Deventer, J.S.J., Hanna, J.V. & Provis, J.L., 2018. New Structural Model of Hydrous Sodium Aluminosilicate Gels and the Role of Charge-Balancing Extra-Framework Al. *The Journal of Physical Chemistry C,* 122(10), pp. 5673-5685.

Wang, D., Wang, Q., Zhuang, S. & Yang, J., 2018a. Evaluation of alkali-activated blast furnace ferronickel slag as a cementitious material: Reaction mechanism, engineering properties and leaching behaviors. *Construction and Building Materials,* 188, pp. 860-873.

Wang, J., Lyu, X., Wang, L., Cao, X., Liu, Q. & Zang, H., 2018b. Influence of the combination of calcium oxide and sodium carbonate on the hydration reactivity of alkali-activated slag binders. *Journal of Cleaner Production,* 171, pp. 622-629.

Wekesa, B.W., Steyn, G.S. & Otieno, F.A.O., 2011. A review of physical and socio-economic characteristics and intervention approaches of informal settlements. *Habitat International,* 35(2), pp. 238-245.

Wells, J., Sinda, S.H. & Haddar, F., 1998. Housing and building materials in low-income settlements in Dar es Salaam. *Habitat International,* 22(4), pp. 397-409.

Yong, R.N. & Ouhadi, V.R., 2007. Experimental study on instability of bases on natural and lime/cement-stabilized clayey soils. *Applied Clay Science,* 35(3), pp. 238-2